Transition Metal Complexes for Solar Fuels Applications

Andrew J. Sadler

A thesis submitted to the University of Sheffield in partial fulfilment of the requirements for the degree of Doctor of Philosophy.

November 2018

Department of Chemistry – The University of Sheffield

Abstract

Plants and photosynthetic organisms have utilised the energy sent to Earth by the sun for millions of years. As the population rapidly increases and the energy demand rises, it is important to develop new ways of harnessing solar energy; mimicking these organisms remains a viable option. These photosynthetic apparatuses have had millions of years to adapt and are therefore highly sophisticated. An efficient photosynthetic mimic remains elusive due to the complexity of these natural systems and the synthetic difficulties associated with assembling an integrated molecular assembly with the ability to achieve and maintain a photoinduced charge separated state (CSS). CSS's are key to photosynthesis and the production of solar fuels. Prevention of back electron transfer and thus charge recombination is one of the greatest challenges in the design of artificial photosynthetic systems. It is therefore of great importance that new ways of prolonging charge separation are developed.

A series of rhenium(I) tricarbonyl complexes have been synthesised containing strongly electron accepting bis-aryl-acenaphthene/phenanthrene ligands. Their suitability towards the catalytic reduction of CO_2 (an important component of artificial photosynthetic systems) was investigated, along with their ground state and excited state properties.

A variety of square planar platinum(II) diimine dithiolates were synthesised to investigate structural reorganisation in the excited state; a potential method of prolonging the lifetime the CSS.

A family of isotopically labelled platinum(II) *trans*-acetylide donor-bridge-acceptor assemblies were synthesised that are known to demonstrate the phenomenon of "vibrational control" a method of controlling the products of photoinduced charge separation through the means of an external perturbation.

Contents

Abbreviations

2DIR	Two-Dimensional Infrared
A	Acceptor
Å	Angstrom
ADP	Adenosine diphosphate
ATP	Adenosine triphosphate
ATR	Attenuated Total Reflectance
aq	Aqueous
ASAP	Atmospheric Solids Analysis Probe
atm	Standard atmosphere
B	Bridge
bpy	2,2'-bipyridyl
BuLi	n-butyl lithium
C	Chromophore
CCD	Charge Coupled Device
Chl a	Chlorophyll a
Chl b	Chlorophyll b
cm	centimetre
CO	carbon monoxide
CO_2	carbon dioxide
conc	concentrated
CSS	Charge Separated State
CT	Charge Transfer
CV	Cyclic Voltammetry
$\Delta_r G^+$	Gibbs free energy
d	doublet
D	Donor
d_8-bpy	d_8-2,2'-bipyridyl

d_{12}-dmbpy	d_{12}-4,4’-dimethyl-2,2’-bipyridyl
DFT	Density Functional Theory
dmbpy	4,4’-dimethyl-2,2’-bipyridyl
DMF	dimethylformamide
DMSO	dimethyl sulfoxide
dt	doublet of triplets
e^-	an electron
EAS	Electronic Absorption Spectroscopy
EI	Electron Ionisation
eq	equivalents
ES	Electrospray
ES-2DIR	Excited State Two-Dimensional Infrared
Et	ethyl
eV	electron Volt
Fc	Ferrocene
Fc^+	Ferrocinium
FLUPS	Fluorescence Up-Conversion Spectroscopy
fs	femtosecond
FTIR	Fourier Transform Infrared
g	grams
H_2O	water
HOMO	highest occupied molecular orbital
hrs	Hours
hv	A photon
Hz	Hertz
I	current
IC	internal conversion
ILCT	intraligand charge transfer

IR	infrared
ISC	intersystem crossing
J	coupling constant
K	Kelvin
kHz	kiloHertz
l	Litre
Laser	Light Amplification by Stimulated Emission of Radiation
LL'CT	Ligand to ligand charge transfer
LMCT	Ligand to metal charge transfer
LUMO	lowest unoccupied molecular orbital
m	multiplet
mA	milliAmperes
MALDI	Matrix Assisted Laser Desorption Ionisation
Me	methyl
Me_2bpy	4,4'-dimethyl-2,2'-bipyridyl
$Me_2bpy\text{-}d_{12}$	4,4'-dimethyl-2,2'-bipyridyl-d_{12}
MeCN	acetonitrile
mesBIAN	bis(mesitylimino)acenaphthene
mesBIPhen	bis(mesitylimino)phenanthrene
mg	milligram
min	minutes
mJ	milliJoule
ml	millilitre
MLCT	Metal-to-Ligand Charge Transfer
MMLLCT	Mixed Metal-to-Ligand Charge Transfer
MS	Mass Spectrometry
mV	millivolt
$NADP^+$	nicotinamide adenine dinucleotide phosphate

NADPH	reduced form of nicotinamide adenine dinucleotide phosphate
NAP	1,8-Napthalimide
$NAP^{\cdot -}$	1,8-Napthalimide radical anion
NDI	1,4,5,8-Napthalene diimide
$NDI^{\cdot -}$	1,4,5,8-Napthalene diimide radical anion
NHE	Normal hydrogen electrode
nm	nanometre
NMR	Nuclear Magnetic Resonance
ns	Nanosecond
O_2	dioxygen
OD	optical density
P680	photosystem II primary donor
P700	photosystem I primary donor
Pc	plastocyanin
phen	1,10-phenanthroline
ppm	parts per million
PQ	plastoquinone
PQH_2	dihydroplastoquinone
ps	picosecond
PSI	photosystem I
PSII	photosystem II
PTZ	phenothiazine
$PTZ^{\cdot +}$	phenothiazine radical cation
q	quartet
Redox	reduction oxidation
Reflns.	reflections
r.t	room temperature
RAL	Rutherford Appleton Laboratory
RMM	relative molecular mass
s	singlet

sat	saturated
SED	sacrificial electron donor
t	triplet
tt	triplet of triplets
TA	Transient Absorption
td	triplet of doublets
$TBAPF_6$	tetrabutylammonium hexafluorophosphate
TEAS	Transient Electronic Absorption Spectroscopy
TEOA	triethanolamine
THF	tetrahydrofuran
TLC	thin layer chromatography
TMS	trimethylsilyl
TOF	time of flight
TON	turn over number
TRIR	Time Resolved Infrared
TVAS	Transient Vibrational Absorption Spectroscopy
TW	terawatt
UV	ultraviolet
UV-Vis	Ultraviolet-visible Spectroscopy
V	Volt
W	Watt
°	degrees
δ	chemical shift
ε	extinction coefficient
λ	wavelength
μ	x-ray absorption correction coefficient
μs	microsecond
τ	lifetime

1 Introduction

1.1 Motivation

1.1.1 Global Energy Demand

The world's population is estimated to reach around 10 billion by the year 2050. This projected growth, coupled with the increasing energy demand of the developing world means that the global power requirement is set to increase from 15 TW per year to 40 TW per year.[1,2] Currently the majority of Earth's energy is provided by fossil fuels, and fossil fuel consumption is still increasing resulting in the rapid depletion of known reserves (Figure 1.1)[2,3] If new methods of energy conversion and storage are not developed soon, then we will be unable to meet the energy requirements of the planet when these fossil fuels inevitably deplete (Figure 1.2). There are many sources of renewable energy but solar energy is without doubt the most abundant of them all. It is estimated that Earth receives 14 TW from the sun in one hour, which is enough to power the planet for one year.[4]

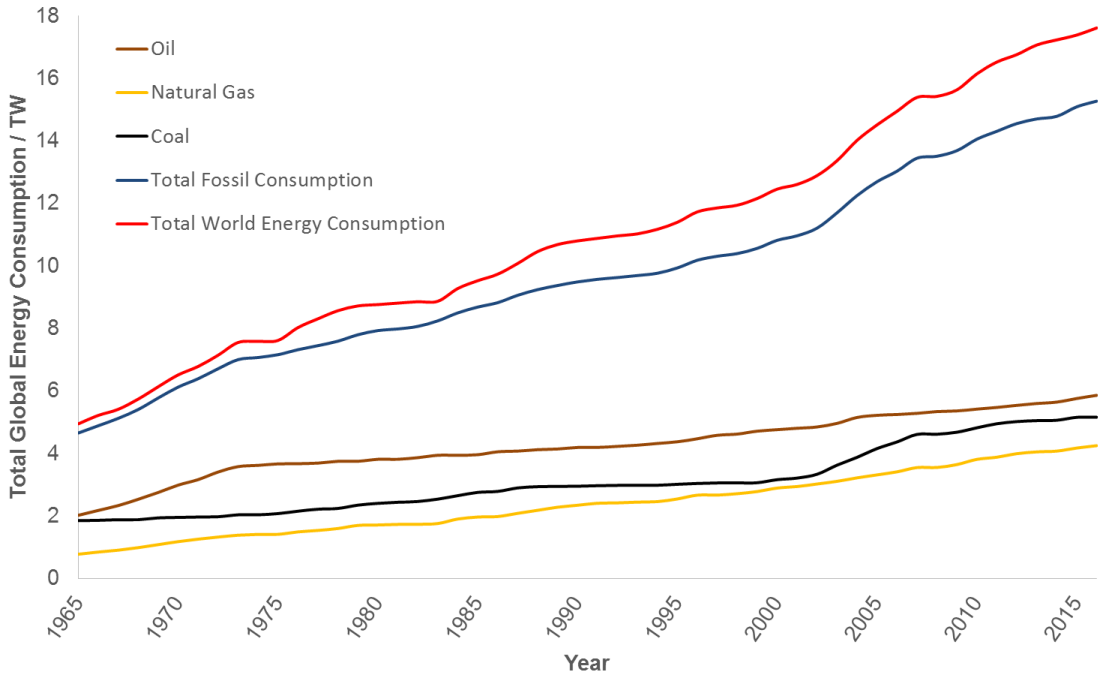

Figure 1.1 A graph to show the increase in global energy consumption between 1965 and 2016 from fossil fuels for oil, natural gas and coal. Produced using data from BP's 2017 statistical review of world energy.[3]

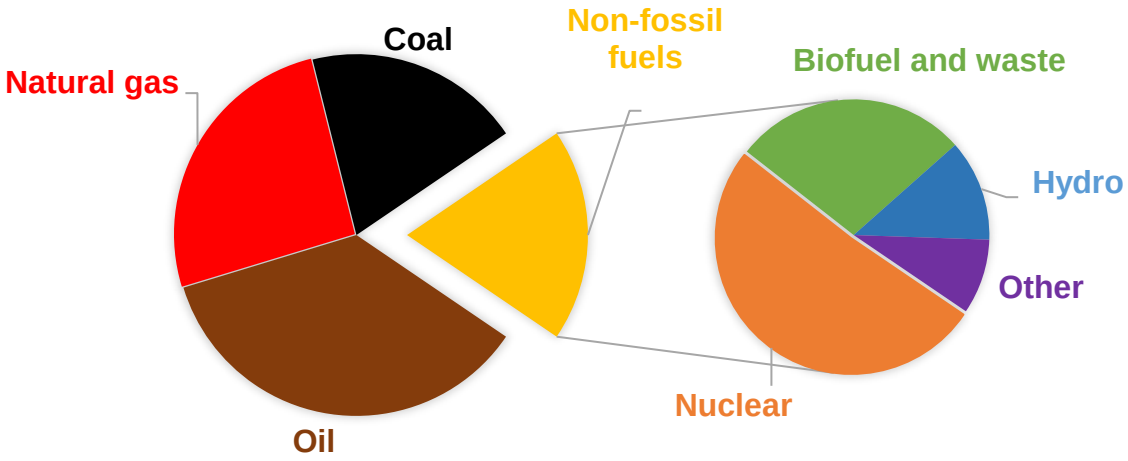

Figure 1.2 A pie chart to illustrate the proportions of the main sources of energy in 2013. Constructed using the IEA Key World Energy Statistics 2014.[2]

Earth receives 120,000 TW per year from the sun (entire planet); when considering the proportion of the sunlight arriving on land this figure reduces to 36,000 TW per year; when accounting for atmospheric losses this figure drops to 23,000 TW per year. When comparing the potential obtainable energy of solar power with other energy sources, it is evident that it exceeds them all (Figure 1.3)[5] Solar energy is also much greener than burning fossil fuels which produced 31,600 tonnes of CO_2 emissions alone, in 2008. New methods of solar energy conversion need to be developed to achieve the full potential of solar power such as dye-sensitized solar cells (DSSC) and artificial photosynthesis.[6,7]

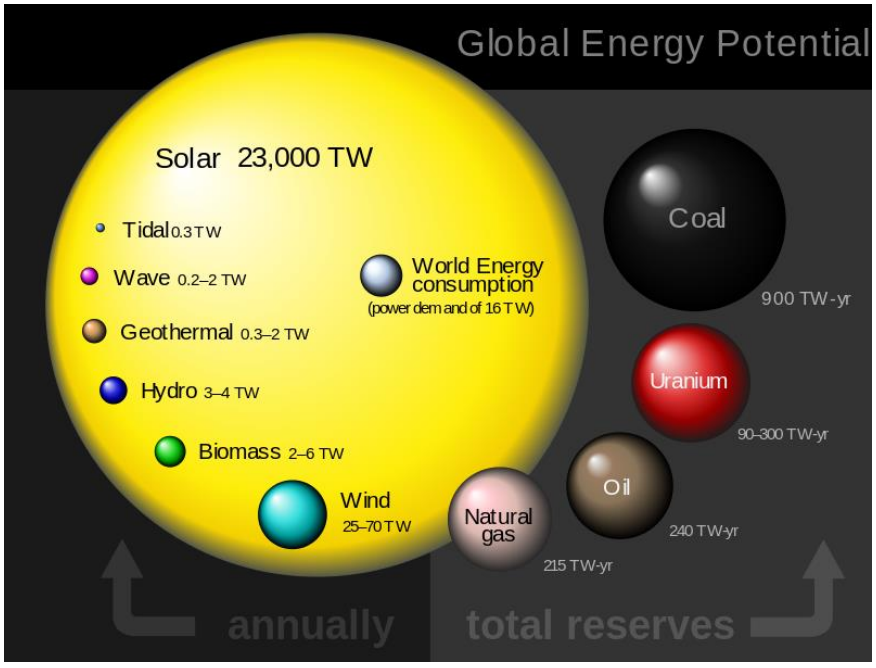

Figure 1.3 The potential of renewable sources of energy vs known reserves of non-renewables, the central sphere depicts the current annual global demand.[5]

1.2 Photosynthesis

1.2.1 Natural photosynthesis

A large amount of the solar radiation received by earth is lost due to absorption by atmospheric gases. Much of the ultra-violet radiation is absorbed by ozone and dioxygen, whilst CO_2 and water absorb in the infrared (Figure 1.4).

In nature, plants have adapted photosynthetic apparatus that capture light in the visible and near infrared region of the spectrum, so that they can store energy via photosynthesis.

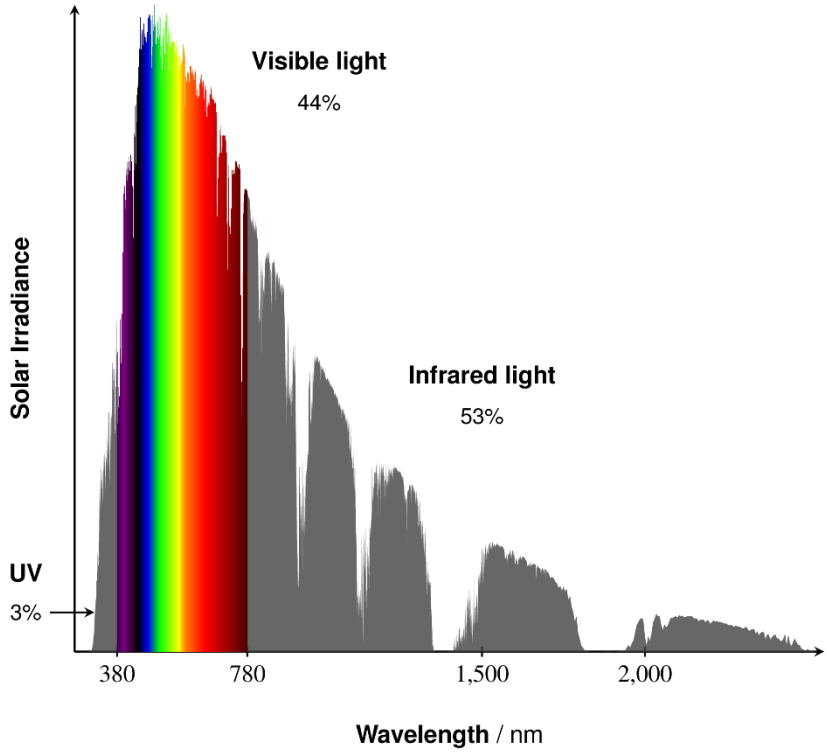

Figure 1.4 The solar irradiance spectrum after atmospheric losses. Produced using the Air Mass 1.5 reference spectrum, courtesy of Dr Theo Keane.[8]

Photosynthesis is the conversion of light energy into chemical energy in the form of carbohydrates, such as glucose, via the reduction of CO_2 and the oxidation of water to dioxygen (Equation 1.1).[9]

$$6CO_2 + 6H_2O \xrightarrow{\text{Light}} C_6H_{12}O_6 + 6O_2 \quad \Delta_rG^{+}=+2880 \text{ kJ mol}^{-1}$$

Equation 1.1 Overall equation for photosynthesis.

The reaction is endergonic with a large positive change in free energy ($\Delta_rG^{\neq}$ 2880 kJ mol^{-1}) and therefore requires light to drive it forward. Many plants utilise chlorophylls a and b (Figure 1.5), alongside carotenoids as “antenna” units in two complex photosystems (PS), PSI and PSII. These highly conjugated molecules

exhibit strong absorptions in the visible region of the spectrum, making them ideal light harvesters for plant life on earth.

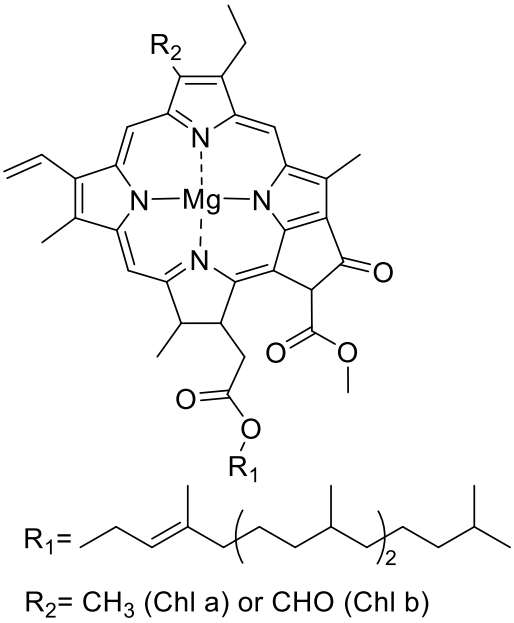

Figure 1.5 The structure of Chlorophyll a (Chl a) and Chlorophyll b (Chl b).

The light induced electron transfer processes in plants result in the oxidation of water to dioxygen as outlined below (Figure 1.6), this is complemented by the reduction of $NADP^+$ to NADPH with the simultaneous production of ATP. ATP and NADPH then reduce CO_2 to carbohydrate in separate reactions.[10]

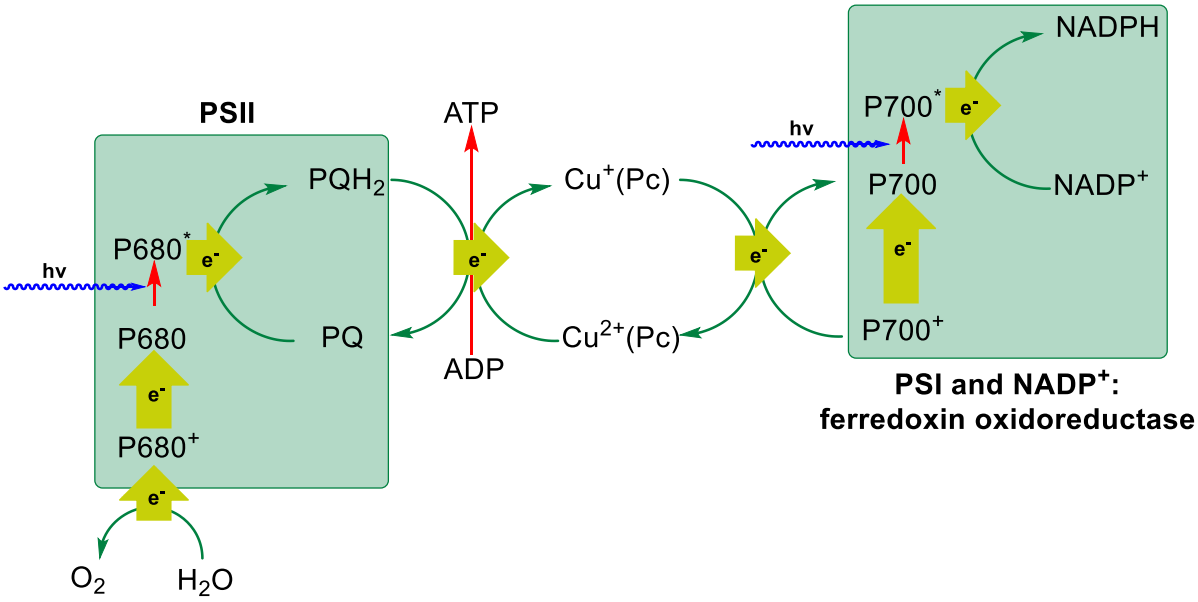

Figure 1.6 A summary of the general electron flow in photosystems I and II, the cytochrome b_6f complex, and ferredoxin: $NADP^+$ oxidoreductase. Adapted from "physical chemistry"[10] PQ=plastoquinone, PQH_2=dihydroplastoquinone, P680=photosystem II primary donor, P700=photosystemnI primary donor, Pc=plastocyanin, ADP=adenosine diphosphate, ATP=adenosine triphosphate, NADP+=nicotinamide adenine dinucleotide phosphate, NADPH=reduced form of nicotinamide adenine dinucleotide phosphate.

1.2.2 Energy storage inspired by nature

The process of photosynthesis is a complex one and involves many intermediate electron carriers to proceed. In a very simplified view the process can be summarised as an oxidation-reduction process, the water is oxidised whilst the CO_2 is reduced (Equation 1.2).

Step 1: water oxidation

$$2H_2O + 2NADP^+ \xrightarrow{\text{Light, PSI and PSII}} O_2 + 2NADPH + 2H^+ \qquad \Delta_rG^+ = +438 \text{ kJ mol}^{-1}$$

$$(2H_2O \longrightarrow O_2 + 4H^+)$$

Step 2: carbon dioxide reduction

$$2H^+ + CO_2 + 2NADPH \longrightarrow (CH_2O) + H_2O + 2NADP^+ \quad \Delta_rG^+ = +2442 \text{ kJ mol}^{-1}$$

$$(4H^+ + CO_2 \longrightarrow (CH_2O) + H_2O)$$

Overall

$$6CO_2 + 6H_2O \xrightarrow{\text{photosynthesis}} C_6H_{12}O_6 + 6O_2 \qquad \Delta_rG^+ = +2880 \text{ kJ mol}^{-1}$$

$$(CO_2 + H_2O \longrightarrow (CH_2O) + O_2)$$

Equation 1.2 The redox processes involved in photosynthesis.

The use of molecular systems to mimic these redox processes via photoinduced charge separation has become a popular area of research in recent years.[11] These molecular systems comprise three main components, a chromophore (C), an acceptor (A) and a donor (D), which can be attached to an oxidation catalyst at the donor terminus and a reduction catalyst and the acceptor terminus (Figure 1.7).[12]

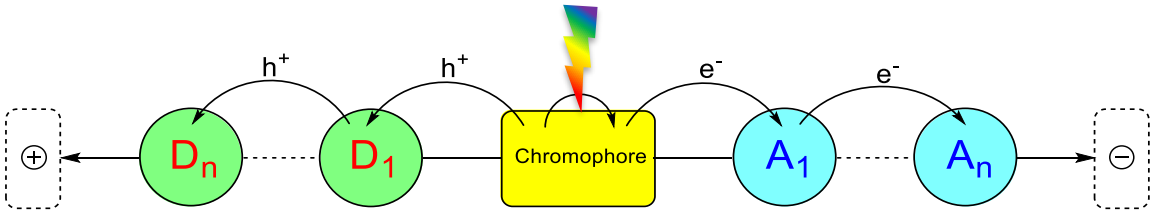

Figure 1.7 A schematic representation of a molecular system for photoinduced charge separation that utilises multiple electron donors and acceptors. Adapted from [11]

Photoinduced charge separation in D-C-A systems involves key steps (1-6) as illustrated below (Scheme 1.1).

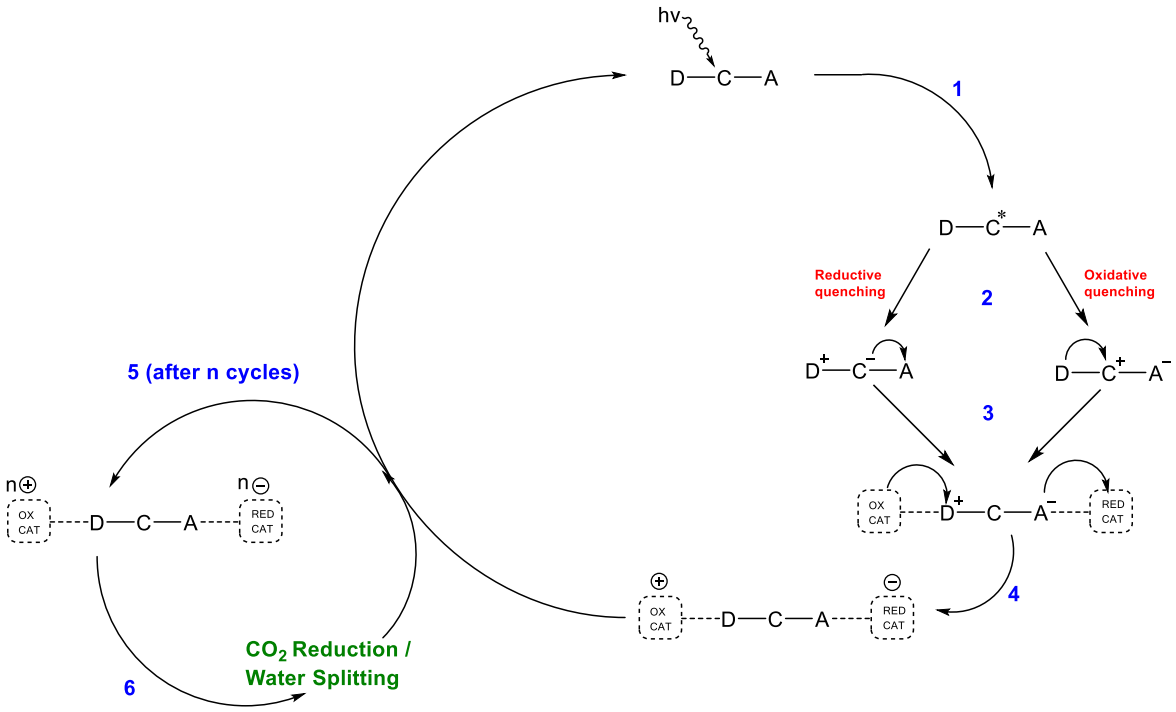

Scheme 1.1 Photoinduced charge separation in a D-C-A system.

1. The chromophore absorbs light to form an excited state.
2. Quenching of the excited state of the chromophore by electron transfer from the donor (reductive quenching) or to the acceptor (oxidative quenching).
3. Charge separation then occurs from either of the previous states to form a charge separated state.
4. Electron transfer then occurs from the oxidation catalyst to D^+ and from A^- to the reduction catalyst.
5. These electron transfer processes (1-4) lead to a system with charges available and/or stored at catalytic sites.

Redox reactions such as CO_2 reduction and water splitting can then be activated at the catalysts returning the system to the initial state. Some ideal candidates for these charge separation systems are based on transition metal complexes as they are excellent absorbers of visible light to generate charge-transfer excited states. The charge-transfer excited states in transition metal complexes are either MLCT,

LL’CT or a mixed metal-ligand to ligand charge transfer (MMLL’CT) in origin.[13] For optimal performance, these transition metal based charge separation systems need to have:

1. Strong visible light absorption
2. Sufficient excited state lifetime (slow charge recombination) to transfer electron/hole to the catalyst(s).
3. Sufficient energy to drive the process of interest.

1.3 Electronic excited states

The primary step in a photosynthetic system is the absorption of light providing the system with the energy needed to initiate the electron transfer cascade. To understand the different ways in which a molecule can interact with electromagnetic radiation is important when designing systems that convert sunlight into other useful forms of energy.

1.3.1 Selection rules for electronic transitions

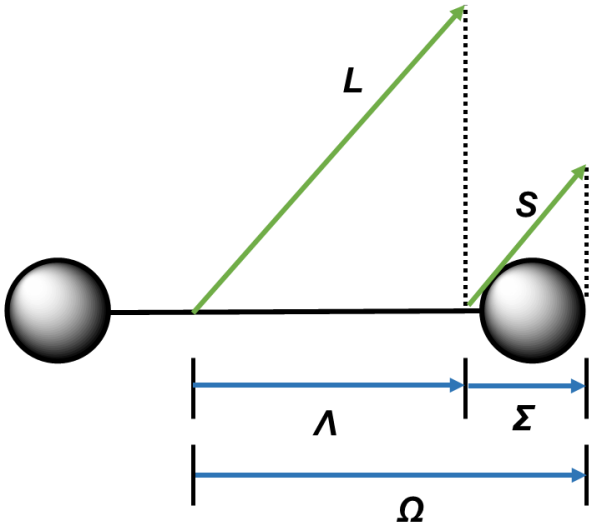

Figure 1.8 For a linear molecule, the coupling of spin and orbital angular momenta is shown. Where; L = total orbital angular momentum quantum number, S = spin quantum number, Λ = orbital angular momentum, Σ = spin angular momentum, Ω = total angular momentum.

Selection rules give an indication of the likelihood of whether or not an interaction between an atom or molecule with electromagnetic radiation is possible. Summarised below are the angular momentum selection rules (Equation 1.3) which refer to the diagram of a linear diatomic molecule above (Figure 1.8).

$$\Delta\Lambda = 0, \pm 1 \qquad \Delta S = 0 \qquad \Delta\Sigma = 0 \qquad \Delta\Omega = 0, \pm 1$$

Equation 1.3 The selection rules concerning changes in angular momentum.

The Laporte selection rule is a symmetry selection rule which states that for atoms and centrosymmetric molecules (those with a centre of inversion), “the only allowed transitions are transitions that are accompanied by a change of parity” and therefore g→u and u→g are allowed and g→g and u→u are forbidden (“g” and “u” standing for “gerade” – centrosymmetric, and “ungerade”).

1.3.2 d-d transitions

Upon the absorption of energy transition metal complexes can undergo an electronic transition, whereby an electron is promoted from a lower energy d orbital to a higher energy one. In octahedral metal complexes, this transition is from a t_{2g} orbital to an e_g orbital; as the energy difference often falls in the visible region these transitions are responsible for the bright colours observed in transition metal complexes. These transitions are forbidden by the Laporte selection rule as there is no change in parity, but are partially allowed due to the disruption of the symmetry arising from Jahn-Teller effect and asymmetric vibrations.[14] Due to these transitions being only partially allowed, they have small extinction coefficients in the order of a few hundred $dm^3\ mol^{-1}\ cm^{-1}$.

1.3.3 Metal to ligand charge transfer (MLCT) transitions

A metal to ligand charge transfer (MLCT) occurs when an electron is promoted from the highest occupied molecular orbital (HOMO) located on a metal centre to the lowest unoccupied molecular orbital (LUMO) which is located on a ligand that is coordinated to the metal. An example of this is when an electron is transferred from a d orbital of a metal, for example rhenium, to the π^* antibonding orbital on an aromatic ligand, for example bipyridine.[15] .

1.3.4 Ligand to metal charge transfer (LMCT) transitions

The opposite of an MLCT transition is simply the reverse situation in which a complex absorbs radiation due to the transfer of an electron from a coordinated ligand to the d-orbitals of the metal centre. An example of this is the electron migration from an orbital of an oxoanion ligand to the manganese d-orbitals in the permanganate ion (MnO_4^-), which gives rise to the intensely strong violet colour.

1.3.5 Ligand to ligand charge transfer (LL'CT) and intraligand charge transfer (ILCT) transitions

A ligand to ligand charge transfer (LL'CT) is an electron transfer in a metal complex which corresponds to excitation populating an electronic state in which considerable shift of electron density between two ligands has occurred. If there is promotion of an electron from a HOMO to a LUMO within the same ligand then this is called an intraligand charge transfer (ILCT).

1.3.6 π→π* transitions

A π→π* transition corresponds to a shift of electron density from a π bonding molecular orbital to a π* antibonding molecular orbital, for example in a C=C double bond. π→π* transitions tend to be symmetry allowed and have extinction coefficients in the order of 10^5 dm^3 mol^{-1} cm^{-1}.

1.3.7 n→π* transitions

An n→π* is an electronic transition from a lone pair, that is not involved in bonding, to a π* antibonding molecular orbital. An example of such a transition is the electronic absorption in ketones, where an electron may be promoted from the lone pair associated with the oxygen atom to the π* antibonding molecular orbital of the carbonyl group which have energy difference of about 4 eV, corresponding to an absorption band at around 290 nm. n→π* transitions are often symmetry forbidden, and therefore have weak absorptions.

1.4 Fates of excited states

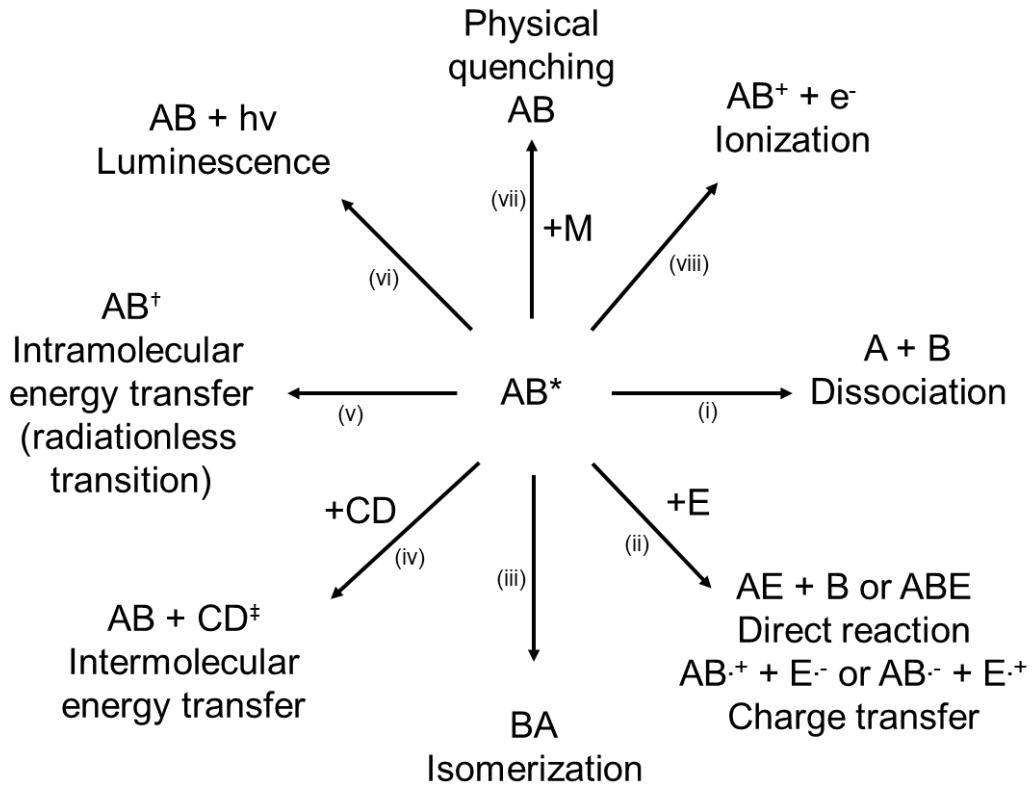

Figure 1.9 Routes to deactivation of an electronically excited species AB. Discussed further below.*

Once a chemical species has absorbed radiation and become electronically excited it will either react to form a new species or relax back to the ground state either by using or losing this excess energy. These processes are summarised above and explained in further detail below (Figure 1.9).

i. Dissociation or photolysis is when the excess energy of the molecular species is sufficient to rupture a bond leading to fragmentation.
ii. The excess energy is sufficient to overcome an activation barrier to an intermolecular reaction with another species (E) or the new electronic arrangement results in a charge transfer. The species may also undergo an intramolecular reaction in which one part of the molecule attacks another.
iii. The excited species can undergo a structural isomerisation or rearrangement, an example of this is the photo-isomerisation of stilbene in which the character of the double bond in excited state stilbene changes, allowing free rotation (Figure 1.10).

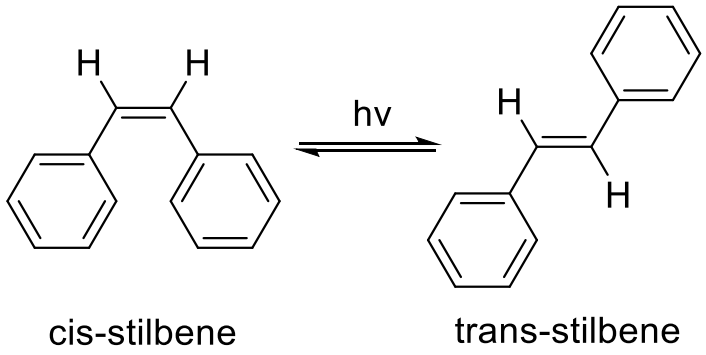

Figure 1.10 The photo-isomerisation of stilbene.[16]

iv. The excited species transfers its energy to another molecule (CD) via an intermolecular collision.
v. Another excited species is formed via an intramolecular pathway that is different to the initial excited species this may then undergo any of the other deactivation pathways (i-viii).
vi. Luminescence is when the excited species emits radiation to lose the excess energy. The term ‘luminescence’ encompasses both fluorescence and phosphorescence. Fluorescence is the radiative loss of energy from a singlet excited state, this is spin-allowed and therefore a faster process, average lifetime; $<10^{-10}$ to 10^{-7} s. Phosphorescence is the radiative loss of

energy in a spin-forbidden process (for example, from a triplet excited state to the singlet ground state), average lifetime in organic molecules 10^{-3} to $>10^{3}$ s. In transition metal complexes, this process is strongly enhanced by the spin-orbit coupling due to the presence of a metal atom, consequently, phosphorescence lifetime in transition metal complexes could be as short as nanoseconds.[11]

vii. Physical quenching or deactivation is a collisional process with a molecule (M) in which the excited species transfers its energy to the molecule resulting in the vibrational or translational excitation of that species.

viii. The excited species can ionise, this is often called photoionisation and is observed in the upper atmosphere in species such as nitric oxide (Equation 1.4).

$$NO + hv \rightarrow NO^{+} + e^{-}$$

Equation 1.4 The photoionisation of nitric oxide.

A useful diagrammatic tool for representing the intramolecular deactivation routes of an excited species (v, vi) is the Jablonski diagram (Figure 1.11).

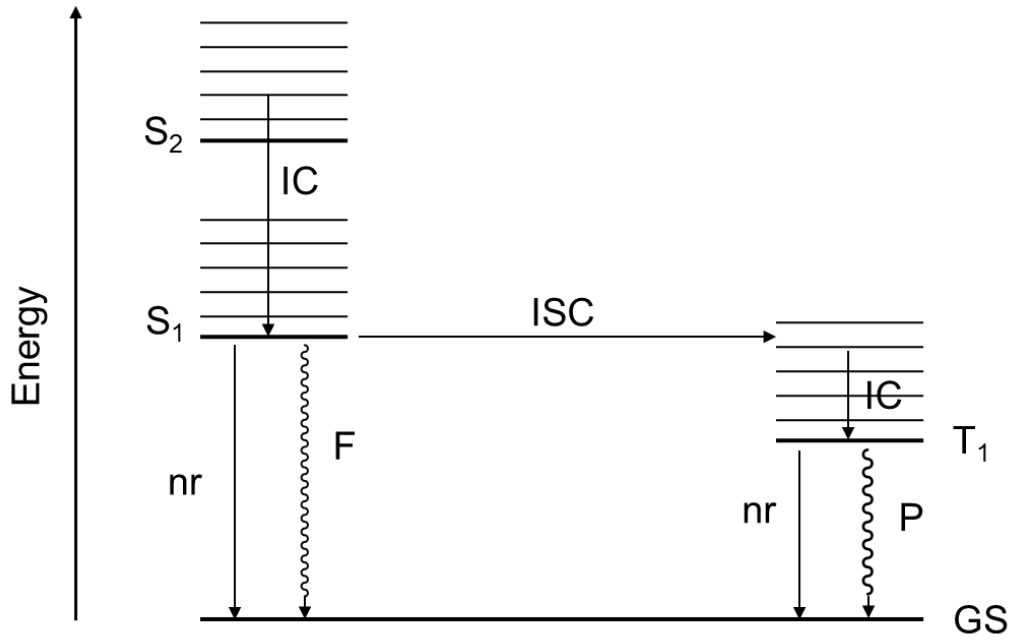

Figure 1.11 A simplified Jablonski diagram showing the various deactivation routes of an excited species. Where; GS = ground state, S = singlet state, T = triplet state, IC = internal conversion, ISC = intersystem crossing, nr = non-radiative decay, F = fluorescence, P = phosphorescence.

1.5 Charge separation

1.5.1 Charge separated states (CSS)

The generation of charge separated states is an important step in natural and artificial photosynthetic systems. In man-made systems it would be desirable to achieve charge separation in a much simpler way. The donor-chromophore-acceptor (D-C-A) model for molecular systems can also be represented as donor-bridge-acceptor (D-B-A) which is perhaps more suitable for many of the complexes discussed and investigated in this study as it does not assume which part of the molecule is behaving as the chromophore (Figure 1.12). Charge separated states within the same molecule are more likely to undergo charge recombination then those in Nature, due to the much closer proximity of the donor end to the acceptor end and the fact that the charge transport is an intramolecular process compared to the multiple intermolecular processes present in nature.[17,18]

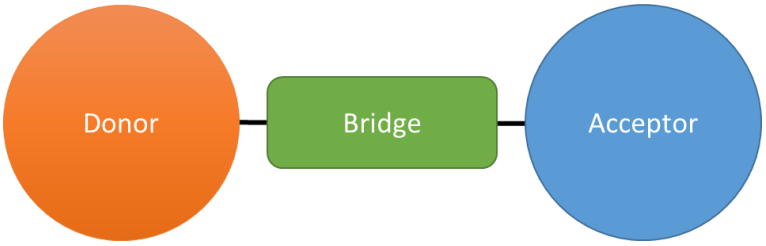

Figure 1.12 The donor-bridge-acceptor (D-B-A) design for molecular systems for photo induced charge transfer.

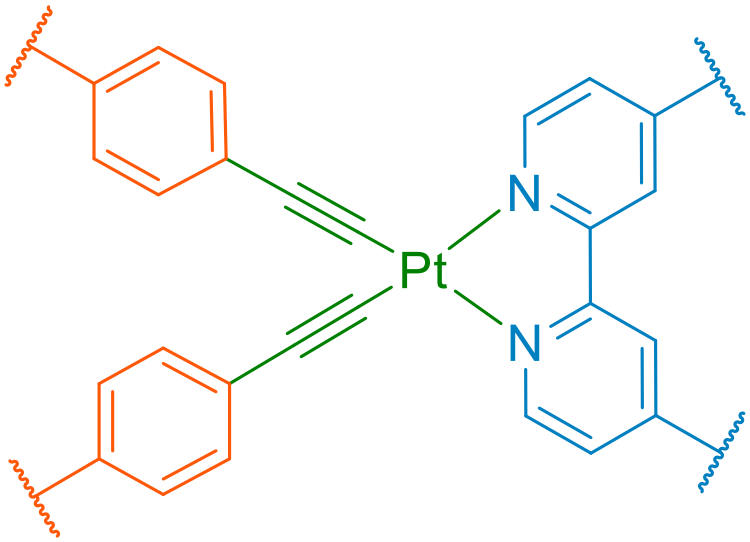

Figure 1.13 An example of a simple D-B-A system is a platinum(II) cis-acetylide complex with an electron accepting ligand (bpy) and electron donors on the other side.

An example of a D-B-A complex is shown above (Figure 1.13), bipyridine (bpy) is a popular electron acceptor as it is cheap and easy to functionalise in a variety of

ways. The use of acetylides on the donor sides is desirable as they as strong infrared reporters and form part of the electron transfer bridge, there are also a wealth of functionalised acetylides available with electron donating groups attached.

1.5.2 Stabilisation of charge separated states

Once a charge separated state is populated, it needs to exist long enough to be utilised, otherwise it will undergo charge recombination and the energy will be wasted. The main approaches to CSS stabilisation are:

i. Extended conjugation

ii. Energy cascade systems

iii. Structural reorganisation of the molecule

1.5.2.1 Extended conjugation

A popular method of CSS stabilisation is to use extended conjugation, which separates the donor and acceptor with a series of conjugated double or triple bonds. This approach has been demonstrated notably by the Wasielewski group with numerous examples. [19–25]

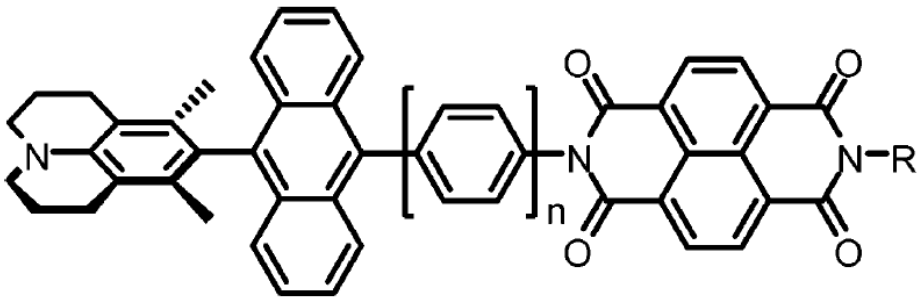

DMJ An Ph NI

1 - 4 (n = 1-4, respectively)

1-3: R = n-C_8H_{17} ; **4**: R = 2,5-di-t-butylphenyl

Figure 1.14 An example of a system in which the lifetime of the charge-separated state was dependent on the length of the conjugation.[21]

In the system above (Figure 1.14) a series of D-B-A systems were investigated where, the donor was a dimethyl-4-(9-anthracenenyl)julolide (DMJ-An) that was bridged by a varying number (n) of phenyl groups to a naphthalene-1,8:4,5-bis(dicarboximide) (NI) acceptor. It was observed that the lifetime of the CSS increased from 6.5 ps when the number of phenyl rings was n=1 to 614 ps for n=4.[21]

1.5.2.2 Energy cascade systems

Energy cascades consist of multiple donors and acceptors covalently linked to one another resulting in a series of electron transfer steps along an energy gradient.

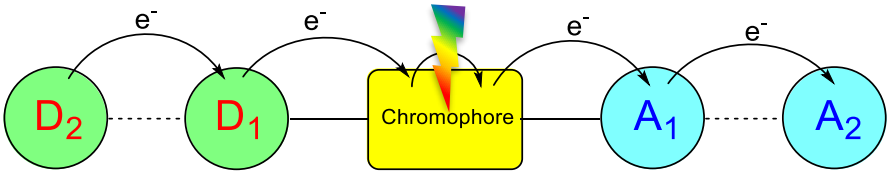

Figure 1.15 Schematic of an extended cascade system.

Electron cascade systems are designed around a central chromophore that can undergo electron transfer to an acceptor upon light absorption. This acceptor (A_1) is connected to a second, more accepting moiety (A_2), and therefore the electron is transferred again. Likewise the donor (D_1) provides the electron to the chromophore and itself is provided an electron from a more donating moiety (D_2) (Figure 1.15). The result is charge separation through space, slowing the rate or charge recombination.

1.5.2.3 Structural reorganisation of the molecule

Upon light absorption systems may undergo structural rearrangement. This can involve the formation of a new bond/bonds that must be broken to return to the ground state or bonds that lead to isomerisation of the excited state species thus inhibiting charge recombination.

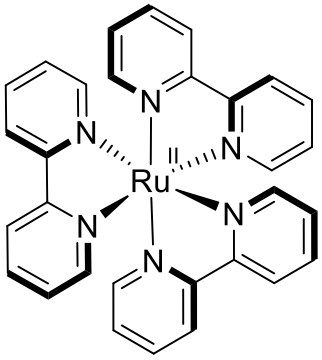

Figure 1.16 The structure of $[Ru(bpy)_3]^{2+}$

An example of this are the modifications made by Hammarstrom *et al.* to the $[Ru(bpy)_3]^{2+}$ complex (Figure 1.16).[26–32] $[Ru(bpy)_3]^{2+}$ is one of the most studied metal complexes due to its chemical stability, excited state reactivity, luminescence emission, excited state lifetime and redox properties.[33]

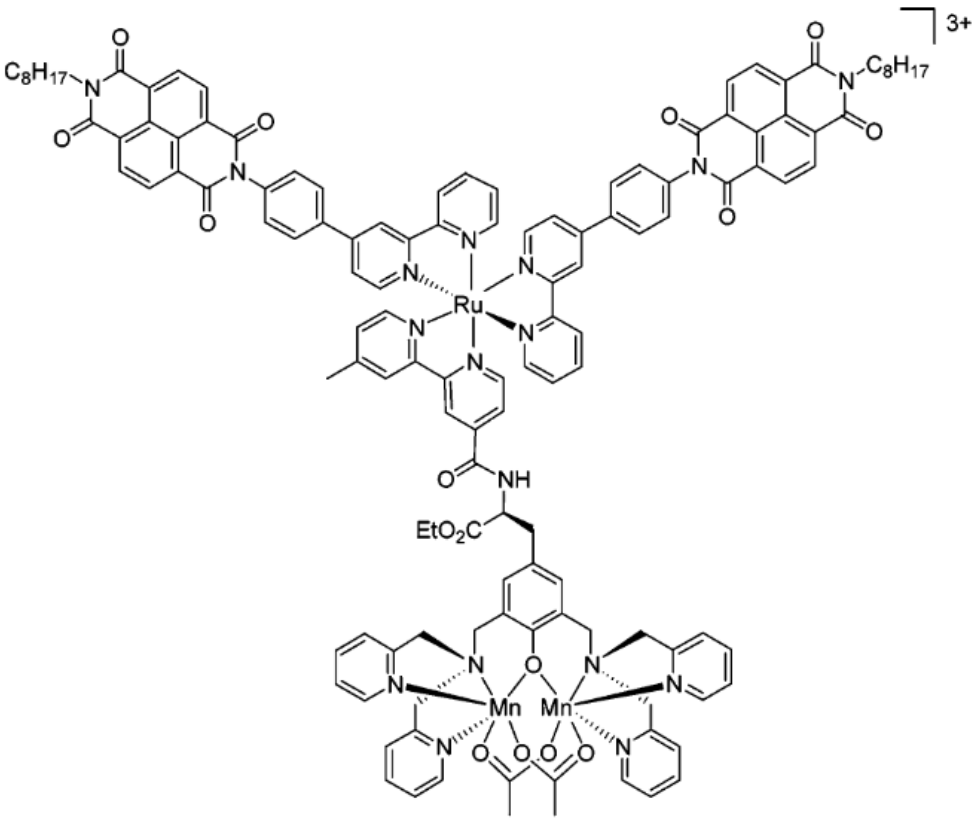

Figure 1.17. The $Ru(bpy)_3$-Mn triad complex reported by Hammarstrom et al.

By linking a manganese complex to a $Ru(bpy)_3$ chromophore the complex was provided with a means of intramolecular electron transfer (Figure 1.17). Upon light absorption Ru(III) is generated which is returned to Ru(II) through electron donation from the Mn(II) complex. A structural rearrangement of the Mn-ligand bonds. is thought to occur upon oxidation of Mn(II) to Mn(III).[27]

1.6 Studying the ground state: steady state spectroscopy

1.6.1 Ultraviolet-Visible Spectroscopy (UV-Vis) and Electronic Absorption Spectroscopy (EAS)

The absorption of light by molecules is integral to understanding the photophysics of that species excited state. For the types of complexes studied in this work the MLCT transition gives rise to a strong absorption band in the visible region of the electromagnetic spectrum. The linear relationship between absorbance and concentration of an absorbing species is given by the Beer-Lambert law (Equation 1.5).

$$A = \varepsilon c l$$

Equation 1.5 The Beer-Lambert law where; A=Absorbance, ε=extinction coefficient, c=concentration, l=path length

The extinction coefficient of a species is indicates the ability of that species to absorb light at a given wavelength. The shape and position of the electronic absorptions in a spectrum gives information on the electronic transitions in the molecule.

The UV-Vis spectrometer is typically set up as shown below, where the monochromatic beam is split and passes through the sample and an internal reference before being processed (Figure 1.18).[34] The measurements are usually made on solutions although measurements on gases and solids are possible.

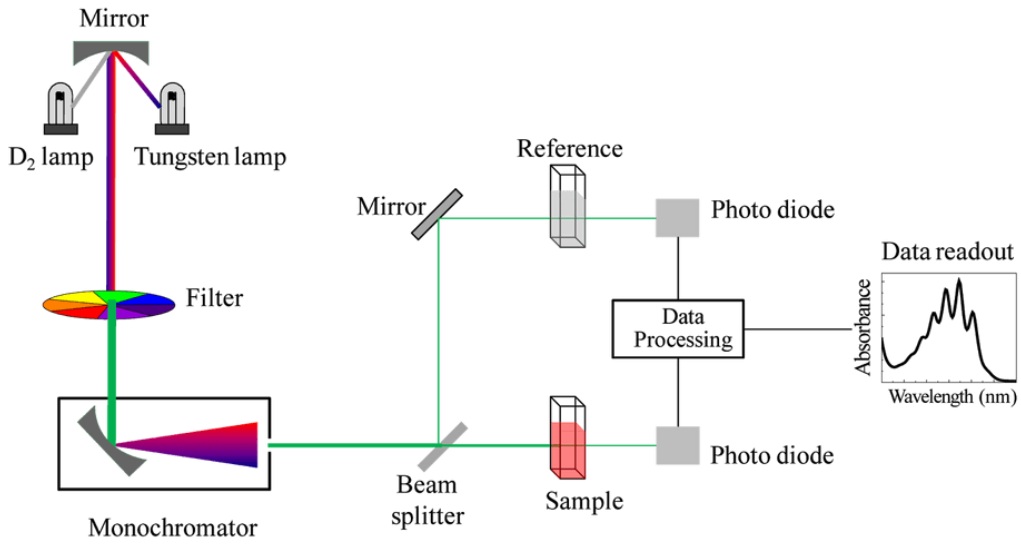

Figure 1.18 A UV-Vis spectrometer layout.[34]

1.6.2 Fourier Transform Infrared Spectroscopy (FTIR)

Infrared radiation is absorbed by chemical bonds in molecules and from this we can determine what bonds are present in that species. Fourier transform infrared spectroscopy is the preferred method of infrared spectroscopy. A typical set-up is shown below (Figure 1.19).

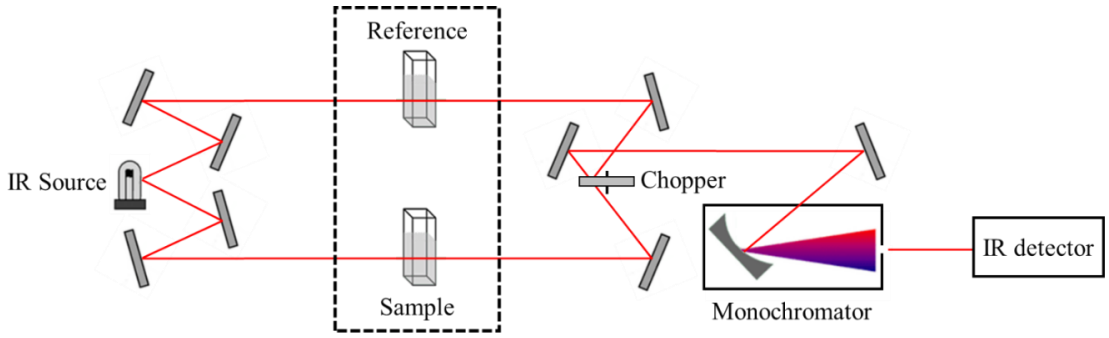

Figure 1.19 An FTIR spectrometer layout. Adapted from Aavos int.[34]

FTIR spectrometers work by passing two beams from the same IR source through the sample and a reference chamber independently. These beams are alternately focussed on the detector via the use of an optical chopper. After the beam passes through the sample, the emitted radiation is dispersed by a monochromator into its component frequencies onto the detector. The detector converts the analogue spectral output into electrical signal which are processed using algorithms to produce the final spectrum.

1.7 Studying the Excited State: Pump Probe Spectroscopy

1.7.1 Time-Resolved Infrared (TRIR) / Transient Vibrational Absorption Spectroscopy (TVAS)

TRIR spectroscopy is used to examine the vibrational properties of a molecules excited state. Firstly an ultra-violet laser is used to create an electronically excited state of the compound in the sample. Secondly broadband infrared laser probes the sample recording any differences in optical density that may arise. The infrared beam is split into two so that one path can act as a reference that allows for any small variations that may occur in the beam energy from shot to shot. The spectra are recorded over different time delays which can be varied with picosecond resolution on an optical delay line. The samples contained within a Harrick cell that is rastered in two dimensions whilst the solution is flowed through it via a peristaltic pump to minimise the affect of repeated irradiating of the same part of the sample.

1.8 References

1 *United Nations Popul. Div. Dep. Econ. Soc. Aff.*

2 International Energy Agency, .

3 British Petroleum, *BP Stat. Rev. World Energy*.

4 N. S. Lewis, Powering the Planet, http://nsl.caltech.edu/energy.

5 R. Perez and M. Perez, *IEA SHC Sol. Updat.*, 2009, **50**, 2–3.

6 S. Chu and A. Majumdar, *Nature*, 2012, **488**, 294–303.

7 EIA, *U.S. Energy Inf. Adm.*, 2017, **IEO2017**, 143.

8 K. Emery, Reference Solar Spectral Irradiance: Air Mass 1.5, http://rredc.nrel.gov/solar/spectra/am1.5/, (accessed 19 July 2017).

9 I. McConnell, G. Li and G. W. Brudvig, *Chem. Biol.*, 2010, **17**, 434–447.

10 P. Atkins and J. De Paula, *Physical Chemistry*, Oxford university press, Oxford, 8th edn., 2006.

11 S. Archer and J. A. Weinstein, *Coord. Chem. Rev.*, 2012, **256**, 2530–2561.

12 R. Eisenberg, *Science (80-.).*, 2009, **324**, 44–45.

13 A. Vlček, *Coord. Chem. Rev.*, 2000, **200**–**202**, 933–977.

14 E. T. H. A. Jahn, *Proc. R. Soc. London. Ser. A, Contain. Pap. a Math. Phys. Character*, 1937, **161**, 220–235.

15 S. C. Marker, S. N. MacMillan, W. R. Zipfel, Z. Li, P. C. Ford and J. J. Wilson, *Inorg. Chem.*, 2018, **57**, 1311–1331.

16 F. Bejarano, I. Alcon, N. Crivillers, M. Mas-Torrent, S. T. Bromley, J. Veciana and C. Rovira, *RSC Adv.*, 2017, **7**, 15278–15283.

17 M. Đokić and H. Sen Soo, *Chem. Commun.*, , DOI:10.1039/C8CC02156B.

18 M. M. Najafpour and B. Pashaei, *Adv. Photosynth. – Fundam. Asp.*, 2006, 3–13.

19 T. M. Wilson, M. J. Tauber and M. R. Wasielewski, *J. Am. Chem. Soc.*, 2009, **131**, 8952–8957.

20 E. M. Giacobbe, Q. Mi, M. T. Colvin, B. Cohen, C. Ramanan, A. M. Scott, S. Yeganeh, T. J. Marks, M. A. Ratner and M. R. Wasielewski, *J. Am. Chem. Soc.*, 2009, **131**, 3700–3712.

21 Z. E. X. Dance, M. J. Ahrens, A. M. Vega, A. B. Ricks, D. W. McCamant, M. A. Ratner and M. R. Wasielewski, *J. Am. Chem. Soc.*, 2008, **130**, 830–832.

22 M. R. Wasielewski, *J. Org. Chem.*, 2006, **71**, 5051–5066.

23 E. A. Margulies, J. L. Logsdon, C. E. Miller, L. Ma, E. Simonoff, R. M. Young, G. C. Schatz and M. R. Wasielewski, *J. Am. Chem. Soc.*, 2017, **139**, 663–671.

24 S. A. Odom, R. F. Kelley, S. Ohira, T. R. Ensley, C. Huang, L. A. Padilha, S. Webster, V. Coropceanu, S. Barlow, D. J. Hagan, E. W. Van Stryland, J. L. Brédas, H. L. Anderson, M. R. Wasielewski and S. R. Marder, *J. Phys. Chem. A*, 2009, **113**, 10826–10832.

25 Z. An, S. A. Odom, R. F. Kelley, C. Huang, X. Zhang, S. Barlow, L. A. Padilha, J. Fu, S. Webster, D. J. Hagan, E. W. Van Stryland, M. R. Wasielewski and S. R. Marder, *J. Phys. Chem. A*, 2009, **113**, 5585–5593.

26 M. Borgström, N. Shaikh, O. Johansson, M. F. Anderlund, S. Styring, B. Åkermark, A. Magnuson and L. Hammarström, *J. Am. Chem. Soc.*, 2005, **127**, 17504–17515.

27 M. Falkenström, O. Johansson and L. Hammarström, *Inorganica Chim. Acta*, 2007, **360**, 741–750.

28 L. Sun, L. Hammarström, B. Åkermark and S. Styring, *Chem. Soc. Rev.*, 2001, **30**, 36–49.

29 M. L. A. Abrahamsson, H. Berglund Baudin, A. Tran, C. Philouze, K. E. Berg, M. K. Raymond-Johansson, L. Sun, B. Åkermark, S. Styring and L. Hammarström, *Inorg. Chem.*, 2002, **41**, 1534–1544.

30 H. Berglund-Baudin, L. Sun, R. Davidov, M. Sundahl, S. Styring, B. Åkermark, M. Almgren and L. Hammarström, *J. Phys. Chem. A*, 1998, **102**, 2512–2518.

31 L. Sun, L. Hammarström, T. Norrby, H. Berglund, R. Davydov, M. Andersson, A. Börje, P. Korall, C. Philouze, M. Almgren, S. Styring and B. Åkermark, *Chem. Commun.*, 1997, 607–608.

32 K. E. Berg, A. Tran, M. K. Raymond, M. Abrahamsson, J. Wolny, S. Redon, M. Andersson, L. Sun, S. Styring, L. Hammarström, H. Toftlund and B. Åkermark, *Eur. J. Inorg. Chem.*, 2001, 1019–1029.

33 A. Juris, V. Balzani, F. Barigelletti, S. Campagna, P. Belser and A. von Zelewsky, *Coord. Chem. Rev.*, 1988, **84**, 85–277.

34 UV – Vis spectroscopy, https://aavos.eu/glossary/uv-vis-spectrometry/.

Research Objectives

The overall aim of this work is to explore different ways of controlling and manipulating excited states in transition metal complexes with the end application in “solar fuels”. This will be achieved in the following ways:

1. Synthesis and characterisation of octahedral rhenium(I) tricarbonyl complexes with novel accepting ligands and an investigation into whether they are suitable catalysts for the reduction of CO_2 to CO via photochemical and electrochemical means. The development of strongly electron accepting diimine ligands based on the bis-aryl-amino-acenaphthene/ phenantherene unit in order to tune the energy of the LUMO (and hence the reduction potential and the ability to reduce CO_2).
2. Exploring structural reorganization in the excited state as a means to control charge recombination. Specifically, this approach has been developed in a series of platinum(II) diimine dithiolate complexes and their diphenolate analogues. Isotopic substitution has also been explored to understand excited state dynamics.
3. To develop better understanding of “vibrational control” of electron transfer – whereby intermediate perturbation of the excited state by a transient IR pulse can affect excited state reactivity – by preparing a series of isotopically substituted model compounds, Donor-(CC)-Pt-(CC)-acceptor.

2 Experimental Methods

2.1 Materials and General Procedures

Commercially available starting materials were obtained from Sigma-Aldrich, Alfa-Aesar, Acros Organics, Manchester Organics, Fluorochem, Apollo Scientific and were used without further purification unless otherwise stated. All solvents (Fisher Scientific, Sigma-Aldrich, VWR) were HPLC grade and used without further purification unless otherwise stated. Dry solvents were obtained from the University of Sheffield Grubbs purification system and stored under a nitrogen atmosphere. Solvent deaeration was performed by sparging with argon for a period of at least 20 min. Column chromatography was performed using either silica gel (60 Å mesh, Fluorochem) or aluminium oxide (Brockmann III grade, Acros). Unless otherwise state, all syntheses were carried out under an atmosphere of argon using Schlenk line techniques.

2.2 Instrumentation and Analysis

2.2.1 NMR Spectroscopy

One dimensional ^{1}H, ^{13}C NMR spectra were recorded at either 400 MHz or 250 MHz on Bruker Avance 400, Bruker Avance II 400 HD, Bruker DPX-400 and Bruker Avance 250 Spectrometer; unless otherwise stated, in which the 250 MHz spectra were recorded on a Bruker Avance 250 spectrometer. ^{31}P NMR spectra were either recorded on a 250 MHz Bruker Avance 250 or 400 MHz Bruker DPX-400 spectrometer, with carrier frequencies for phosphorous nuclei of 101.1 MHz and 161.9 MHz respectively. Spectra were recorded for the compounds in spectroscopic grade deuterated solvents and the ^{1}H spectra calibrated against the residual solvent peak as published by Fulmer *et. al.*[1]

2.2.2 Mass Spectrometry

All experiments were performed by the University of Sheffield mass spectrometry service. Positive electrospray (ES+) mass spectra were recorded on a Waters LCT time of flight (TOF) mass analyzer. Electroionisation (EI) spectra were recorded

using a VG AutoSpec magnetic sector instrument. Solid state mass spectra were recorded using an atmospheric solids analysis probe (ASAP). Matrix assisted laser desorption ionisation (MALDI) mass spectra were recorded on a Bruker Reflex III instrument equipped with a TOF mass analyser utilising a DCTB (*trans*-2-[3-(4-*tert*-butylphenyl)-methyl-2-propenylidene] malononitrile) matrix.

2.2.3 UV-Vis Spectroscopy

UV/vis spectra were recorded on a Cary 50 Bio. A quartz cuvette with 1 cm pathlength was used to take the spectra of samples in solution.

2.2.4 FTIR Spectroscopy

Infra-red spectra were recorded in solution or the solid state. Solution phase infra-red spectra were recorded on a Perkin Elmer Spectrum One FTIR instrument using an MCT detector at 4 cm-1 resolution in demountable solution cells with sodium chloride windows.

2.2.5 Cyclic Voltammetry

Cyclic voltammetry was performed on a solution of sample complex (2 mM) in acetonitrile with TBAPF (0.2 M) as the electrolyte. A Princeton Applied Research VersaSTAT 3 potentiostat was used to control the potential. The working electrode was glassy carbon (0.07 cm^2), the counter electrode was platinum wire and the reference electrode was Ag/AgCl (0.1 M). Values of potential are quoted against Fc/Fc^+. Initial scans were measured using a scan rate of 100 mV s^{-1} and reversibility was assessed using scan rates of 20 – 200 mV s^{-1}. A solvent saturated atmosphere of nitrogen was used to degas the sample and all scans were recorded under and inert atmosphere of nitrogen. To test for current enhancement the samples were thoroughly bubbled with CO_2 and their voltammograms recorded. A Bronsted acid (water, 0.3 ml) was then added and the voltammograms rerecorded.

2.2.6 Single Crystal X-Ray Diffraction

Single crystals of **3.7**, **3.8**, and **3.9** suitable for structure determination were selected and collected by Mr Harry Adams (X-ray Technician, Department of Chemistry, University of Sheffield) from samples extracted from the mother liquor,

suspended in perfluoropolyether oil (FOMBLIN Y) and mounted onto a mylar tip. Data were collected on a Smart APEX-2 CCD diffractometer equipped with a graphite-monochromator Mo-Kα sealed-tube source. Sample temperature was maintained using an Oxford Cryosystems Cryostream device. Data were corrected for absorption using empirical methods (SADABS) based on symmetry-equivalent reflections and measurements at different azimuthal angles.[2–4] Structure solution was achieved by direct methods and the crystal structure was refined using full-matrix least-squares against weighted F2 values using SHELXL4 within a SHELX suite.[5] Non-hydrogen were refined anisotropically. Hydrogen atoms were placed in calculated positions, refined to idealized geometries (riding model) and assigned a fixed isotropic displacement parameter.

2.2.7 Time-Resolved Infrared Spectroscopy

Experiments were conducted at the Ultrafast Spectroscopy Laboratory, Rutherford Appleton Laboratory (RAL), Science and Technology Facilities Council (STFC), UK, ULTRA facility.[6] A 65 MHz, 40 fs titanium sapphire laser operating with a repetition rate of 10 kHz was used to pump a series of optical parametric amplifiers (OPA's). The pump beam (400 nm) is generated from the second harmonic of the titanium sapphire laser, whilst another portion of the initial laser beam is used to generate tuneable mid-IR probe light with a 400 cm^{-1} bandwidth. The pump energy is typically 1 – 1.5 μJ per pulse. Changes in IR absorbance were determined via three HgCdTe linear IR-array detectors. Experiments were performed on solutions contained within Harrick cells with 2mm thick CaF_2 windows with 500 to 1000 μm sample pathlength and a typical optical density of between 0.5 and 1 at 400 nm

2.3 Computational methods

All optimisation, frequency and excited state calculations were carried out by Heather Carson at the University of Sheffield, using the Gaussian 09 software package, revision D.01.[7] The solvent, dichloromethane was simulated using the integral equation formalism polarisable continuum model (IEFPCM).[8–10] All calculations utilized the PBE0 functional.[11] The Karlsruhe basis set, def2-SVP, was employed for all atoms except Pt, for which the Dirac-Hartree-Fock basis set, dhf-

SVP, was used instead.[12,13] The absence of imaginary frequencies confirmed that energy minima had been found, within the harmonic approximation. For all calculations, ultrafine integrals were used and no symmetry constraints were applied. For all excited state calculations the first 20 excited states were calculated. All samples were mounted to a 2D-raster stage and solutions were flowed using a peristaltic pump to ensure photostability

2.4 References

1 G. R. Fulmer, A. J. M. Miller, N. H. Sherden, H. E. Gottlieb, A. Nudelman, B. M. Stoltz, J. E. Bercaw and K. I. Goldberg, *Organometallics*, 2010, **29**, 2176–2179.

2 G. M. Sheldrick, *SADABS, Empirical Absorption Correct program*, 1995.

3 L. Krause, R. Herbst-Irmer, G. M. Sheldrick and D. Stalke, *J. Appl. Crystallogr.*, 2015, **48**, 3–10.

4 R. H. Blessing, *Acta Crystallogr. Sect. A*, 1995, **51**, 33–38.

5 G. M. Sheldrick, *Acta Crystallogr. Sect. C Struct. Chem.*, 2015, **71**, 3–8.

6 P. A. Scattergood, M. Delor, I. V Sazanovich, O. V Bouganov, S. A. Tikhomirov, A. S. Stasheuski, A. W. Parker, G. M. Greetham, M. Towrie, E. S. Davies, A. J. H. M. Meijer and J. A. Weinstein, *Dalt. Trans.*, 2014, **43**, 17677–17693.

7 M. J. Frisch, G. W. Trucks, H. B. Schlegel, G. E. Scuseria, M. A. Robb, G. Cheeseman, J. R. Scalmani, V. Barone, B. Mennucci, G. A. Petersson, H. Nakatsuji, M. Caricato, X. Li, H. P. Hratchian, A. F. Izmaylov, J. Bloino, G. Zheng, J. L. Sonnenberg, M. Hada, M. Ehara, K. Toyota, R. Fukuda, J. Hasegawa, M. Ishida, T. Nakajima, Y. Honda, O. Kitao, H. Nakai, T. Vreven, J. Montgomery, J. A., J. E. Peralta, F. Ogliaro, M. Bearpark, J. J. Heyd, E. Brothers, K. N. Kudin, R. Staroverov, V. N. Kobayashi, J. Normand, K. Raghavachari, A. Rendell, J. C. Burant, S. S. Iyengar, J. Tomasi, M. Cossi, N. Rega, N. J. Millam, M. Klene, J. E. Knox, J. B. Cross, V. Bakken, C. Adamo, J. Jaramillo, R. Gomperts, R. E. Stratmann, O. Yazyev, A. J. Austin, R. Cammi, C. Pomelli, J. W. Ochterski, R. L. Martin, K. Morokuma, V. G. Zakrzewski, G. A. Voth, P. Salvador, J. J. Dannenberg, S. Dapprich, A. D. Daniels, Ö. Farkas, J. B. Foresman, J. V. Ortiz and J. Cioslowski, 2010.

8 S. Miertus, E. Scrocco and J. Tomasi, *Chem. Phys.*, 1981, **55**, 117–129.

9 S. Miertuš and J. Tomasi, *Chem. Phys.*, 1982, **65**, 239–245.

10 J. L. Pascual-Ahuir, E. Silla and I. Tunon, *J. Comput. Chem.*, 1994, **15**, 1127–1138.

11 C. Adamo and V. Barone, *J. Chem. Phys.*, 1999, **110**, 6158–6170.

12 F. Weigend and R. Ahlrichs, *Phys. Chem. Chem. Phys.*, 2005, **7**, 3297.

13 D. Andrae, U. H, M. Dolg, H. Stoll and H. Preub, *Theor. Chim. Acta*, 1990, **77**, 123–141.

3. Rhenium (I) tricarbonyl α-diimmine complexes for the reduction of CO_2

3.1 Introduction

3.1.1 Carbon fixation by the reduction of CO_2

Carbon fixation is the process by which organisms convert namely CO_2, into organic compounds. Photosynthesis is the archetypal process by which carbon fixation occurs, as discussed in Chapter 1. CO_2 fixation via photosynthesis typically results in complex organic molecules such as sugars that would be challenging to achieve in a simple catalytic system. When designing systems for CO_2 fixation, simpler chemical processes are considered that require lesser energy input (Equations 1-6).

$$CO_2 + 2H^+ + 2e^- \rightarrow CO + H_2O \quad \mathbf{E^0 = -0.53\ V}\ (\boldsymbol{Eq.1})$$

$$CO_2 + 2H^+ + 2e^- \rightarrow HCO_2H \quad \mathbf{E^0 = -0.61\ V}\ (\boldsymbol{Eq.2})$$

$$CO_2 + 4H^+ + 4e^- \rightarrow HCHO + H_2O \quad \mathbf{E^0 = -0.48\ V}\ (\boldsymbol{Eq.3})$$

$$CO_2 + 6H^+ + 6e^- \rightarrow CH_3OH + H_2O \quad \mathbf{E^0 = -0.38\ V}\ (\boldsymbol{Eq.4})$$

$$CO_2 + 8H^+ + 8e^- \rightarrow CH_4 + 2H_2O \quad \mathbf{E^0 = -0.24\ V}\ (\boldsymbol{Eq.5})$$

$$CO_2 + e^- \rightarrow CO_2^- \quad \mathbf{E^0 = -1.90\ V}\ (\boldsymbol{Eq.6})$$

Equations 1-6 The reduction potentials for various reactions of CO_2, recorded at pH7 in aqueous solution versus NHE, 25 °C, 1 atm gas pressure and 1 M for the other solutes.

The one-electron reduction of CO_2 requires a large voltage and only yields the thermodynamically unstable CO_2^-. Consequently, a reduction catalyst is required to act as an electron transfer agent in the (often proton-coupled) multi-electron processes. Some of the reduction products of CO_2, for example methanol, look promising as liquid fuels to be used in existing systems, however production of liquid fuels is kinetically challenging and is therefore often catalysed using solid state catalysts.[1,2] CO_2 reduction to CO is an appealing way of CO_2 reduction as it requires only a relatively small voltage and produces a gaseous product that is easy to separate from the reaction mixture. CO is a technologically important chemical: it is a component of syngas which is used as a feedstock for the Fischer-Tropsch process for the production of useful liquid hydrocarbons;[3] CO can also be converted to hydrogen gas via the water-gas shift reaction, this is becoming

increasing more useful as more systems are developed around hydrogen gas as a source of fuel (Equation 7).

$$CO + H_2O \rightleftharpoons CO_2 + H_2$$

Equation 7 The water-gas shift reaction.

In this chapter, a family of rhenium-based carbonyl complexes of the general structure *fac*-[Re(NN)$(CO)_3$X], where NN is an α-diimmine ligand and X is a halide or pseudohalide ligand, will be discussed for the purpose of catalysing the reduction of CO_2 to CO, and their properties investigated. Complexes of this type are always the facial isomer unless otherwise stated.

3.1.2 Early work on rhenium tricarbonyls

The first published example of a complex in the form [Re(NN)$(CO)_3$X] is [Re(bpy)$(CO)_3$I], published in a 1959 paper from Abel and Wilkinson.[4] Their research focussed on the synthesis and reactivity of rhenium and manganese carbonyls and comparative analysis of their FTIR spectra. This initial discovery was followed by many papers published on these types of compounds, that further explored the reactivity, synthesis and vibrational spectra of rhenium and manganese carbonyls with the main focus on their ligand substitution reactions.[5–10]

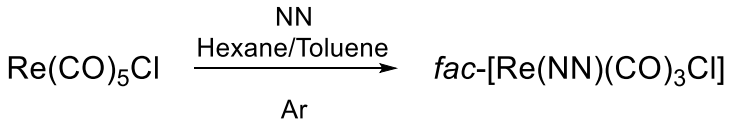

Scheme 3.1 The general method of synthesising complexes of the type [Re(NN)$(CO)_3$X].

This early research demonstrates some of the advantages of such complexes: they are easy to synthesise and always yield the facial isomer due to the presence of the axial carbonyl ligand in trans position to a halide which is bound stronger than the other carbonyls (Scheme 3.1).[7] This synthetic feature results in a symmetry change from C_{4V} of the Re$(CO)_5$X starting material to C_S in the product [Re(NN)$(CO)_3$X] which is easily observed in the FTIR spectrum. FTIR spectroscopy is a useful tool for characterising transition metal carbonyls due the presence of π back-bonding (Figure 3.1). For example in the complex [Re(NN)$(CO)_3$X] changing "X" for a more electron donating halide or pseudohalide ligand will result in more electron density around the rhenium metal centre which can then take part in π back-donation to the antibonding orbital of the carbonyl ligand, which in turn

strengthens the Re-CO bond and weakens the carbon oxygen triple bond, resulting in lower energy v(CO) observed in the infrared spectrum.

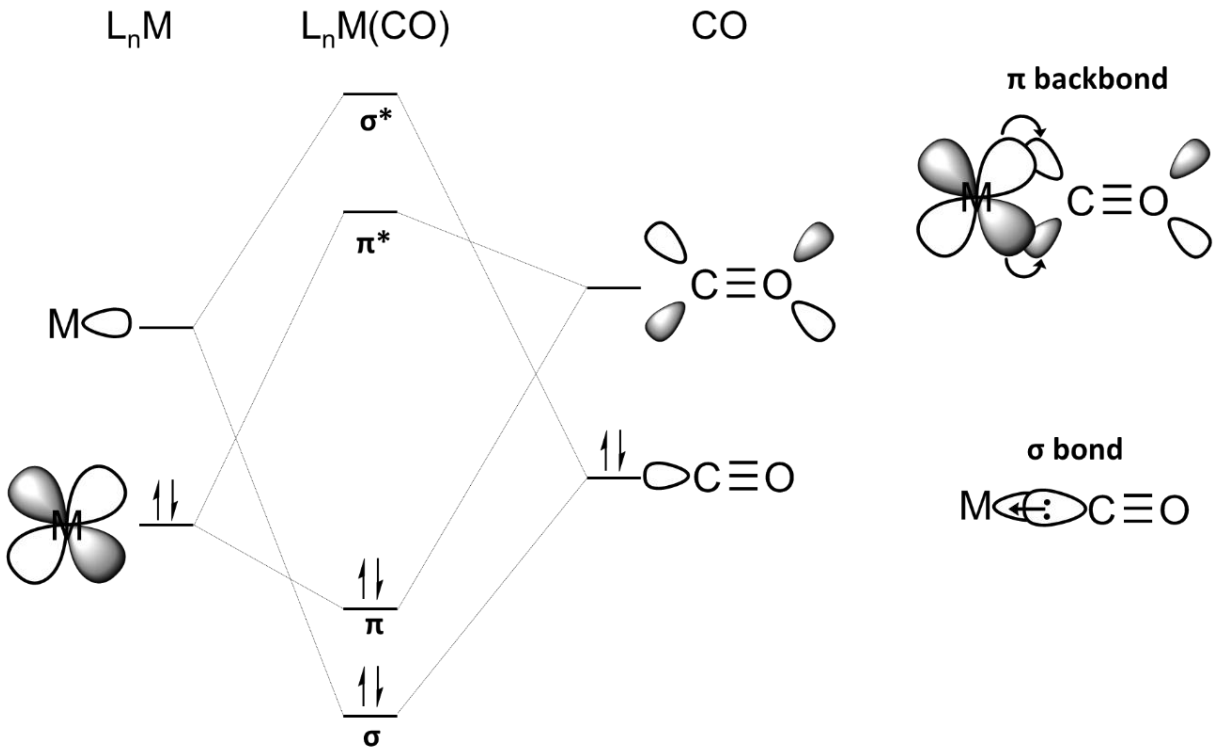

Figure 3.1 A diagram to show how transition metals bond to carbonyl ligands via synergic π back-bonding.

In 1974 Mark S. Wrighton at Massachusetts Institute of Technology published a paper on the lowest excited state of $[Re(phen)(CO)_3Cl]$ and related complexes.[11] This was the first report on metal carbonyls that exhibited luminescence in solution at room temperature, luminescence lifetime reported was relatively long, of ~30 ns.[11] After this discovery, the research on Re(I) complexes focused on their photochemistry and excited state dynamics, with the majority of the studies during this period published by Wrighton and coworkers.[12–19] However, it was Jean-Marie Lehn and co-workers in Strasbourg that first realised the catalytic potential of $[Re(NN)(CO)_3X]$ complexes to reduce CO_2 to CO, in 1982.[20]

3.1.3 Rhenium tricarbonyl based CO_2 reduction catalysts

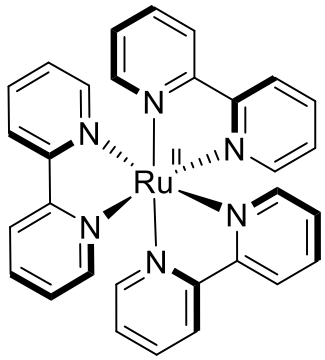

Figure 3.2 The structure of [Ru(2,2'-bipyridine)$_3$]$^{2+}$.

Ziessel and Lehn originally observed the simultaneous generation of H_2 and CO via the visible light irradiation of $[Ru(bpy)_3]^{2+}$ in solutions of $CoCl_2$ and CO_2 in acetonitrile/water/trimethylamine mixture.[21] After the increase in publications focussing on the interesting photophysical properties of $[Re(NN)(CO)_3X]$, Lehn and Ziessel investigated the use of the complexes in the same set-up as described for the ruthenium catalyst (Figure 3.3). Their results showed selective catalytic reduction of CO_2 to CO with turn over numbers (TON) of up to 11 for 1-hour illumination in the presence of tetraethylammonium chloride, without the formation of dihydrogen or formate (side products observed whilst using ruthenium catalyst).[20] This was the first published work on the photocatalytic activity of this family of Re(I) complexes, which since then are referred to as "Lehn-type catalysts".

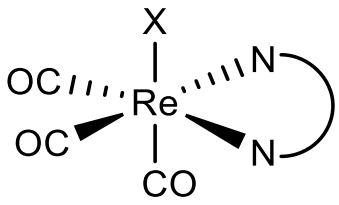

NN = polypyridyl ligand, X = Halide

Figure 3.3 The general structure of the complexes of the type [Re(NN)(CO)$_3$X].

3.1.4 The suitability of rhenium tricarbonyls as CO_2 reduction catalysts

Since the initial discovery in 1982 of the application of Lehn-type catalysts to the reduction of CO_2, there has been a huge increase in research into their implementation.[22] It seems likely that such interest was partially fuelled by the suitability of these complexes for the study of CO_2 reduction over other catalysts

(such as the ruthenium system). For example, the presence of the facial arranged rhenium(I) tricarbonyl moiety gives rise to three strong IR active vibrational modes (A'(1) + A'(2) + A'') which provides an easy method of characterisation of the catalytic processes using FTIR spectroscopy in both the ground and excited state (Figure 3.4).

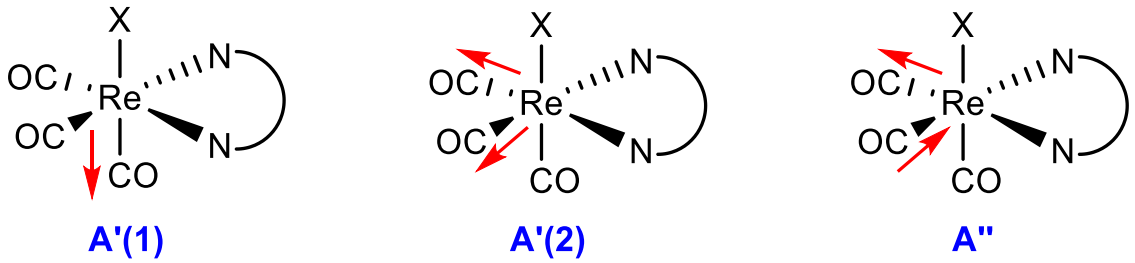

Figure 3.4 The three carbonyl stretching frequencies of [Re(NN)(CO)$_3$X] assuming they are C_S point group.

The rhenium(I) tricarbonyl complexes exhibit interesting excited state properties: they have a low energy excited state that is of mixed MLCT/ intraligand $^3\pi$–π^* character.[23] Their excited states are long lived (hundreds of nanoseconds) and strongly phosphorescent due to strong spin-orbit coupling resulting in enhanced singlet-triplet mixing.[22] The combination of low lying MLCT transitions, long lived excited states, strong phosphorescence and intense stretching vibrations makes these complexes optimal candidates to study the vibrational and electronic structure using steady state and time resolved techniques. The complexes also exhibit a high degree of photostability, they show no signs of degradation in (relatively) high power laser experiments which allows them to be studied using two-dimensional pump-probe experiments to elucidate the structure of the excited state.[24]

There are a broad range of synthetic modifications that can be made to the NN polypiridyl, or α-diimmine, ligand such as the extension of the planar aromatic system to the incorporation of electron donating or withdrawing substituents to the aromatic rings.[11,13,25–27] The variation of the ligand and/or counterion changes the electronic and vibrational properties of the complexes (Table 3.1).

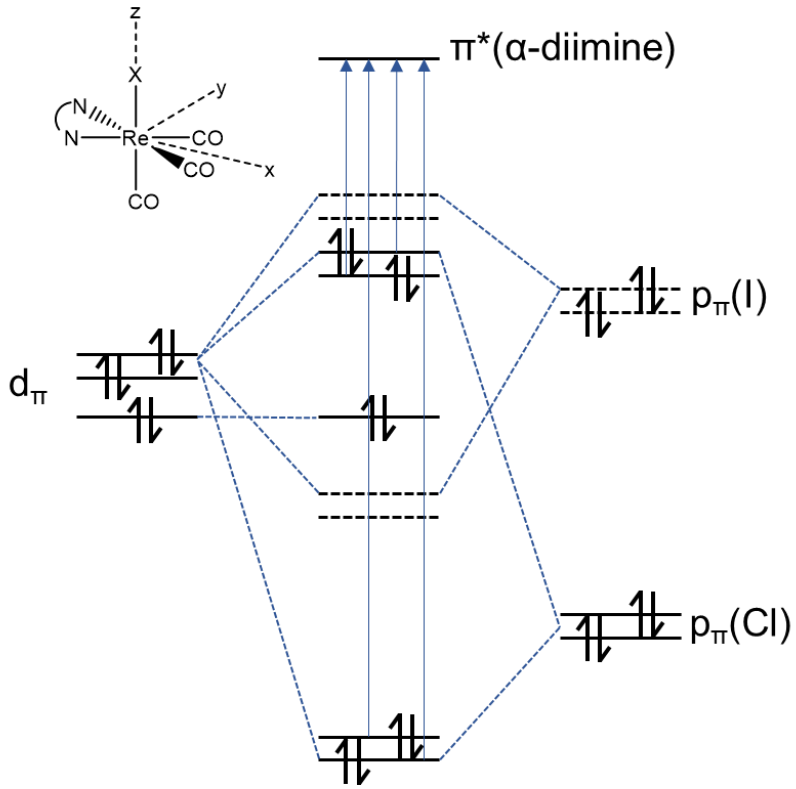

Figure 3.5 Qualitative MO scheme for [Re(NN)(CO)$_3$X]). Solid lines are the orbital diagram where X=Cl and the dashed lines are for X=I.[28]

Altering the halide ligand on the [Re(NN)(CO)$_3$X] complexes alters both the electronic and vibrational properties. This is because the Re(d_π) orbitals, d_{xz} and d_{yz} , interact with the X(p_π), p_x and p_y , orbitals of the halide ligand which results in π-bonding and anti-bonding combinations , the d_{xz} orbital on the Re centre does not interact with the halide p orbitals and is not involved in the bond. The molecular orbital diagram above (Figure 3.5) compares the bonding situation for X=Cl vs X=I: changing from Cl to I leads to an increase in the energy of the p_π orbitals in absolute terms, but also relative to the Re(d_π) orbitals, this means that the lower-lying metal-halide π-bonding orbitals are more metal in character whilst the π-antibonding orbital, the HOMO of the complex, is more halide in character in the I-complex vs. the Cl-complex. This change in character going from Cl to I means that the lowest energy transitions in the molecules will be more XLCT (X=I) than MLCT (X=Cl) and therefore are much less intense due to the smaller overlap with the π*(R-diimmine) orbital for the pπ(X) orbitals than for the dπ(Re) orbital. Hence, the intensity of the transition to π*(R-diimmine) from dπ(Re) - pπ(X) will mainly be determined by the contribution of dπ(Re) to the HOMO, which decreases upon going from Cl to I.

Table 3.1 A summary of photophysical properties of [Re(NN)(CO)$_3$X] complexes, constructed using data from [4,9,11,13,25,26,28–33]

NN/X (year)	**ν(CO) / cm^{-1}**		**Absorption / nm (ε /M^{-1} cm^{-1})**		**Emission / nm**			**Lifetime**		
	Solvent		*Solvent*		*Solvent*	*T / K*		*Solvent*	*T / K*	
bpy/Cl (1974)	CH_2Cl_2	2012	CH_2Cl_2	387 (3500)	2-Me-THF	80	532	2-Me-THF	80	2.7 µs
		1914		316 sh	CH_2Cl_2	298	615	CH_2Cl_2	298	50 ns
		1883		294 (17900)	CH_3CN	298	622	CH_3CN	298	25 ns
				257 sh						
				238 (19300)						
bpy/Br (1972)	CH_3CN	2023	CH_2Cl_2	392 (3700)	2-Me-THF	80	530	2-Me-THF	80	3.7 µs
		1917		295 (20100)						
		1900		245 br (21500)						
bpy/I (1959)	$CHCl_3$	2037	CH_2Cl_2	402(2600)	2-Me-THF	80	525	2-Me-THF	80	7.5 µs
		1917		299 (18500)						
		1900		245 sh (22400)						
				233 sh (24300)						
phen/Cl (1941)	$CHCl_3$	2027	CH_3CN	370 (3900)	CH_3CN	298	612	CH_3CN	298	178 ns
		1924		264 (25000)	CH_2Cl_2	298	604	CH_2Cl_2	298	288 ns
		1896								

3.1.5 Rhenium tricarbonyls for the photocatalytic reduction of CO_2

The following catalytic cycle outlines the key steps involved in the photocatalytic reduction of CO_2 to CO using [Re(dmbpy)$(CO)_3$Cl] as an example (Scheme 3.2).[34]

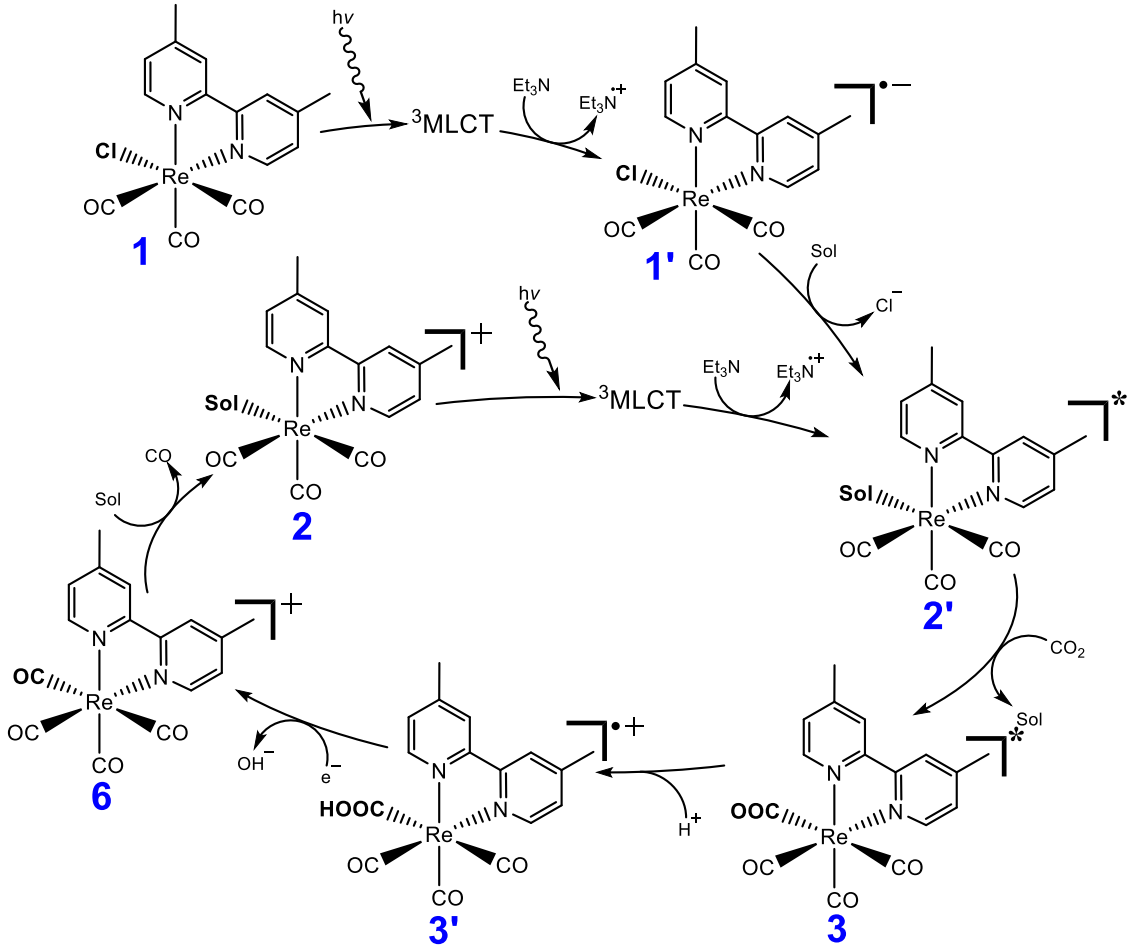

Scheme 3.2 Photochemical CO_2 reduction photosensitised by [Re(dmbpy)$(CO)_3$Cl].[35]

1. Complex 1 absorbs a photon of light, which populates a singlet MLCT state which populates triplet MLCT state on the ultrafast timescale; this ^{3}MLCT state that undergoes one-electron reduction by TEA to yield the radical anion 1'.
2. The chloride ion is eliminated and replaced by the solvent (DMF) to give the one electron reduced form of the solvent-coordinated rhenium complex 2'.
3. Complex 2' undergoes electrophilic attack from CO_2 and subsequent protonation to form the CO_2 adduct of the complex 3'.
4. Complex 3' accepts an electron, from 1', 2' or a carbon radical formed by deprotonation of the triethylamine radical cation, to produce CO and regenerate the complex 2.
5. Complex 2 absorbs a photon of light to form complex 2'.

3.1.6 Rhenium tricarbonyls for the electrocatalytic reduction of CO_2

3.1.7 Previous work on rhenium aryl-BIAN complexes

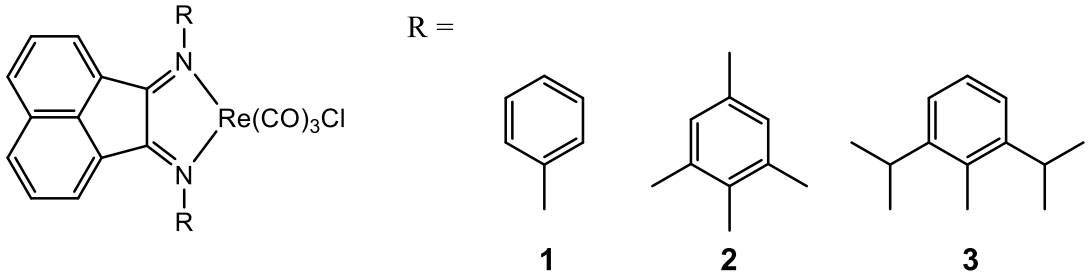

Figure 3.6 Chemical structures of rhenium aryl-BIAN complexes investigated by Portenkirchner and co-workers for CO_2 reduction.[36]

A study published in 2014 by Portenkirchner *et al.* investigated the suitability of rhenium(I) tricarbonyl chloride complexes, bearing three different bis(arylimino)acenaphthene (aryl-BIAN) ligands, for the two-electron reduction of CO_2 (Figure 3.6). They found that compound 1 did not show significant activity as an electrocatalyst for CO_2 reduction whereas compounds 2 and 3 both catalytic current enhancement in a CO_2 saturated solution. The notable difference between complexes 1, 2 and 3 is the variation in steric bulk on the aryl substituents around the rhenium metal centre. The presence of sterically demanding groups in close proximity to the active rhenium tricarbonyl site appears to have a strong influence of the catalytic properties of these systems.[36] As previously discussed, the loss of the halide is a key step in the catalytic cycle as it forms the five-coordinate anion species with a vacant coordination site which is the active catalyst.[37] It has been proposed that the steric bulk of the aryl group which surrounds this active site influences the loss of the halide thus impacting the catalytic performance. The aryl rings in these complexes are orthogonal to the acenaphthene unit which means that they are (largerly) electronically decoupled, which further supports the hypothesis that the effect is a steric one.

3.1.8 Aims

- To synthesise and fully characterise a series of rhenium tricarbonyl halide α-diimmine complexes where the α-diimmine ligand is systematically varied in order to observe the effect of changing the functional group on the aromatic electron acceptor. This will primarily be the modification of the mesBIAN ligand.
- Attempt to crystallise the complexes and determine their solid state structure by x-ray crystallography.

- Characterise the complexes using both infrared spectroscopy and UV-vis spectroscopy to inspect their electronic and vibrational structure in the ground state.
- Characterise the complexes using ultra-fast spectroscopy to understand their behaviour in the excited state.
- Use DFT calculations (in collaboration) to estimate the energy of their HOMOs and the LUMOs, model their geometries, predict both their electronic and vibrational spectra and compare them to experimental spectra.
- Assess whether the complexes are suitable for the photocatalytic reduction of CO_2 to CO by irradiating a sample of the complex with light and collecting a sample of the gas from above the sample to test for the presence of CO using gas chromatography (GC).
- Assess whether the complexes are suitable for the electrocatalytic reduction of CO_2 to CO using cyclic voltammetry.
- Compare the complexes to see what affect the modification of the α-diimmine ligand has on the complexes ability to catalyse CO_2 reduction.

3.2 Experimental

3.2.1 Materials and General Procedures

2,4,6-trimethylaniline (97 %), n-butyl lithium (2.5 M in hexane), 9,10-phenanthrene (95 %), titanium tetrachloride (99.9 %) and pentacarbonylchlororhenium(I) (98 %) were purchased from Acros Organics. 5-bromoacenaphthene was purchased from Manchester Organics. Ethyl chloroformate (97 %) was purchased from Alfa Aesar. Acetic Anhydride was purchased from Fisher Scientific. Chromium trioxide (>98 %) was purchased from Sigma Aldrich. Acenaphthene was purchased from Aldrich. Triethanolamine (>99 %) was purchased from Sigma. Bromopentacarbonylmanganese(I) (98 %) was purchased from STREM. Glacial acetic acid was purchased from VWR. These reagents were used as received without further purification.

Tetrabutyl ammonium hexafluorophosphate was purchased from Sigma-Aldrich and recrystallised from hot ethanol and dried overnight in a vacuum oven. All solvents were of HPLC grade or higher and were used without further purification. Dry solvents were obtained from the University of Sheffield chemistry department Grubbs solvent purification system.

3.2.2 Synthetic Procedures

3.2.2.1 1,2-Bis(mesitylimino)acenaphthene (mesBIAN) (3.1)

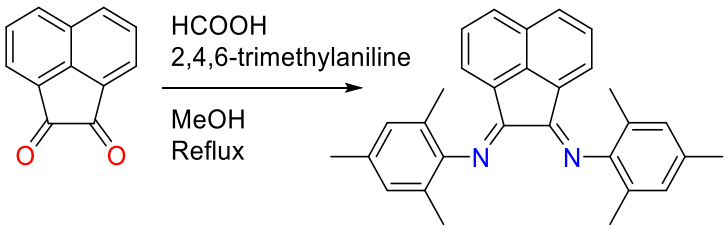

Acenapthenequinone (1.0 g, 5.49 mmol) was dissolved in methanol (50 ml) with stirring. 2,4,6-trimethylanilene (7.42 g, 7.70 ml, 54.9 mmol, 10 eq) and formic acid (2.02 g, 1.65 ml, 43.9 mmol, 8 eq) were added to the solution which turned from light orange to deep red within 2 min. The solution was allowed to stir in the dark for 4 hrs at room temperature. The solvent was removed *in vacuo* to give a bright orange solid which was dissolved in a minimum volume of dichloromethane and subjected to column chromatography on silica (1:1 diethyl ether : 40-60 petroleum ether). The

fractions corresponding to mesBIAN were collected as bright orange band and dried *in vacuo* to give ***3.1*** as a bright orange solid (2.1 g, 92 %).

^{1}H NMR (400 MHz, $CDCl_3$) δ 7.89 (d, J = 8.2 Hz, 2H), 7.40 (dd, J = 8.2, 7.3 Hz, 2H), 6.97 (s, 4H), 6.76 (d, J = 7.1 Hz, 2H), 2.38 (s, 6H), 2.09 (s, 12H).

3.2.2.2 ethyl 1,2-dihydroacenaphthylene-5-carboxylate (3.2)

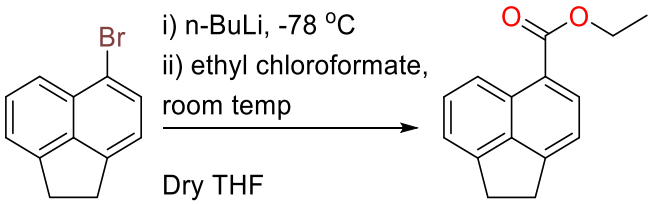

5-Bromoacenaphthene (1.11 g, 4.76 mmol) was added to a flame-dried two neck round bottom flask that had been purged with argon. Anhydrous THF (50 ml) was added to the reaction vessel with stirring to aid dissolution. The solution was cooled to -78 °C (acetone/dry ice), then n-butyl lithium (4.76 mmol) was added dropwise over 5 min and the reaction mixture was allowed to stir. After 50 min, ethyl chloroformate (0.45 ml, 4.76 mmol) was added to the reaction mixture over 5-min period at -78 °C, then the reaction was allowed to warm to room temperature with stirring over 2 hrs. The reaction solvent was removed in vacuo to give a light coloured solid that was dissolved in a minimum volume of DCM. The DCM solution was washed with saturated brine (4 x 50 ml), dried ($MgSO_4$) and the solvent removed in vacuo to give ***3.2*** as a sand coloured powder (0.58 g, 58%).

^{1}H NMR (400 MHz, $CDCl_3$) δ 8.64 (dd, *J* = 8.6, 0.5 Hz, 1H), 8.29 (d, *J* = 7.3 Hz, 1H), 7.59 (dd, *J* = 8.6, 6.9 Hz, 1H), 7.35 (d, *J* = 6.9 Hz, 1H), 7.31 (d, *J* = 7.4 Hz, 1H), 4.46 (q, *J* = 7.1 Hz, 2H), 3.45 – 3.41 (m, 4H), 1.47 (t, *J* = 7.1 Hz, 3H).
MS (EI+, DCM) m/z (%): [***3.2***] 226.1, [***3.2***-CH_4] 211.1, [***3.2***-$CHCH_3$] 198.1, [***3.2***-OCH_2CH_3] 181.1, [***3.2***-$OOCH_2CH_3$] 168.1, [***3.2***-$COOCH_2CH_3$] 153.1.

3.2.2.3 *ethyl 1,2-dioxo-1,2-dihydroacenaphthylene-5-carboxylate (3.3)*

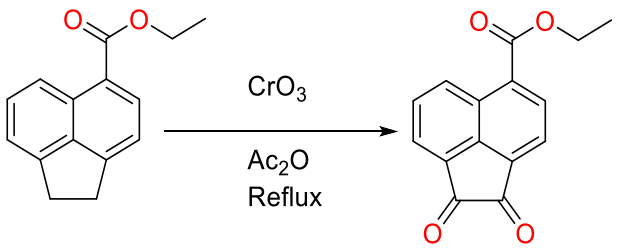

3.2 (0.465 g, 2.21 mmol) and chromium trioxide (2.0 g, 22.1 mmol) were added to acetic anhydride (30 ml) and refluxed at 140 ^{o}C for two hrs. The colour of the reaction solution changed from red to green indicating a change from Cr(IV) to Cr(III). The reaction solution was allowed to cool to room temperature then decanted over ice (100 g). Once the ice had melted the solution was filtered and the solid was washed with a large amount of water to give a sandy precipitate that was dissolved in DCM and dried ($MgSO_4$). The solvent was removed *in vacuo* to give ***3.3*** as a deep red solid (0.43 g, 76 %).

^{1}H NMR (400 MHz, $CDCl_3$) δ 9.29 (dd, *J* = 8.7, 0.5 Hz, 1H), 8.57 (d, *J* = 7.3 Hz, 1H), 8.18 (dd, *J* = 7.0, 0.5 Hz, 1H), 8.11 (d, *J* = 7.4 Hz, 1H), 7.97 (dd, *J* = 8.7, 7.0 Hz, 1H), 4.55 (q, *J* = 7.1 Hz, 2H), 1.51 (t, *J* = 7.1 Hz, 3H).

3.2.2.4 *ethyl(1E,2E)-1,2-bis[(2,4,6-trimethylphenyl)imino]-1,2-dihydroacenaphthylene-5-carboxylate (4-COOEt-mesBIAN) (3.4)*

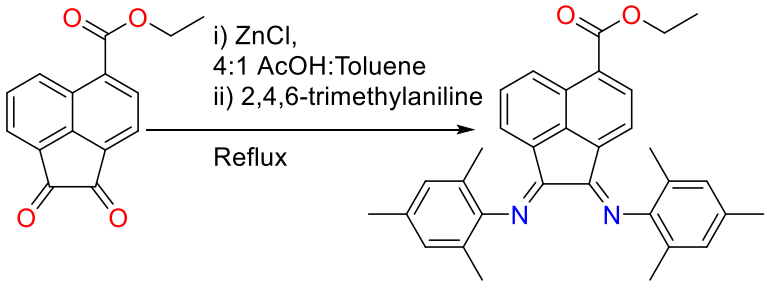

3.3 (0.429 g, 1.69 mmol) and zinc chloride (0.51 g, 5.06 mmol) were added to a dry flask against a flow of argon and a 4:1 mixture of glacial acetic acid: toluene (10 ml) was added. To this solution 2,4,6-trimethylaniline (0.71 ml, 5.06 mmol) was added and

solution was heated to 60 ^{o}C for 5 min with stirring. The solution was then heated to 120 ^{o}C for 1 hour. After cooling to room temperature, water (10 ml) was added to give a deep red organic layer and a colourless aqueous layer. The organic layer was collected and washed with 1.5 eq of potassium oxalate in water (50 ml) for an hour with stirring. The organic layer was dried (over $MgSO_4$) and the solvent removed *in vacuo* to give ***3.4*** as a red solid (0.18 g, 22 %).

^{1}H NMR (400 MHz, $CDCl_3$) δ 8.95 (d, *J* = 8.4 Hz, 1H), 8.19 (d, *J* = 7.6 Hz, 1H), 7.52 (dd, *J* = 8.6, 7.2 Hz, 1H), 6.98 (d, *J* = 1.7 Hz, 4H), 6.85 (d, *J* = 6.9 Hz, 1H), 6.79 (d, *J* = 7.6 Hz, 1H), 4.44 (q, *J* = 7.1 Hz, 2H), 2.38 (s, 6H), 2.09 (s, 6H), 2.08 (s, 6H), 1.41 (t, *J* = 7.2 Hz, 3H).

3.2.2.5 (1E,2E)-5-azido-N1,N2-bis(2,4,6-trimethylphenyl)-1,2-dihydroacenaphthylene-1,2-diimmine (4-N_3-mesBIAN) (3.5)

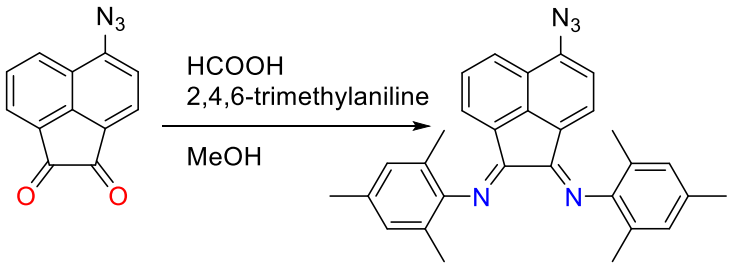

4-azidoacenapthenequinone (200 mg, 0.897 mmol) was dissolved in methanol (12 ml) with stirring. 2,4,6-trimethylanilene (1.20 g, 1.25 ml, 8.88 mmol) and formic acid (0.4 ml) were added to the solution which turned from light orange to deep red within ~2 min. The solution was allowed to stir in the dark for 4 hrs at room temperature. The solvent was removed *in vacuo* to give a bright orange solid which was dissolved in a minimum volume of dichloromethane and separated by column chromatography on silica (1:1 diethyl ether: 40-60 petroleum ether). The fractions corresponding to 4-N_3-mesBIAN were collected and dried *in vacuo* to give ***3.5*** as a bright orange solid (400 mg, 92 %).

^{1}H NMR (400 MHz, CDCl3) δ 7.99 (d, J = 8.4 Hz, 1H), 7.39 (dd, J = 8.4, 7.3 Hz, 1H), 7.13 (d, J = 7.8 Hz, 1H), 6.97 (s, 4H), 6.78 (d, J = 7.1 Hz, 1H), 6.73 (d, J = 7.8 Hz, 1H), 2.37 (s, 6H), 2.08 (s, 12H).

3.2.2.6 10-[(2,4,6-trimethylphenyl)imino]-4a,9,10,10a-tetrahydrophenanthren-9-one (3.6)

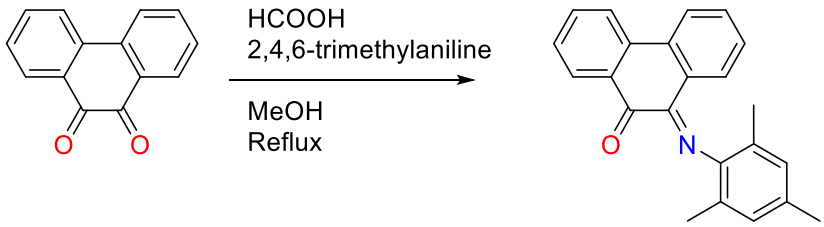

9,10-phenanthrenequinone (1.00 g, 4.80 mmol) and 2,4,6-trimethylaniline (6.49 g, 6.74 ml, 10 eq) were stirred in methanol (50 ml), to this formic acid (1.77 g,1.45 ml, 8 eq) was added dropwise of 5 min. The reaction mixture was allowed to stir for 18 hrs in the dark at room temperature. The solvent was removed *in vacuo* and the remaining oily residue was dissolved in DCM (20 ml) and washed with water (4 x 50 ml) the organic layer was dried ($MgSO_4$) and filtered. The solvent was removed *in vacuo* and the oily residue was passed through silica using 50:50 petroleum ether : diethyl ether to remove the excess 2,4,6-trimethylaniline. The bright blue solution was reduced to an oily residue *in vacuo*. To this oil, hexane (50 ml) was added dropwise over 1 hour and the solution was placed in the freezer overnight. A green solid precipitated out which was collected by vacuum filtration which was impure by TLC (4 spots) and NMR. This solid was dissolved in a minimum volume of DCM and purified by column chromatography (80:20 petroleum ether : diethyl ether) to give ***3.6*** as a bright green solid (0.86 g, 55 %).

^{1}H NMR (400 MHz, $CDCl_3$) δ 8.43 (d, *J* = 7.3 Hz, 1H), 8.08 – 7.97 (m, 3H), 7.73 – 7.66 (m, 1H), 7.65 – 7.58 (m, 1H), 6.89 (s, 2H), 2.31 (s, 3H), 1.95 (s, 6H).
MS (ES+, MeCN) m/z (%): [***3.6***H]$^{+}$ 326.2 (100%).

3.2.2.7 (9E,10Z)-N9,N10-bis(2,4,6-trimethylphenyl)-4a,9,10,10a-tetrahydrophenanthrene-9,10-diimmine, bis(mesitylimino)phenanthrene (mesBIPHEN) (3.7)

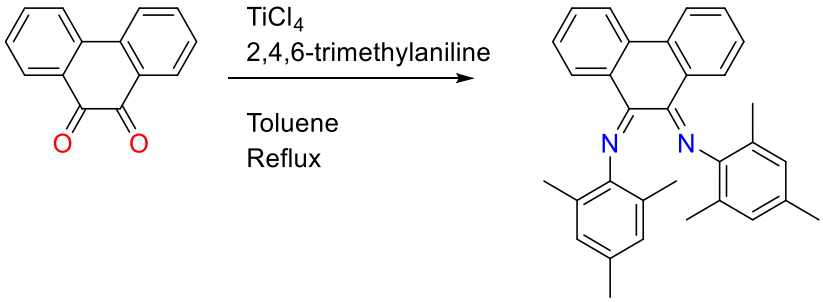

9,10-Phenanthrenequinone (1.0 g, 4.80 mmol) and 2,4,6-trimethylaniline (3.89 g, 4.04 ml, 28.81 mmol, 6 eq) were stirred in toluene (30 ml) under an inert atmosphere. $TiCl_4$ (0.91 g, 0.53 ml, 4.80 mmol) was added dropwise over 5 min and the solution was stirred for 18 hrs at 70 ^oC. The reaction solution was washed with water (3 x 10 ml) and the organic layer was collected, dried ($MgSO_4$) and filtered. The reaction mixture was reduced to a dark coloured oil *in vacuo*, after 48 hrs large square crystals had grown out of the oil that were washed with hexane to remove any excess 2,4,6-trimethylaniline to give ***3.7*** as bright red crystals (580 mg, 27 %).

^1H NMR (400 MHz, $CDCl_3$) δ 8.32 (dd, *J* = 7.7, 1.1 Hz, 1H), 7.91 (dd, *J* = 10.8, 8.0 Hz, 2H), 7.61 (td, *J* = 7.7, 1.4 Hz, 1H), 7.50 (td, *J* = 7.6, 0.9 Hz, 1H), 7.40 (td, *J* = 8.0, 1.2 Hz, 1H), 6.94 (dd, *J* = 15.2, 0.9 Hz, 1H), 6.80 (s, 2H), 6.75 (dd, *J* = 7.8, 0.9 Hz, 1H), 6.65 (s, 2H), 2.25 (d, *J* = 12.8 Hz, 3H), 2.17 (d, *J* = 7.4 Hz, 3H), 2.00 (s, 6H), 1.35 (s, 6H).

MS (ES+, DCM) m/z (%): [***3.7***H]+ 443.3 (100%).

3.2.2.8 [Re(mesBIAN)(CO)$_3$Cl] (3.8)

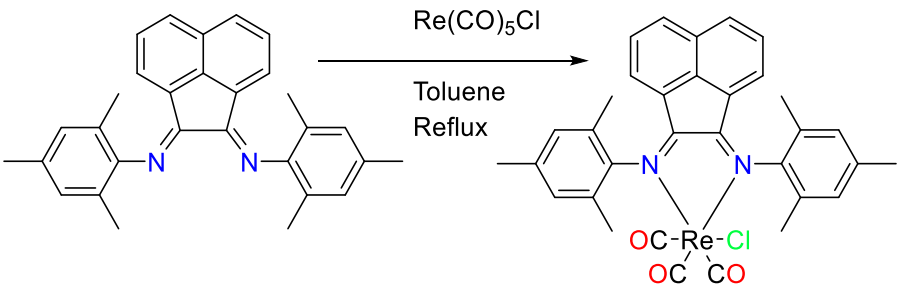

Pentacarbonylchlororhenium(I) (200 mg, 0.553 mmol) and ***3.1*** (230 mg, 0.553 mmol) were dissolved in toluene (30 ml) and brought to reflux. After 2 hrs, the reaction mixture which by then turned deep purple was allowed to cool to room temperature. The slow addition of n-hexane (~70 ml) induced the precipitation of a dark purple crystalline powder which was collected by vacuum filtration. The product was dried *in vacuo* to give ***3.8*** as dark purple needles (380 mg, 95 %).

^{1}H NMR (400 MHz, $CDCl_3$) d 8.05 (d, J = 8.0 Hz, 2H), 7.49 (dd, J = 8.3, 7.3 Hz, 2H), 7.13 (s, 2H), 7.02 (s, 2H), 6.74 (d, J = 7.2 Hz, 2H), 2.63 (s, 6H), 2.43 (s, 6H), 2.14 (s, 6H).
MS (ES+, MeCN) m/z (%): $[(mesBIAN)(CO)_3Re + MeCN]^+$ 728.00 (100%), $[(mesBIAN)(CO)_3Re]^+$ 687.00 (40%).

3.2.2.9 [Re(4-COOEt-mesBIAN)(CO)$_3$Cl] (3.9)

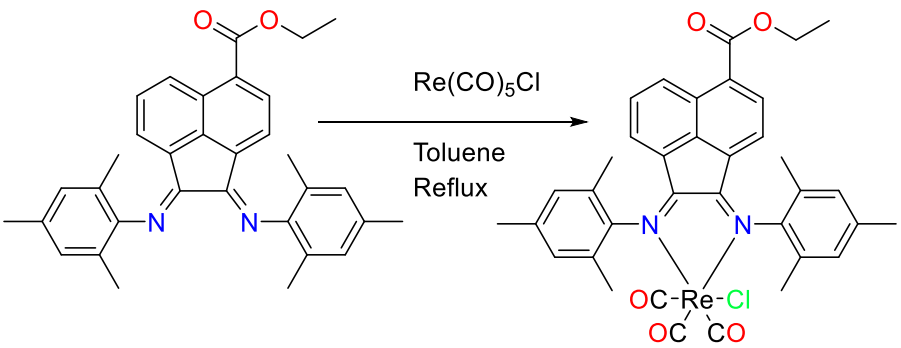

Pentacarbonylchlororhenium(I) (134 mg, 0.371 mmol) and ***3.4*** (181 mg, 0.371 mmol) were dissolved in toluene (30 ml) and brought to reflux. After 2 hrs the deep purple

reaction mixture was allowed to cool to room temperature before the slow addition of n-hexane (~70 ml) which induced the precipitation of a dark red powder which was collected by vacuum filtration. The product was dried *in vacuo* to give ***3.9*** as a fine red powder (212 mg, 72 %).

^{1}H NMR (400 MHz, $CDCl_3$) δ 9.08 (d, *J* = 8.2 Hz, 1H), 8.24 (d, *J* = 7.6 Hz, 1H), 7.59 (dd, *J* = 8.7, 7.3 Hz, 1H), 7.14 (s, 2H), 7.02 (s, 2H), 6.78 (d, *J* = 6.9 Hz, 1H), 6.74 (d, *J* = 7.6 Hz, 1H), 4.46 (q, *J* = 7.1 Hz, 2H), 2.62 (s, 6H), 2.43 (s, 6H), 2.11 (d, *J* = 3.6 Hz, 6H), 1.42 (t, *J* = 7.1 Hz, 3H).
MS (ES+, MeCN) m/z (%):[(4-COOEt-mesBIAN)$(CO)_3$Re + MeCN]$^+$ 800.00 (100%), [(4-COOEt-mesBIAN)$(CO)_3$Re]$^+$ 759.00 (70%).

3.2.2.10 Re(4-N_3-mesBIAN)$(CO)_3$Cl (3.10)

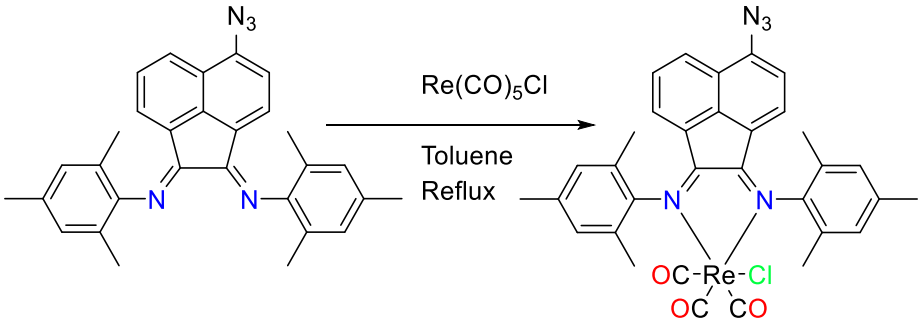

Pentacarbonylchlororhenium(I) (200 mg, 0.553 mmol) and ***3.5*** (253 mg, 0.553 mmol) were dissolved in toluene (30 ml) and brought to reflux. After 2 hrs the deep purple reaction mixture was allowed to cool to room temperature before the slow addition of n-hexane (~70 ml) which induced the precipitation of a dark purple powder which was collected by vacuum filtration. The product was dried *in vacuo* to give ***3.10*** as a dark purple powder (215 mg, 51 %).

^{1}H NMR (400 MHz, $CDCl_3$) δ 7.80 (d, *J* = 8.4 Hz, 1H), 7.09 (d, *J* = 9.1 Hz, 2H), 7.02 (s, 1H), 6.99 (d, *J* = 7.2 Hz, 2H), 6.60 (d, *J* = 7.2 Hz, 1H), 6.51 (d, *J* = 3.4 Hz, 1H), 2.62 (d, *J* = 6.4 Hz, 6H), 2.40 (d, *J* = 4.6 Hz, 6H), 2.14 (d, *J* = 7.1 Hz, 6H).

3.2.2.11 Re(mesBIPHEN)(CO)$_3$Cl (3.11)

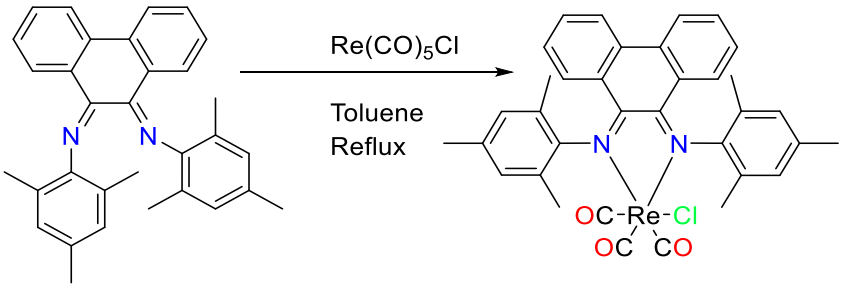

Pentacarbonylchlororhenium(I) (50 mg, 0.138 mmol) and ***3.7*** (61 mg, 0.138 mmol) were dissolved in toluene (30 ml) and brought to reflux. After 2 hrs the deep blue reaction mixture was allowed to cool to room temperature before the slow addition of n-hexane (~70 ml) which induced the precipitation of a black crystalline powder which was collected by vacuum filtration. The product was dried *in vacuo* to give ***3.11*** (46 mg, 76 %).

^{1}H NMR (400 MHz, $CDCl_3$) δ 8.17 (d, *J* = 7.6 Hz, 2H), 7.58 (dd, *J* = 8.4, 1.0 Hz, 2H), 7.56 – 7.51 (m, 1H), 7.13 (s, 2H), 7.09 (ddd, *J* = 8.4, 7.3, 1.1 Hz, 2H), 6.83 (s, 2H), 2.80 (s, 6H), 2.38 (s, 6H), 1.76 (s, 6H).
MS (ES+, MeCN) m/z (%):[(mesBIPHEN)$(CO)_3$Re + MeCN]$^+$ 754.00 (100%), [(mesBIPHEN)$(CO)_3$Re]$^+$ 713.00 (70%).

3.2.3 Instrumentation and Analysis

3.2.3.1 Photocatalysis

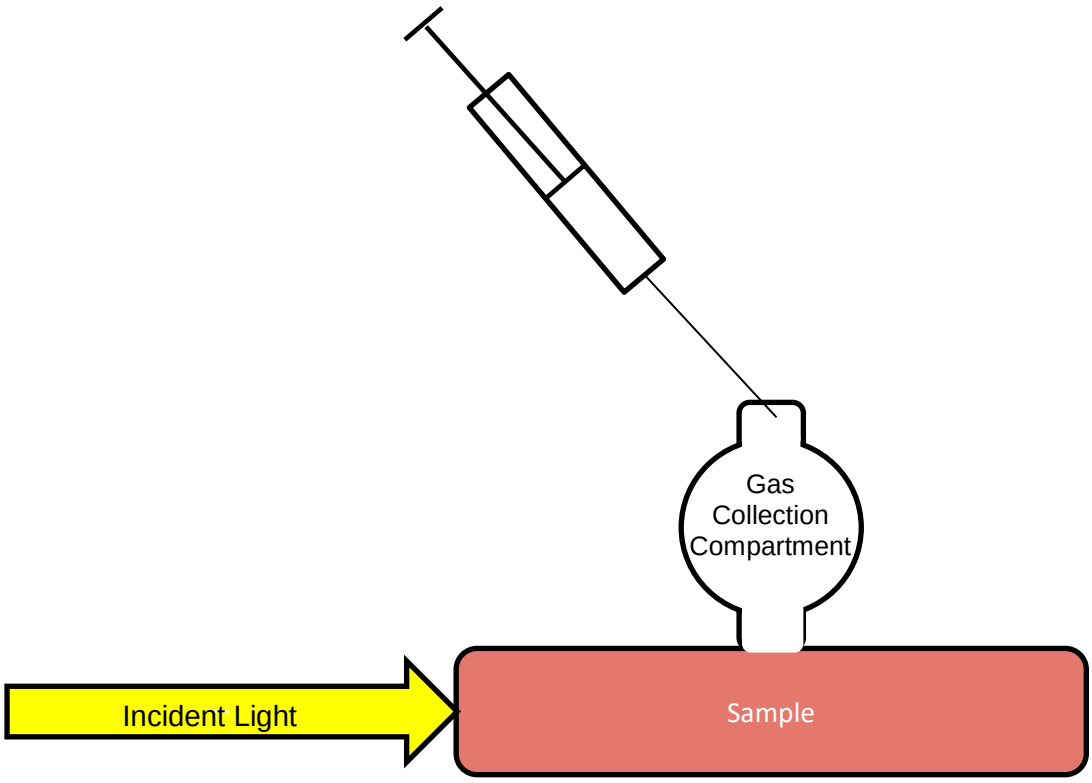

Figure 3.7 The setup used to assess whether the rhenium tricarbonyl complexes were photocatalytically active towards the reduction of CO_2 to CO.

Using a piece of modified equipment (Figure 3.7) the suitability of the complexes towards the photocatalytic reduction of CO_2 to CO could be assessed. The glassware consisted of a 10 cm path length sample space with a 25 ml round bottom flask joined to the top that could be fitted with a rubber suba seal. A sample complex was dissolved in acetonitrile (24 ml, 0.11 mM) and bubbled with CO_2. Triethanolamine (TEOA) (4.5 ml) was added via syringe as a SED. The sample compartment was irradiated with light (xenon lamp) and gas samples were taken from the headspace using a gas syringe at one hour intervals. These samples were analysed by gas chromatography to detect whether CO was present.

3.3 Results and discussion

3.3.1 Synthesis

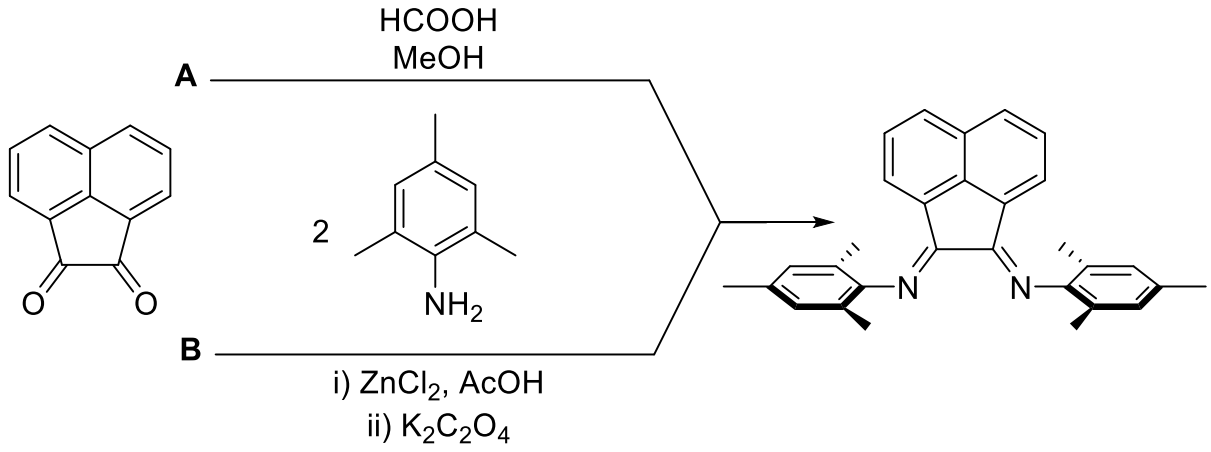

Scheme 3.3 Synthetic routes to mesBIAN

The synthesis of mesBIAN is often carried out in one of two methods, starting from acenaphthenequinone and 2,4,6-trimethylaniline (Scheme 3.3). Route A is the acid catalysed condensation between acenaphthenequinone and 2,4,6-trimethylaniline to give mesBIAN in good yields.[38–47] Route B is the zinc templated synthesis of mesBIAN which uses a zinc metal centre to assemble the ligand around before removing the zinc by washing with potassium oxalate, this route is more versatile and can be used to attach aromatic groups other than mesityl rings.[47–49]

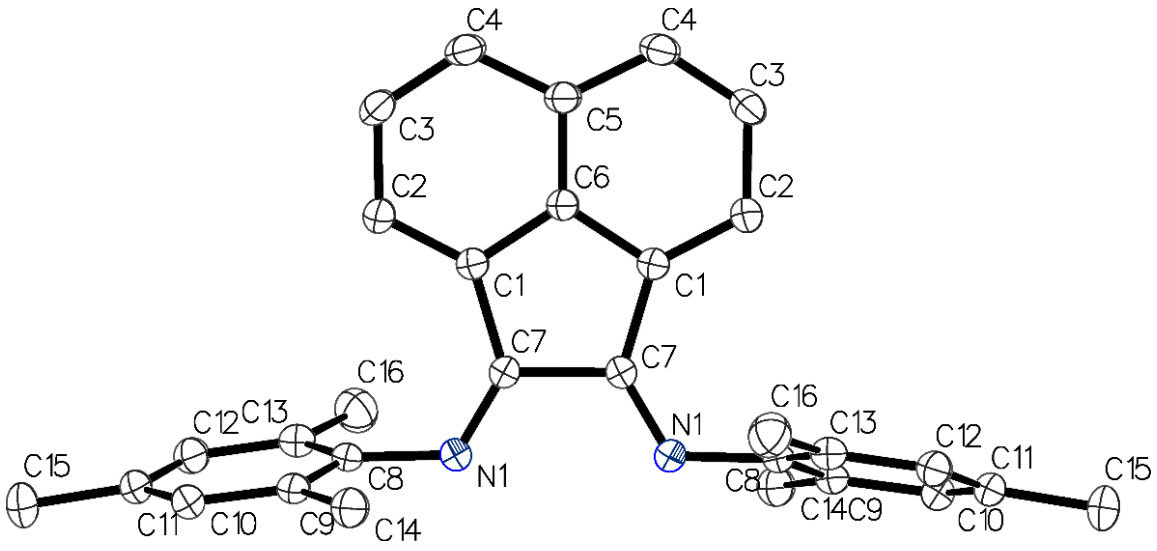

Figure 3.8 The crystal structure of mesBIAN as reported by Fukuda et al [47]

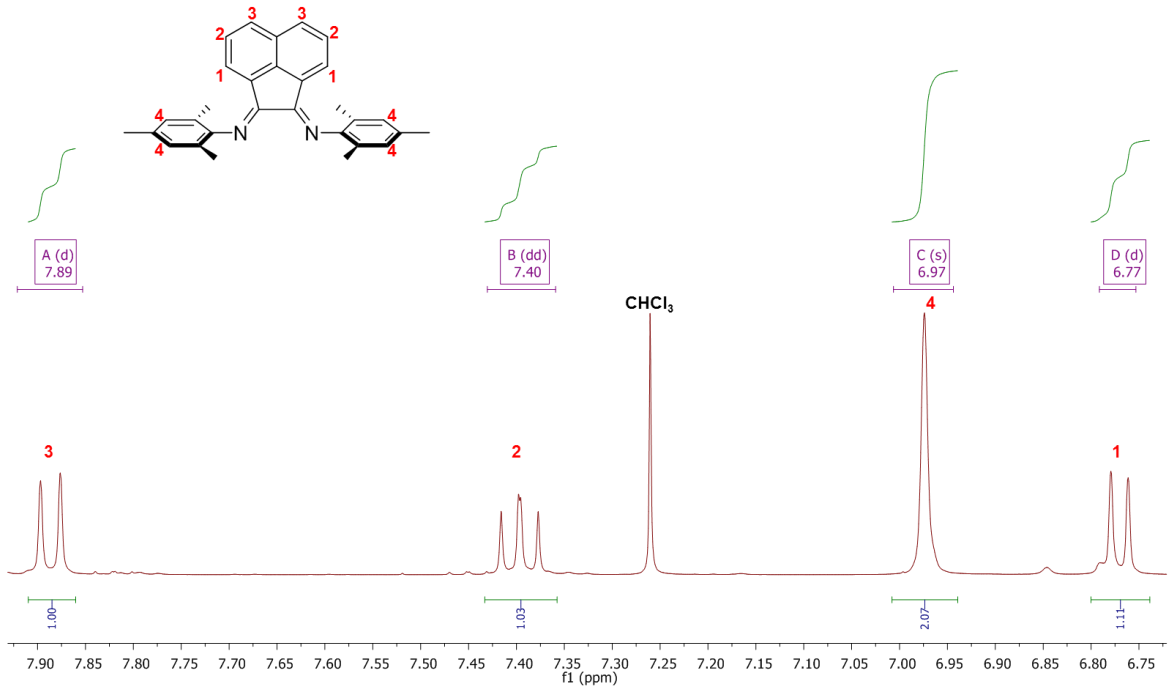

Figure 3.9 The aromatic region of the ^{1}H NMR spectrum of mesBIAN recorded in $CDCl_3$, proton environments labelled in red.

The crystal structure of mesBIAN reported by Fukuda clearly shows the orthogonal arrangement of the mesityl rings to the acenaphthene unit (Figure 3.8).[47] Due to this arrangement, mesBIAN has a plane of symmetry that gives it four aromatic environments in the ^{1}H NMR spectrum (Figure 3.9). One of the major side products of the synthesis of mesBIAN is the mono-iminated acenaphthene quinone, this is however easily removed from the reaction mixture via column chromatography due to the difference in polarity when compared to the symmetric mesBIAN. The mono-iminated product is also very easy to distinguish via ^{1}H NMR due to the asymmetry which gives eight aromatic environments compared to the four seen in mesBIAN (Figure 3.10).

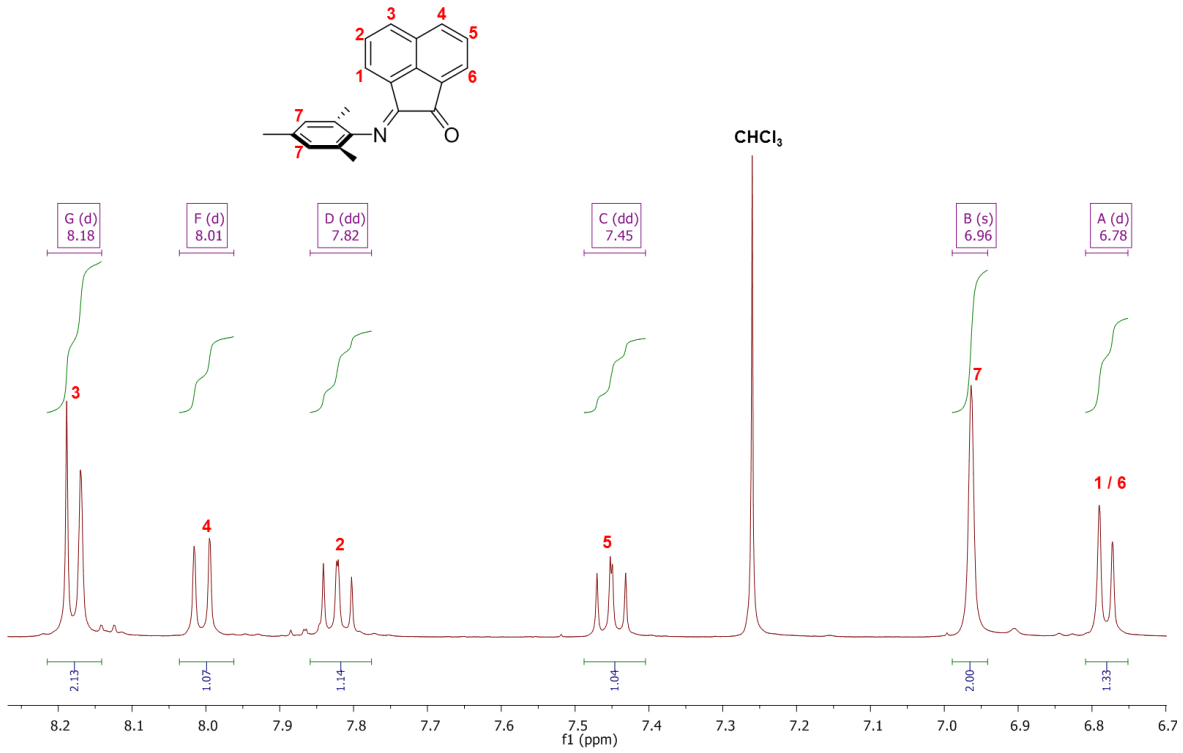

Figure 3.10 The aromatic region of the ^{1}H NMR spectrum of mono-mesBIAN recorded in $CDCl_3$, proton environments labelled in red.

The synthetic routes to the substituted mesBIANs are highlighted below and were improved within the research group by Dr Stuart Archer (Scheme 3.4).The ^{1}H NMR spectra of both the 4-substituted azido and ethyl ester mesBIAN break the symmetry of the acenaphthene ring resulting in increased number of proton environments. Both the azide and the ethyl ester substituent on aromatic systems are seen to be mildly electron withdrawing groups.[50] When comparing the Hammett substituent constants and resonance and field parameters for an aromatic azides and an ethyl ester it is found that the azide is more electron withdrawing than the ester.[51] This can be seen in both ligands ^{1}H NMR spectra as the proton with the largest chemical shift is shifted higher than in that of the standard mesBIAN (Figure 3.11, Figure 3.12).

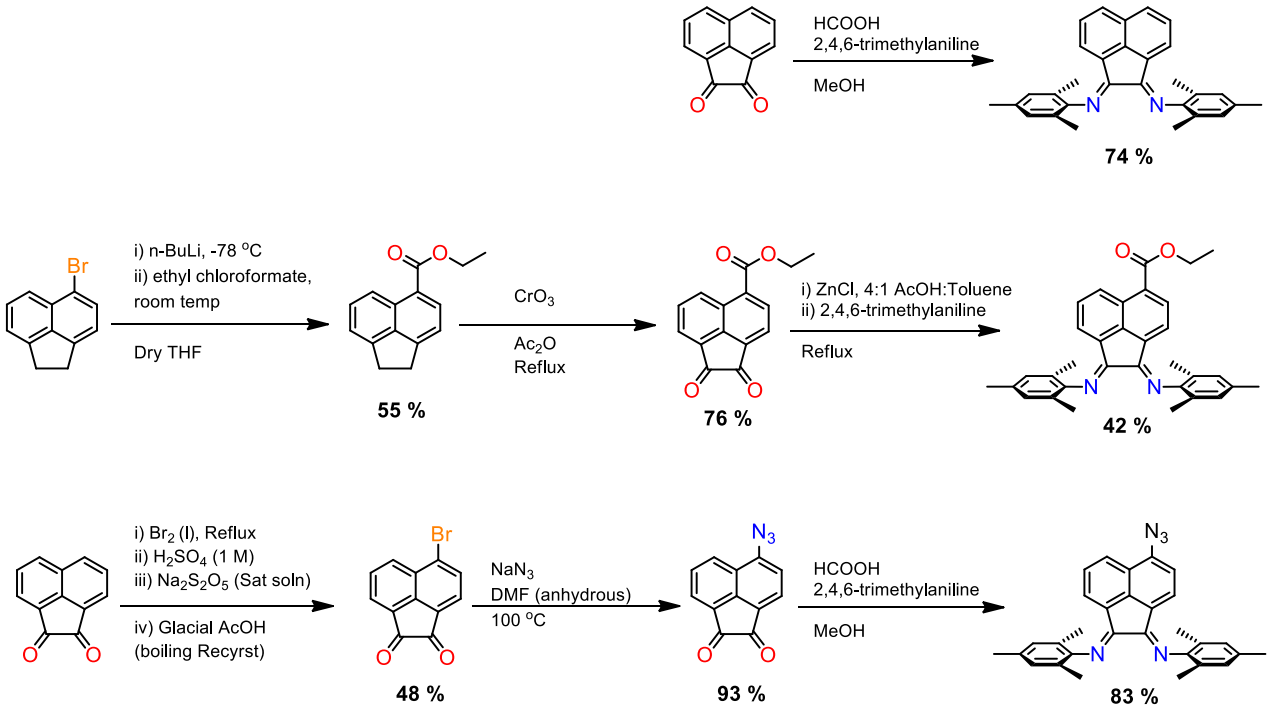

Scheme 3.4 The synthetic routes used to make the mesBIAN ligands discussed in this chapter.

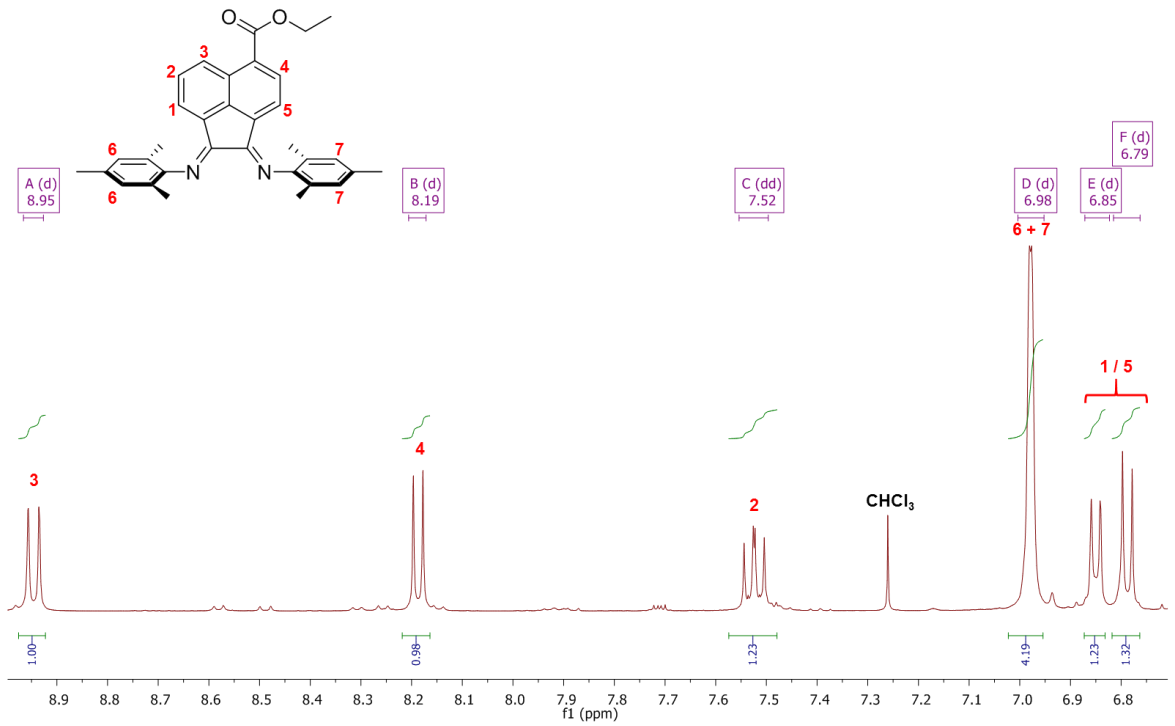

Figure 3.11 The aromatic region of the ^{1}H NMR spectrum of 4-COOEt-mesBIAN recorded in $CDCl_3$, proton environments labelled in red.

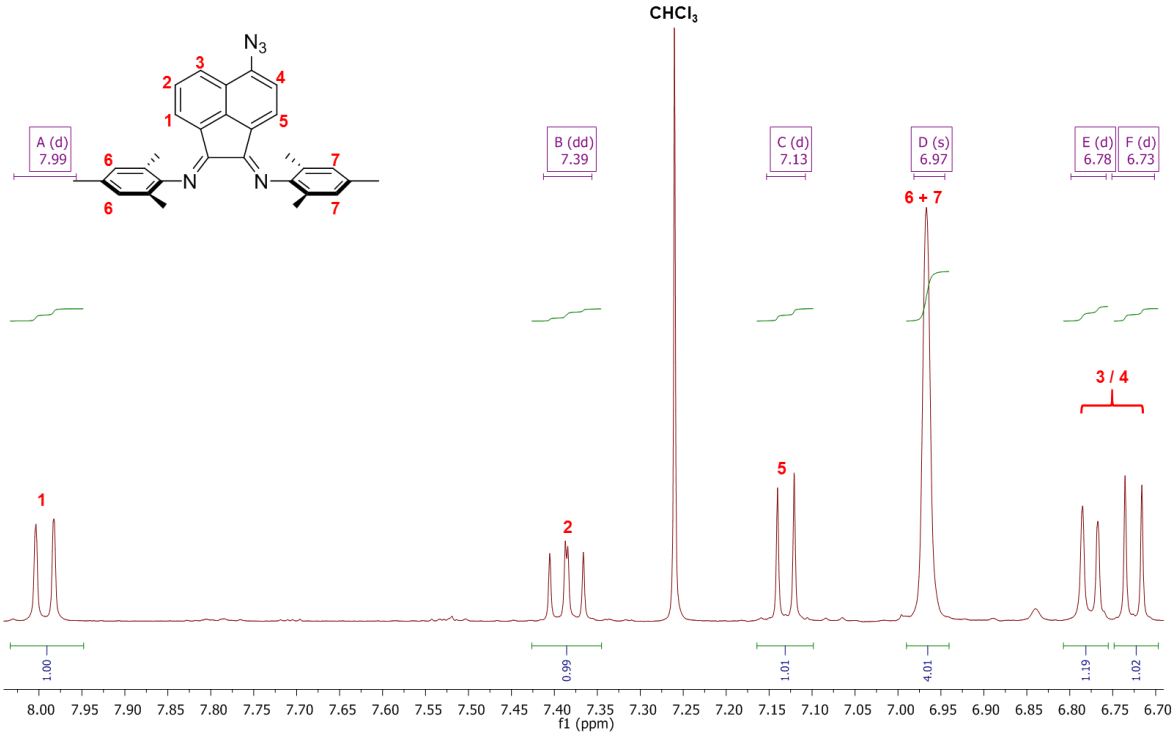

Figure 3.12 The aromatic region of the ^{1}H NMR spectrum of 4-N_3-mesBIAN recorded in $CDCl_3$, proton environments labelled in red.

One of the current challenges in photocatalysis is lack of compounds which absorb in the red part of visible spectrum, and/or are panchromatic absorbers, whilst retaining the sufficiently long excited state lifetime to engage in the catalytic process. To address this problem, we proposed to use an "extended mesBIAN" ligand, which has a 6-membered ring in place of the 5-membered ring in the mesBIAN. In such a molecule, a more extended π-system would lower the energy of the LUMO, thus tuning the absorption spectrum of the potential catalyst further into the red region of the spectrum. This ligand is based on phenanthrene, and is named bis-mesitylimino-phenanthrene or mesBIphen.

The synthesis of this ligand was attempted using the acid catalysed and zinc templated imination routes that proved successful with the synthesis of mesBIAN (route A) from acenaphthenequinone. The major product of this reaction was a mono-iminated phenanthrenequinone (Scheme 3.5). The mono-iminated compound was distinctively blue in solution with a varied shade of blue depending on the polarity of the solvent that is was dissolved in (Figure 3.13). This phenomenon of a chemical species changing colour depending on the polarity of the solvent that it is dissolved in is known as solvatochromism, and is usually indicative of a charge-transfer electronic transition being responsible for the color observed. This effect in 3.2 may be due to a shift in the

energy of a charge transfer band arising from electron donation from the oxygen atom of the carbonyl group to the nitrogen atom of the imide group.

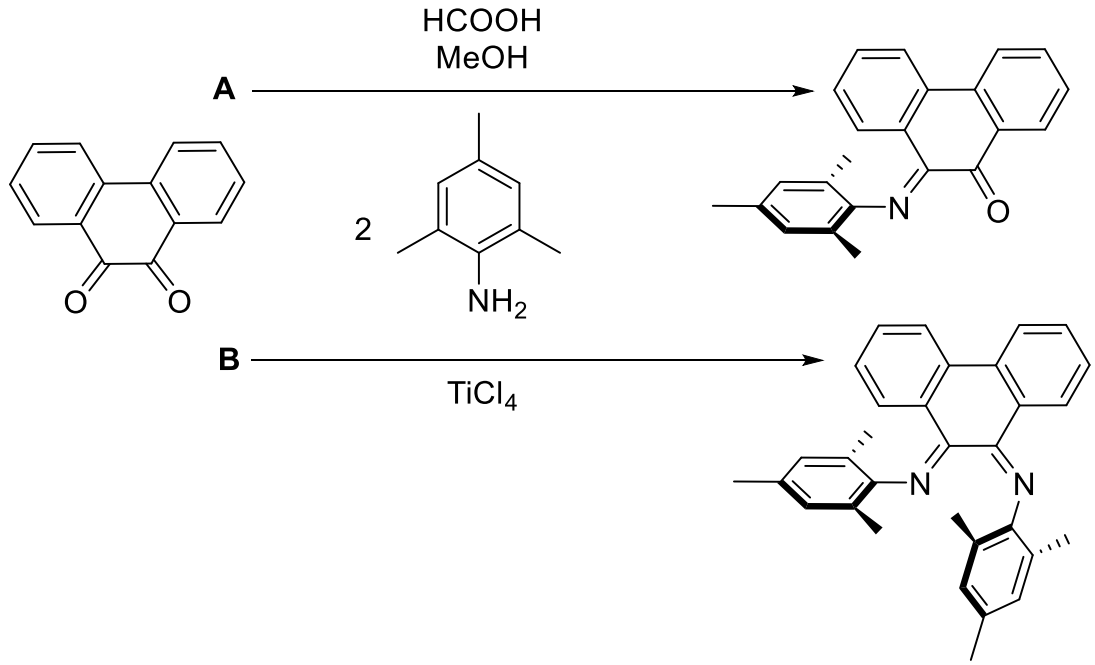

Scheme 3.5 Synthetic routes to mono-mesBIphen and mesBIPHEN.

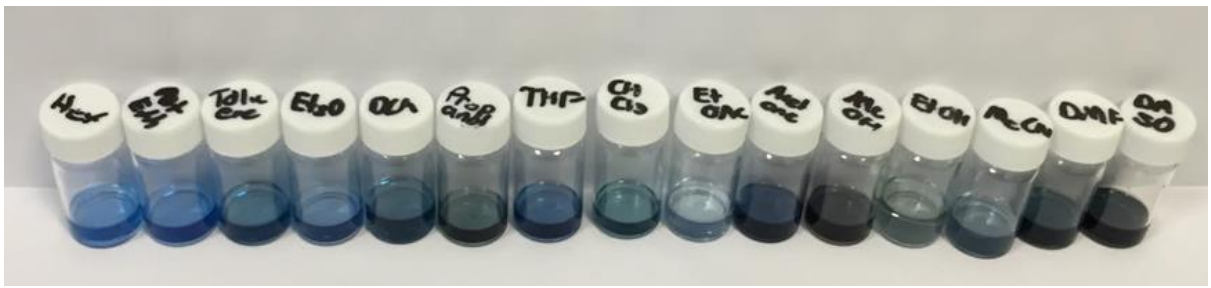

Figure 3.13 mono-mesBIPHEN in different solvents; left to right (hexane, petroleum ether, toluene, diethyl ether, CH_2Cl_2, propanol, THF, chloroform, ethyl acetate, acetone, methanol, ethanol, acetonitrile, DMF, DMSO).

Another method of synthesising mesBIphen was employed (route B) using a titanium(IV) chloride templated route as described for similar molecules in the literature that used different aniline derivatives.[52–54] The use of titanium(IV) chloride was a viable route to synthesising mesBIphen as it enhances the propensity of the C=O group to nucleophilic attack by coordinating to its oxygen atom, thus increasing the partial positive charge on the carbon atom (Scheme 3.6). An interesting structural feature of mesBIphen is the E,Z arrangement of the mesityl rings around the R-N=C bond, which becomes is apparent in the aromatic region of the ^{1}H NMR spectrum (Figure 3.15)

when compared to the mono substituted version (Figure 3.14). A consequence of this arrangement is that there are 9 proton environments in the aromatic region as the molecule does not possess the plane of symmetry seen in mesBIAN.

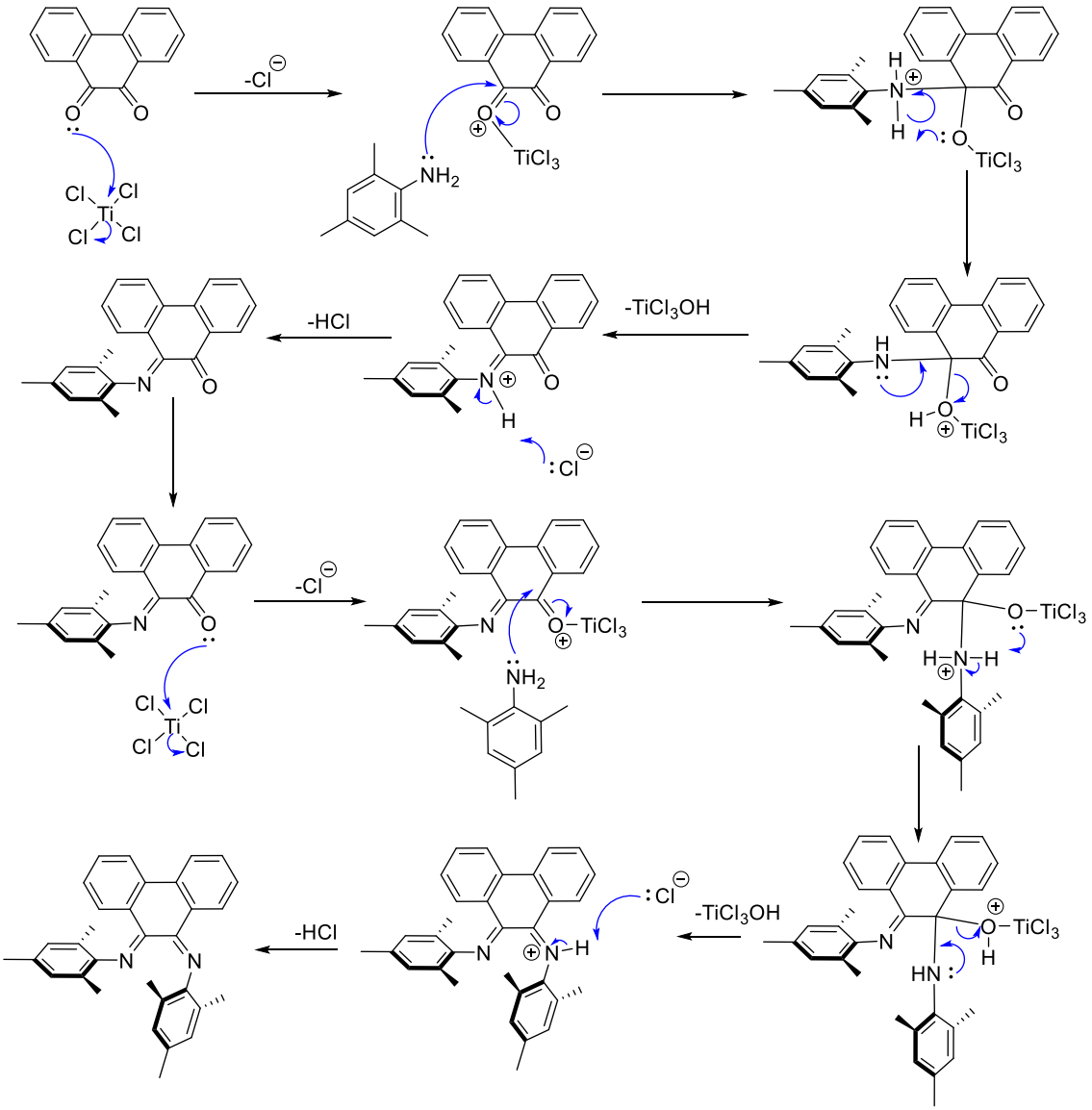

Scheme 3.6 The mechanism for the $TiCl_4$ templated synthesis of mesBIphen.

The mesBIphen product formed large red rectangular crystals once purified which made it an ideal candidate for single crystal X-ray crystallography. The E,Z structural arrangement was also confirmed from the X-ray crystal structure (Figure 3.16).

3.3.2 Synthesis of mesBIPhen

All of the ligands discussed so far were coordinated to rhenium pentacarbonyl chloride to form complexes of the type $[Re(NN)(CO)_3X]$ by refluxing the two in a 1:1 ratio in toluene and then recrystallizing the product from diethyl ether. The recrystallized product was often of high purity as seen by ^1H NMR (Figure 3.17 Figure 3.18).

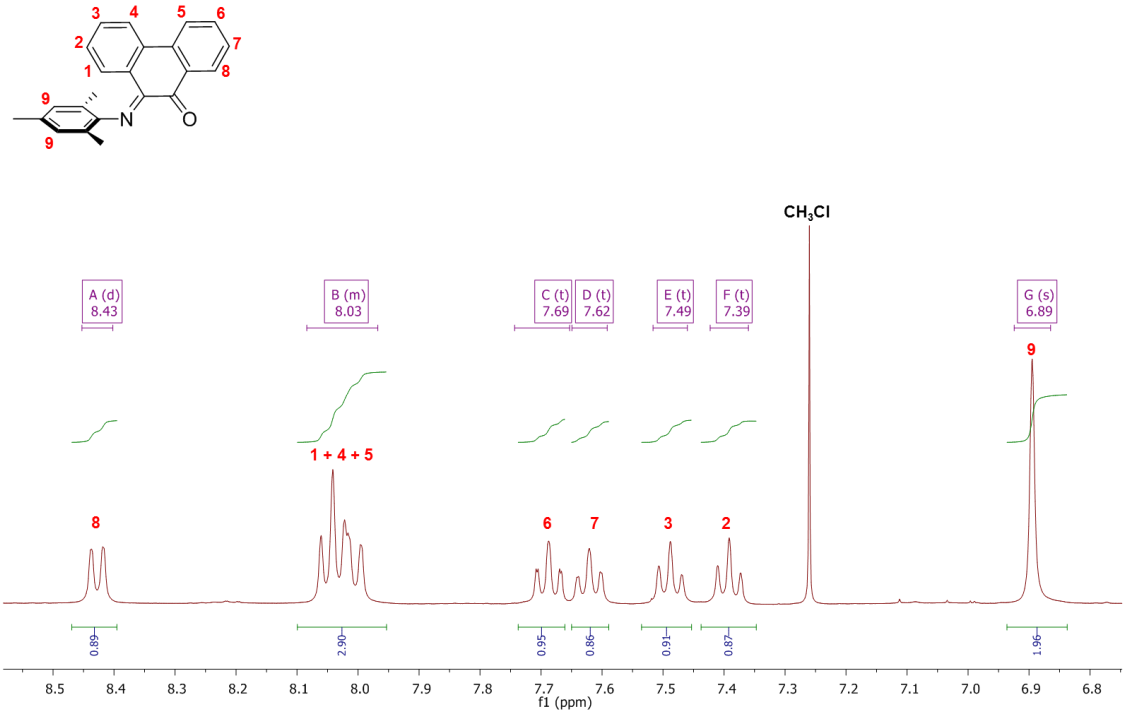

Figure 3.14 The aromatic region of the ^1H NMR spectrum of mono-mesBIphen recorded in $CDCl_3$, proton environments labelled in red.

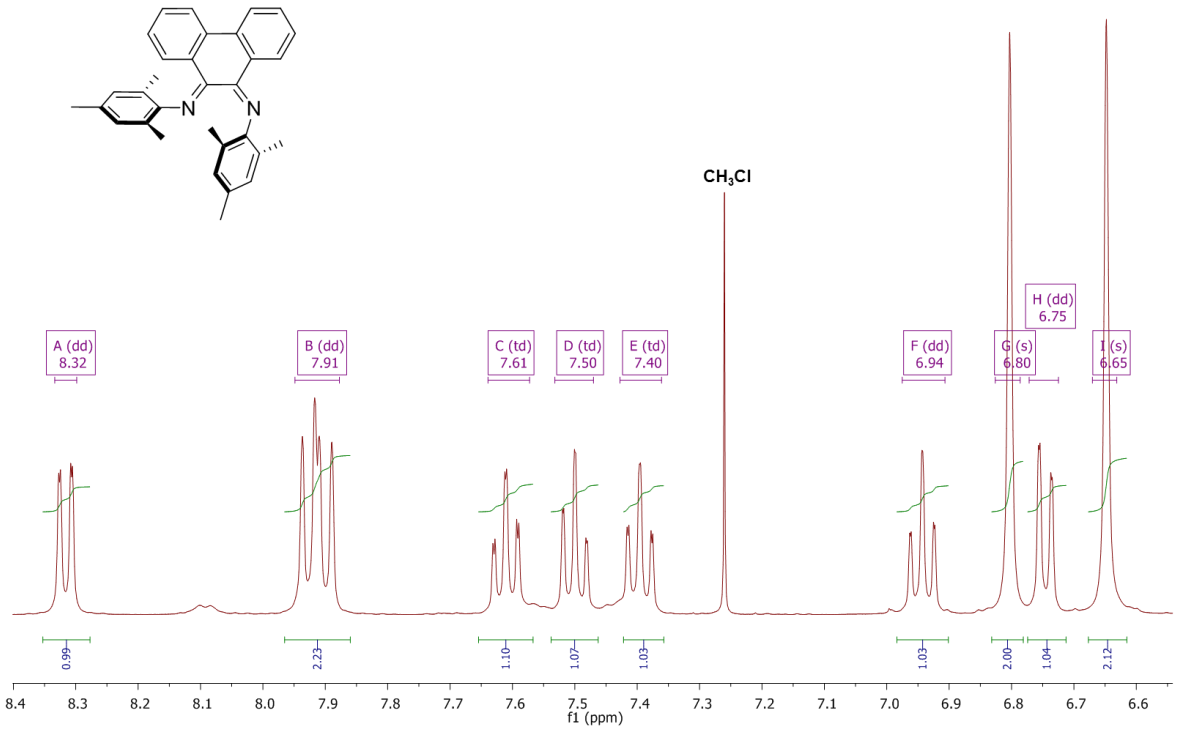

Figure 3.15 The aromatic region of the 1H NMR spectrum of mesBIphen recorded in $CDCl_3$

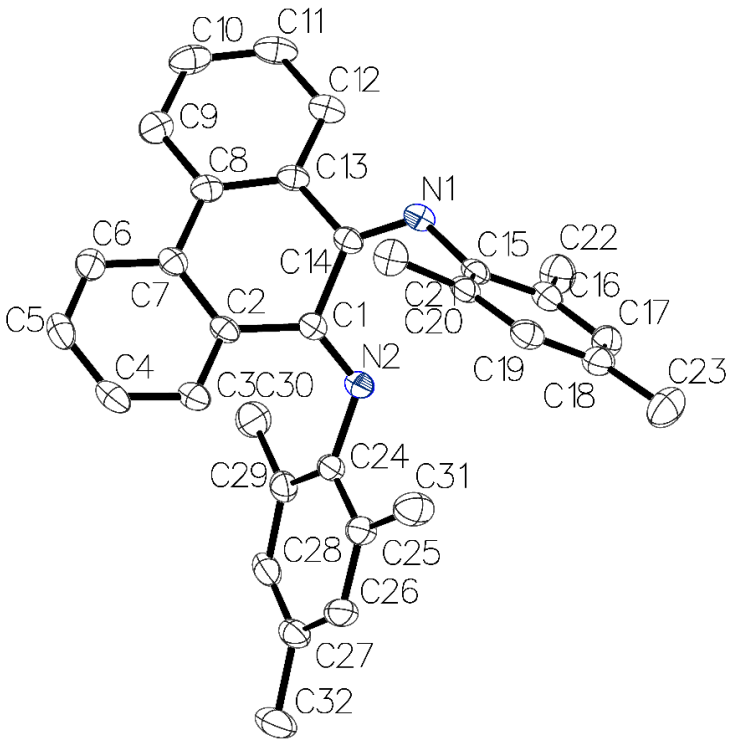

Figure 3.16 The crystal structure of mesBIphen ligand.

An interesting feature of the product [Re(mesBIphen)(CO)$_3$Cl] was that the mesityl rings were apparently orthogonal to the ring system as in the mesBIAN. This was noticed as the aromatic region of the ^{1}H NMR spectrum now only contained five environments which suggested that the ligand was now somewhat symmetrical (Figure 3.17, Figure 3.18). Both of the complexes [Re(mesBIAN)(CO)$_3$Cl] and [Re(mesBIphen)(CO)$_3$Cl] formed crystalline needles that were analysed using X-ray crystallography and in both cases the orthogonal arrangement of the mesityl rings was observed (Figure 3.19, Figure 3.20). The difference in structure of the mesBIphen ligand between the free ligand and the product suggests that the compound undergoes a structural rearrangement during the coordination process.

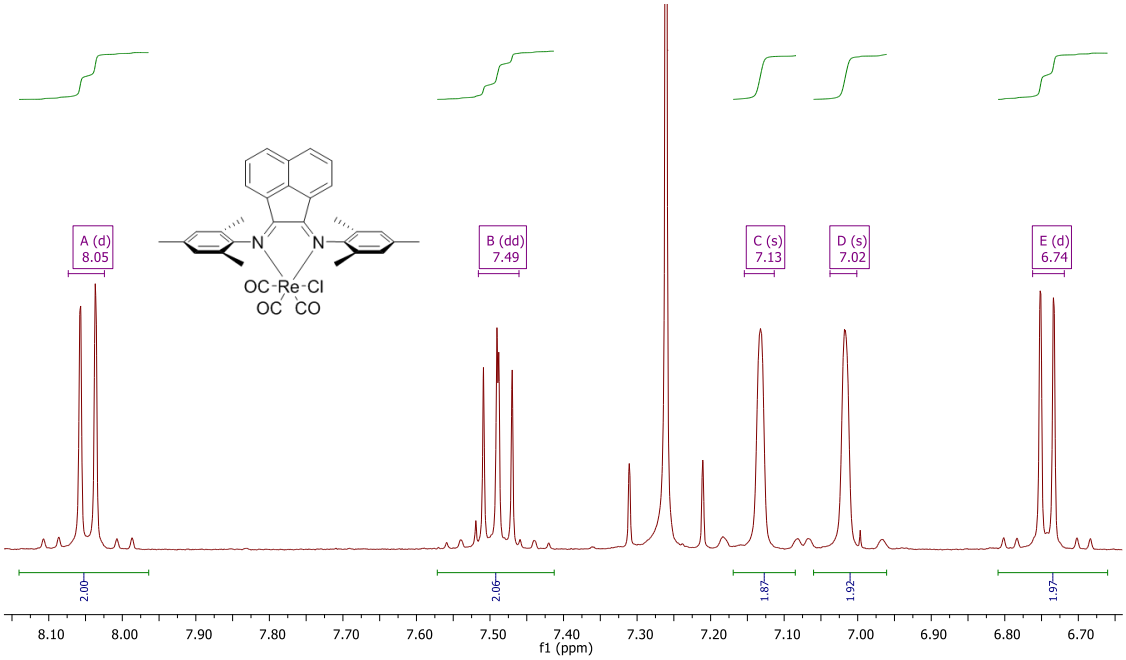

Figure 3.17 The aromatic region of the ^{1}H NMR spectrum of [Re(mesBIAN)(CO)$_3$Cl] recorded in CDCl$_3$

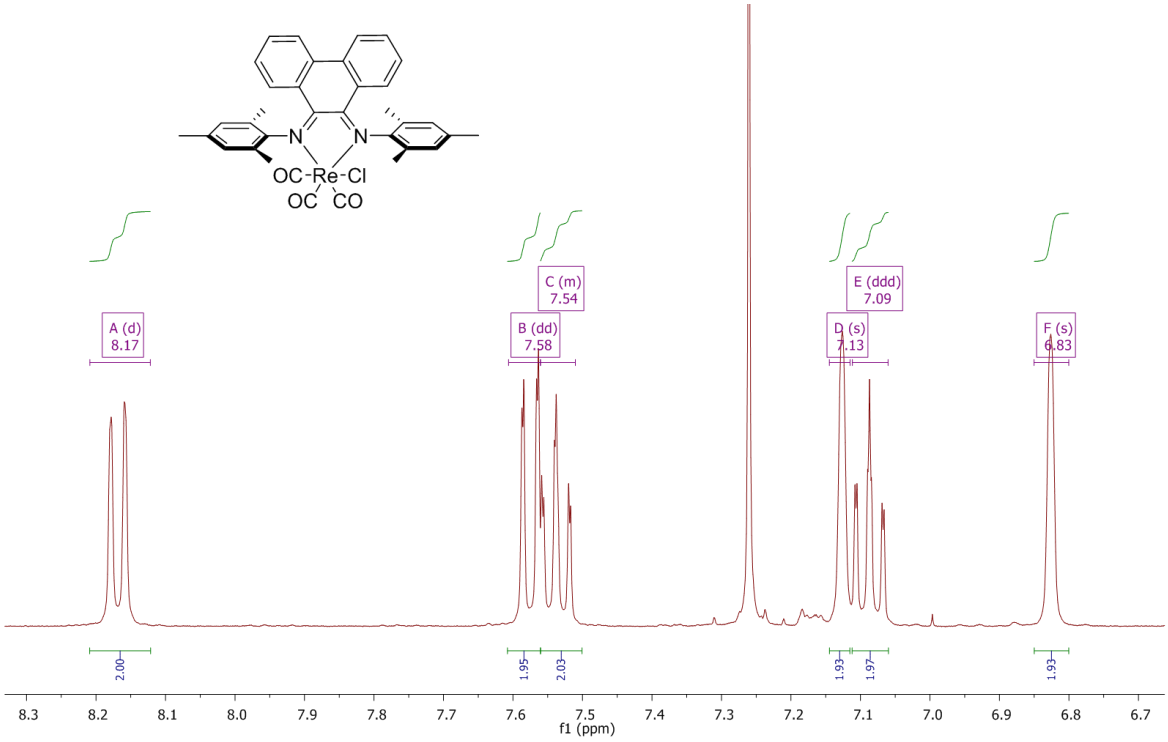

Figure 3.18 The aromatic region of the ^{1}H NMR spectrum of [Re(mesBIphen)(CO)$_3$Cl] recorded in $CDCl_3$

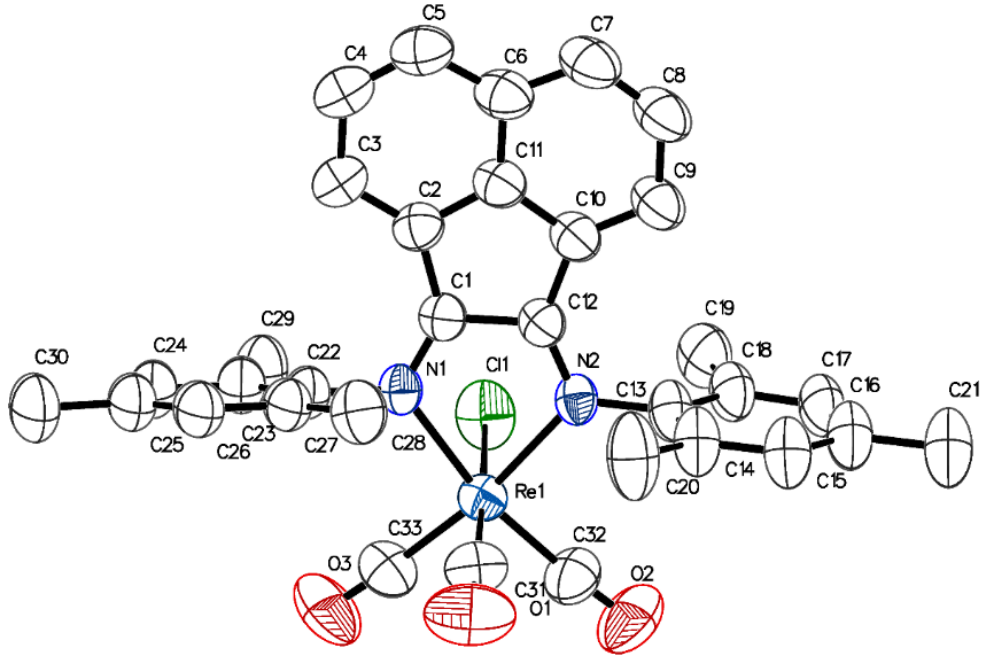

Figure 3.19 The crystal structure of [Re(mesBIAN)(CO)$_3$Cl]

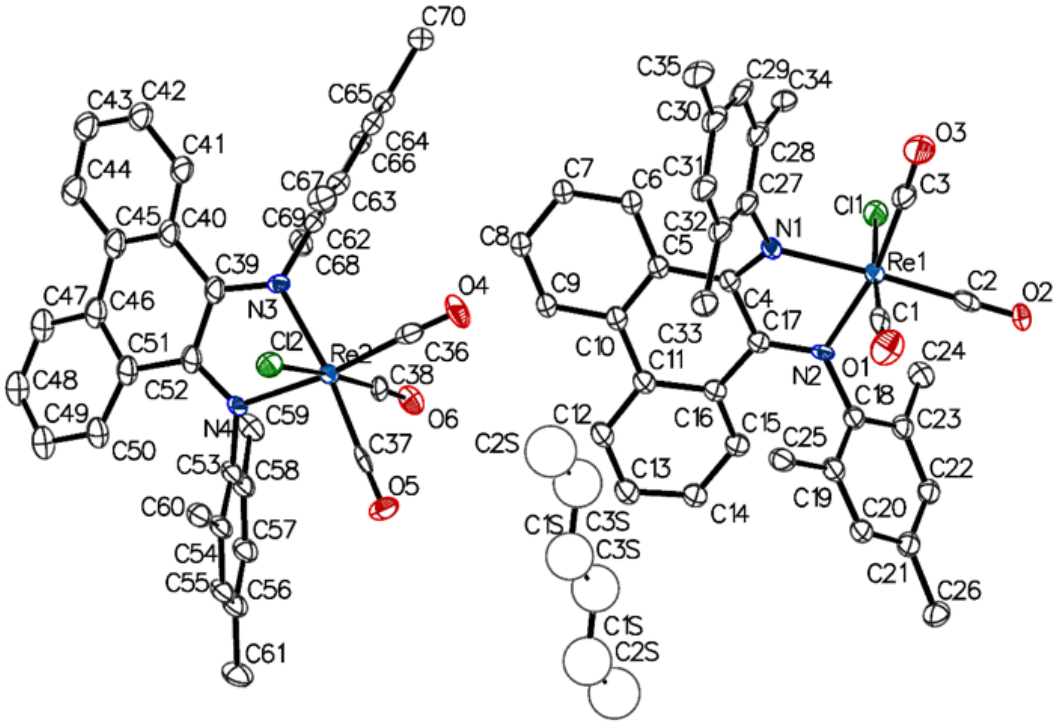

Figure 3.20 The crystal structure of [Re(mesBIphen)(CO)$_3$Cl]

3.3.3 Theoretical calculations

Calculations were performed on the complexes discussed in this chapter by Heather Carson. Using these calculations, the frontier orbitals HOMO and LUMO were visualised along with the optimised geometries, and vibrational and electronic spectra (discussed later) were obtained.

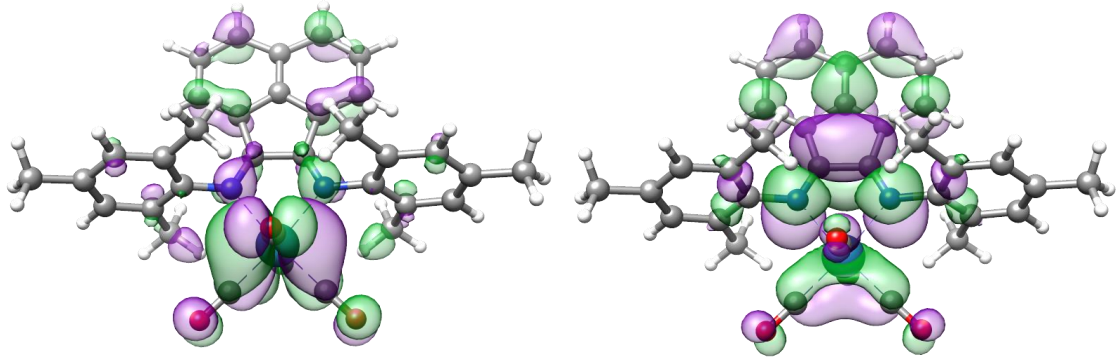

Figure 3.21 [Re(mesBIAN)(CO)$_3$Cl] HOMO (left) LUMO (right).

Both the HOMO and the LUMO of the [Re(mesBIAN)(CO)$_3$Cl] complex are symmetric and have little involvement from the mesityl rings. The HOMO is centred on the metal and the LUMO is extended into the π-system on the acenaphthene unit (Figure 3.21).

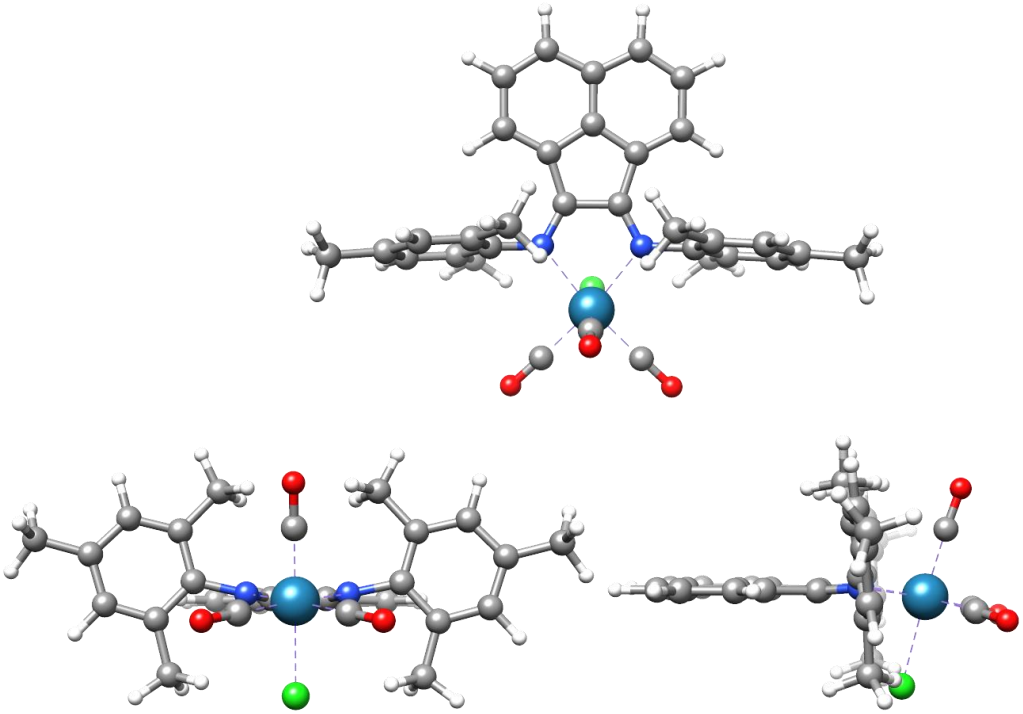

Figure 3.22 Optimised geometries for [Re(mesBIAN)(CO)$_3$Cl].

The optimised structure for [Re(mesBIAN)(CO)$_3$Cl] shows the planar acenaphthene unit with the mesityl rings positioned orthogonally. The chloride is angled upward toward the mesBIAN ligand between the mesityl rings (Figure 3.22).

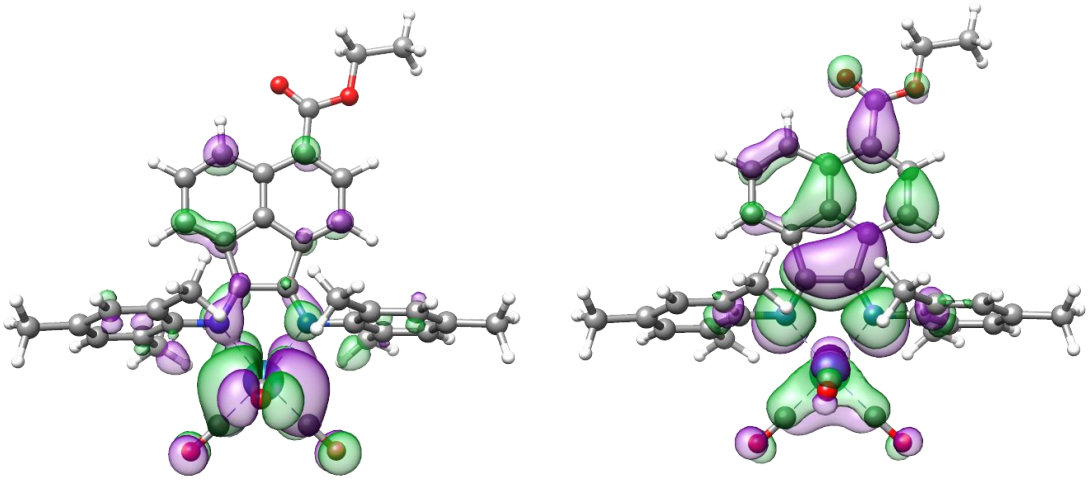

Figure 3.23 [Re(4-COOEt-mesBIAN)(CO)$_3$Cl] HOMO (left) LUMO (right).

The HOMO and the LUMO of the [Re(4-COOEt-mesBIAN)(CO)$_3$Cl] complex are different when compared to the unsubstituted complex. They are asymmetric due to the introduction of an electron withdrawing substituent at the 4 position and also have little involvement from the mesityl rings. The HOMO is centred on the metal and the LUMO is extended into the π-system of the acenaphthene unit and into the ester functional group (Figure 3.23).

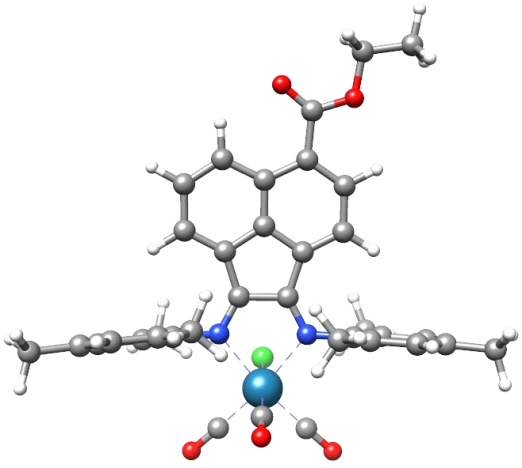

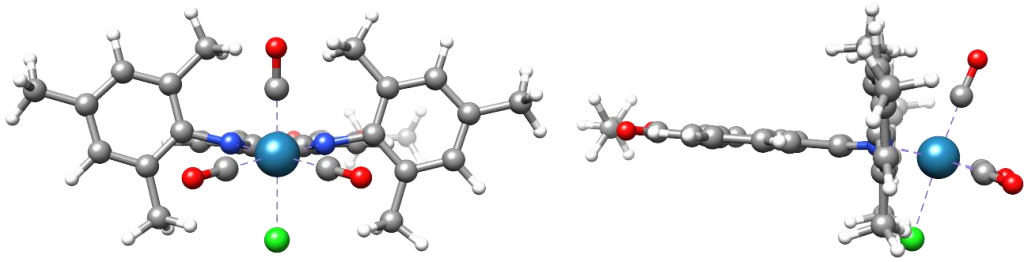

Figure 3.24 Optimised geometries for [Re(4-COOEt-mesBIAN)(CO)$_3$Cl].

The optimised structure for [Re(4-COOEt-mesBIAN)(CO)$_3$Cl] is very similar to the unsubstituted complex with the ethyl ester substituent positioned in-plane with the acenaphthene ring (Figure 3.24).

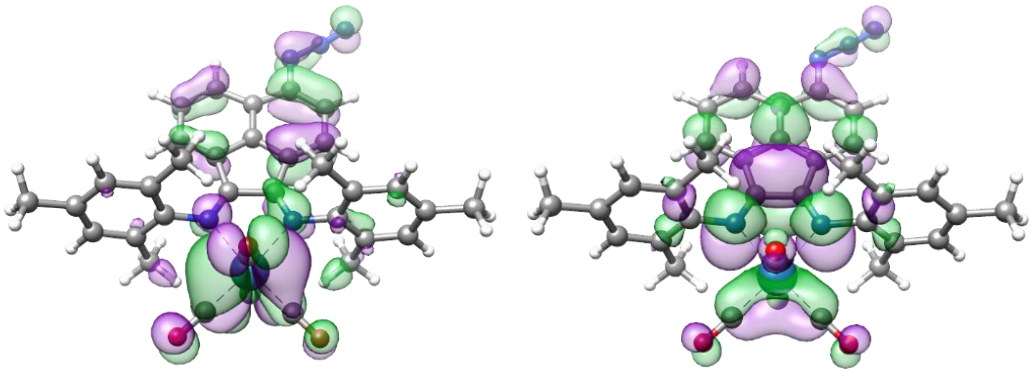

Figure 3.25 [Re(4-N$_3$-mesBIAN)(CO)$_3$Cl] HOMO (left) LUMO (right).

As with [Re(4-COOEt-mesBIAN)(CO)$_3$Cl] the HOMO and the LUMO of the [Re(4-N$_3$-mesBIAN)(CO)$_3$Cl] complex are asymmetric due to the introduction of an electron withdrawing substituent at the 4 position. The HOMO has a much larger involvement with the acenaphthene ring and the 4- substituent the LUMO is also extended into the electron withdrawing azide (Figure 3.25).

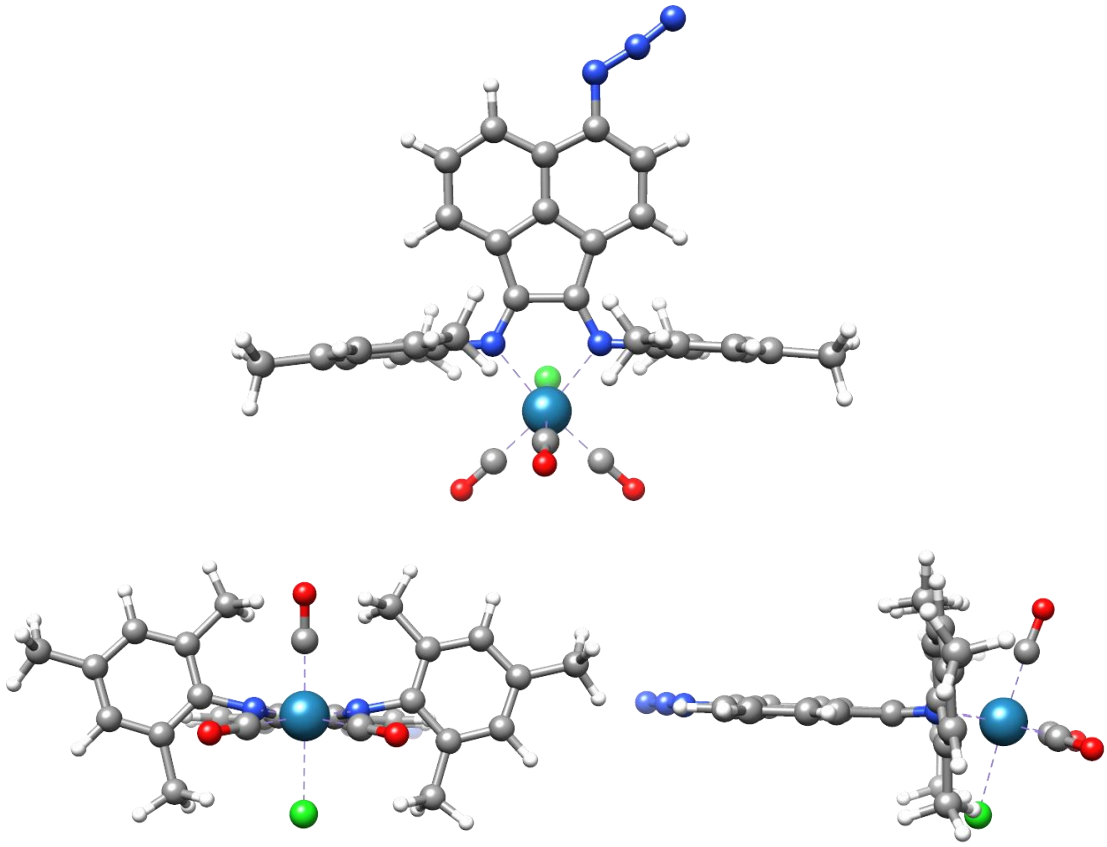

Figure 3.26 Optimised geometries for [Re(4-N3-mesBIAN)(CO)$_3$Cl]

The optimised structure for [Re(4-N$_3$-mesBIAN)(CO)$_3$Cl] is very similar to the ethyl ester complex, the azide substituent also lies in-plane with the acenaphthene unit (Figure 3.26).

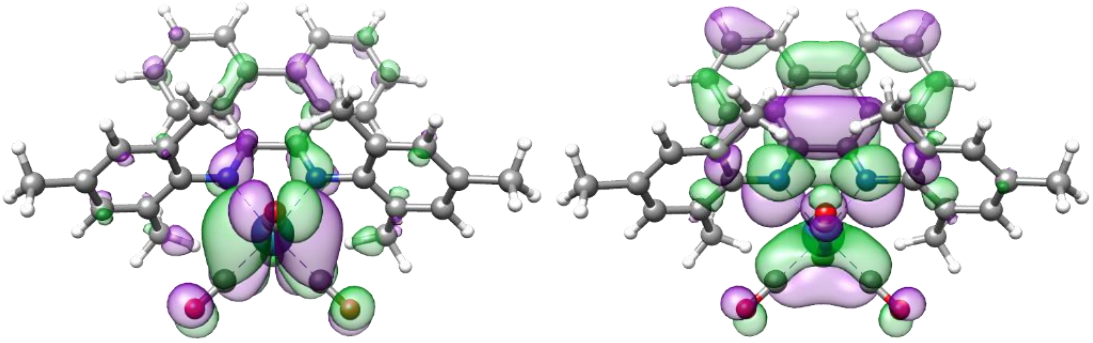

Figure 3.27 [Re(CO)$_3$Cl(mesBIphen)] HOMO (left) LUMO (right).

The frontier orbitals for the [Re(mesBIphen)(CO)$_3$Cl] complex are similar to [Re(mesBIAN)(CO)$_3$Cl] both the HOMO and the LUMO of the complex are symmetric

and have little involvement from the mesityl rings. The HOMO is centred on the metal and the LUMO is extended into the π-system on the phenanthrene unit (Figure 3.27).

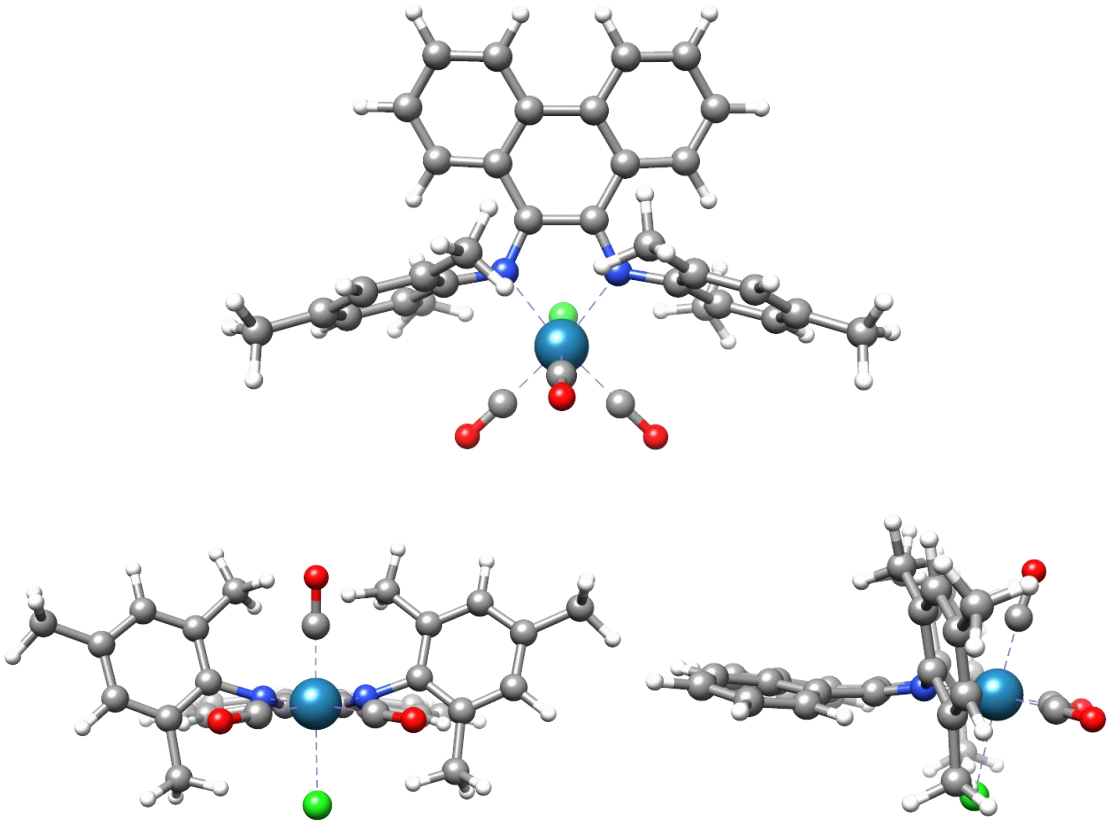

Figure 3.28 Optimised geometries for [Re(mesBIphen)(CO)$_3$Cl].

The optimised structure for [Re(mesBIphen)(CO)$_3$Cl] is interesting when compared to the mesBIAN complex. The additional carbon in the ring breaks the aromaticity of the ring system and therefore it is slightly bent. This bend is towards the chloride side of the complex and the mesityl rings sit slightly off centre and pushed out from the chloride relative to the mesBIAN complexes (Figure 3.28).

3.3.4 UV/Vis Electronic Absorption Spectroscopy

The electronic absorption spectra of complexes [Re(mesBIAN)(CO)$_3$Cl], [Re(4-N$_3$-mesBIAN)(CO)$_3$Cl], [Re(4-COOEt-mesBIAN)(CO)$_3$Cl] and [Re(mesBIphen)(CO)$_3$Cl] were recorded in CH_2Cl_2 at room temperature to determine the energy of the electronic excited states (Figure 3.29, Table 3.2).

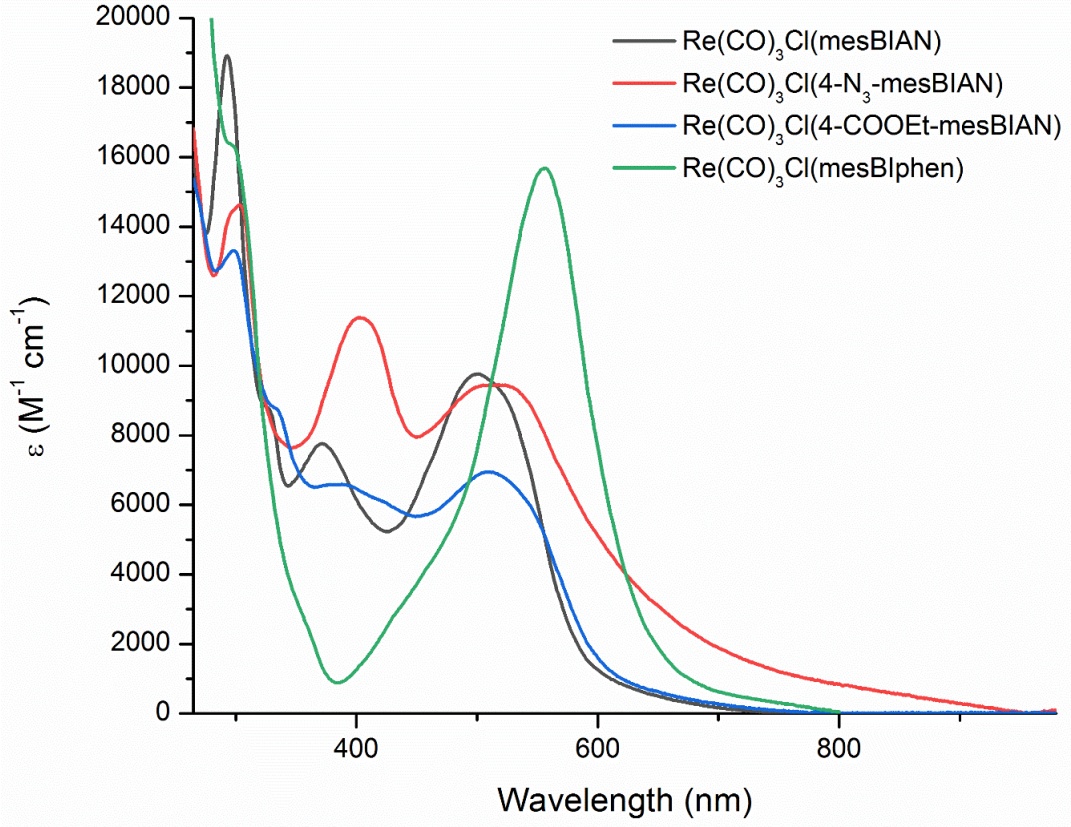

Figure 3.29 Steady state electronic absorption spectra of complexes [Re(4-R-mesBIAN)(CO)$_3$Cl] in CH_2Cl_2 at r.t. Black line – [Re(mesBIAN)(CO)$_3$Cl], Blue line – [Re(4-COOEt-mesBIAN)(CO)$_3$Cl], Red line – [Re(4-N$_3$-mesBIAN)(CO)$_3$Cl].

Table 3.2 Electronic absorption data for complexes [Re(NN)(CO)$_3$Cl] in CH_2Cl_2 at r.t

Complex	**λ_{max} / nm (ε / M^{-1} cm^{-1})**
[Re(mesBIAN)(CO)$_3$Cl]	294 (18900), 332 (8790), 374 (7740), 502 (9760)
[Re(4-COOEt-mesBIAN)(CO)$_3$Cl]	300 (13300), 336 (8660), 396 (6500), 510 (6940)
[Re(4-N$_3$-mesBIAN)(CO)$_3$Cl]	308 (14500), 407 (11400), 511 (9400)
[Re(mesBIphen)(CO)$_3$Cl]	300 (16400), 555 (15700)

The set of intense absorption bands below 350 nm observed in the spectra of all complexes are assigned to intraligand transitions, most likely π-π* transitions based on the ring system of aryl-BIAN/BIphen ligands. All of the complexes also had an absorption band in the region of 500-550 nm which was assigned to the MLCT of each complex. The MLCT bands for the complexes [Re(mesBIAN)$(CO)_3$Cl] and [Re(4-N_3-mesBIAN)$(CO)_3$Cl] had a similar position and intensity, 502 nm (9760 M^{-1} cm^{-1}) and 511 nm (9440 M^{-1} cm^{-1}), respectively, however this band in [Re(4-N_3-mesBIAN)$(CO)_3$Cl] was much broader and tailed off to wavelengths above 900 nm. The electronic absorption profile for [Re(4-COOEt-mesBIAN)$(CO)_3$Cl] was most similar to that of [Re(mesBIAN)$(CO)_3$Cl] but with a less intense (6940 M^{-1} cm^{-1}) MLCT transition (510 nm). For the complex [Re(mesBIphen)$(CO)_3$Cl], MLCT transition was assigned to a very intense electronic absorption (15700 M^{-1} cm^{-1}) band at a longer wavelength to the other complexes (550 nm).

The absorption spectra show good agreement with the predicted spectra obtained from the optimised geometries calculated by Heather Carson. These spectra are shown below, red sticks indicate the wavelength at with the transition is predicted to occur and the height of the stick indicating its predicted intensity (Figure 3.30 - Figure 3.33).

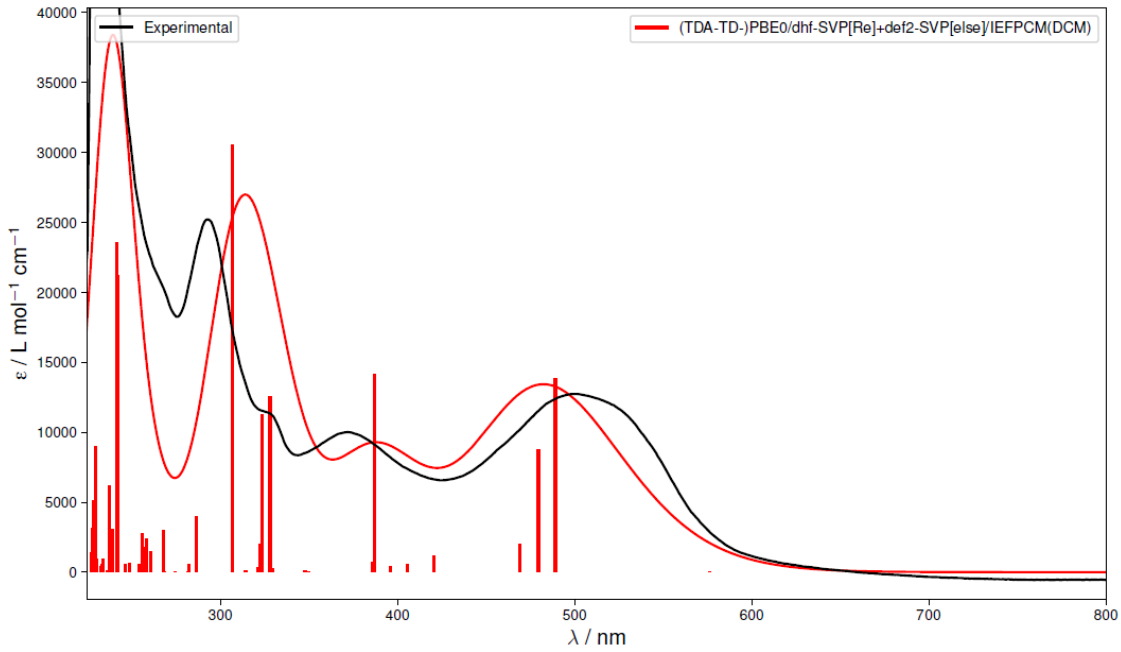

Figure 3.30 Experimental electronic absorption spectrum - black line, calculated spectrum - red line, for the complex [Re(mesBIAN)$(CO)_3$Cl].

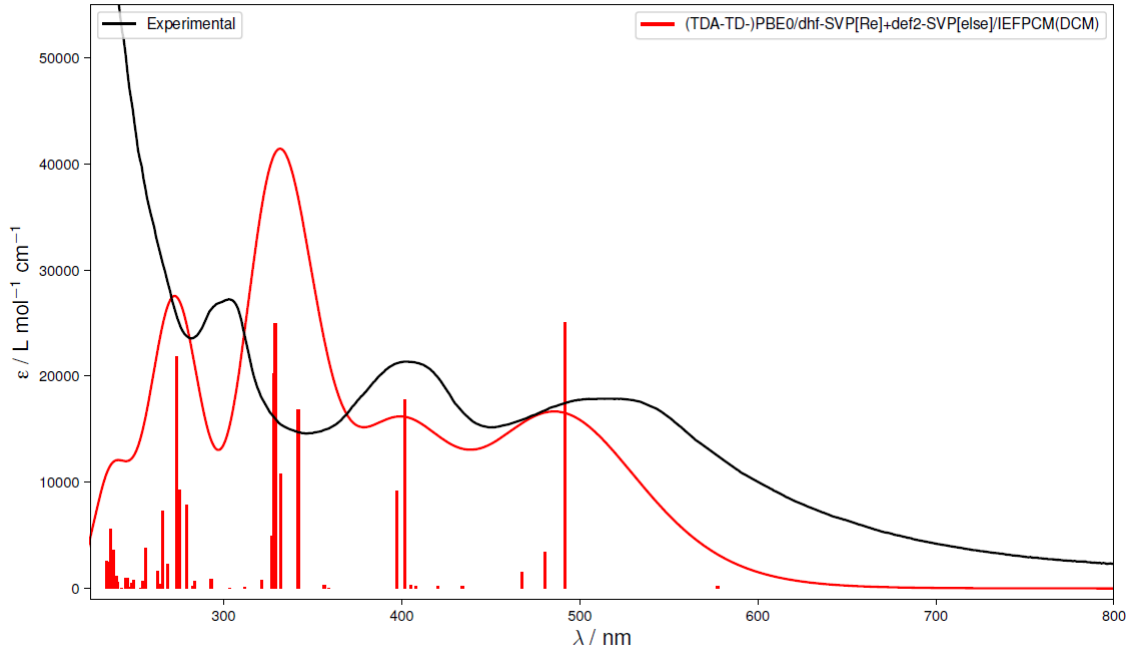

Figure 3.31 Experimental electronic absorption spectrum - black line, calculated spectrum - red line, for the complex [Re(4-COOEt-mesBIAN)(CO)$_3$Cl].

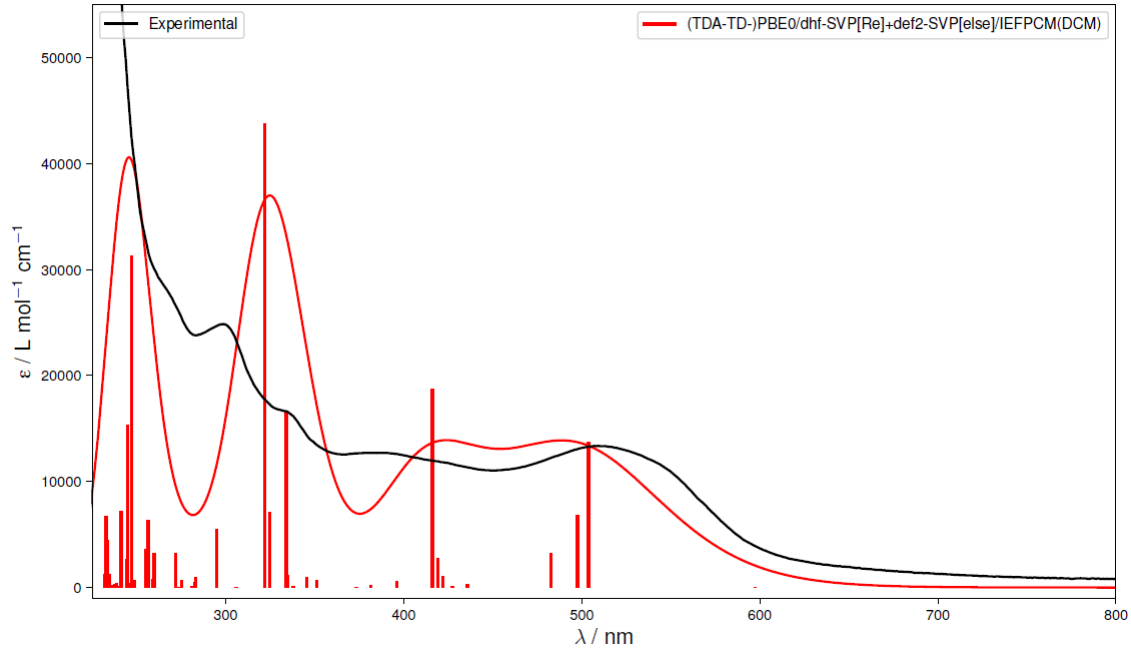

Figure 3.32 Experimental electronic absorption spectrum - black line, calculated spectrum - red line, for the complex [Re(4-N$_3$-mesBIAN)(CO)$_3$Cl].

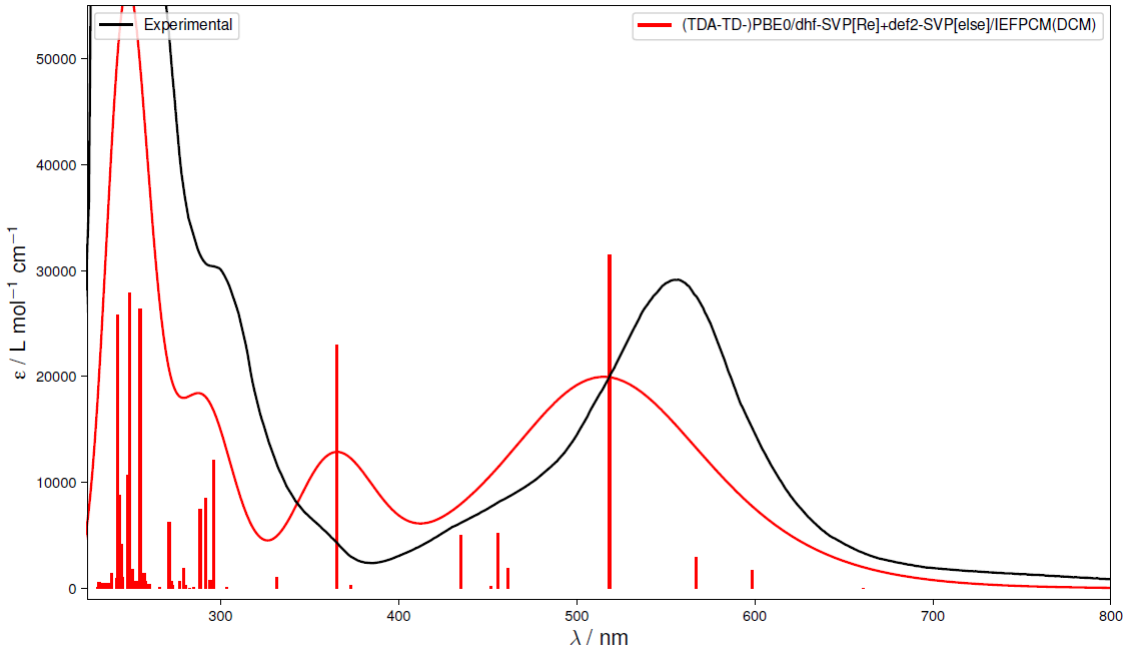

Figure 3.33 Experimental electronic absorption spectrum - black line, calculated spectrum - red line, for the complex [Re(mesBIphen)(CO)$_3$Cl].

3.3.5 FTIR absorption spectroscopy

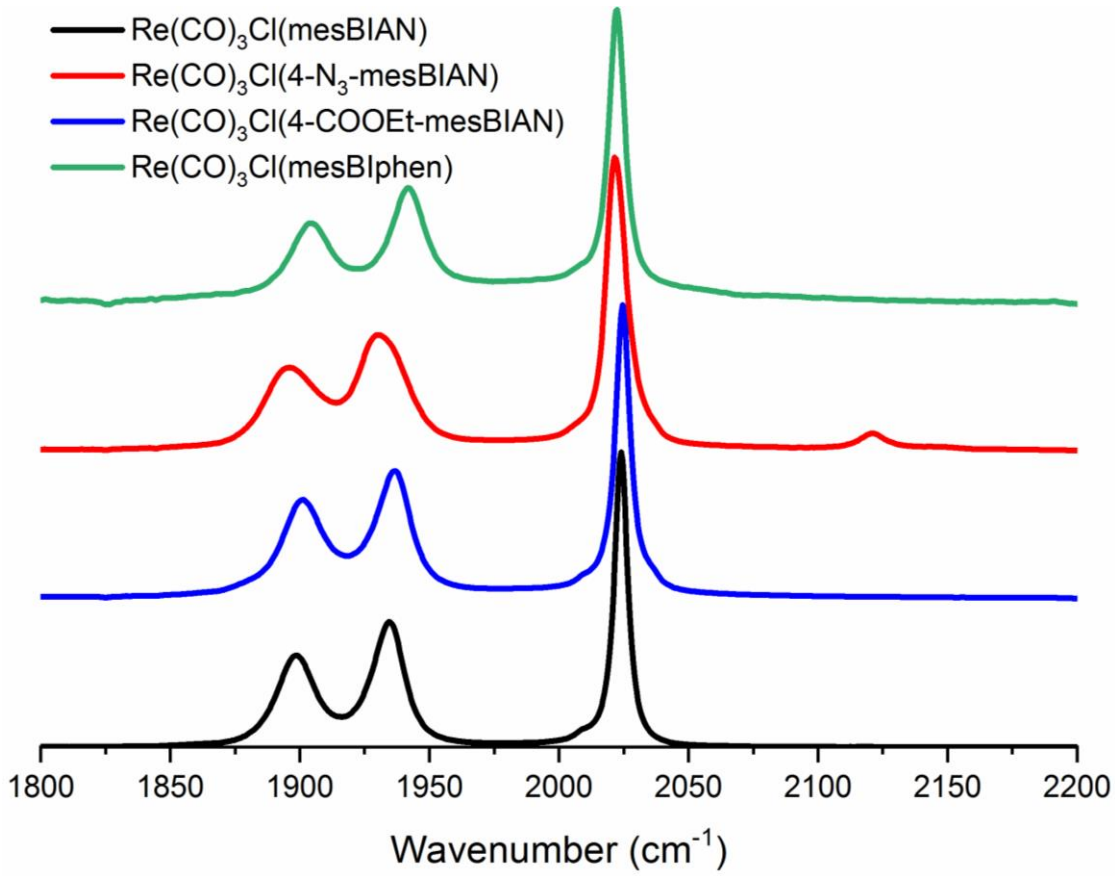

Figure 3.34 Steady state IR vibrational absorption spectra of complexes [Re(4-R-mesBIAN)(CO)$_3$Cl] in CH_2Cl_2 at r.t. Black line – [Re(mesBIAN)(CO)$_3$Cl] Blue line – [Re(4-COOEt-mesBIAN)(CO)$_3$Cl] Red line – [Re(4-N$_3$-mesBIAN)(CO)$_3$Cl], Green line – [Re(mesBIphen)(CO)$_3$Cl].

Table 3 Vibrational absorption bands for complexes [Re(NN)(CO)$_3$Cl] in CH_2Cl_2 at r.t

Complex	**$\tilde{\nu}$ / cm^{-1}**
[Re(mesBIAN)(CO)$_3$Cl]	1899, 1935, 2024
[Re(4-COOEt-mesBIAN)(CO)$_3$Cl]	1720, 1901, 1937, 2025
[Re(4-N$_3$-mesBIAN)(CO)$_3$Cl]	1896, 1931, 2022, 2121
[Re(mesBIphen)(CO)$_3$Cl]	1904, 1942, 2023

The FTIR spectra for all four complexes, which are C_S point group, contained three intense carbonyl stretching vibrations associated with the A'(1) + A'(2) + A'' stretches at 1899, 1935 and 2024 cm^{-1} for the unsubstituted mesBIAN complex; 1901, 1937 and 2025 cm^{-1} for [Re(4-COOEt-mesBIAN)$(CO)_3$Cl]; 1896, 1931 and 2022 cm^{-1} for the azido-mesBIAN complex; 1904, 1942 and 2023 cm^{-1} for the mesBIphen complex. The complex [Re(4-N_3-mesBIAN)$(CO)_3$Cl] also featured an azide stretch at 2121 cm^{-1}.

The calculated spectra shown below were plotted by Heather Carson and show a good agreement with the experimental spectra (Figure 3.35 - Figure 3.38). The predicted spectra show good agreement with all three stretching modes of the metal carbonyls for the complexes ***3.8***, ***3.9***, ***3.10*** and ***3.11*** along with the additional ester carbonyl at 1700 cm^{-1}. Complex ***3.10*** also shows an azide band at approximately 2120 cm^{-1}

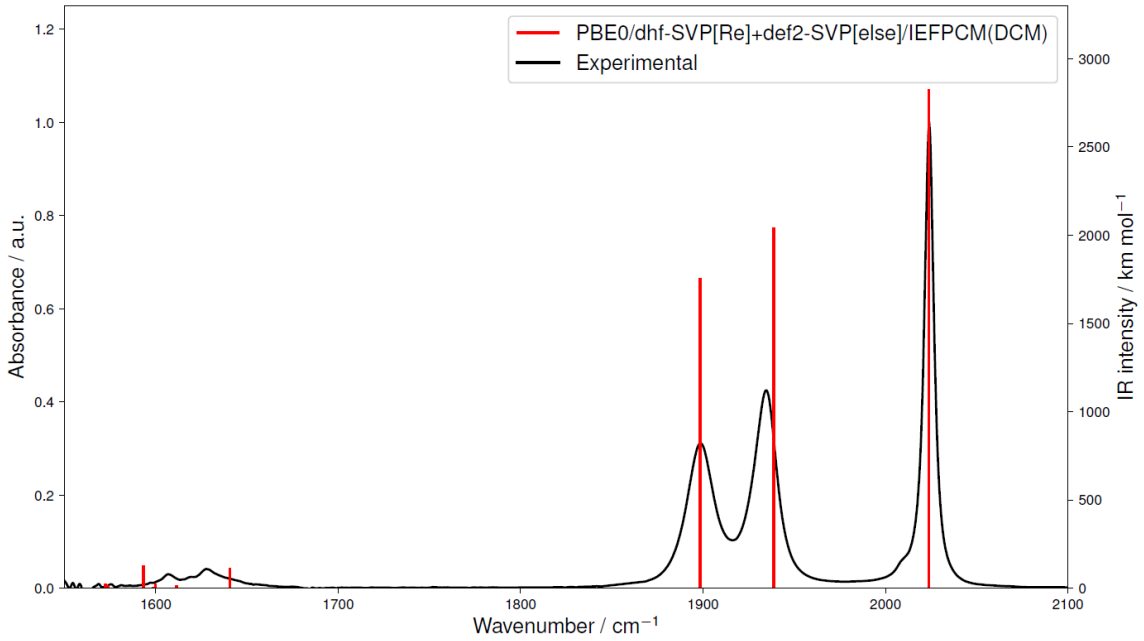

Figure 3.35 Experimental vibrational spectrum - black line, calculated spectrum - red line, for the complex [Re(mesBIAN)$(CO)_3$Cl].

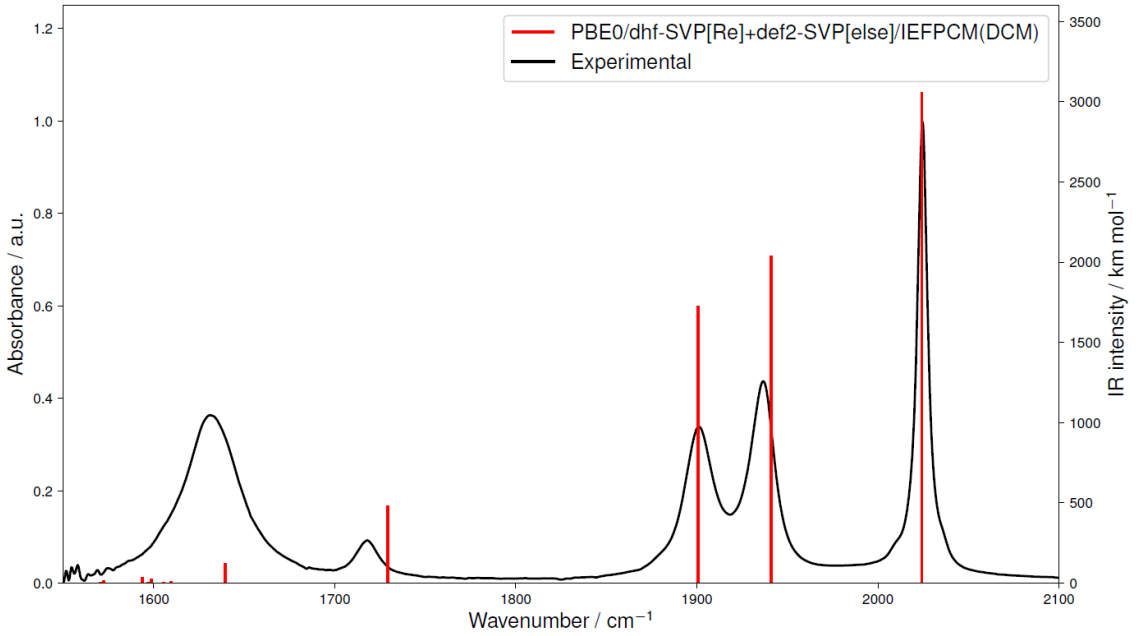

Figure 3.36 Experimental vibrational spectrum - black line, calculated spectrum - red line, for the complex [Re(4-COOEt-mesBIAN)(CO)$_3$Cl]

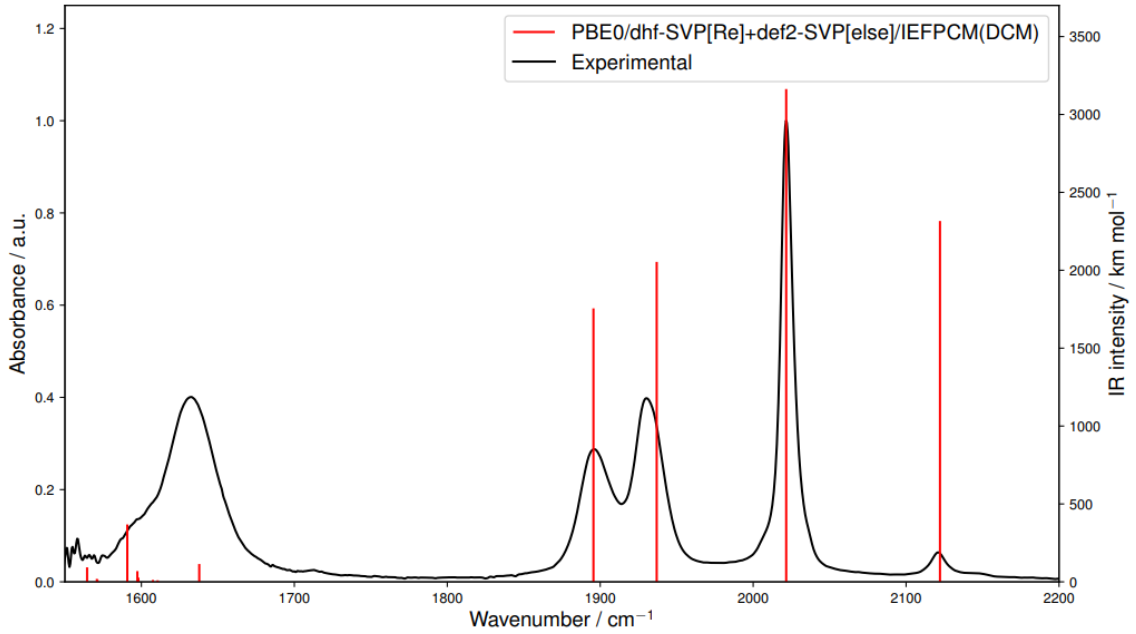

Figure 3.37 Experimental vibrational spectrum - black line, calculated spectrum - red line, for the complex [Re(4-N$_3$-mesBIAN)(CO)$_3$Cl].

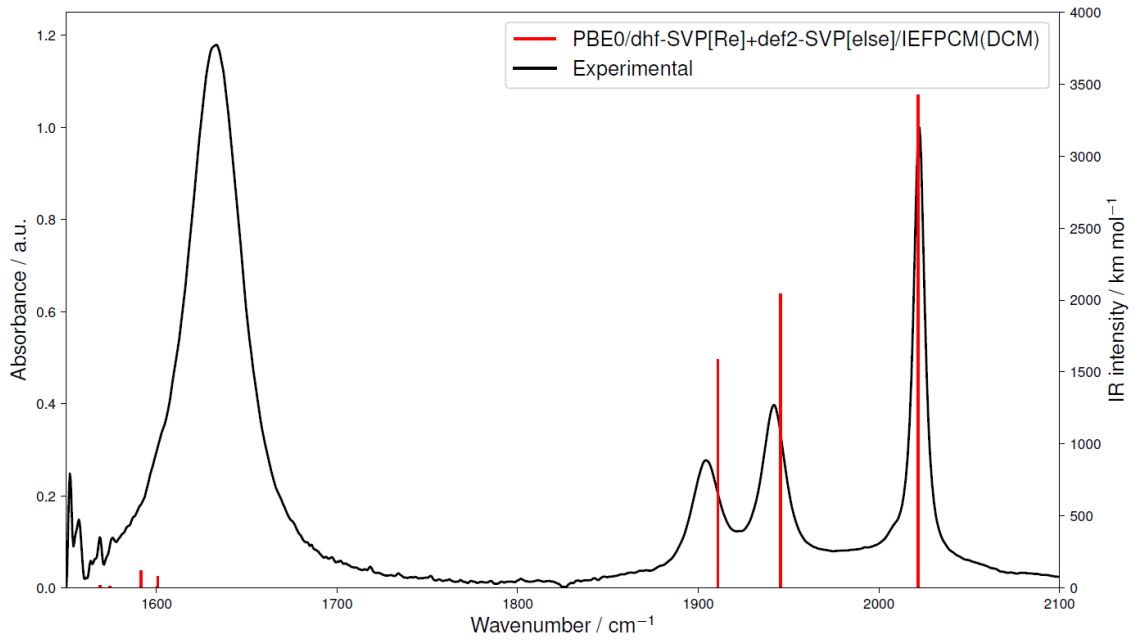

Figure 3.38 Experimental vibrational spectrum - black line, calculated spectrum - red line, for the complex [Re(mesBIphen)(CO)$_3$Cl].

3.3.6 Cyclic voltammetry

In order to evaluate the catalytic activity of the compounds, cyclic voltammetry studies have been performed. Briefly, an approximately 1mM solution of a complex would be investigated under N_2 atmosphere, CO_2 atmosphere in dry solvent, and CO_2 atmosphere in presence of a Bronsted acid. The catalytic activity would be evidenced by current enhancement in the presence of CO_2. The ratio of the current observed under CO_2 vs. under N_2 can be used as an indication of catalytic efficiency. Of course such comparisons need to be evaluated with care, and generally are only valid for a series of similar compounds (size, charge). Dr. Steven Spall assisted with the collection of the following data (Figure 3.39 - Figure 3.41).

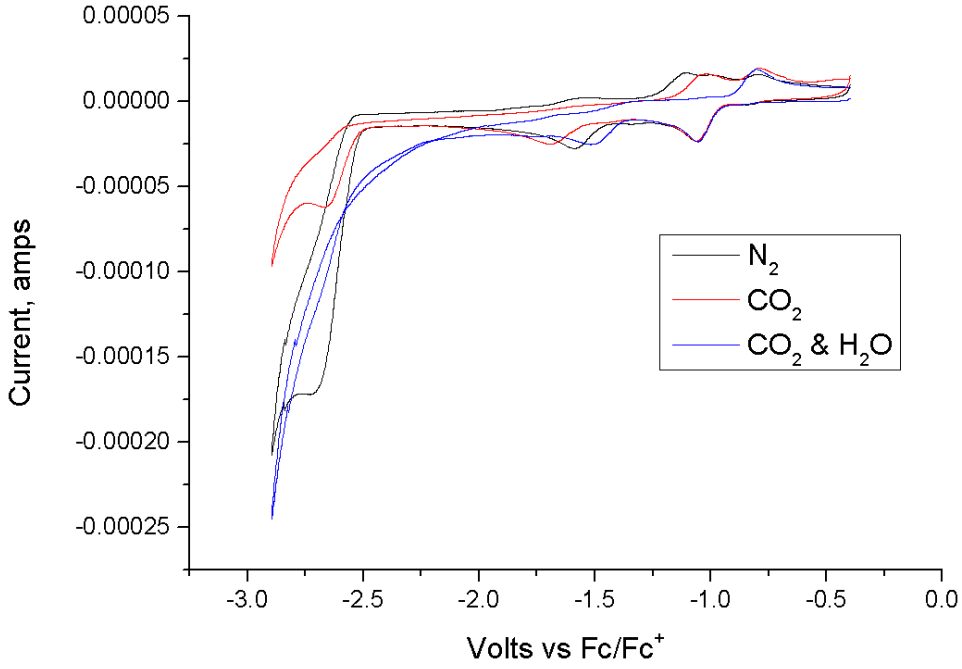

Figure 3.39 CV traces of [Re(mesBIAN)(CO)$_3$Cl] under N_2, CO_2 and CO_2 with 0.3 ml of H_2O in 6 ml of dry MeCN with 0.2 M TBAPF.

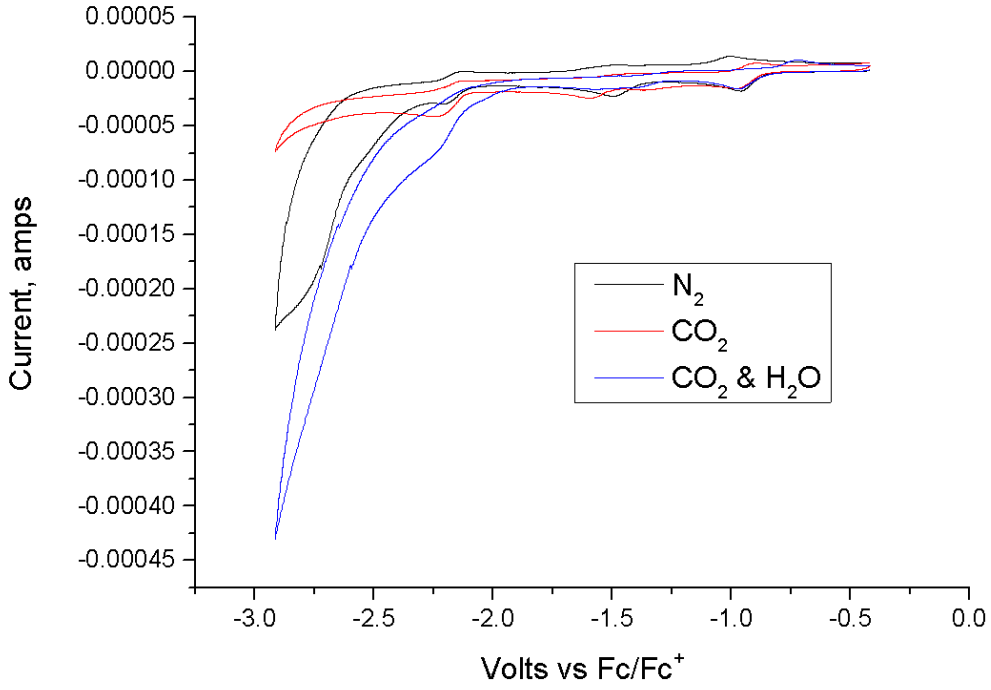

Figure 3.40 CV traces of [Re(4-COOEt-mesBIAN)(CO)$_3$Cl] under N_2, CO_2 and CO_2 with 0.3 ml of H_2O in 6 ml of dry MeCN with 0.2 M TBAPF.

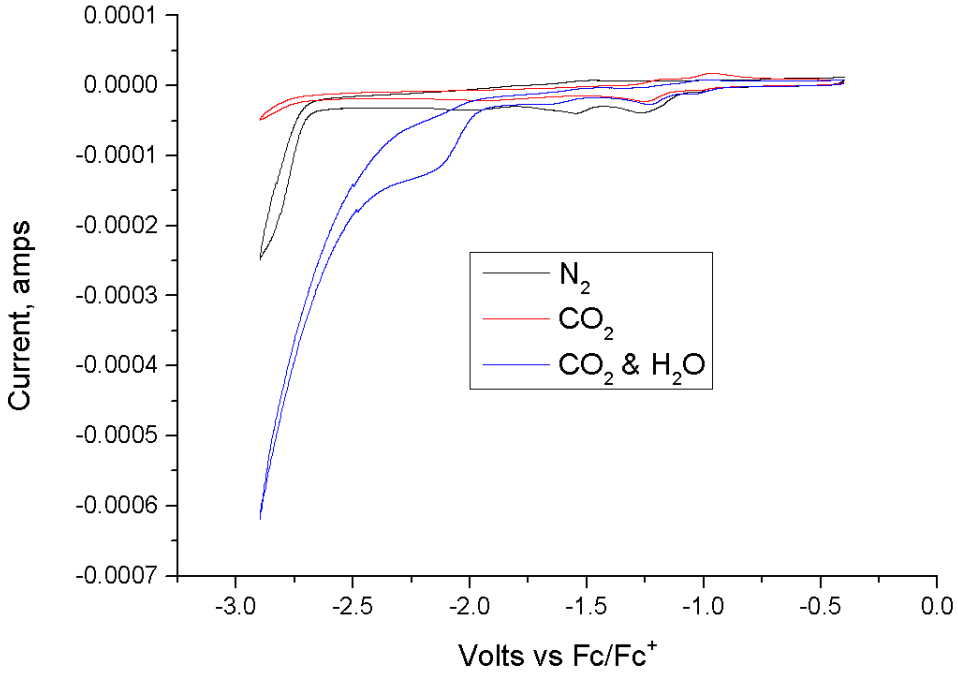

Figure 3.41 CV traces of [Re(4-N_3-mesBIAN)$(CO)_3$Cl] under N_2, CO_2 and CO_2 with 0.3 ml of H_2O in 6 ml of dry MeCN with 0.2 M TBAPF.

The CV data show current enhancement observed between the experiments performed under "CO_2 + water" vs. CO_2 alone. The control experiment (no compound, "solvent + electrolyte + CO_2 + water") showed no current enhancement in comparison to "solvent + electrolyte + CO_2 + dry acetonitrile".

3.3.7 X-ray crystallography

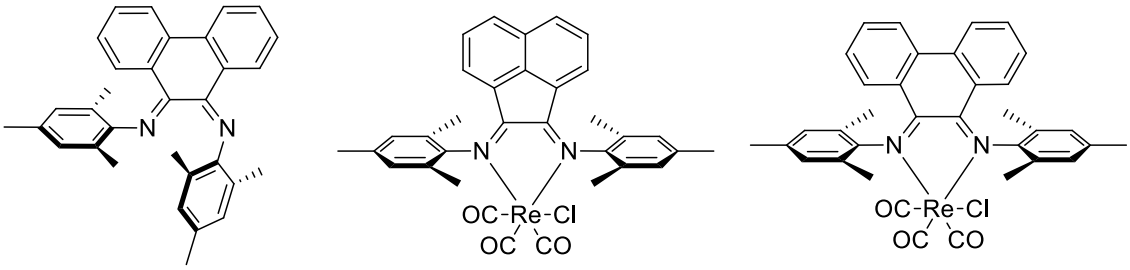

*Figure 3.42 Chemical structures of **3.7** (left), **3.8** (middle), **3.11** (right).*

Summary of the single-crystal data of **3.7 3.8 3.11**			
	3.7	**3.8**	**3.11**
	mesBIPhen	**Re(mesBIAN)(CO)$_3$Cl**	**Re(mesBIPhen)(CO)$_3$Cl**
	$C_{32}H_{30}N_2$	$C_{33}H_{28}ClN_2O_3Re$	$C_{73}H_{67}Cl_2N_4O_6Re_2$
Crystal habit	Block	Plate	Needle
Crystal colour	Red	Red	Colourless
Crystal size (mm)	0.430 x 0.320 x 0.290	0.280 x 0.210 x 0.120	0.310 x 0.110 x 0.110
Crystal system	Monoclinic	Monoclinic	Triclinic
Space group	C2/c	P21/n	P-1
a (Å)	34.032(5)	11.035(5)	12.6447(7)
b (Å)	7.9843(12)	16.273(8)	14.3999(7)
c (Å)	18.503(3)	16.829(9)	17.8420(9)
α (˚)	90	90	83.833(3)
β (˚)	97.517(2)	92.29(2)	86.968(4)
γ (˚)	90	90	88.142(3)
V (Å^3)	4984.5(13)	3020(3)	3224.2(3)
Density (g cm^{-3})	1.18	1.589	1.586
Temperature (K)	97(2)	296(2)	97(2)
μ (mm^{-1})	0.068	4.148	3.89
Wavelength (Å)	0.71073	0.71073	0.71073
θ range (˚)	2.220 to 27.460	1.741 to 27.790	1.149 to 24.943
Reflns. collected	18946	44266	52167
Independent reflns. (R_{int})	5268 [R(int) = 0.0395]	6486 [R(int) = 0.0470]	10887 [R(int) = 0.0851]
Reflns. used in refinement, *n*	5268	6486	10887
LS parameters, *p*	313	367	758
Restraints, *r*	0	268	570
R1 (*F*)[a] *I>2.0s(I)*	0.0418	0.0366	0.0515
wR2 (*F2*)[a], all data	0.1186	0.0966	0.1551
σ(*F2*)[a], all data	1.010	1.012	1.076

a =*R1*(*F*) = Σ(|*Fo*| – |*Fc*|)/Σ|Fo| ; *wR2*(*F2*) =[Σw(*Fo2* – *Fc2*)^2/ΣwFo4]$^{1/2}$; *S*(*F2*) = [Σw(*Fo2* – *Fc2*)^2/(*n* + *r* – *p*)]$^{1/2}$

Table 3.4 A summary of the crystallographic for the compounds 3.7, 3.8 and 3.11.

3.3.8 Evaluating potential of Re(I) complexes as photocatalysts.

In order to evaluate the potential of new Re(I) complex as photocatalysts for CO_2 reduction, one first needs to investigate the nature of their lowest excited states, and the excited state dynamics. The presence of CO-vibrations allowed us to use time-resolved IR spectroscopy to answer these questions as they are strong IR reporters.

3.3.9 Time resolved infrared spectroscopy

The TRIR studies were conducted at the Rutherford Appleton Laboratory, STFC. The details of the experimental set up are given in Chapter 2, and by Greetham *et al.*[55]
The TRIR studies were conducted in CH_2Cl_2 solution (approx.. 1 mM concentration) under 400 nm, ~100 fs laser excitation. The spectra were collected in the range from ~1200 to 2300 cm^{-1}, over the time span from ~100 fs to 4 ns (the experimental limit of the set-up used).

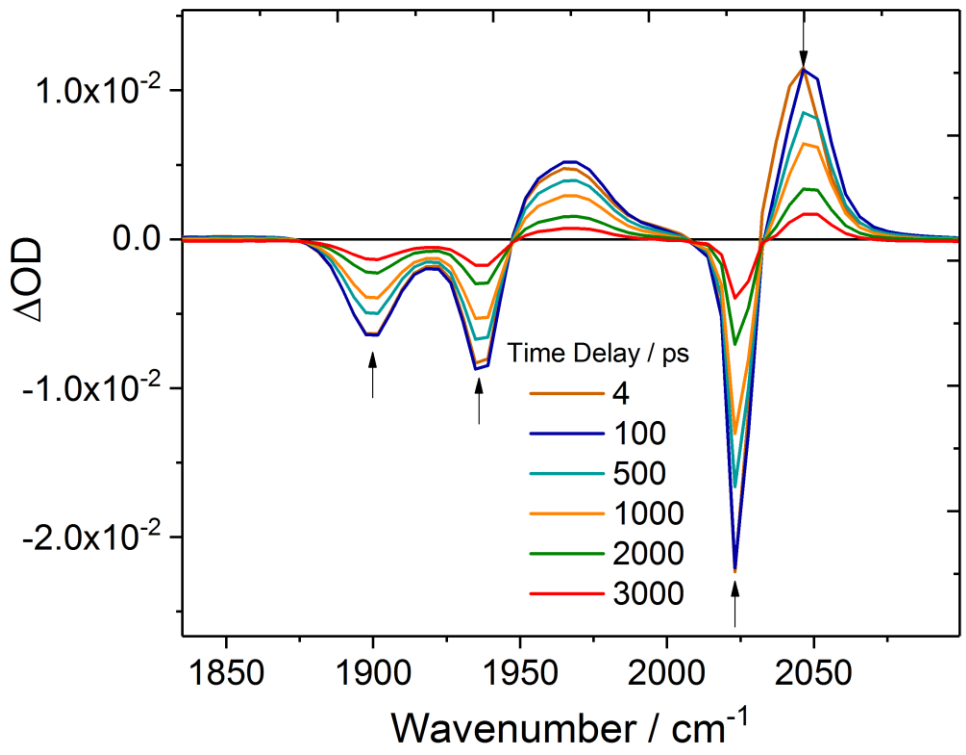

Figure 3.43 The TRIR spectra at selected time delays for [Re(mesBIAN)(CO)$_3$Cl].

Time resolved infrared spectra for [Re(mesBIAN)(CO)$_3$Cl] at selected time delays are shown in (Figure 3.43). Excitation of the complex at the MLCT band leads to formation of the transient bands at 1965 and 2046 cm^{-1} and carbonyl bleaches at 1900, 1935 and 2023 cm^{-1} which rise with the instrument response. The transient at 2046 cm^{-1} decays with a lifetime of ca 600 ps which is concurrent with the recovery of the bleach at 2023 cm^{-1} (Figure 3.44). The fact that the transients grow in at a higher energy than the bleaches confirms the assignment of the lowest excited state as an MLCT state: due to the decreased electron density on the rhenium centre which weakens the metal-to-carbonyl back-donation, in turn increasing the carbonyl CO bond strength thus shifting the vibration to a higher energy. The lifetime of the ^{3}MLCT state is 605 ps. It is important to note that such short lifetime is not sufficient for electron transfer to a molecule of CO_2 in a bimolecular reaction. Therefore, this compound will either be a poor photocatalyst, or needs to operate via first forming a complex with CO_2, which then undergoes electron transfer inside the complex.

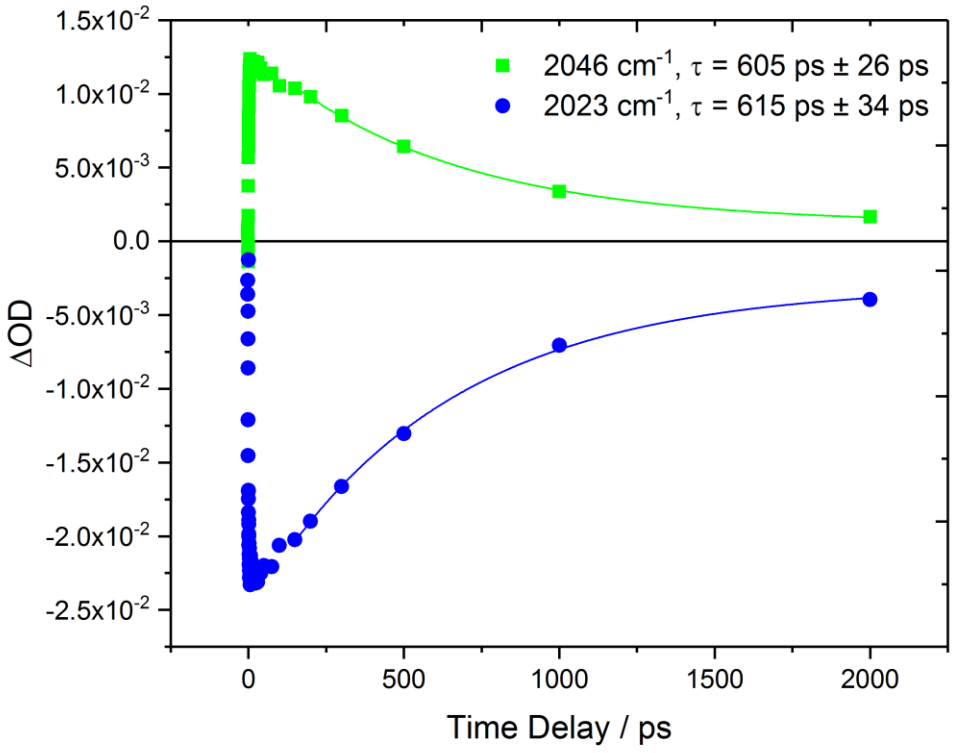

Figure 3.44 Single point kinetic analysis for [Re(mesBIAN)(CO)$_3$Cl] at 2046 cm^{-1} and 2023 cm^{-1}.

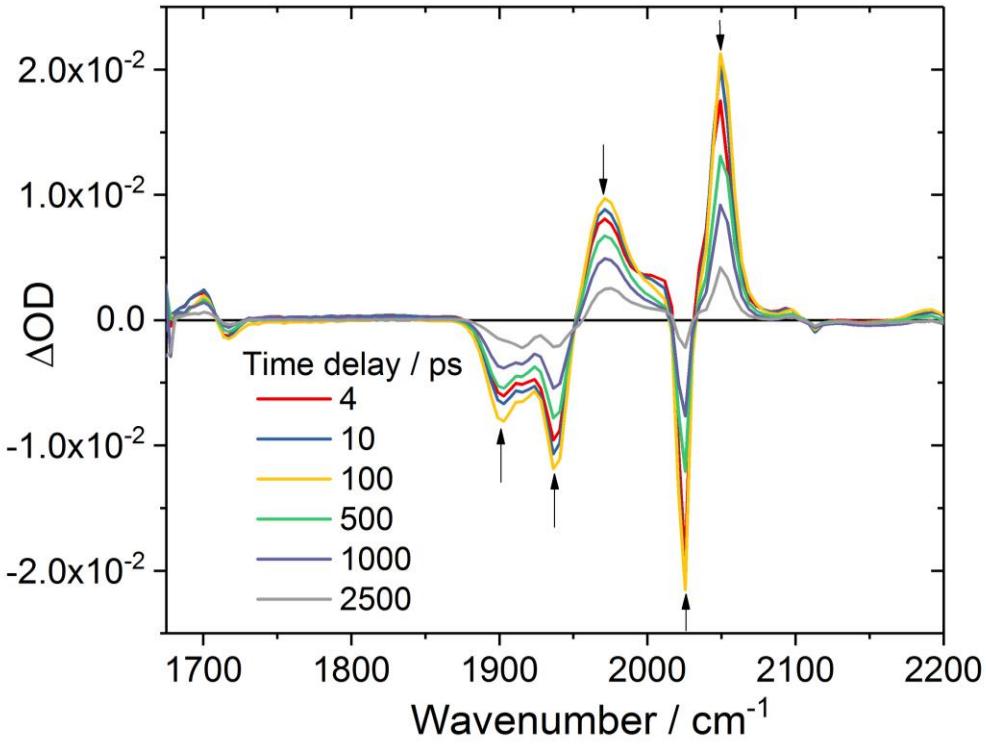

Figure 3.45 The TRIR spectra at selected time delays for [Re(4-COOEt-mesBIAN)(CO)$_3$Cl].

Time resolved infrared spectra for [Re(4-COOEt-mesBIAN)(CO)$_3$Cl] at selected time delays are shown in (Figure 3.45). Excitation of the complex at the MLCT band leads to formation of the transient bands at 1700, 1971 and 2049 cm^{-1} and carbonyl bleaches at 1717, 1901, 1937 and 2027 cm^{-1} which rise with the instrument response. The transient at 2049 cm^{-1} decays with a lifetime of ca 1500 ps which is different to the 1190 ps recovery time of the bleach at 2025 cm^{-1}(Figure 3.46). This difference is likely due to the fact that there is slight overlap with the transient and bleaches in this region, and this was determined from a single-point kinetics. As stated above for [Re(mesBIAN)(CO)$_3$Cl] the transients grow in at a higher energy than the bleaches confirms the assignment of the lowest excited state as an MLCT state: due to the decreased electron density on the rhenium centre which weakens the metal-to-carbonyl back-donation, in turn increasing the carbonyl CO bond strength thus shifting the vibration to a higher energy. The lifetime of the ^{3}MLCT state is 1506 ps. As stated with the [Re(mesBIAN)(CO)$_3$Cl] complex short lifetimes are not sufficient for electron transfer to a molecule of CO_2 in a bimolecular reaction. The lifetime is more than double that of the unsubstituted mesBIAN complex. Therefore, this compound will either be a poor photocatalyst, or needs to operate via first forming a complex with CO_2, which then undergoes electron transfer inside the complex.

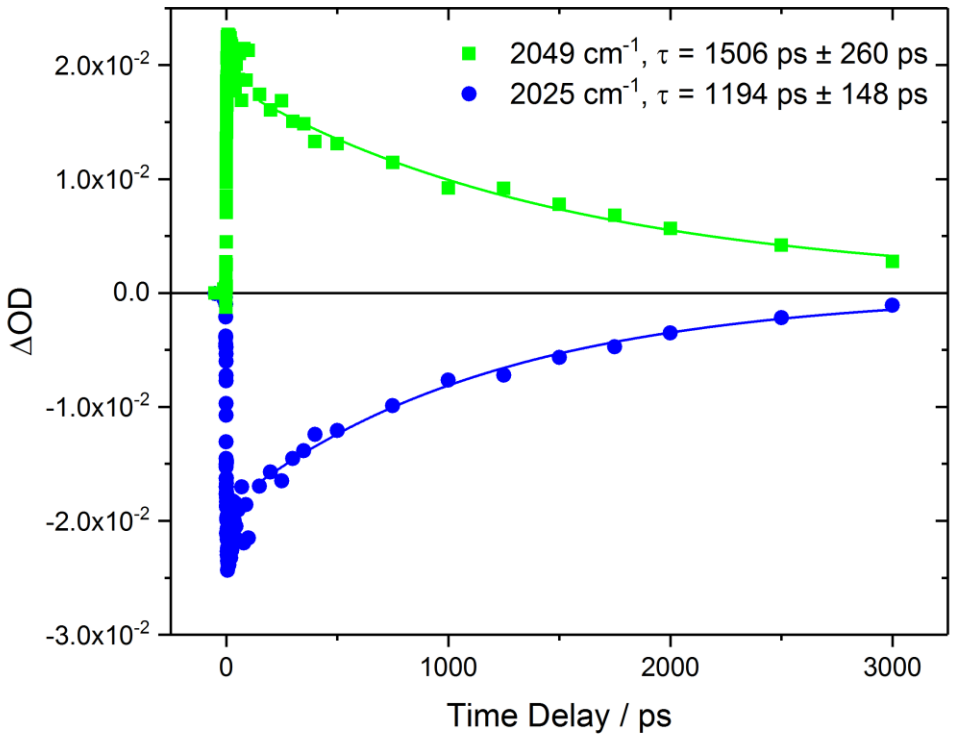

Figure 3.46 Single point kinetic analysis for [Re(4-COOEt-mesBIAN)(CO)$_3$Cl] at 2049 cm^{-1} and 2025 cm^{-1}.

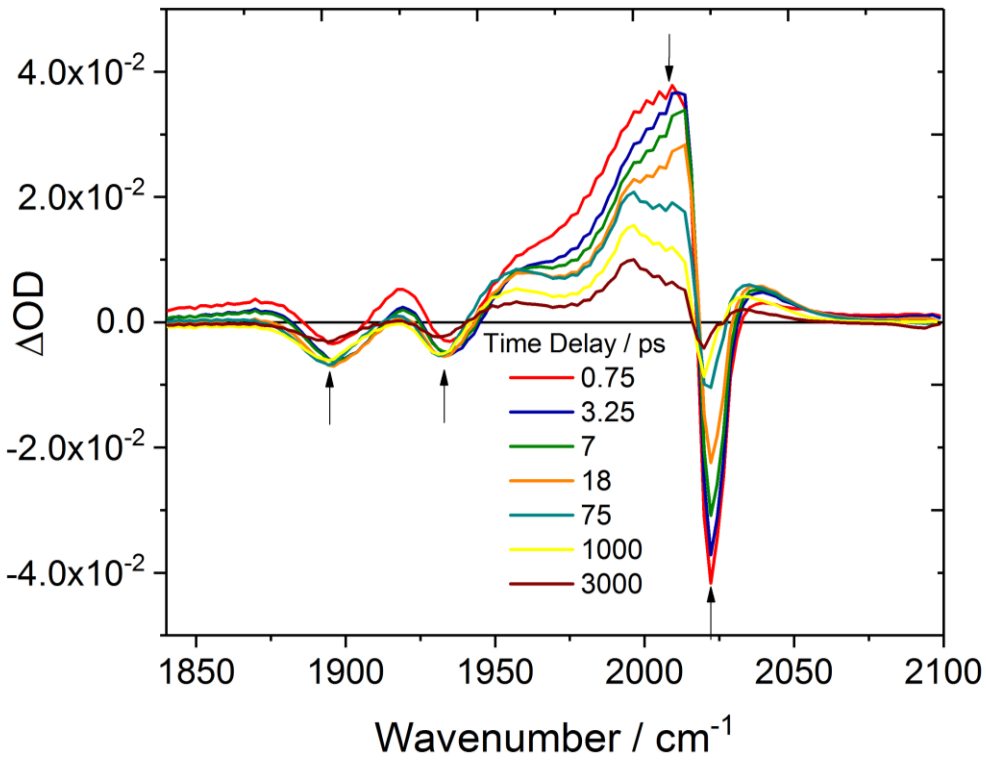

Figure 3.47 The TRIR spectra at selected time delays for [Re(4-N$_3$-mesBIAN)(CO)$_3$Cl].

Time resolved infrared spectra for [Re(4-N_3-mesBIAN)$(CO)_3$Cl] at selected time delays are shown in (Figure 3.47). Excitation of the complex at the MLCT band leads to formation of the transient bands at 1918, 1960 and 2009 cm^{-1} and carbonyl bleaches at 1894, 1933, and 2022 cm^{-1} which rise with the instrument response. The transient at 2009 cm^{-1} decays in a biexponential manner with lifetimes of 36 and 1984 ps. The recovery of the bleach at 2022 cm^{-1} is also biexponential with lifetimes of 29 and 1336 ps (Figure 3.48). The biexponential decay, and the change in the spectral position of the transients with time in the case of [Re(4-N_3-mesBIAN)$(CO)_3$Cl] indicates that the initially populated excited state is converting into either a different excited state, or retains its CT-character but undergoes structural reorganization which involves the N_3-group. It is also possible that the ~30 ps component is due to metal carbonyl vibrational relaxation. Global analysis of the data is currently underway in order to accertain excited state dynamics.

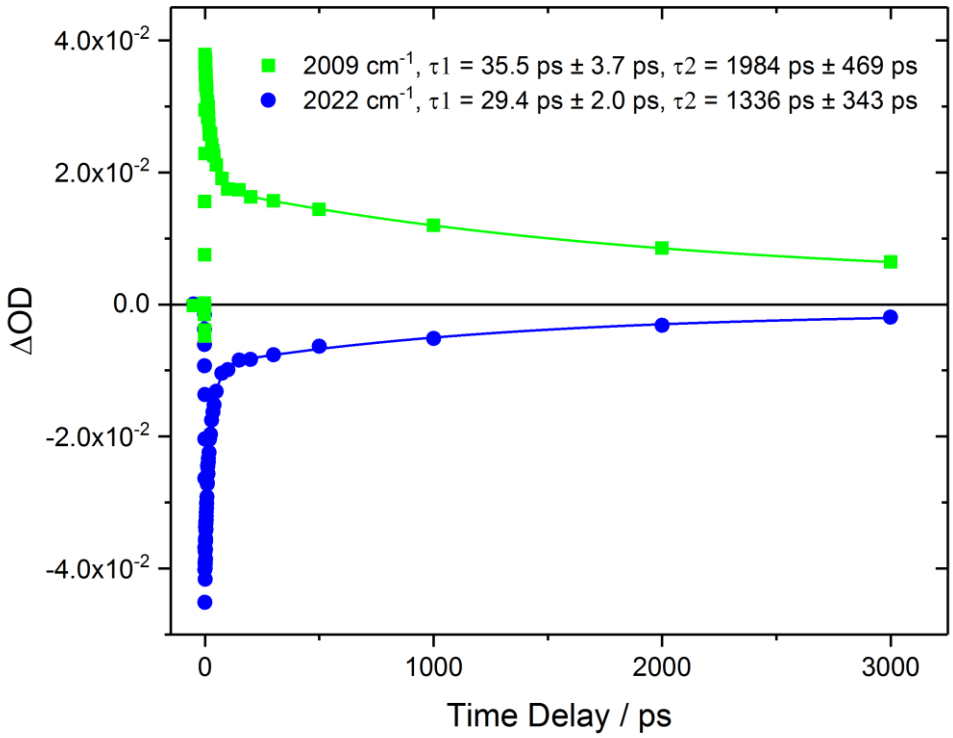

Figure 3.48 Single point kinetic analysis for [Re(4-N_3-mesBIAN)$(CO)_3$Cl] at 2009 cm^{-1} and 2022 cm^{-1}.

3.3.10 Assessment of photocatalytic activity

The experiment was initially tested using a known photocatalyst [Re(dmbpy)$(CO)_3$Cl] which showed a strong CO peak in the GC trace after one hour that increased in strength over one-hour time intervals. This control confirmed that the experiment was suitable to test whether the complexes discussed in this chapter were photocatalysts for the reduction of CO_2 to CO.
Complexes ***3.8***, ***3.9***, ***3.10*** and ***3.11*** were all tested under the conditions described with 6 hours of irradiation. No CO was detected by GC for any of the complexes and therefore it was concluded that they were not photo catalytically active towards the reduction of CO_2 to CO.

3.4 Conclusions

A series of novel rhenium(I) tricarbonyl complexes with systematically varied α-diimmine ligands have been synthesised and their ground and excited state properties investigated (Table 3.5). The diimmine ligands were mesBIAN, 4-COOEt-mesBIAN, 4-N_3-mesBIAN and mesBIPhen.

Whilst the series of complexes reported here did not show any function as photo-catalysts in the experiments conducted, they do show interesting photophysics that change upon altering of the ligands electronic properties. Preliminary data indicate that the compounds can be electrocatalytically active towards CO_2 reduction, the detailed studies are currently underway.

Complex	**ν (ground state) / cm^{-1}**		**ν (excited state) / cm^{-1}**	**Excited state lifetime / ps**	**Absorption / nm (ε /M^{-1} cm^{-1})**	
	Solvent				*Solvent*	
[Re(mesBIAN)(CO)$_3$Cl]	CH_2Cl_2	2024	2046	605 ± 26	CH_2Cl_2	502 (9760)
		1935	1965			374 (7740)
		1889				332 (8790)
						294 (18900)
[Re(4-COOEt-mesBIAN)(CO)$_3$Cl]	CH_2Cl_2	2025	2027	1506 ± 260	CH_2Cl_2	510 (6940)
		1937	1937			396 (6500)
		1901	1901			336 (8660)
		1720	1700			300 (13300)
[Re(4-N$_3$-mesBIAN)(CO)$_3$Cl]	CH_2Cl_2	2121	2009	1984 ± 469	CH_2Cl_2	511 (9440)
		2022	1960			407 (11400)
		1931	1918			308 (14500)
		1896				
[Re(mesBIphen)(CO)$_3$Cl]	CH_2Cl_2	2023	-	-	CH_2Cl_2	555 (15700)
		1942				300 (16400)
		1904				

Table 3.5 A summary of the properties of the rhenium complexes studied in this chapter

3.5 Future work

Rhenium(I) α-diimmine tricarbonyl halide complexes have shown huge promise as photocatalysts for the reduction of CO_2 to useable fuels, and they are still of interest.[56,57] However research in recent years has shown a shift towards cheaper, more sustainable catalysts that utilise earth abundant metals in contrast to rare earth metals.[58] A wealth of research focuses on manganese(I) α-diiimine tricarbonyl halide catalysts as cheaper alternatives,[59] however these are often photo-unstable and have been shown to proceed via much different mechanisms than their rhenium counterparts.[60]

In future it would be of interest to synthesise manganese complexes bearing the ligands described in this chapter to study. The ligands of the type *bis*-aryl-imino acenaphthene are modifiable at the aryl group where more steric bulk can be introduced around the metal centre, this is of interest as catalysts based on manganese have been shown to degrade via formation of a Mn-Mn dimer that may not be possible to form with too much steric hindrance around the Mn centre.[61]

3.6 References

1 E. E. Benson, C. P. Kubiak, A. J. Sathrum and J. M. Smieja, *Chem. Soc. Rev.*, 2009, **38**, 89–99.

2 A. J. Morris, G. J. Meyer and E. Fujita, *Acc. Chem. Res.*, 2009, **42**, 1983–1994.

3 B. A. De Klerk and E. Furimsky,*Catalysis in the Refining of Fischer-Tropsch Syncrude,* 2010, 11–23.

4 E. W. Abel and G. Wilkinson, *J. Chem. Soc.*, 1959, 1501–1505.

5 Manfred Noak and T. Kruck, *Eur. J. Inorg. Chem.*, 1963, **96**, 3028–3034.

6 M. Hofler and T. Kruck, *Eur. J. Inorg. Chem.*, 1963, **96**, 3035–3043.

7 U. Sartorelli, F. Canziani and F. Zingales, *Inorg. Chem.*, 1966, **5**, 2233–2236.

8 E. W. Abel and S. P. Tyfield, *Can. J. Chem.*, 1969, **47**, 4627–4633.

9 D. Vitali and F. Calderazzo, *Gazz. Chim. Ital.*, 1972, **102**, 587–596.

10 J. G. Dunn and D. A. Edwards, *J. Organometalic Chem.*, 1973, **61**, 323–328.

11 M. Wrighton and D. L. Morse, *J. Am. Chem. Soc.*, 1974, **96**, 998–1003.

12 M. S. Wrighton, D. S. Ginley and D. L. Morse, *J. Phys. Chem.*, 1974, **78**, 2229–2233.

13 M. S. Wrighton, D. L. Morse and L. Pdungsap, *J. Am. Chem. Soc.*, 1975, **97**, 2073–2079.

14 D. L. Morse and M. S. Wrighton, *J. Am. Chem. Soc.*, 1976, **98**, 3931–3934.

15 J. C. Luong, L. Nadjo and M. S. Wrighton, *J. Am. Chem. Soc.*, 1978, **100**, 5790–5795.

16 P. J. Giordano and M. S. Wrighton, *J. Am. Chem. Soc.*, 1979, **101**, 2888–2897.

17 S. M. Fredericks, J. C. Luong and M. S. Wrighton, *J. Am. Chem. Soc.*, 1979, **101**, 7415–7417.

18 J. C. Luong, R. A. Faltynek and M. S. Wrighton, *J. Am. Chem. Soc.*, 1979, **101**, 1597–1598.

19 J. C. Luong, R. A. Faltynek and M. S. Wrighton, *J. Am. Chem. Soc.*, 1980, **102**, 7892–7900.

20 J. Hawecker, J.-M. Lehn and R. Ziessel, *Chem. Commun.*, 1983, 536–538.

21 J.-M. Lehn and R. Ziessel, *Proc. Natl. Acad. Sci. U. S. A.*, 1982, **79**, 701–704.

22 A. Coleman, C. Brennan, J. G. Vos and M. T. Pryce, *Coord. Chem. Rev.*, 2008, **252**, 2585–2595.

23 S. Ranjan, S. Y. Lin, K. C. Hwang, Y. Chi, W. L. Ching, C. S. Liu, Y. T. Tao, C.

H. Chien, S. M. Peng and G. H. Lee, *Inorg. Chem.*, 2003, **42**, 1248–1255.

24 M. Fumanal, E. Gindensperger and C. Daniel, *Phys. Chem. Chem. Phys.*, 2018, **20**, 1134–1141.

25 J. R. Wagner and D. G. Hendricker, *J. Inorg. Nucl. Chem.*, 1975, **37**, 1375–1379.

26 K. Kalyanasundaram, *J. Chem. Soc. Faraday Trans. 2 Mol. Chem. Phys.*, 1986, **82**, 2401–2415.

27 P. Kurz, B. Probst, B. Spingler and R. Alberto, *Eur. J. Inorg. Chem.*, 2006, 2966–2974.

28 B. D. Rossenaar, D. J. Stufkens and A. Vlček, *Inorg. Chem.*, 1996, **35**, 2902–2909.

29 W. Hieber and H. Fuchs, *Zeitschrift für Anorg. und Allg. Chemie*, 1941, **248**, 269–275.

30 J. E. Yarnell, J. C. Deaton, C. E. McCusker and F. N. Castellano, *Inorg. Chem.*, 2011, **50**, 7820–7830.

31 R. Heydová, E. Gindensperger, R. Romano, J. Sýkora, A. Vlček, S. Záliš and C. Daniel, *J. Phys. Chem. A*, 2012, **116**, 11319–11329.

32 G. J. Stor, F. Hartl, J. W. M. Van Outersterp and D. J. Stufkens, *Organometallics*, 1995, **14**, 1115–1131.

33 M. Rajkumar, J. Bhuvaneswari, M. Velayudham, E. Rajkumar and S. Rajagopal, *J. Fluoresc.*, 2011, **21**, 1729–1737.

34 Y. Kou, Y. Nabetani, D. Masui, T. Shimada, S. Takagi, H. Tachibana and H. Inoue, *J. Am. Chem. Soc.*, 2014, **136**, 6021–6030.

35 Y. Kou, Y. Nabetani, D. Masui, T. Shimada, S. Takagi, H. Tachibana and H. Inoue, *J. Am. Chem. Soc.*, 2014, **136**, 6021–6030.

36 E. Portenkirchner, E. Kianfar, N. S. Sariciftci and G. Knör, *ChemSusChem*, 2014, **7**, 1347–1351.

37 F. P. A Johnson, M. W. George, F. Hartl and J. J. Turner, *Organometallics*, 1996, **15**, 3374–3387.

38 C. J. Adams, N. Fey and J. A. Weinstein, *Inorg. Chem.*, 2006, **45**, 6105–7.

39 G. A. Grasa, R. Singh, E. D. Stevens and S. P. Nolan, *J. Organomet. Chem.*, 2003, **687**, 269–279.

40 J. Yuan, Z. Zhang, W. Xu, J. Zhao, Y. Mu and J. Chen, *Transit. Met. Chem.*, 2014, **39**, 769–779.

41 E. Kianfar, C. Schafer, M. R. Lornejad-Schafer, E. Portenkirchner and G. Knör,

Inorganica Chim. Acta, 2015, **435**, 174–177.

42 M. J. Supej, A. Volkov, L. Darko, R. A. West, J. M. Darmon, C. E. Schulz, K. A. Wheeler and H. M. Hoyt, *Polyhedron*, 2016, **114**, 403–414.

43 X. Wang, L. Fan, C. Huang, T. Liang, C. Y. Guo and W. H. Sun, *J. Polym. Sci. Part A Polym. Chem.*, 2016, **54**, 3609–3615.

44 M. Khoshsefat, N. Beheshti, G. H. Zohuri, S. Ahmadjo and S. Soleimanzadegan, *Polym. Sci. - Ser. B*, 2016, **58**, 487–494.

45 A. K. Leone, K. D. Souther, A. K. Vitek, A. M. LaPointe, G. W. Coates, P. M. Zimmerman and A. J. McNeil, *Macromolecules*, 2017, **50**, 9121–9127.

46 F. Wang, R. Tanaka, Z. Cai, Y. Nakayama and T. Shiono, *Polymers (Basel).*, , DOI:10.3390/polym8040160.

47 U. El-Ayaan, F. Murata, S. El-Derby and Y. Fukuda, *J. Mol. Struct.*, 2004, **692**, 209–216.

48 T. Tu, Z. Sun, W. Fang, M. Xu and Y. Zhou, *Org. Lett.*, 2012, **14**, 4250–4253.

49 K. Hasan and E. Zysman-Colman, *J. Phys. Org. Chem.*, 2013, **26**, 274–279.

50 D. Huang and G. Yan, *Adv. Synth. Catal.*, 2017, **359**, 1600–1619.

51 C. Hansch, A. Leo and R. W. Taft, *Chem. Rev.*, 1991, **91**, 165–195.

52 G. A. Abakumov, N. O. Druzhkov, T. N. Kocherova, K. A. Kozhanov, A. V. Murugova and E. N. Egorova, *Dokl. Chem.*, 2016, **467**, 109–112.

53 L. Li, M. Jeon and S. Y. Kim, *J. Mol. Catal. A Chem.*, 2009, **303**, 110–116.

54 V. K. Cherkasov, N. O. Druzhkov, T. N. Kocherova, A. S. Shavyrin and G. K. Fukin, *Tetrahedron*, 2012, **68**, 1422–1426.

55 G. M. Greetham, P. Burgos, Q. Cao, I. A. N. P. Clark, P. S. Codd, R. C. Farrow, M. W. George, P. Matousek, A. W. Parker, M. R. Pollard, A. Robinson, Z. Xin and M. Towrie, *Appl. Spectrosc.*, 2010, **64**, 1311–1319.

56 A. Nakada and O. Ishitani, *ACS Catal.*, 2018, **8**, 354–363.

57 Y. Kuramochi, O. Ishitani and H. Ishida, *Coord. Chem. Rev.*, 2018, **373**, 333–356.

58 M. F. Kuehnel, C. D. Sahm, G. Neri, J. R. Lee, K. L. Orchard, A. J. Cowan and E. Reisner, *Chem. Sci.*, 2018, **9**, 2501–2509.

59 D. C. Grills, M. Z. Ertem, M. McKinnon, K. T. Ngo and J. Rochford, *Coord. Chem. Rev.*, 2018, **374**, 173–217.

60 G. Neri, J. J. Walsh, G. Teobaldi, P. M. Donaldson and A. J. Cowan, *Nat. Catal.*, 2018, 1.

61 H. Arakawa, M. Aresta, J. N. Armor, M. A. Barteau, E. J. Beckman, A. T. Bell, J. E. Bercaw, C. Creutz, E. Dinjus, D. A. Dixon, K. Domen, D. L. Dubois, J. Eckert, E. Fujita, D. H. Gibson, W. A. Goddard, D. W. Goodman, J. Keller, G. J. Kubas, H. H. Kung, J. E. Lyons, L. E. Manzer, T. J. Marks, K. Morokuma, K. M. Nicholas, R. Periana, L. Que, J. Rostrup-nielson, W. M. H. Sachtler, L. D. Schmidt, A. Sen, G. A. Somorjai, P. C. Stair, B. R. Stults, W. Tumas, X. C. Creutz, O. E. Dinjus and O. D. H. Gibson, *Chem. Rev.*, 2001, **101**, 953–996.

4 Structural reorganisation in the excited state of platinum(II) diimmine dithiolates

4.1 Introduction

4.1.1 Structural reorganisation via a transient S∴S

As previously discussed photoinduced charge transfer is an elementary process that is used in a variety of natural or man-made processes, *e.g*. photosynthesis and photocatalysis. The Donor-Bridge-Acceptor (D-B-A) complex is responsible for the photoinduced electron transfer step, involving $[D^{+}\text{-B-}A^{-}]^{*}$ as key transient. The reactivity of this state is dependant on the back-electron transfer to the ground state. Controlling back electron transfer in D-B-A complexes remains a challenge. The following work discusses a series of platinum(II) diimmine dithiolate complexes, D-B-A complexes where aromatic thiolates are the electron donors attached to platinum with bipyridyl acceptors. Previous work on these complexes has suggested the presence of a transient three electron sulfur-sulfur bond, S∴S.[1]

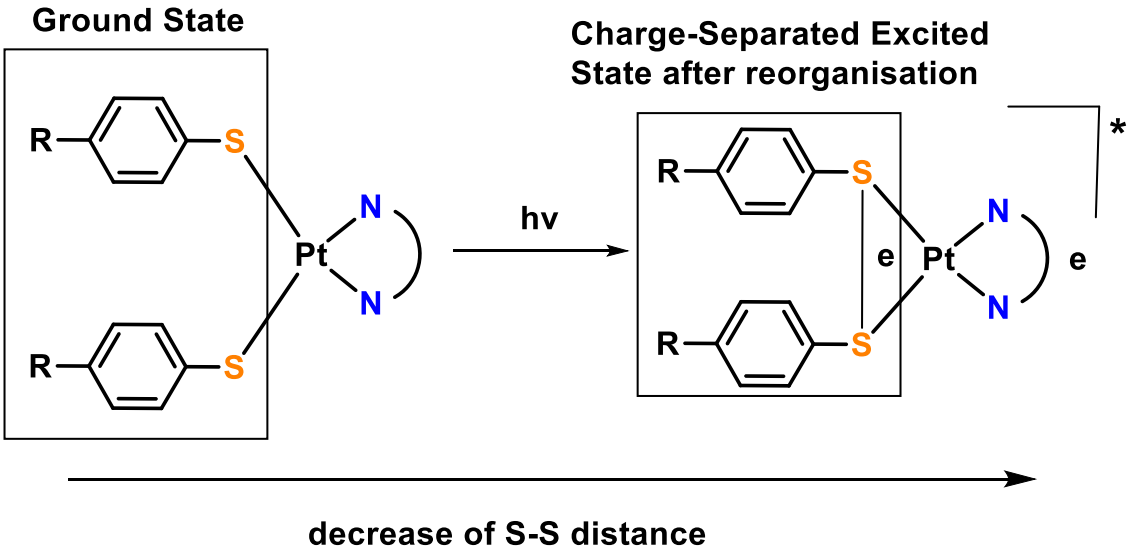

Figure 4.1 The proposed formation of the transient S∴S bond with concomitant shortened sulfur sulfur distance in the excited state

Platinum(ii) diimmine dithiolates $[Pt(NN)(SR_2)_2]$ are model complexes for these studies as the HOMO has thiolate/Pt(d) origin and the LUMO is mostly localised on the diimmine ligand. Upon light absorption these complexes undergo electron transfer from the thiolate moiety to the diimmine resulting in a thiolate anion and

thiyl radical which can interact with one another via the metal centre (Figure 4.1).[2–4] The formation of a new bond in the excited state such as this proposed S∴S bond would provide a barrier to back electron transfer, a route for deactivation of the excited state, thus giving a tool to control the rate of this process.

4.1.2 Using TR^3 to detect the transient S∴S bond

Time-resolved resonance Raman(TR^3) is an ideal tool for obtaining structural information on the excited states of metal chromophores (Figure 4.2).[5–7] The presence of a S-S bond in the excited state is detectable using this technique as it is strongly Raman active.

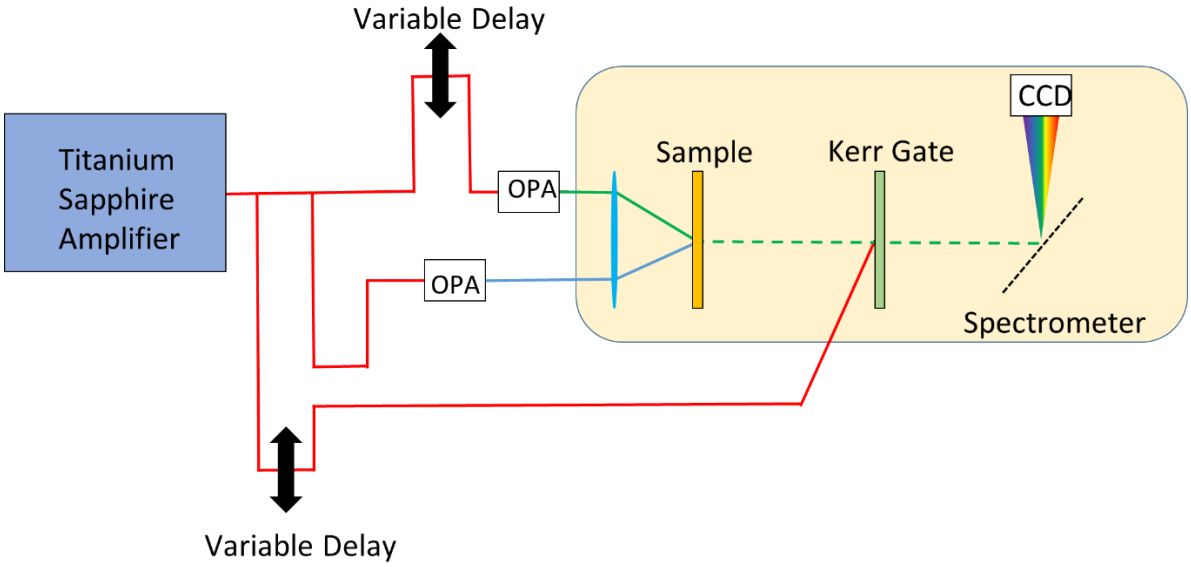

Figure 4.2 The Kerr-gated TR^3 setup, OPA = Optical Parametric Amplifier, CCD = Charge-coupled device

The TR^3 set-up uses picosecond Kerr gating to reject fluorescence from the sample so that it does not swamp the Raman signal (Figure 4.3).

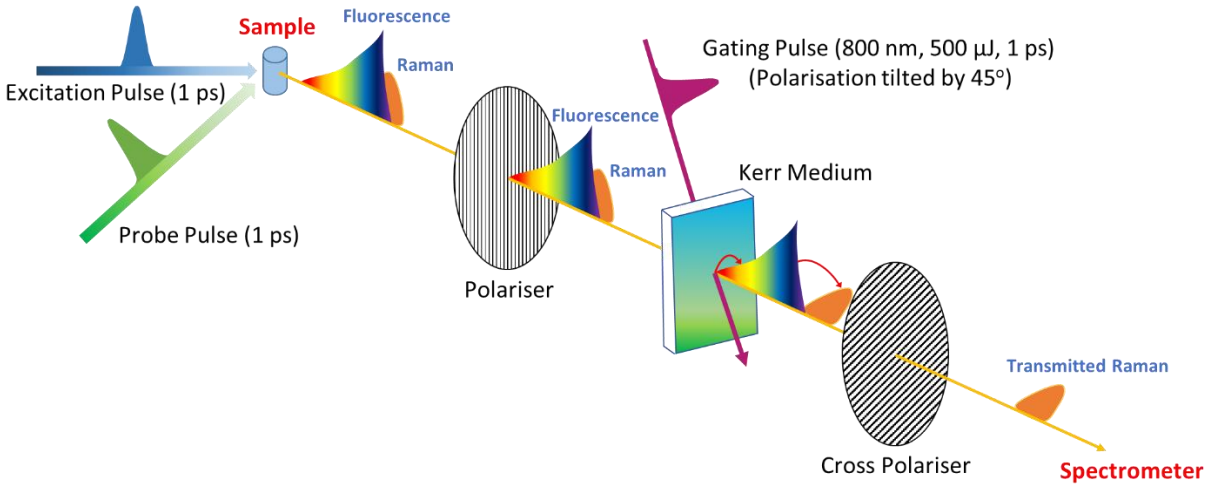

Figure 4.3 The method by which the Kerr medium removes unwanted fluorescence signal from the sample. Adapted from reference 8 [8]

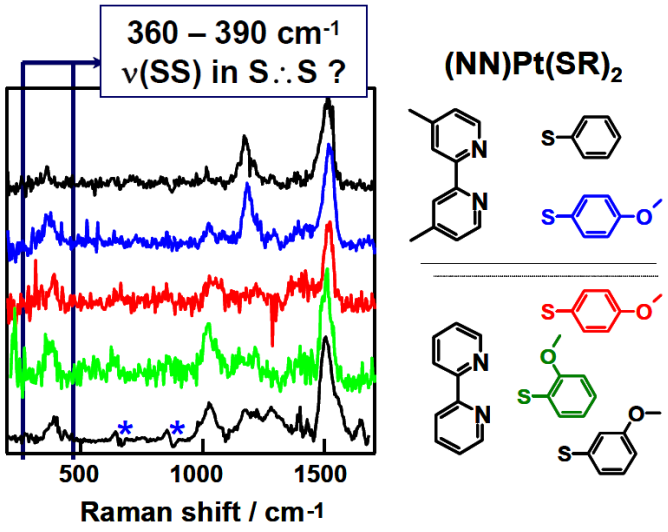

Figure 4.4 Previous work on complexes of the type $Pt(NN)(SR)_2$, where NN = bpy, dmbpy

Previous work showed a peak at approximately 360 cm^{-1} (Figure 4.4) which was tentatively assigned to a SS three electron bond in the excited state. The peak at 360 cm^{-1} was possibly due to bipyridyl localised vibrations and therefore more work was required to investigate the origin of the band. The research described in the chapter aimed to address this issue by altering the diimine ligand so that if the peak did originate from the bipyridyl vibrations then it would be expected to shift. This was attempted by using deuterated analogues of 2,2'-bipyridine and 4,4'-dimethyl-2,2'-bipyridine which would have lower energy vibrations. Platinum(II) diimmine diphenolate complexes were also of interest as they are should not exhibit the behaviour predicted in the dithiolate complexes.

4.1.3 Aims

- To synthesise and purify a series of Platinum(II) diimmine dithiolate /diphenolates and their deuterated analogues (Figure 4.5).
- To use TR[3] to search for the presence of the transient S∴S bond in the Platinum(II) diimmine dithiolates

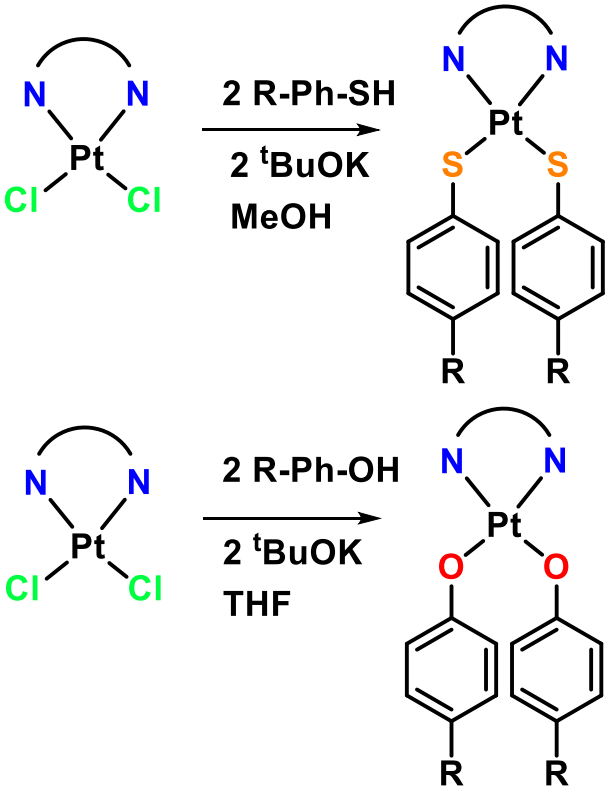

Figure 4.5 The synthetic routes to the complexes investigated in this chapter

4.2 Experimental

4.2.1 Materials and General Procedures

2,2'-bipyridyl (≥99 %), thiophenol (97 %), methyl 4-hydroxybenzoate (≥99.0 %), 4-methoxyphenol (99 %), 4-methoxythiophenol (97 %), methyl 4-sulfanylbenzoate (95 %) were purchased from Aldrich and 4,4'-Dimethyl-2,2'-bipyridine (≥99 %) from Fisher.

Dichlorobis(dimethylsulfoxide)platinum(II) was prepared as follows. To 100 ml flask, potassium tetrachloroplatinate (626 mg, 1.51 mmol) dissolved in water (10 ml) was added. To this solution, DMSO was added and was then stirred for 15 hours. The light-yellow precipitate formed was filtered off and washed with water (3 x 5 ml) and acetone (3 x 5 ml) to leave a yellow crystalline powder (494 mg, 1.17 mmol). Yield: 77.5 %

4.2.2 Synthetic Procedures

4.2.2.1 Synthesis of [Pt(bpy)Cl$_2$] (4.1)

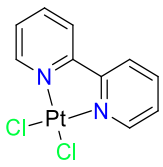

2,2′-Dipyridyl (bpy) (305 mg, 1.95 mmol) and *cis*-dichlorobis(dimethyl sulfoxide)platinum(II) (824 mg, 1.95 mmol) were dissolved in CH_2Cl_2 (50 ml) and stirred at room temperature for 48 hours. Solvent was removed *in vacuo* to give a yellow powder that gradually turned orange then red upon drying. This red solid was dissolved in a minimum volume of CH_2Cl_2 and precipitated out with the addition of diethyl ether to give a bright yellow powder that was collected by vacuum filtration and washed with diethyl ether (3 x 15 ml) to give ***4.1*** as a bright yellow powder (734 mg, 89 %)

^{1}H NMR (400 MHz, DMSO-d6) δ 9.13 (d, *J* = 6.0 Hz, 2H), 8.60 (d, *J* = 5.8 Hz, 2H), 8.37 (t, *J* = 6.0 Hz, 2H), 7.82 (t, *J* = 5.9 Hz, 2H).

4.2.2.2 Synthesis of [Pt(d$_8$-bpy)Cl$_2$] (4.2)

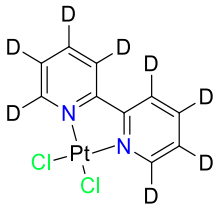

2,2′-Dipyridyl-d$_8$ (d$_8$-bpy) (296 mg, 1.80 mmol) and *cis*-dichlorobis(dimethyl sulfoxide)platinum(II) (760 mg, 1.80 mmol) were dissolved in CH_2Cl_2 (50 ml) and stirred at room temperature for 48 hours. Solvent was removed *in vacuo* to give a yellow powder that gradually turned orange then red upon drying. This red solid was dissolved in a minimum volume of CH_2Cl_2 and precipitated out with the addition of diethyl ether to give a bright yellow powder that was collected by vacuum filtration and washed with diethyl ether (3 x 15 ml) to give ***4.2*** as a bright yellow powder (640 mg, 83 %)

4.2.2.3 Synthesis of [Pt(dmbpy)Cl$_2$] (4.3)

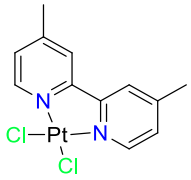

4,4'-dimethyl-2,2'-bipyridine (dmbpy) (200 mg, 1.09 mmol) and *cis*-Dichlorobis(dimethyl sulfoxide)platinum(II) (458 mg, 1.09 mmol) were suspended in dry dichloromethane (100 ml) and refluxed under argon for 6 hours. The reaction mixture was cooled to room temperature, filtered to obtain some of the product and the remaining product was precipitated using diethyl ether which was again collected by filtration. The solid yellow product was washed with diethyl ether and dried under vacuum to yield ***4.3*** (347 mg, 71 %).

^{1}H NMR (400 MHz, DMSO-d$_6$) δ 9.27 (d, *J* = 6.0 Hz, 2H), 8.44 (s, 2H), 7.66 (d, *J* = 6.0 Hz, 2H), 2.48 (s, 6H).

4.2.2.4 Synthesis of [Pt(d_{12}-dmbpy)Cl_2] (4.4)

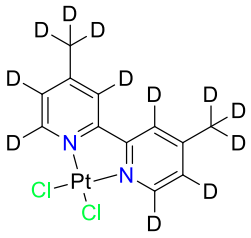

4,4'-dimethyl-2,2'-bipyridine-d_{12} (d_{12}-dmbpy) (170 mg, 1.01 mmol) and *cis*-dichlorobis(dimethyl sulfoxide)platinum(II) (426 mg, 1.01 mmol) were suspended in dry dichloromethane (100 ml) and refluxed under argon for 6 hours. The reaction mixture was cooled to room temperature, filtered to obtain some of the product and the remaining product was precipitated using diethyl ether which was again collected by filtration. The solid yellow product was washed with diethyl ether and dried under vacuum to yield ***4.4*** (324 mg, 69 %).

4.2.2.5 Synthesis of [Pt(bpy)(SPh)$_2$] (4.5)

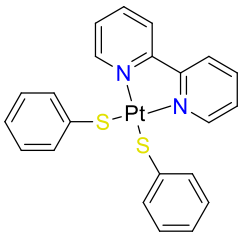

Thiophenol (198 mg, 0.18 ml, 1.8 mmol) and potassium tert-butoxide (200 mg, 1.8 mmol) were added to a Schlenk tube containing methanol (50 ml) that had been deaerated by bubbling argon for 30 minutes. The reagents were stirred under argon for 30 minutes to allow deprotonation of the thiol. The thiol solution was then added via cannula transfer to a second Schlenk tube containing a suspension of platinum(II) bpy dichloride (380 mg, 0.9 mmol) in methanol (50 ml) that had been deaerated by bubbling argon for 30 minutes, to give a yellow suspension. The reaction mixture was sonicated at room temperature for 30 minutes to give a red suspension that was filtered under vacuum and washed with cold methanol (3 x 15 ml). to give ***4.5*** as a fine red solid (430 mg, 84 %).

^{1}H NMR (400 MHz, DMSO-d$_6$) δ 9.64 (d, *J* = 5.6 Hz, 2H), 8.66 (d, *J* = 8.2 Hz, 2H), 8.36 (t, *J* = 7.9 Hz, 2H), 7.79 (t, *J* = 6.4 Hz, 2H), 7.48 (d, *J* = 7.9 Hz, 4H), 6.91 (t, *J* = 7.5 Hz, 4H), 6.81 (t, *J* = 7.2 Hz, 2H).

4.2.2.6 Synthesis of [Pt(d$_8$-bpy)(SPh)$_2$] (4.6)

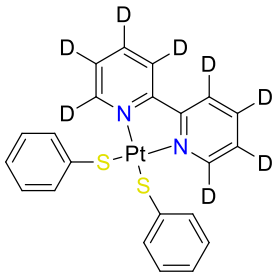

Thiophenol (198 mg, 0.18 ml, 1.8 mmol) and potassium tert-butoxide (200 mg, 1.8 mmol) were added to a Schlenk tube containing methanol (50 ml) that had been deaerated by bubbling argon for 30 minutes. The reagents were stirred under argon for 30 minutes to allow deprotonation of the thiol. The thiol solution was then added via cannula transfer to a second Schlenk tube containing a suspension of platinum(II) d$_8$-bpy dichloride (387 mg, 0.9 mmol) in methanol (50 ml) that had been deaerated by bubbling argon for 30 minutes, to give a yellow suspension. The reaction mixture was sonicated at room temperature for 30 minutes to give a red suspension that was filtered under vacuum and washed with cold methanol (3 x 15 ml). to give ***4.6*** as a fine red solid (467 mg, 90 %).

^{1}H NMR (400 MHz, DMSO-d$_6$) δ 7.48 (d, *J* = 7.9 Hz, 4H), 6.91 (t, *J* = 7.5 Hz, 4H), 6.81 (t, *J* = 7.2 Hz, 2H).

4.2.2.7 Synthesis of [Pt(dmbpy)(SPh)$_2$] (4.7)

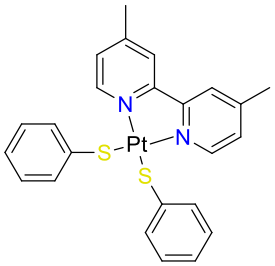

Thiophenol (198 mg, 0.18 ml, 1.8 mmol) and potassium tert-butoxide (200 mg, 1.8 mmol) were added to a Schlenk tube containing methanol (50 ml) that had been deaerated by bubbling argon for 30 minutes. The reagents were stirred under argon for 30 minutes to allow deprotonation of the thiol. The thiol solution was then added via cannula transfer to a second Schlenk tube containing a suspension of platinum(II) dmbpy dichloride (405 mg, 0.9 mmol) in methanol (50 ml) that had been deaerated by bubbling argon for 30 minutes, to give a yellow suspension. The reaction mixture was sonicated at room temperature for 30 minutes to give a red suspension that was filtered under vacuum and washed with cold methanol (3 x 15 ml). to give ***4.7*** as a fine red solid (494 mg, 92 %).

^{1}H NMR (400 MHz, DMSO-d$_6$) δ 9.44 (d, *J* = 5.9 Hz, 2H), 8.54 (s, 2H), 7.61 (d, *J* = 5.9 Hz, 2H), 7.48 (d, *J* = 6.5 Hz, 4H), 6.92 (t, *J* = 7.0 Hz, 4H), 6.81 (t, *J* = 6.5 Hz, 2H), 2.46 (s, 6H).

4.2.2.8 Synthesis of [Pt(dmbpy)(SPh)$_2$] (4.8)

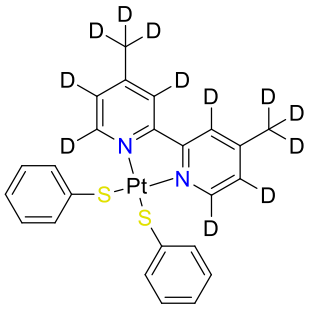

Thiophenol (198 mg, 0.18 ml, 1.8 mmol) and potassium tert-butoxide (200 mg, 1.8 mmol) were added to a Schlenk tube containing methanol (50 ml) that had been deaerated by bubbling argon for 30 minutes. The reagents were stirred under argon for 30 minutes to allow deprotonation of the thiol. The thiol solution was then added via cannula transfer to a second Schlenk tube containing a suspension of platinum(II) d_{12}-dmbpy dichloride (416 mg, 0.9 mmol) in methanol (50 ml) that had been deaerated by bubbling argon for 30 minutes, to give a yellow suspension. The reaction mixture was sonicated at room temperature for 30 minutes to give a red suspension that was filtered under vacuum and washed with cold methanol (3 x 15 ml). to give ***4.8*** as a fine red solid (505 mg, 92 %).

^{1}H NMR (400 MHz, DMSO-d_6) δ 7.49 (d, *J* = 6.5 Hz, 4H), 6.91 (t, *J* = 7.0 Hz, 4H), 6.81 (t, *J* = 6.5 Hz, 2H).

4.2.2.9 Synthesis of [Pt(bpy)(SPhOMe)$_2$] (4.9)

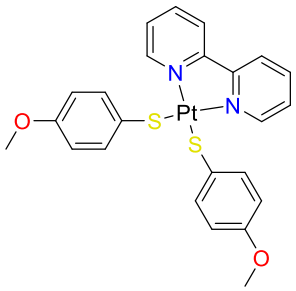

4-methoxythiophenol (302 mg, 0.27 ml, 2.16 mmol) and potassium tert-butoxide (237 mg, 2.16 mmol) were added to a Schlenk tube containing methanol (50 ml) that had been deaerated by bubbling argon for 30 minutes. The reagents were stirred under argon for 30 minutes to allow deprotonation of the thiol. The thiol solution was then added via cannula transfer to a second Schlenk tube containing a suspension of platinum(II) bpy dichloride (455 mg, 1.08 mmol) in methanol (50 ml) that had been deaerated by bubbling argon for 30 minutes, to give a yellow suspension. The reaction mixture was sonicated at room temperature for 30 minutes to give a purple suspension that was filtered under vacuum and washed with cold methanol (3 x 15 ml). to give ***4.9*** as a fine purple solid (615 mg, 95 %).

^{1}H NMR (400 MHz, DMSO-d$_6$) δ 9.64 (d, *J* = 5.7 Hz, 2H), 8.61 (d, *J* = 7.8 Hz, 2H), 8.35 (t, *J* = 7.9 Hz, 2H), 7.77 (t, *J* = 6.4 Hz, 2H), 7.35 (d, *J* = 8.9 Hz, 4H), 6.54 (d, *J* = 8.9 Hz, 4H), 3.61 (s, 6H).

4.2.2.10 Synthesis of [Pt(d$_8$-bpy)(SPhOMe)$_2$] (4.10)

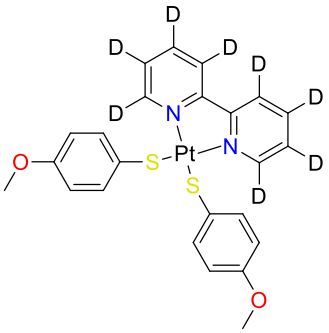

4-methoxythiophenol (63 mg, 0.056 ml, 0.45 mmol) and potassium tert-butoxide (50 mg, 0.45 mmol) were added to a Schlenk tube containing methanol (20 ml) that had been deaerated by bubbling argon for 30 minutes. The reagents were stirred under argon for 30 minutes to allow deprotonation of the thiol. The thiol solution was then added via cannula transfer to a second Schlenk tube containing a suspension of platinum(II) d$_8$-bpy dichloride (96 mg, 0.22 mmol) in methanol (50 ml) that had been deaerated by bubbling argon for 30 minutes, to give a yellow suspension. The reaction mixture was sonicated at room temperature for 30 minutes to give a purple suspension that was filtered under vacuum and washed with cold methanol (3 x 15 ml) to give ***4.10*** as a fine purple solid (111 mg, 78 %).

^{1}H NMR (400 MHz, DMSO-d$_6$) δ 7.40 – 7.33 (m, 4H), 6.58 – 6.51 (m, 4H), 3.62 (s, 6H).

4.2.2.11 Synthesis of [Pt(dmbpy)(SPhOMe)$_2$] (4.11)

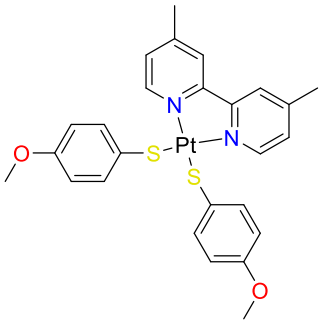

4-methoxythiophenol (62 mg, 0.055 ml, 0.44 mmol) and potassium tert-butoxide (50 mg, 0.44 mmol) were added to a Schlenk tube containing methanol (20 ml) that had been deaerated by bubbling argon for 30 minutes. The reagents were stirred under argon for 30 minutes to allow deprotonation of the thiol. The thiol solution was then added via cannula transfer to a second Schlenk tube containing a suspension of platinum(II) dmbpy dichloride (100 mg, 0.22 mmol) in methanol (50 ml) that had been deaerated by bubbling argon for 30 minutes, to give a yellow suspension. The reaction mixture was sonicated at room temperature for 30 minutes to give a orange/brown suspension that was filtered under vacuum and washed with cold methanol (3 x 15 ml). The sinter was then washed with CH_2Cl_2 to dissolve the solid to a dark purple coloured solution. The solvent was removed *in vacuo* to give ***4.11*** as a brownish purple film (124 mg, 85 %).

^{1}H NMR (400 MHz, DMSO-d$_6$) δ 9.44 (d, *J* = 5.9 Hz, 2H), 8.50 (s, 2H), 7.60 (d, *J* = 6.0 Hz, 2H), 7.38 – 7.32 (m, 4H), 6.58 – 6.50 (m, 4H), 3.62 (s, 6H), 2.44 (s, 6H).

4.2.2.12 Synthesis of [Pt(d_{12}-dmbpy)(SPhOMe)$_2$] (4.12)

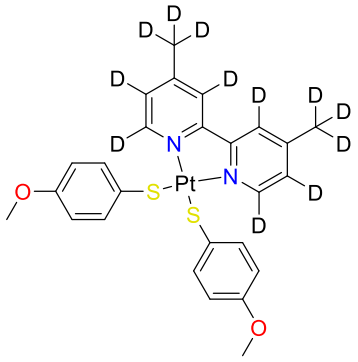

4-methoxythiophenol (55 mg, 0.049 ml, 0.39 mmol) and potassium tert-butoxide (44 mg, 0.39 mmol) were added to a Schlenk tube containing methanol (20 ml) that had been deaerated by bubbling argon for 30 minutes. The reagents were stirred under argon for 30 minutes to allow deprotonation of the thiol. The thiol solution was then added via cannula transfer to a second Schlenk tube containing a suspension of platinum(II) d_{12}-dmbpy dichloride (90 mg, 0.19 mmol) in methanol (50 ml) that had been deaerated by bubbling argon for 30 minutes, to give a yellow suspension. The reaction mixture was sonicated at room temperature for 30 minutes to give a brown suspension that was filtered under vacuum and washed with cold methanol (3 x 15 ml). The sinter was then washed with CH_2Cl_2 to dissolve the solid to a dark purple coloured solution. The solvent was removed *in vacuo* to give ***4.12*** as a brownish purple film (98 mg, 75 %).

^{1}H NMR (400 MHz, DMSO-d_6) δ 7.38 – 7.32 (m, 4H), 6.58 – 6.50 (m, 4H), 3.62 (s, 6H), 2.44 (s, 6H).

4.2.2.13 Synthesis of [Pt(dmbpy)(OPhOMe)$_2$] (4.13)

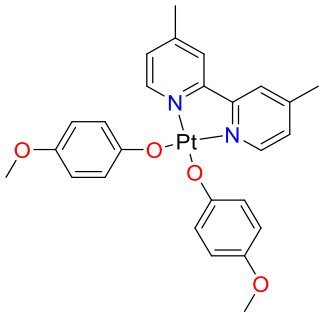

4-methoxyphenol (53 mg, 0.43 mmol) and potassium tert-butoxide (48 mg, 0.43 mmol) were added to a Schlenk tube containing THF (20 ml) that had been deaerated by bubbling argon for 30 minutes. The reagents were stirred under argon for 30 minutes to allow deprotonation of the thiol. The thiol solution was then added via cannula transfer to a second Schlenk tube containing a suspension of platinum(II) dmbpy dichloride (96 mg, 0.21 mmol) in THF (50 ml) that had been deaerated by bubbling argon for 30 minutes, to give a yellow suspension. The reaction mixture was sonicated at room temperature for 30 minutes to give a red suspension that was filtered under vacuum and washed with cold THF (3 x 15 ml). The sinter was then washed with CH_2Cl_2 to dissolve the solid to a deep red coloured solution. The solvent was removed *in vacuo* to give ***4.13*** as a red solid (102 mg, 78 %).

^{1}H NMR (400 MHz, DMSO-d_6) δ 9.30 (d, *J* = 6.0 Hz, 2H), 8.57 (s, 2H), 7.64 (dd, *J* = 5.9, 0.9 Hz, 2H), 6.99 – 6.91 (m, 4H), 6.55 – 6.49 (m, 4H), 3.65 (s, 6H), 2.47 (s, 6H).

4.2.2.14 Synthesis of [Pt(d$_{12}$-dmbpy)(OPhOMe)$_2$] (4.14)

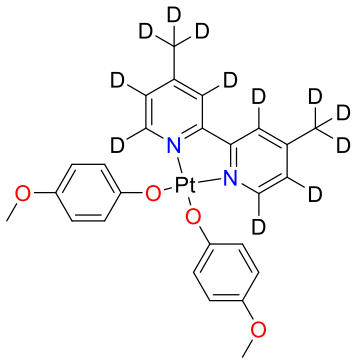

4-methoxyphenol (46 mg, 0.37 mmol) and potassium tert-butoxide (42 mg, 0.37 mmol) were added to a Schlenk tube containing THF (20 ml) that had been deaerated by bubbling argon for 30 minutes. The reagents were stirred under argon for 30 minutes to allow deprotonation of the thiol. The thiol solution was then added via cannula transfer to a second Schlenk tube containing a suspension of platinum(II) d$_{12}$-dmbpy dichloride (86 mg, 0.18 mmol) in THF (50 ml) that had been deaerated by bubbling argon for 30 minutes, to give a yellow suspension. The reaction mixture was sonicated at room temperature for 30 minutes to give a red suspension that was filtered under vacuum and washed with cold THF (3 x 15 ml). The sinter was then washed with CH_2Cl_2 to dissolve the solid to a deep red coloured solution. The solvent was removed *in vacuo* to give ***4.14*** as a red solid (78 mg, 66 %).

^{1}H NMR (400 MHz, DMSO-d$_6$) δ 6.99 – 6.91 (m, 4H), 6.55 – 6.49 (m, 4H), 3.65 (s, 6H).

4.2.2.15 Synthesis of [Pt(dmbpy)(SPhCOOMe)$_2$] (4.15)

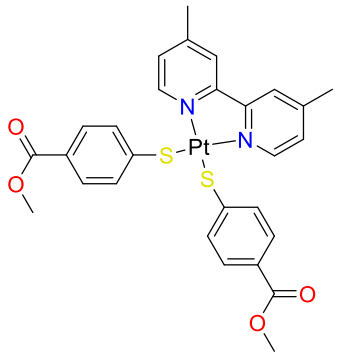

Methyl 4-sulfanylbenzoate (245 mg, 1.46 mmol) and potassium tert-butoxide (164 mg, 1.46 mmol) were added to a Schlenk tube containing methanol (60 ml) that had been deaerated by bubbling argon for 30 minutes. The reagents were stirred under argon for 30 minutes to allow deprotonation of the thiol. The thiol solution was then added via cannula transfer to a second Schlenk tube containing a suspension of platinum(II) dmbpy dichloride (328 mg, 0.729 mmol) in methanol (50 ml) that had been deaerated by bubbling argon for 30 minutes, to give a yellow suspension. The reaction mixture was sonicated at room temperature for 30 minutes to give a brown suspension that was filtered under vacuum and washed with cold methanol (3 x 30 ml). The sinter was then washed with CH_2Cl_2 to dissolve the solid to a deep red coloured solution. The solvent was removed *in vacuo* to give ***4.15*** as a brownish purple film (505 mg, 97 %).

^{1}H NMR (400 MHz, DMSO) δ 9.31 (d, *J* = 5.9 Hz, 2H), 8.57 (s, 2H), 7.64 (dd, *J* = 5.9, 0.9 Hz, 2H), 7.61 – 7.57 (m, 4H), 7.50 – 7.46 (m, 4H), 3.74 (s, 6H), 2.47 (s, 6H).

4.2.2.16 Synthesis of [Pt(d_{12}-dmbpy)(SPhCOOMe)$_2$] (4.16)

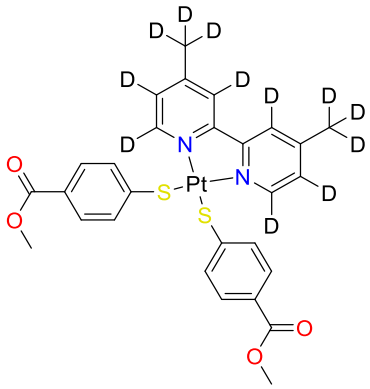

Methyl 4-sulfanylbenzoate (69 mg, 0.41 mmol) and potassium tert-butoxide (46 mg, 0.41 mmol) were added to a Schlenk tube containing methanol (20 ml) that had been deaerated by bubbling argon for 30 minutes. The reagents were stirred under argon for 30 minutes to allow deprotonation of the thiol. The thiol solution was then added via cannula transfer to a second Schlenk tube containing a suspension of platinum(II) d_{12}-dmbpy dichloride (95 mg, 0.21 mmol) in methanol (50 ml) that had been deaerated by bubbling argon for 30 minutes, to give a yellow suspension. The reaction mixture was sonicated at room temperature for 30 minutes to give a brown suspension that was filtered under vacuum and washed with cold methanol (3 x 15 ml). The sinter was then washed with CH_2Cl_2 to dissolve the solid to a deep red coloured solution. The solvent was removed *in vacuo* to give ***4.16*** as a brownish purple film (65 mg, 44 %).

^{1}H NMR (400 MHz, DMSO-d_6) δ 7.61 – 7.56 (m, 4H), 7.51 – 7.46 (m, 4H), 3.74 (s, 6H).

4.2.2.17 Synthesis of [Pt(dmbpy)(OPhCOOMe)$_2$] (4.17)

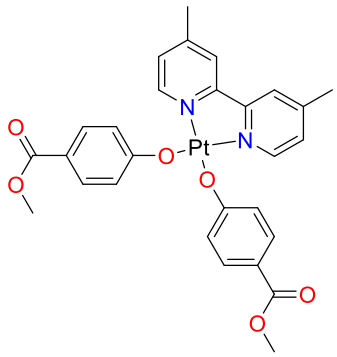

Methyl 4-hydroxybenzoate (84 mg, 0.55 mmol) and potassium tert-butoxide (62 mg, 0.55 mmol) were added to a Schlenk tube containing THF (20 ml) that had been deaerated by bubbling argon for 30 minutes. The reagents were stirred under argon for 30 minutes to allow deprotonation of the thiol. The thiol solution was then added via cannula transfer to a second Schlenk tube containing a suspension of platinum(II) dmbpy dichloride (124 mg, 0.28 mmol) in THF (50 ml) that had been deaerated by bubbling argon for 30 minutes, to give a yellow suspension. The reaction mixture was sonicated at room temperature for 30 minutes to give a red suspension that was filtered under vacuum and washed with cold THF (3 x 15 ml). The sinter was then washed with CH_2Cl_2 to dissolve the solid to a deep red coloured solution. The solvent was removed *in vacuo* to give ***4.17*** as a red solid (101 mg, 54 %).

^{1}H NMR (400 MHz, DMSO-d$_6$) δ 8.50 – 8.36 (m, 4H), 7.62 (d, *J* = 5.6 Hz, 2H), 7.57 (d, *J* = 8.8 Hz, 4H), 7.09 (d, *J* = 8.8 Hz, 4H), 3.70 (s, 6H), 2.47 (s, 6H).

4.2.2.18 Synthesis of [Pt(d$_{12}$-dmbpy)(OPhCOOMe)$_2$] (4.18)

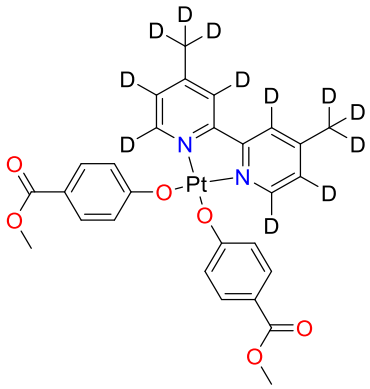

Methyl 4-hydroxybenzoate (70 mg, 0.46 mmol) and potassium tert-butoxide (52 mg, 0.46 mmol) were added to a Schlenk tube containing THF (20 ml) that had been deaerated by bubbling argon for 30 minutes. The reagents were stirred under argon for 30 minutes to allow deprotonation of the thiol. The thiol solution was then added via cannula transfer to a second Schlenk tube containing a suspension of platinum(II) d$_{12}$-dmbpy dichloride (107 mg, 0.23 mmol) in THF (50 ml) that had been deaerated by bubbling argon for 30 minutes, to give a yellow suspension. The reaction mixture was sonicated at room temperature for 30 minutes to give a red suspension that was filtered under vacuum and washed with cold THF (3 x 15 ml). The sinter was then washed with CH_2Cl_2 to dissolve the solid to a deep red coloured solution. The solvent was removed *in vacuo* to give ***4.18*** as a red solid (30 mg, 19 %).

1H NMR (400 MHz, DMSO-d$_6$) δ 7.59 – 7.54 (m, 4H), 7.12 – 7.06 (m, 4H), 3.70 (s, 6H).

4.3 Results and discussion

4.3.1 Optimised geometries

The optimised geometries calculated by Heather Carson are summarised below (Figure 4.6-Figure 4.12). There was no difference between the protonated complexes and their deuterated analogues so they are not shown below.

4.3.1.1 Pt(bpy)(SPh)$_2$

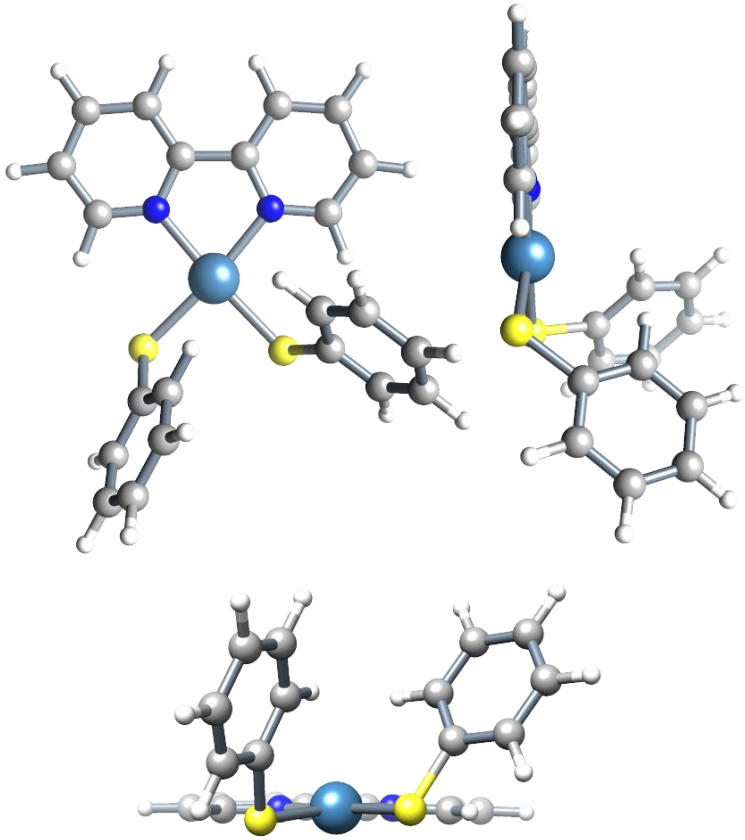

Figure 4.6 Optimised geometries for Pt(bpy)(SPh)$_2$

4.3.1.2 Pt(dmbpy)(SPh)$_2$

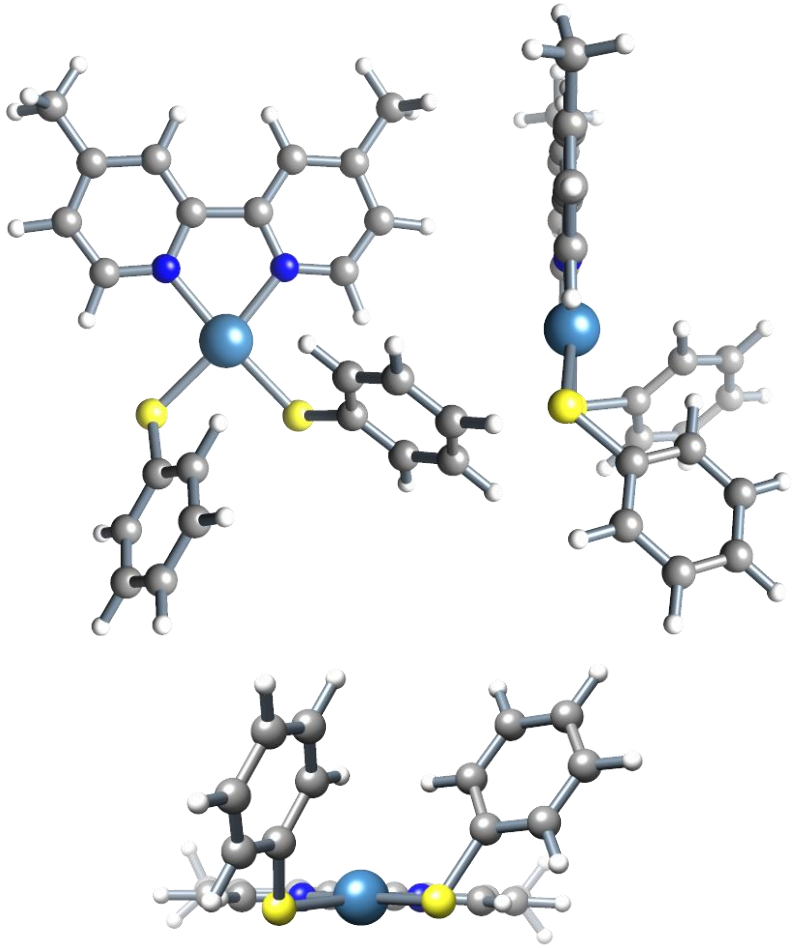

Figure 4.7 Optimised geometries for Pt(dmbpy)(SPh)$_2$

4.3.1.3 $Pt(bpy)(SPhOMe)_2$

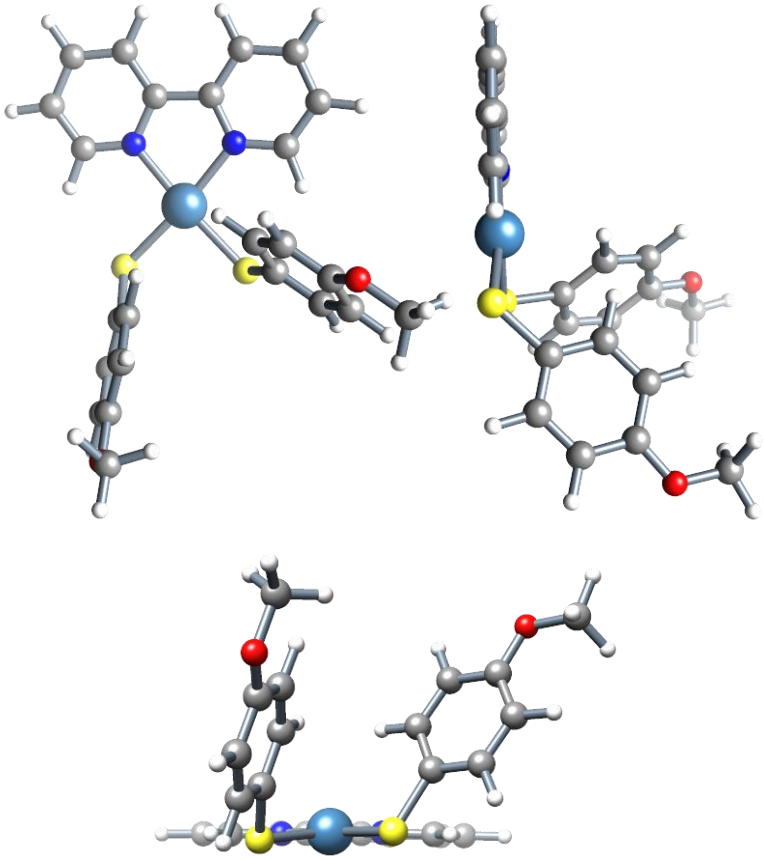

Figure 4.8 Optimised geometries for $Pt(bpy)(SPhOMe)_2$

4.3.1.4 Pt(dmbpy)(SPhOMe)$_2$

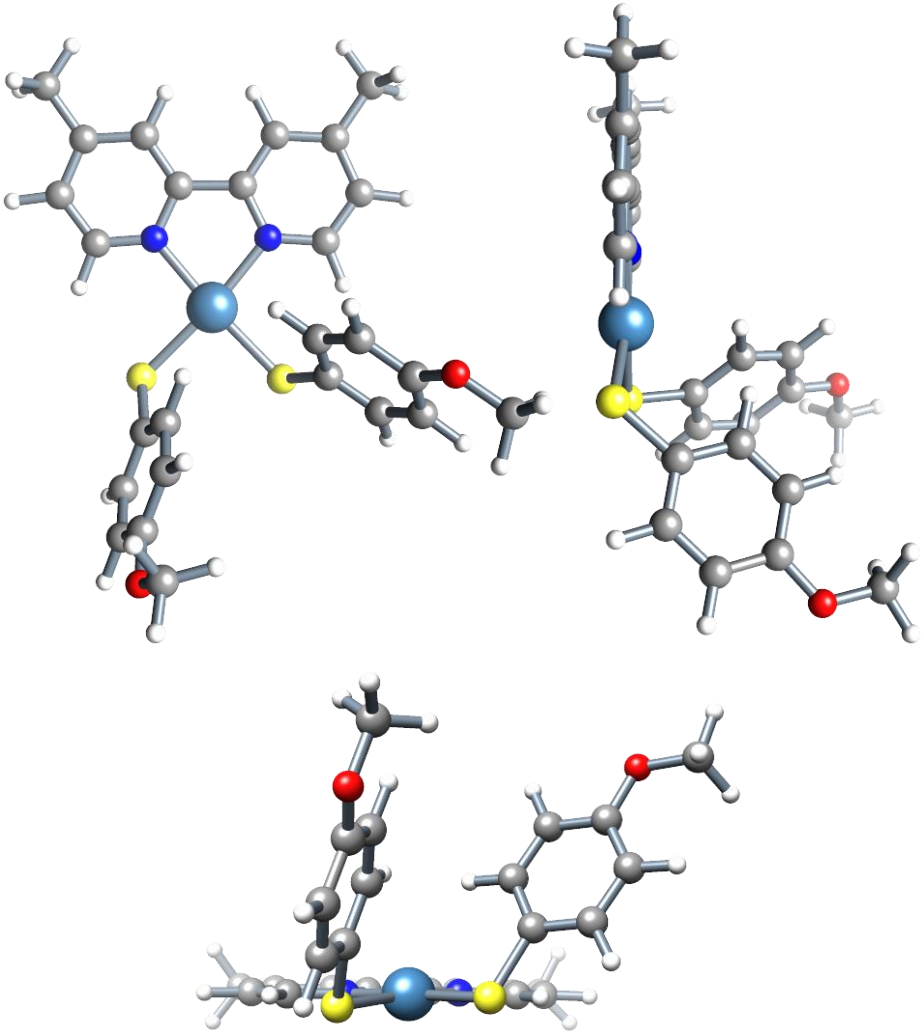

Figure 4.9 Optimised geometries for Pt(dmbpy)(SPhOMe)$_2$

4.3.1.5 Pt(dmbpy)(OPhOMe)$_2$

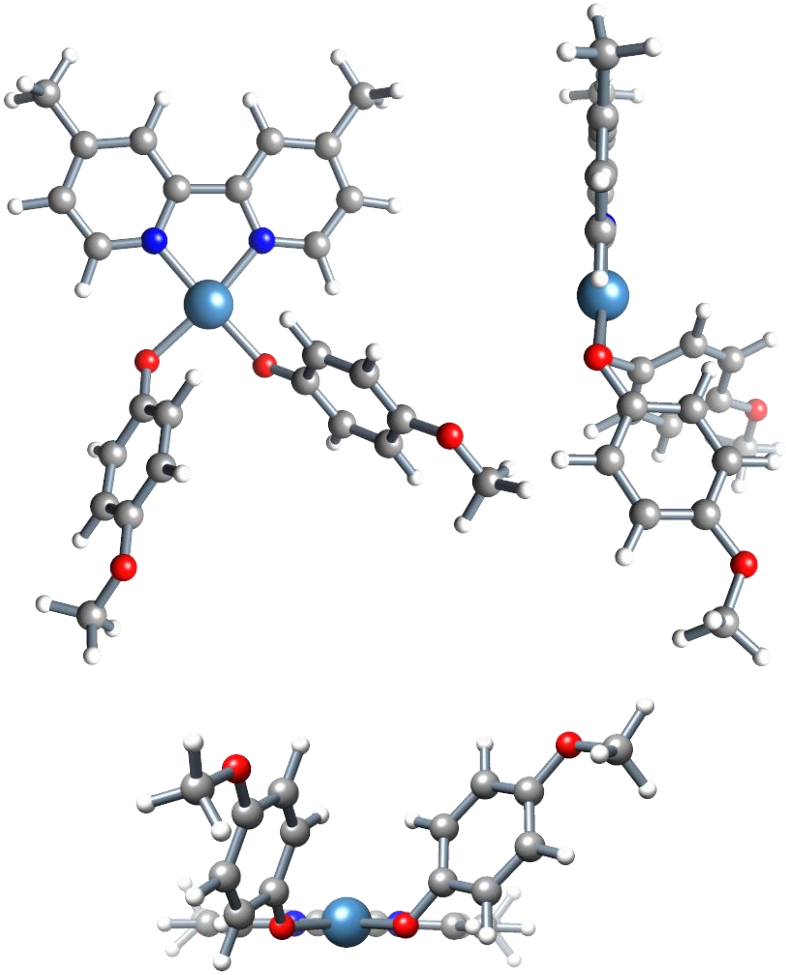

Figure 4.10 Optimised geometries for Pt(dmbpy)(OPhOMe)$_2$

4.3.1.6 Pt(dmbpy)(SPhCOOMe)$_2$

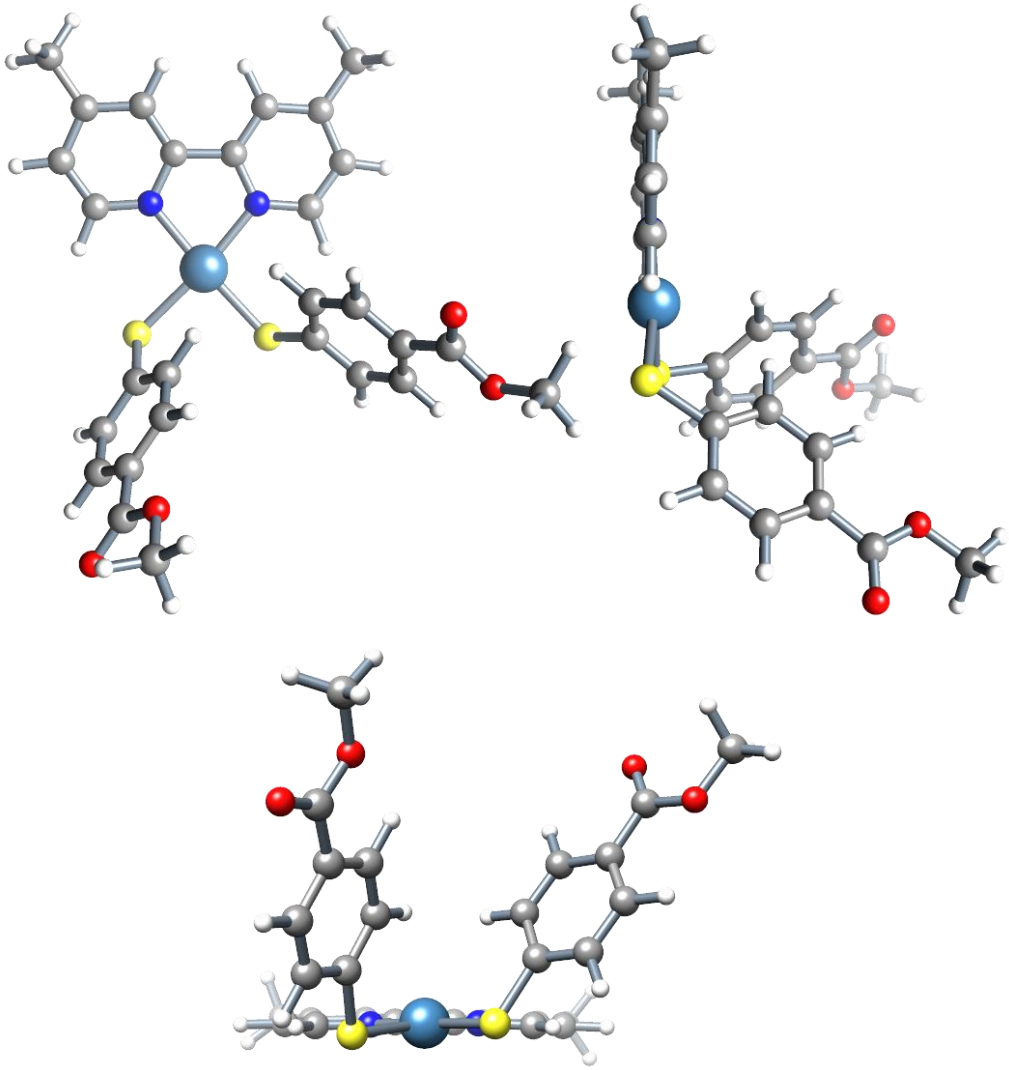

Figure 4.11 Optimised geometries for Pt(bpy)(SPhCOOMe)$_2$

4.3.1.7 Pt(dmbpy)(OPhCOOMe)$_2$

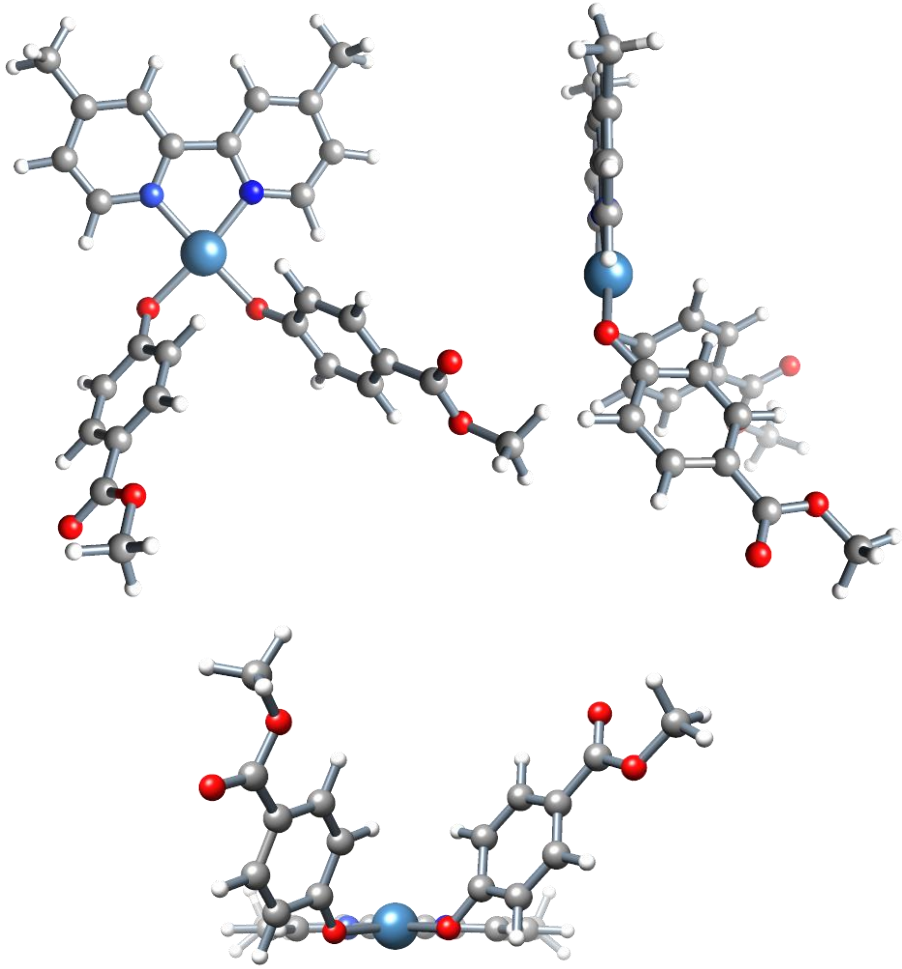

Figure 4.12 Optimised geometries for Pt(dmbpy)(OPhCOOMe)$_2$

4.3.2 UV/Vis Electronic Absorption Spectroscopy

The electronic absorption spectra of complexes ***4.5*** - ***4.18*** were recorded in CH_2Cl_2 at room temperature to determine the energy of the electronic excited states (Figure 4.13 - Figure 4.19). The absorption spectra have been normalised to the absorbance of most intense band. The absorptions are summarised in the table below (Table 4.1).

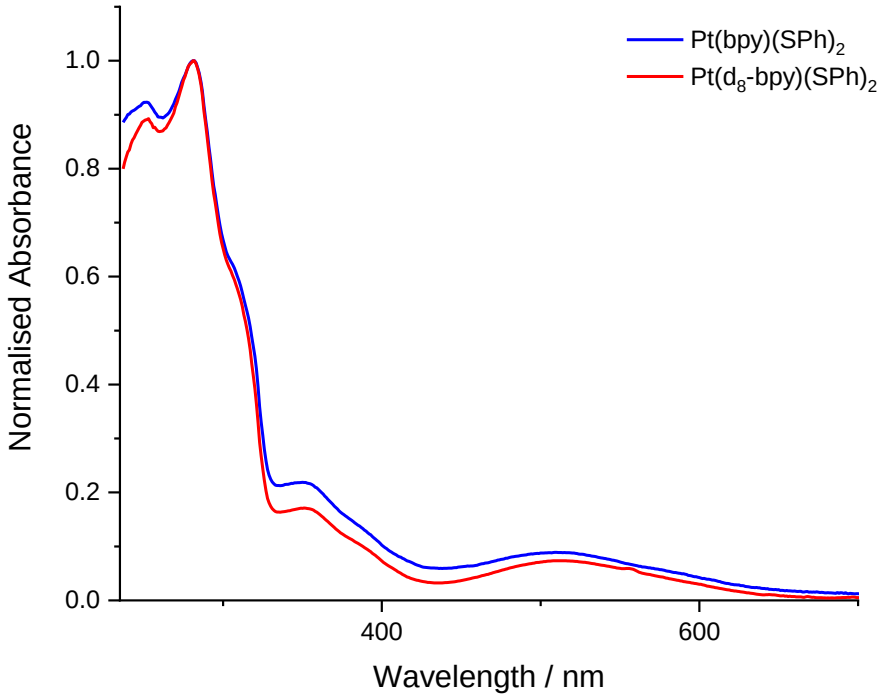

Figure 4.13 Steady state electronic absorption spectra of complexes Pt(bpy)(SPh)$_2$ and Pt(d$_8$-bpy)(SPh)$_2$ in CH_2Cl_2 at r.t. Blue line – Pt(bpy)(SPh)$_2$), Red line – Pt(d$_8$-bpy)(SPh)$_2$

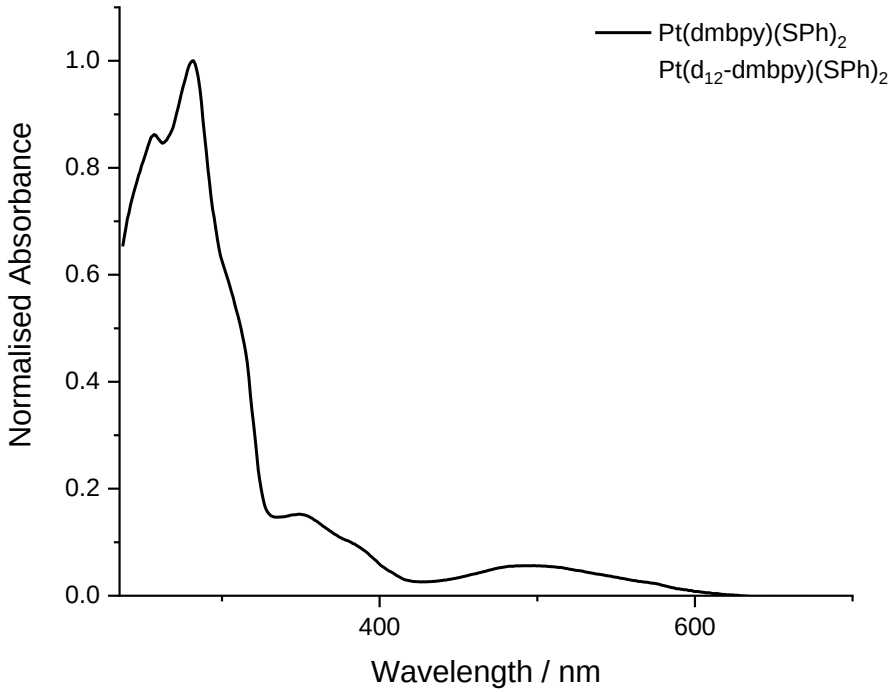

Figure 4.14 Steady state electronic absorption spectrum of Pt(dmbpy)(SPh)$_2$ and Pt(d$_{12}$-dmbpy)(SPh)$_2$ in CH_2Cl_2 at r.t. The spectra closely followed one another so only one line is shown for clarity.

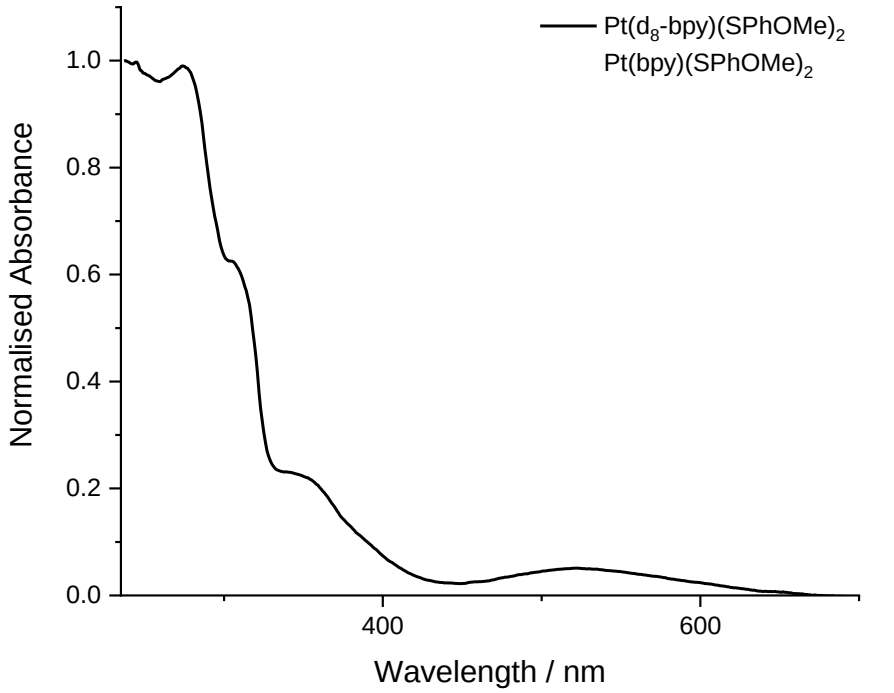

Figure 4.15 Steady state electronic absorption spectrum of Pt(bpy)(SPhOMe)$_2$ and Pt(d$_8$-bpy)(SPhOMe)$_2$ in CH_2Cl_2 at r.t. The spectra closely followed one another so only one line is shown for clarity.

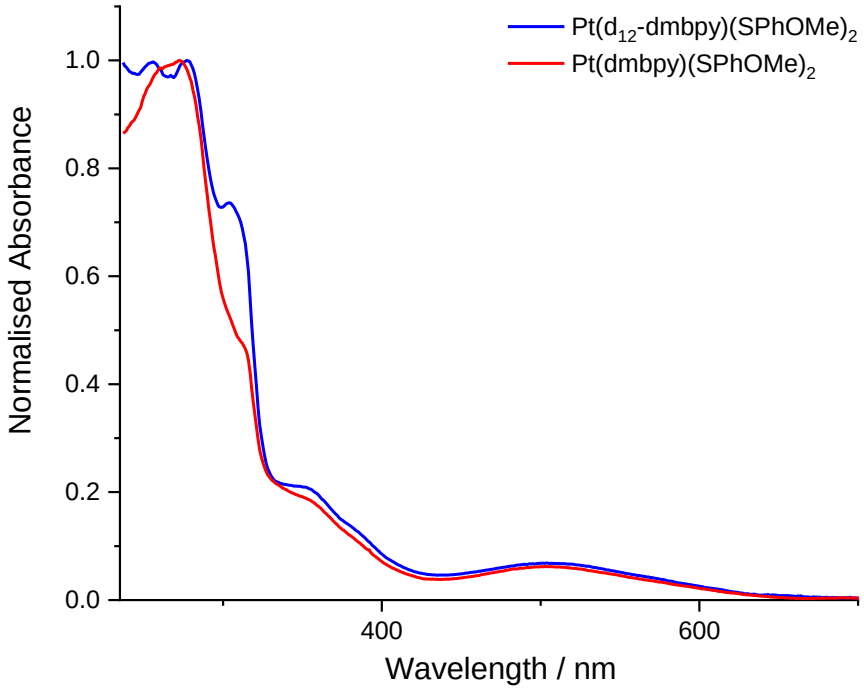

Figure 4.16 Steady state electronic absorption spectra of complexes Pt(dmbpy)(SPhOMe)₂ and Pt(d₁₂-dmbpy)(SPhOMe)₂ in CH_2Cl_2 at r.t. Blue line – Pt(d₁₂-dmbpy)(SPhOMe)₂), Red line – Pt(dmbpy)(SPhOMe)₂

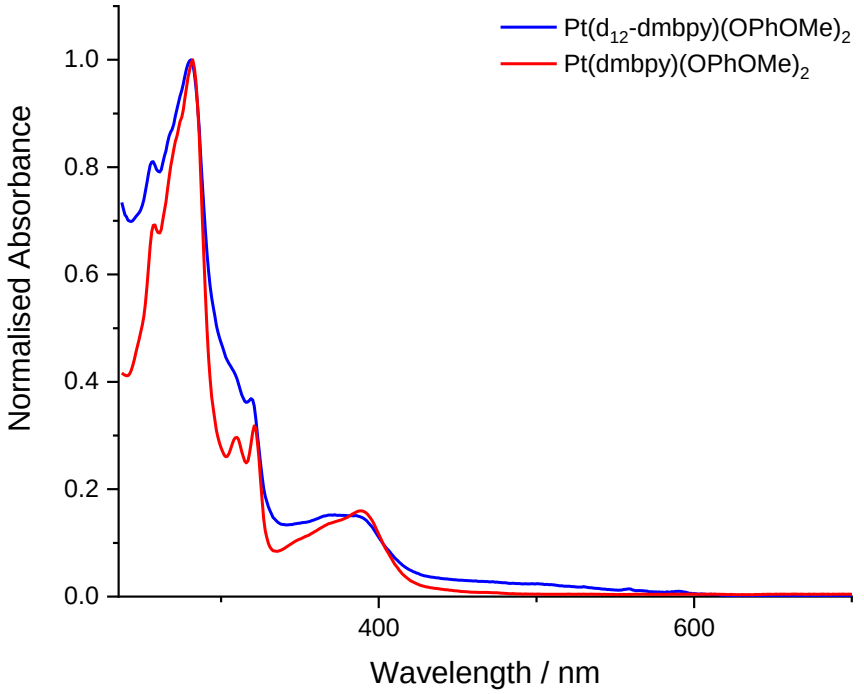

Figure 4.17 Steady state electronic absorption spectra of complexes Pt(dmbpy)(OPhOMe)₂ and Pt(d₁₂-dmbpy)(OPhOMe)₂ in CH_2Cl_2 at r.t. Blue line – Pt(d₁₂-dmbpy)(OPhOMe)₂), Red line – Pt(dmbpy)(OPhOMe)₂

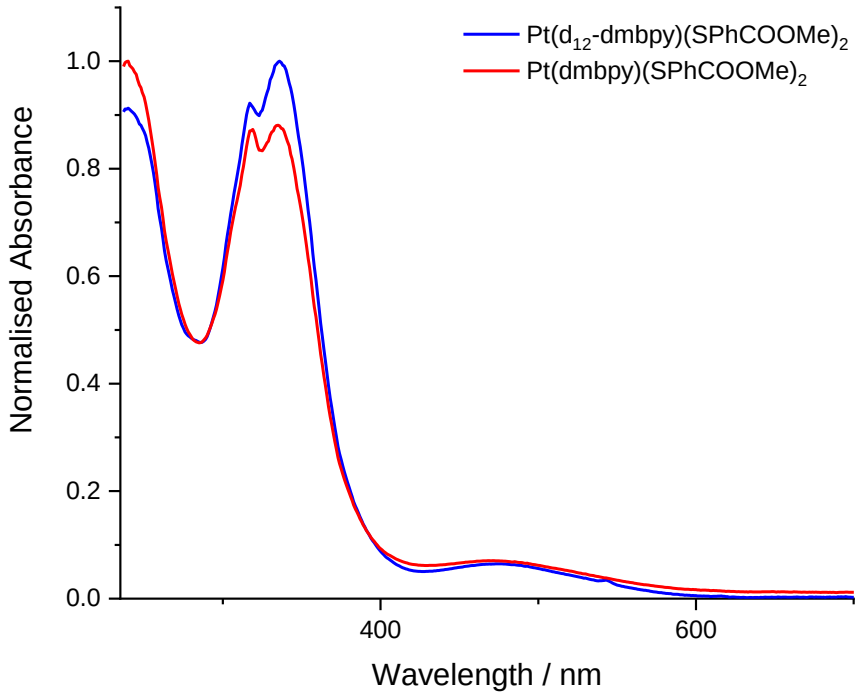

Figure 4.18 Steady state electronic absorption spectra of complexes Pt(dmbpy)(SPhCOOMe)$_2$ and Pt(d$_{12}$-dmbpy)(SPhCOOMe)$_2$ in CH_2Cl_2 at r.t. Blue line – Pt(d$_{12}$-dmbpy)(SPhCOOMe)$_2$), Red line – Pt(dmbpy)(SPhCOOMe)$_2$

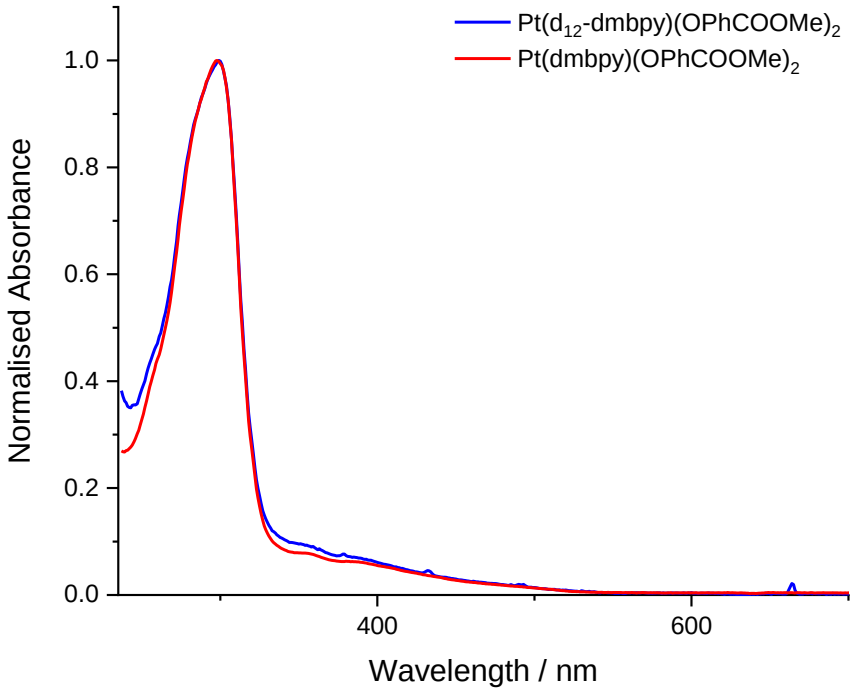

Figure 4.19 Steady state electronic absorption spectra of complexes Pt(dmbpy)(OPhCOOMe)$_2$ and Pt(d$_{12}$-dmbpy)(OPhCOOMe)$_2$ in CH_2Cl_2 at r.t. Blue line – Pt(d$_{12}$-dmbpy)(OPhCOOMe)$_2$), Red line – Pt(dmbpy)(OPhCOOMe)$_2$

Table 4.1 Electronic absorption data for complexes 4.5-4.14 in CH_2Cl_2 at r.t

Complex	**λ_{max} / nm**
Pt(bpy)(SPh)$_2$	252, 281, 308 (sh), 352, 385 (sh), 510
Pt(dmbpy)(SPh)$_2$	257, 281, 308 (sh), 350, 383 (sh), 496
Pt(bpy)(SPhOMe)$_2$	274, 305, 346, 374 (sh), 524
Pt(dmbpy)(SPhOMe)$_2$	256, 277, 305, 351, 376 (sh), 504
Pt(dmbpy)(OPhOMe)$_2$	256, 270 (sh), 281, 310, 322, 369, 390
Pt(dmbpy)(SPhCOOMe)$_2$	240, 317, 336, 472
Pt(dmbpy)(OPhCOOMe)$_2$	257 (sh), 285 (sh), 299, 354, 384

The absorption spectra of the platinum(II) diimmine dithiolates and phenolates produced the same absorption spectra as their deuterated analogues and any spectral differences appear to be merely due to sample concentration. Whilst it was attempted to run the absorption spectra of the complexes and their deuterated analogues at the same concentration, it was challenging due to the small quantities required to run them (*ca.* 1-2 mg in 3 ml of solvent). Ideally these spectra would have been presented with extinction coefficient values, however there was not enough of each sample to perform the UV/vis titrations to obtain this data.

The platinum(II) thiolate complexes exhibit a broad asymmetric absorption of medium intensity in the visible region centred around 470-510 nm. The variation of the substituent in the 4- position on the thiolate ligand shifts the transition to lower energies depending on the electron donating ability of the substituent. The observed trend for both Pt(bpy)(S-Ph-X) and Pt(dmbpy)(S-Ph-X) is that the energy of the transition decreases as X changes from OMe to COOMe to H. This is due to the decrease in the HOMO-LUMO band gap with donor ligand donicity. In previous studies on platinum(II) diimmine dithiolates, where the diimmine is a derivative of bipyridine, the lowest excited state has been assigned as CT-to-diimmine,[9] or LLCT.[10]

The absorption spectra for the platinum(II) diimmine dithiolates show good agreement with the predicted spectra obtained from the optimised geometries calculated by Heather Carson (Figure 4.20 - Figure 4.24). These spectra are shown below, red sticks indicate the wavelength at with the transition is predicted to occur and the height of the stick indicating its predicted intensity.

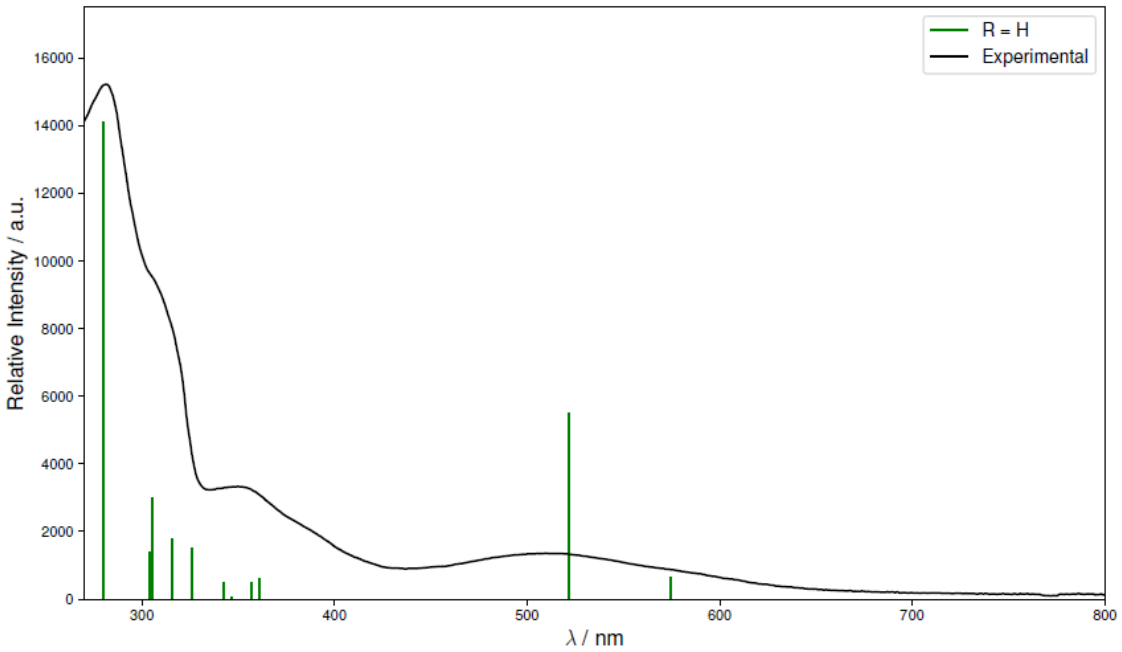

Figure 4.20 Experimental electronic absorption spectrum - black line, calculated spectrum – green sticks, for the complex Pt(bpy)(S-Ph)$_2$.

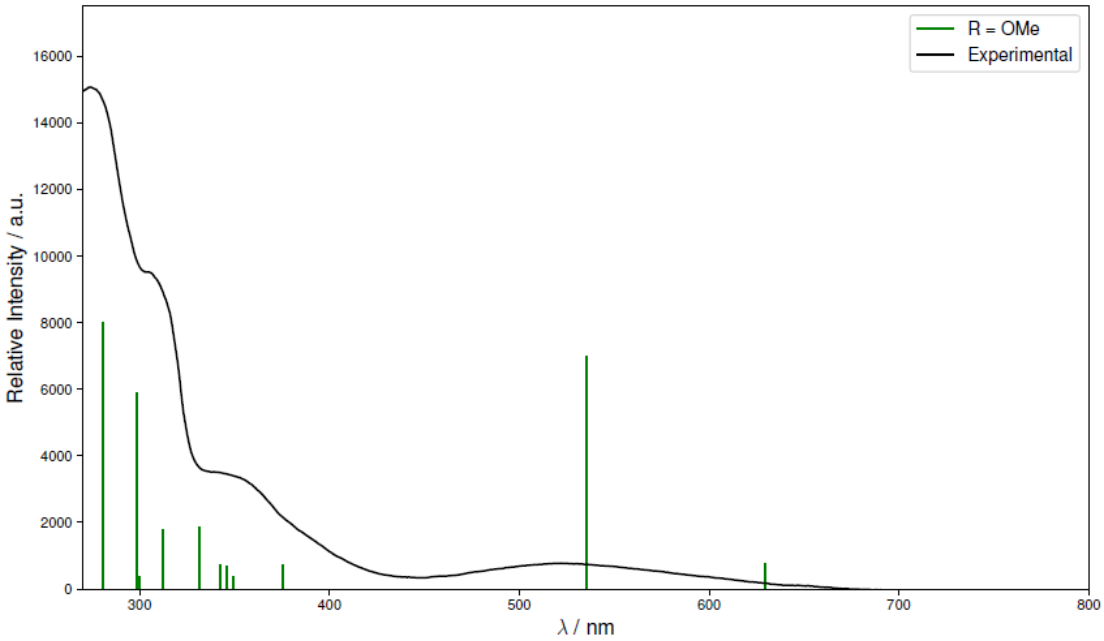

Figure 4.21 Experimental electronic absorption spectrum - black line, calculated spectrum – green sticks, for the complex Pt(bpy)(S-Ph-OMe)$_2$.

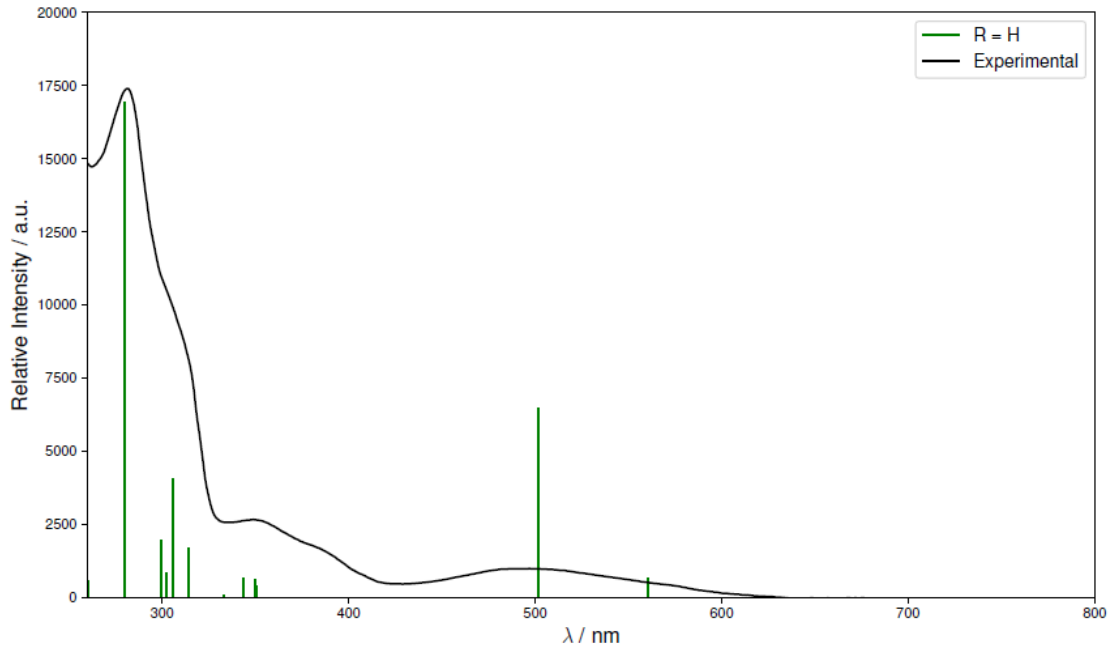

Figure 4.22 Experimental electronic absorption spectrum - black line, calculated spectrum – green sticks, for the complex Pt(dmbpy)(S-Ph)₂.

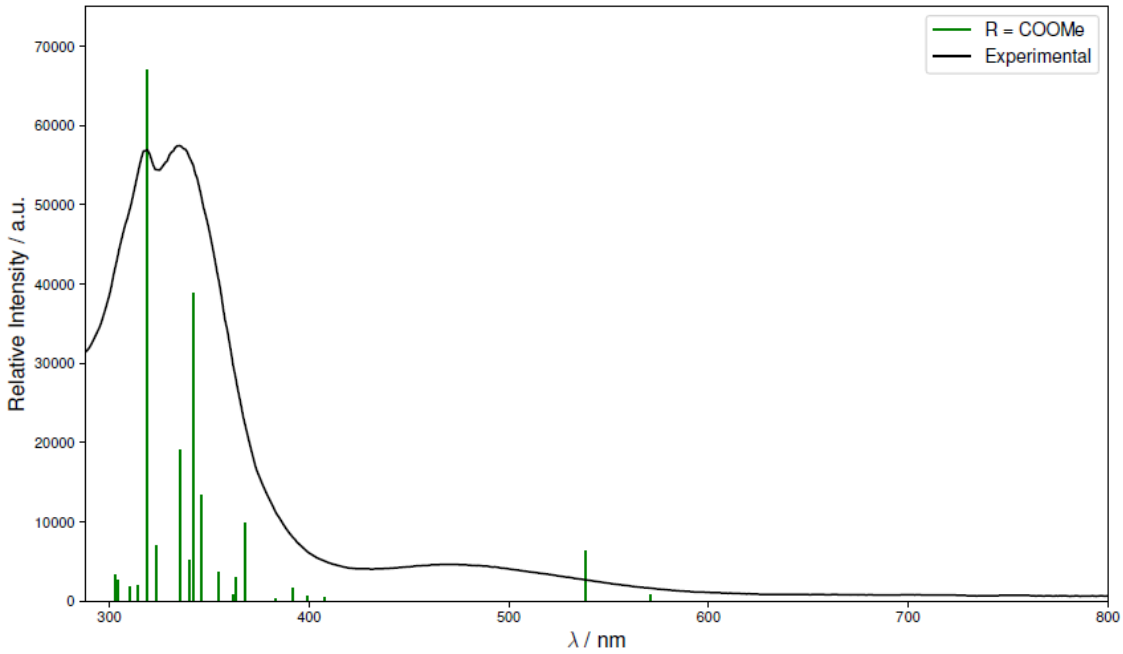

Figure 4.23 Experimental electronic absorption spectrum - black line, calculated spectrum – green sticks, for the complex Pt(dmbpy)(S-Ph-COOMe)₂.

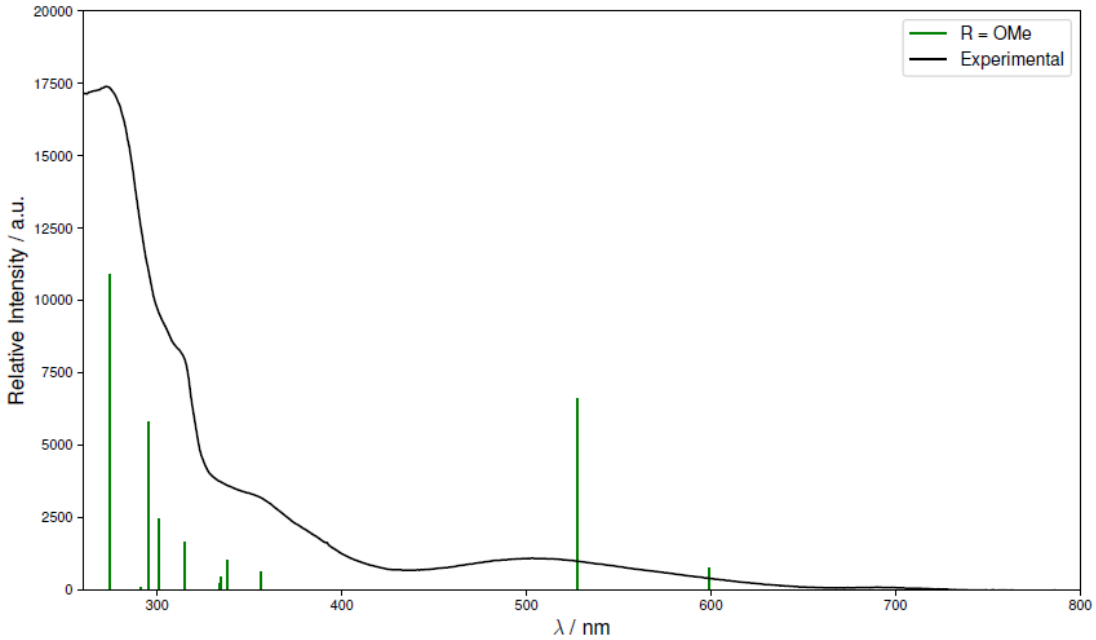

Figure 4.24 Experimental electronic absorption spectrum - black line, calculated spectrum – green sticks, for the complex Pt(dmbpy)(S-Ph-OMe)₂.

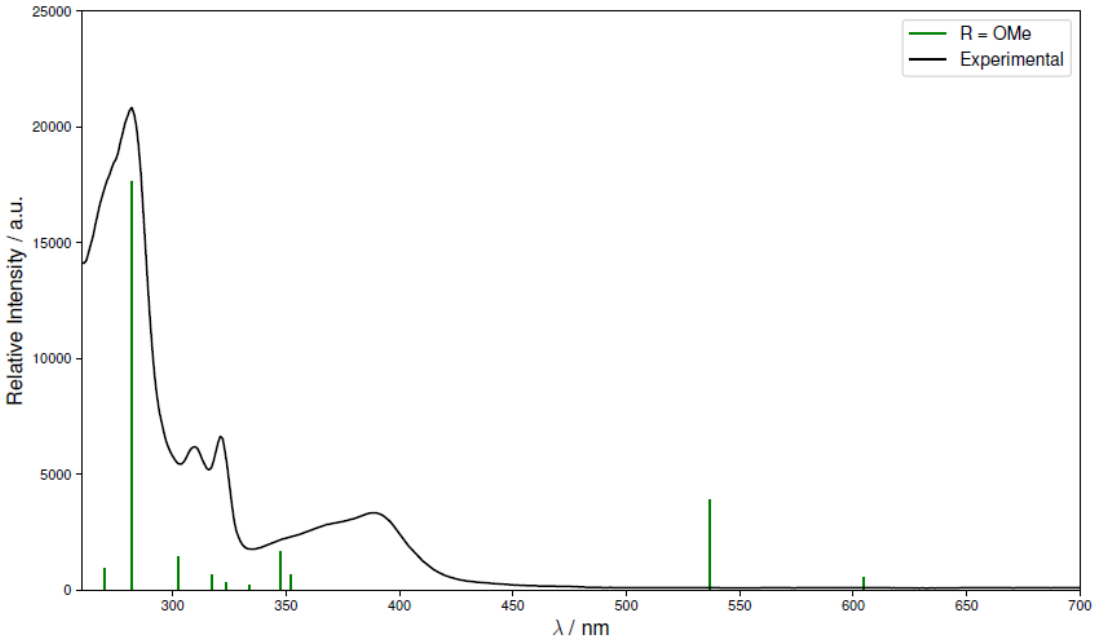

Figure 4.25 Experimental electronic absorption spectrum - black line, calculated spectrum – green sticks, for the complex Pt(dmbpy)(O-Ph-OMe)₂.

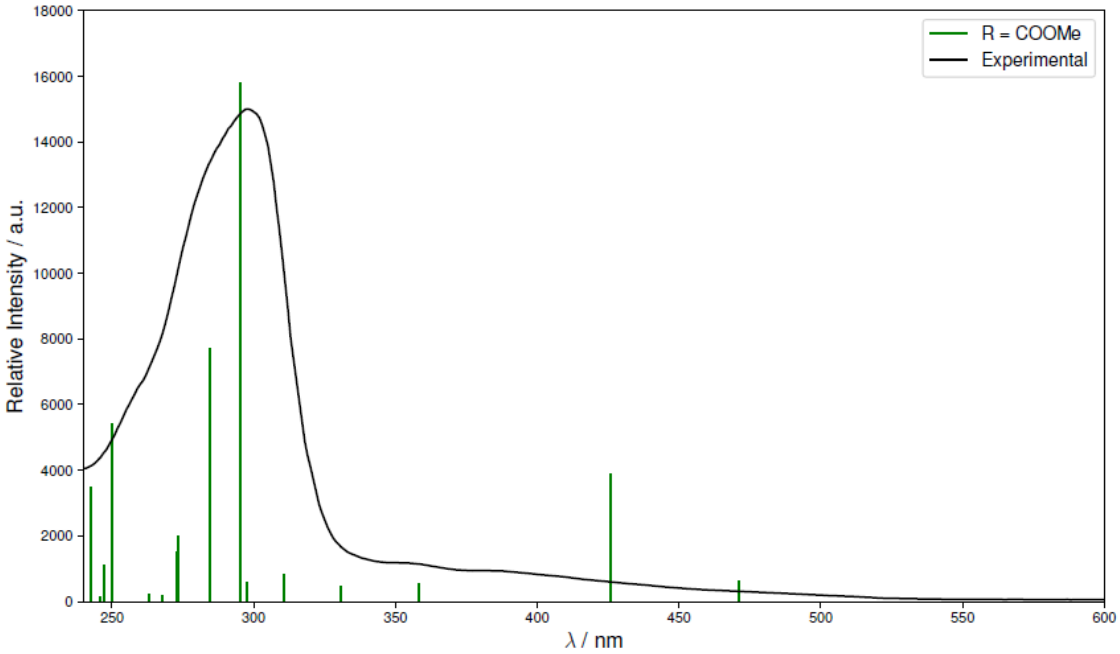

Figure 4.26 Experimental electronic absorption spectrum - black line, calculated spectrum – green sticks, for the complex Pt(dmbpy)(O-Ph-COOMe)$_2$.

4.3.3 Time-resolved Resonance Raman (TR^3)

Unfortunately the TR^3 set-up rapidly decomposed all of the complexes before any signal could be detected. The nature of the decomposition results in precipitation of a product that introduces scattering to the experiment and therefore makes it difficult to detect Raman signal.

4.4 Conclusions

A series of 5 platinum(II) diimmine dithiolates and their 5 deuterated analogues were synthesised along with 2 platinum(II) diimmine phenolates and their 2 deuterated analogues. The absorption spectra of the complexes were recorded and showed good agreement with calculated spectra. Unfortunately the TR^3 experiment did not work as desired and therefore no data was obtained for the investigation of the structural reorganisation in the excited state.

4.5 Future Work

It is clear that stability is an issue when studying these complexes under high power laser experiments. It would be of interest to synthesise platinum(II) diimine dithiolates in which the dithiolate ligand was chelating to increase the rigidity of the complexes which may in turn stabilise the excited state.

4.6 References

1 M. Y. Mel'nikov, J. a. Weinstein, M. Y. Mel'nikov and J. a. Weinstein, *High Energy Chem.*, 2008, **42**, 287–289.

2 J. A. Weinstein, N. N. Zheligovskaya, M. Y. Mel'nikov and F. Hartl, *Dalt. Trans.*, 1998, 2459–2466.

3 J. A. Weinstein, A. J. Blake, E. S. Davies, A. L. Davis, M. W. George, D. C. Grills, I. V. Lileev, A. M. Maksimov, P. Matousek, M. Y. Mel'Nikov, A. W. Parker, V. E. Platonov, M. Towrie, C. Wilson and N. N. Zheligovskaya, *Inorg. Chem.*, 2003, **42**, 7077–7085.

4 S. Huertas, M. Hissler, J. E. McGarrah, R. J. Lachicotte and R. Eisenberg, *Inorg. Chem.*, 2001, **40**, 1183–1188.

5 J. R. Schoonover and G. F. Strouse, *Chem. Rev.*, 1998, **98**, 1335–1356.

6 J. L. Wootton and J. I. Zink, *J. Phys. Chem.*, 1995, **99**, 7251–7257.

7 S. K. Sahoo, S. Umapathy and A. W. Parker, *Appl. Spectrosc.*, 2011, **65**, 1087–1115.

8 P. Matousek, M. Towrie and a W. Parker, *Appl. Spectr.*, 1999, **53**, 1485–1489.

9 M. Hissler, J. E. McGarrah, W. B. Connick, D. K. Geiger, S. D. Cummings and R. Eisenberg, *Coord. Chem. Rev.*, 2000, **208**, 115–137.

10 A. Vogler, H. Kunkely, J. Hlavatsch and A. Merz1, *Inorg. Chem.*, 1984, **23**, 506–509.

5 Isotopic labelling of *bis*-acetylide platinum(II) complexes containing 1,8-Naphthalimide

5.1 Introduction

5.1.1 Platinum(II) trans-acetylides donor-bridge-acceptor assemblies

Electron transfer is a fundamental mechanism in many natural processes including respiration and photosynthesis. The process of electron transfer in solar energy technologies and molecular electronic devices has implications for their efficiency. In recent years there have been developments in controlling electron transfer through using light as an external perturbation, enabling more predictive design of molecular devices.[1]

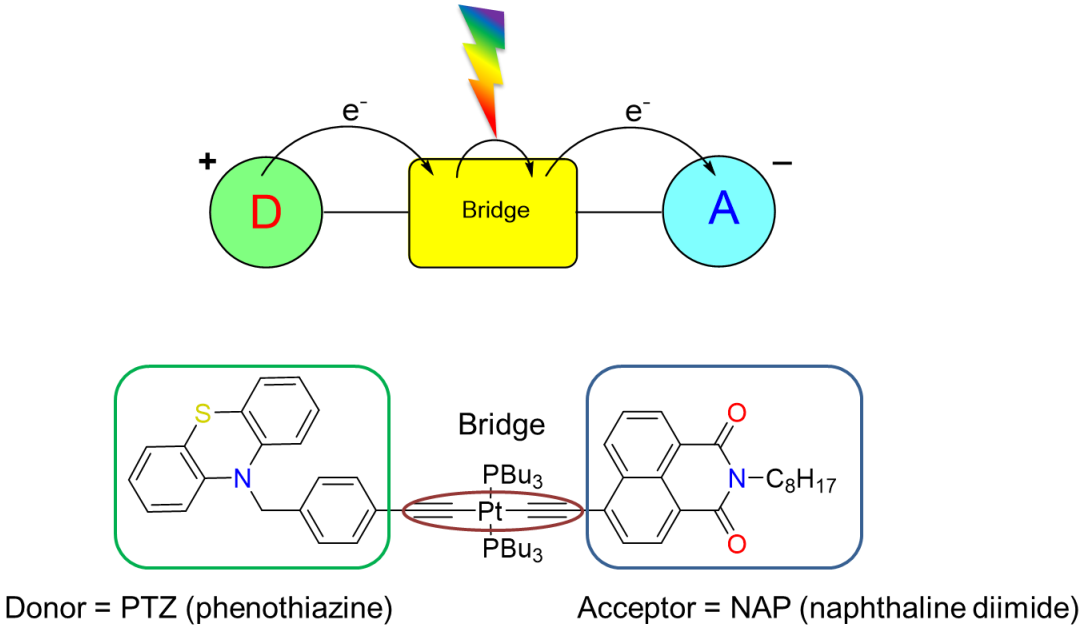

Figure 5.1. Platinum(II) trans-acetylide complexes investigated in this chapter, showing the donor bridge and acceptor components of the system.

Ultrafast spectroscopic techniques are employed to study electron transfer, which occurs on sub-picosecond timescales, in real-time. Intramolecular photoinduced electron transfer can involve the formation of a charge-separated excited state which is formed due to a rearrangement of electron density from the donor, D, part of the molecule to the electron acceptor, A. This often occurs via a bridge, B, which can have affect the rate of the electron transfer.

In this chapter linear, asymmetric platinum(II) trans-acetylides will be investigated as Donor-Bridge-Acceptor complexes (Figure 5.1). The molecular design of these systems employ the platinum(II) bridge to adopt a square planar geometry which provides directionality to the electron transfer. The presence of donor acetylide ligands aid the formation of long-lived stable charge separated states. These systems utilise the strong electron donor phenothiazine (PTZ) and the electron acceptor 4-ethynyl-*N*-octyl-1,8-naphthalimide (NAP). The complexes also contain neutral phosphine ligands which lack low lying π* orbitals and therefore do not interfere in the charge transfer process.

5.1.2 Previous work in the group on vibrational control

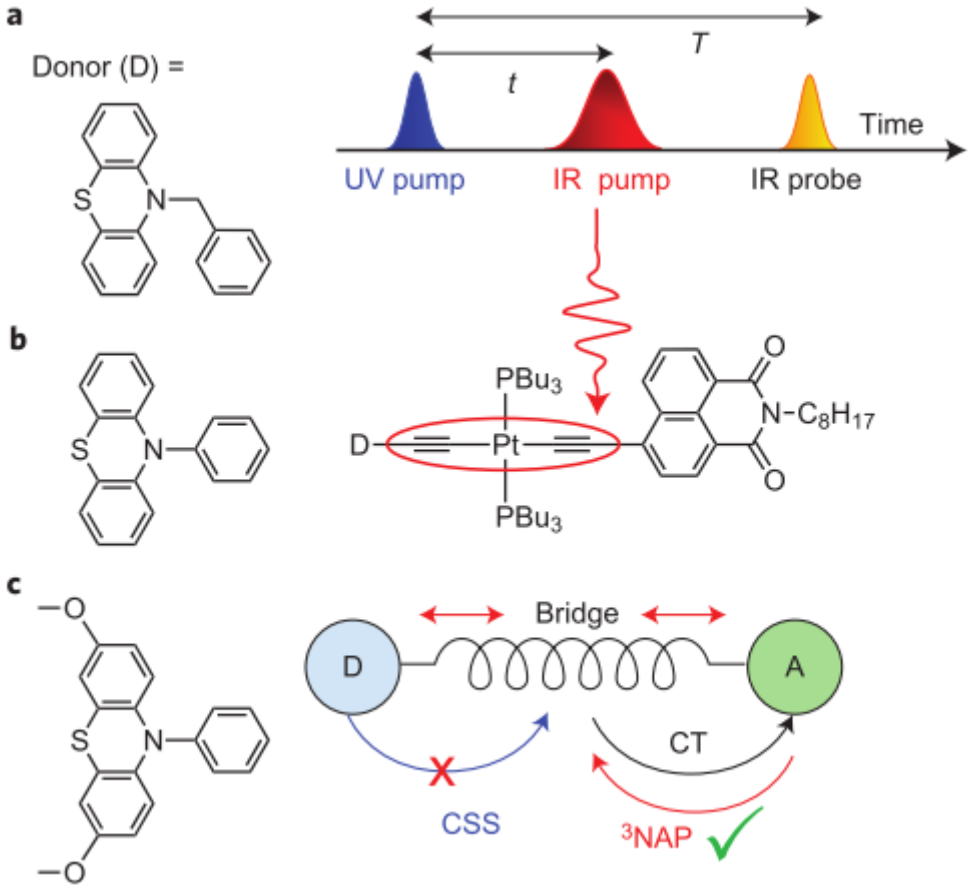

Figure 5.2 Summary of infrared-control experiments. ***a,****The* UV_{pump}–IR_{pump}– IR_{probe} *pulse sequence used in infrared control experiments, with the infrared pump chopped at half the ultraviolet pump repetition rate to facilitate collection of* IR_{pump}*(on–off) measurements. Time-resolved infrared measurements were carried out without the intermediate infrared pump.* ***b,*** *Structures of the three DBA triads investigated, where the donor side was varied to systematically change the driving force of charge separation.* ***c,*** *Schematic electron transfer (ET) pathways initiated by 400 nm light: bridge-to-acceptor charge transfer (CT), followed by population of an acceptor-localized π–π* triplet state (*^{3}*NAP) or reductive quenching by the donor to form the full charge-separated state (CSS). The latter process is switched off by intermediate infrared excitation. Reproduced with permission from* [1]*.*

Previous work in the Weinstein group studied a series of platinum(II) *trans*-acetylide complexes of the type D-C≡C-Pt(PBu_3)$_2$-C≡C-NAP, where D was one of three phenothiazine based donor ligands as outlined above (Figure 5.2).[1–4] It was observed that infrared excitation of the platinum(II) *trans*-acetylide bridge after ultraviolet initiated charge separation changed the yields of light induced product states.[1,4]

The infrared excitation pump had a frequency of 2087 cm^{-1} to match the vibrational frequency of the acetylides on the bridge.[2] Both of the acetylide groups absorb at this wavelength and therefore there is no way of selectively exciting them separately.

5.1.3 Aims

The aims of this chapter are to synthesise and purify isotopically labelled analogues of the complex PTZ-CH_2-Ph-C≡C-Pt(PBu_3)$_2$-C≡C-NAP. The synthesis of the complex will be modified to incorporate carbon-13 labelled acetylides on either acetylide, *i.e.* donor-side or acceptor-side of the platinum centre, and both sides in the same molecule. The aim of this is to shift the vibrational frequencies of the acetylides by enough to selectively excite one side of the complex either the donor or acceptor. Using simple mathematics the shift in vibrational frequency between a non-labelled carbon-12 acetylide and a carbon-13 labelled acetylide can be estimated as shown:

$$\tilde{\nu} = \frac{1}{2\pi c}\sqrt{\frac{k}{\mu}}$$

Equation 5.1. Where ν̃ = the wavenumber of the molecular vibration, c=the speed of light in a vacuum, k= the force constant, μ= the reduced mass.

$$\mu = \frac{m_1 \times m_2}{m_1 + m_2}$$

Equation 5.2. Where μ = the reduced mass, m_1= the mass of atom 1, m_2 = the mass of atom 2.

For C^{12}≡C^{12}:

$$m_1 = 12 \times 1.67377 \times 10^{-24}\ g = 2.008524 \times 10^{-23}\ g \approx 2.009 \times 10^{-23}\ g$$

$$m_1 = m_2$$

$$\therefore \mu = \frac{{m_1}^2}{2m_1}$$

$$\mu = \frac{(2.009 \times 10^{-23} g)^2}{2(2.009 \times 10^{-23} g)} = 1.0045 \times 10^{-23}\ g\ \approx 1.005 \times 10^{-23}\ g$$

Force constant for triple bond ≃ 15 x 10^5 dyne cm^{-1} (where 1 dyne = 1 g cm s^{-2}) ∴ 15 x 10^5 g s^{-2} :

$$\tilde{\nu} = \frac{1}{2\pi \times 3 \times 10^{10}\ cm\ s^{-1}} \sqrt{\frac{15 \times 10^5 g\ s^{-2}}{1.005 \times 10^{-23}\ g}} = \mathbf{2049.56\ cm^{-1}}$$

For $C^{13} \equiv C^{13}$:

$$m_1 = 13 \times 1.67377 \times 10^{-24}\ g = 2.175901 \times 10^{-23}\ g \approx 2.176 \times 10^{-23}\ g$$

$$m_1 = m_2$$

$$\therefore \mu = \frac{{m_1}^2}{2m_1}$$

$$\mu = \frac{(2.176 \times 10^{-23} g)^2}{2(2.176 \times 10^{-23} g)} = 1.088 \times 10^{-23}\ g$$

$$\tilde{\nu} = \frac{1}{2\pi \times 3 \times 10^{10}\ cm\ s^{-1}} \sqrt{\frac{15 \times 10^5 g\ s^{-2}}{1.088 \times 10^{-23}\ g}} = \mathbf{1969.84\ cm^{-1}}$$

$$2049.56\ cm^{-1} - 1969.84\ cm^{-1} = \ 79.72\ cm^{-1}\ \approx \mathbf{80\ cm^{-1}}$$

Therefore, it is predicted that the vibrational frequency of the acetylide should vary by approximately 80 cm^{-1} between the carbon-12 and carbon-13 analogues of the molecules. It is possible to synthesise these complexes by substituting the trimethylsilylacetylene in the first cross coupling step of the ligand synthesis with carbon-13 labelled trimethylsilylacetylene (Scheme 5.1).

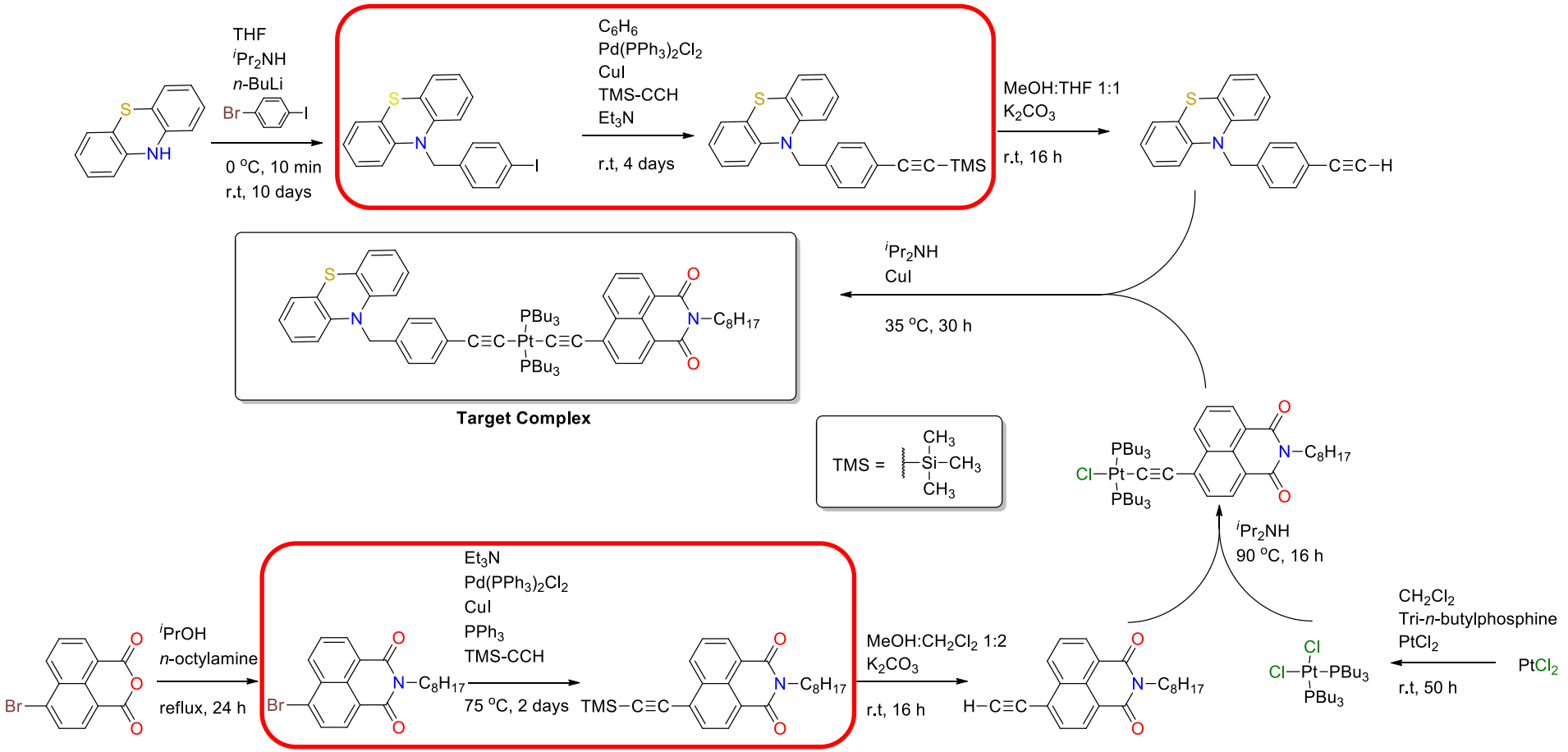

Scheme 5.1. The planned route to the synthesis of the D-B-A Pt(II) trans-acetylide complex where isotopic labelled acetylides can be introduced in the steps highlighted in red boxes.

5.2 Experimental

5.2.1 Materials and General Procedures

Commercially available starting materials were obtained from Sigma-Aldrich, Alfa-Aesar, Acros Organics, Manchester Organics, Fluorochem, Apollo Scientific and were used without further purification unless otherwise stated. All solvents (Fisher Scientific, Sigma-Aldrich, VWR) were HPLC grade and used without further purification unless otherwise stated. Dry solvents were obtained from the University of Sheffield Grubbs purification system and stored under a nitrogen atmosphere. Solvent deaeration was performed by sparging with argon for a period of at least 20 min. Column chromatography was performed using either silica gel (60 Å mesh, Fluorochem) or aluminium oxide (Brockmann III grade, Acros). Unless otherwise state, all syntheses were carried out under an atmosphere of argon using Schlenk line techniques.

5.2.2 Synthetic Procedures

5.2.2.1 Synthesis of cis-Pt(PBu$_3$)$_2$Cl$_2$ (5.1)

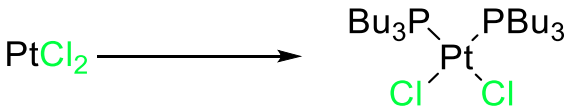

Tri-*n*-butylphosphine (1.85 ml, 1.52 g, 7.519 mmol) was added to a suspension of platinum(II) chloride (1.00 g, 3.760 mmol) in deaerated, dry CH_2Cl_2 (80 ml) and stirred at room temperature under an inert atmosphere (argon) for 7 days. The reaction mixture was filtered remove solid particulates and then the solvent was removed *in vacuo* to leave a grey solid. The solid was washed with hexane (50 ml) and sonicated for one minute and then filtered, the solid on the filter paper was washed with more portions of cold hexane (4 x 20 ml). The solids were then washed on the filter paper with diethyl ether until no solid remained (~ 100 ml), then the solvent was removed *in vacuo* to give the product as an off-white solid (2.01 g, 80 %).

^{1}H NMR ($CDCl_3$, 250 MHz): 0.85-1.04 (m, 18H), 1.34-1.66 (m, 24H), 1.75-2.17 (m, 12H). ^{31}P NMR ($CDCl_3$, 250 MHz): 0.95 ($J_{Pt\text{-}P}$ = 3518 Hz).

5.2.2.2 Synthesis of 4-bromo-N-octyl-1,8-naphthalimide (5.2)

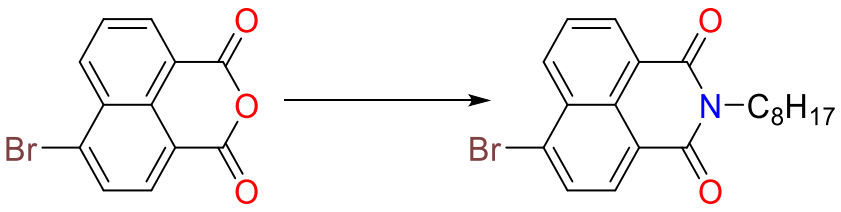

4-bromo-1,8-naphthalic anhydride (4.9 g, 17.7 mmol) and *n*-octylamine (6.05 g, 7.8 ml, 46.8 mmol) were added to deaerated isopropanol (100 ml) and refluxed for 24 hours. The volume of the reaction solution was reduced *in vacuo* and cooled to 0 °C. Methanol (~ 200 ml) was added to induce precipitation of the product which was collected by vacuum filtration and washed with cold methanol (3 x 50 ml) until the filtrate stopped staining thin layer silica plates yellow. The pale yellow solid was dried *in vacuo* to give 4-bromo-*N*-octyl-1,8-naphthalimide (5.25 g, 76 %).

^{1}H NMR (400 MHz, $CDCl_3$) δ 8.66 (d, *J* = 7.2 Hz, 1H), 8.57 (d, *J* = 8.4 Hz, 1H), 8.41 (d, *J* = 7.8 Hz, 1H), 8.04 (d, *J* = 7.8 Hz, 1H), 7.89 – 7.81 (m, 1H), 4.22 – 4.05 (m, 2H), 1.72 (dt, *J* = 15.1, 7.5 Hz, 2H), 1.48 – 1.14 (m, 10H), 0.87 (t, *J* = 6.7 Hz, 3H).
ESMS: m/z = 388.1 (MH^+, 100 %).

5.2.2.3 Synthesis of 4- trimethylsilyl-C≡C-N-octyl-1,8-naphthalimide (5.3)

4-bromo-*N*-octyl-1,8-naphthalimide (1.01 g, 2.601 mmol), copper(I) iodide (51 mg, 0.267 mmol, 10 mol%), bis(triphenylphosphine)palladium chloride (91 mg, 0.130 mmol, 5 mol%) and triphenylphosphine (34 mg, 0.130 mmol, 5.0 mol%) were added to deaerated triethylamine (45 ml) and stirred at room temperature for 15 minutes. Trimethylsilylacetylene (1.48 ml, 0.69 g ml^{-1}, 10.4 mmol) was added which resulted in a colour change from yellow to dark brown/black. The reaction solution was heated at

75 °C for 48 hours, allowed to cool and the solvent removed *in vacuo*. The crude product was dissolved in diethyl ether and passed down a silica plug to yield a bright yellow filtrate which was dried *in vacuo* to give 4-trimethylsilyl-C≡C-*N*-octyl-1,8-naphthalimide (0.95 g, 90 %).

^{1}H NMR (400 MHz, $CDCl_3$) δ 8.62 (d, *J* = 2.0 Hz, 1H), 8.60 (d, *J* = 0.9 Hz, 1H), 8.49 (d, *J* = 7.6 Hz, 1H), 7.87 (d, *J* = 7.6 Hz, 1H), 7.83 – 7.77 (m, 1H), 4.18 – 4.12 (m, 2H), 1.72 (dt, *J* = 15.3, 7.5 Hz, 3H), 1.49 – 1.18 (m, 14H), 0.91 – 0.82 (m, 4H), 0.36 (s, 9H).

5.2.2.4 Synthesis of 4- trimethylsilyl-C^{13}≡C^{13}-N-octyl-1,8-naphthalimide (5.4)

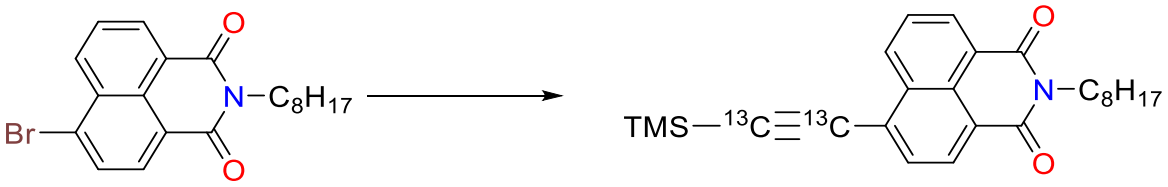

4-bromo-*N*-octyl-1,8-naphthalimide (0.28 g, 0.723 mmol), copper(I) iodide (14 mg, 0.072 mmol, 10 mol%), bis(triphenylphosphine)palladium chloride (25 mg, 0.036 mmol, 5 mol%) and triphenylphosphine (9.48 mg, 0.036 mmol, 5 mol%) were added to deaerate trimethylamine (20 ml) and stirred at room temperature for 15 minutes. Trimethylsilylacetylene (0.42 ml, 0.69 g ml^{-1}, 2.89 mmol) was added which resulted in a colour change from yellow to dark brown/black. The reaction solution was heated at 75 °C for 48 hours, allowed to cool and the solvent removed *in vacuo*. The crude product was dissolved in diethyl ether and passed down a silica plug to yield a bright yellow filtrate which was dried *in vacuo* to give 4- trimethylsilyl-C^{13}≡C^{13}-*N*-octyl-1,8-naphthalimide (0.22 g, 75 %).

^{1}H NMR (400 MHz, $CDCl_3$) δ 8.63 (d, *J* = 1.8 Hz, 1H), 8.61 (s, 1H), 8.51 (d, *J* = 7.6 Hz, 1H), 7.89 (dd, *J* = 7.6, 5.6 Hz, 1H), 7.84 – 7.78 (m, 1H), 4.19 – 4.12 (m, 2H), 1.80 – 1.64 (m, 2H), 1.48 – 1.19 (m, 10H), 0.95 – 0.78 (m, 3H), 0.36 (s, 9H).

5.2.2.5 Synthesis of 4-C≡CH-N-octyl-1,8-naphthalimide (5.5)

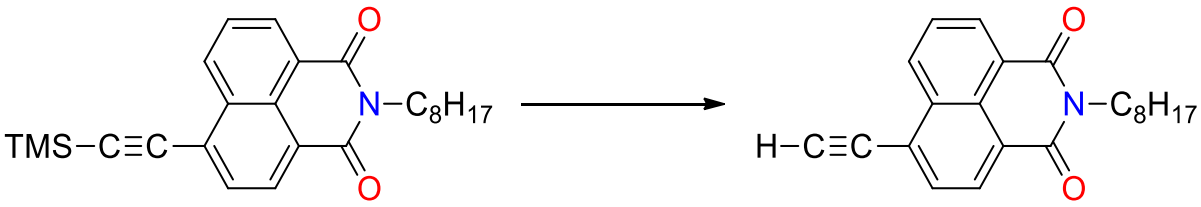

4-trimethylsilyl-C≡C-*N*-octyl-1,8-naphthalimide (0.95 g, 2.342 mmol) was added to a suspension of potassium carbonate (1.424 g, 10.30 mmol) in deaerated 1:2 (v/v) MeOH / CH_2Cl_2 (50 ml) which was stirred at room temperature for 18 hours. Water (60 ml) was added to the reaction solution to quench it and the organic solvent was removed *in vacuo* to give a solid suspension in the water. The product was then extracted with CH_2Cl_2 (2 x 100 ml) and washed with water (50 ml) and dried ($MgSO_4$) and the solvent volume reduce *in vacuo*. The product was purified via column chromatography (SiO_2, CH_2Cl) to yield a yellow solid (0.75 g, 96 %).

^{1}H NMR (400 MHz, $CDCl_3$) δ 8.61 (t, *J* = 6.9 Hz, 1H), 8.49 (d, *J* = 7.6 Hz, 1H), 7.90 (d, *J* = 7.6 Hz, 1H), 7.83 – 7.74 (m, 1H), 4.18 – 4.10 (m, 2H), 3.73 (s, 1H), 1.72 (dt, *J* = 15.3, 7.5 Hz, 2H), 1.46 – 1.18 (m, 10H), 0.86 (t, *J* = 6.8 Hz, 3H). ESMS: m/z = 334.1 (MH^+, 100 %).

5.2.2.6 Synthesis of 4- trimethylsilyl-C^{13}≡C^{13}H-N-octyl-1,8-naphthalimide (5.6)

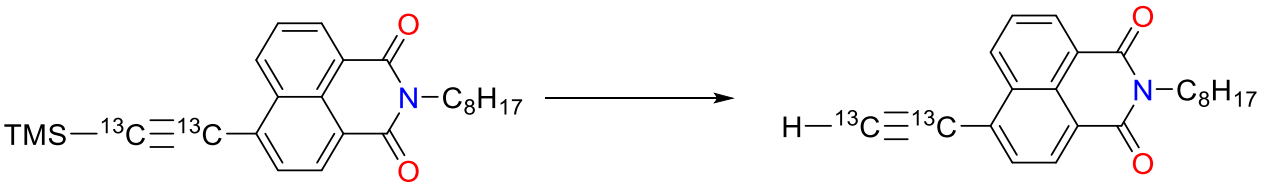

4-TMS-C^{13}≡C^{13}-*N*-octyl-1,8-naphthalimide (0.22 g, 0.540 mmol) was added to a suspension of potassium carbonate (0.40 g, 2.89 mmol) in deaerated 1:2 (v/v) MeOH / CH_2Cl_2 (20 ml) which was stirred at room temperature for 18 hours. Water (25 ml) was added to the reaction solution to quench it and the organic solvent was removed *in vacuo* to give a solid suspension in the water. The product was then extracted with

CH_2Cl_2 (2 x 50 ml) and washed with water (40 ml) and dried ($MgSO_4$) and the solvent volume reduce *in vacuo*. The product was purified via column chromatography (SiO_2, CH_2Cl) to yield a yellow solid (167 mg, 92%).

^{1}H NMR (400 MHz, $CDCl_3$) δ 8.62 (t, *J* = 7.6 Hz, 2H), 8.51 (d, *J* = 7.6 Hz, 1H), 7.91 (dd, *J* = 7.5, 6.0 Hz, 1H), 7.84 – 7.77 (m, 1H), 4.19 – 4.12 (m, 2H), 3.72 (dd, *J* = 249.9, 53.9 Hz, 1H), 1.72 (dt, *J* = 15.3, 7.5 Hz, 2H), 1.48 – 1.14 (m, 10H), 0.86 (t, *J* = 6.8 Hz, 3H).

ESMS: m/z = 336.2 (MH^+, 100 %).

5.2.2.7 Synthesis of N-(4-iodobenzyl)-phenothiazine (5.7)

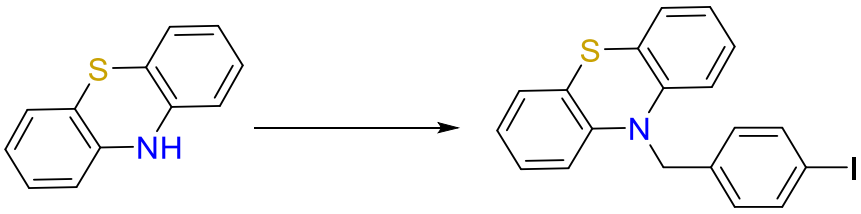

Diisopropylamine (1.8 ml, 0.722 g ml^{-1}, 12.843 mmol) was deaerated by bubbling argon through it for 30 minutes and added to dry deaerated THF (60 ml) and cooled in an ice bath to 0 ^oC. *n*-butyllithium (in hexanes) (4.95 ml, 2.5 mol dm^{-3}, 12.375 mmol) was added dropwise over 5 minutes and the mixture stirred in ice for 45 minutes. Phenothiazine (2.286 g, 11.469 mmol) was dissolved in dry deaerated THF (60 ml) and added to the reaction vessel via cannula to give a bright yellow solution the was stirred in ice for 10 minutes before warming to room temperature. 4-Iododbenzylbromide (3.78 g, 12.729 mmol) was dissolved in dry deaerated THF (60 ml) and was added via cannula transfer to the reaction solution and stirred for 10 days. Removal of the solvent *in vacuo* yielded an oily residue which was redissolved in CH_2Cl_2 (250 ml) and poured quickly into saturated brine solution (350 ml). The organic phase was extracted and washed with saturated brine solution (200 ml) and water (200 ml) before being dried ($MgSO_4$) and filtered. Removal of the solvent *in vacuo* yielded a light brown oily solid which was purified by column chromatography (SiO_2, 1:10 CH_2Cl_2: Hexane) to yield the product as a clear oily solid (3.53 g, 74 %).

^{1}H NMR (400 MHz, $CDCl_3$) δ 7.63 (d, *J* = 8.35 Hz, 2H), 7.04-7.10 (m, 4H), 6.97 (td, *J* = 1.60, 7.71 Hz, 2H), 6.86 (td, *J* = 1.03, 7.47 Hz, 2H), 6.60 (dd, *J* = 0.87, 8.11 Hz, 2H), 5.00 (s, 2H).

5.2.2.8 Synthesis of N-(4-trimethylsilyl-C≡C-benzyl)-phenothiazine (5.8)

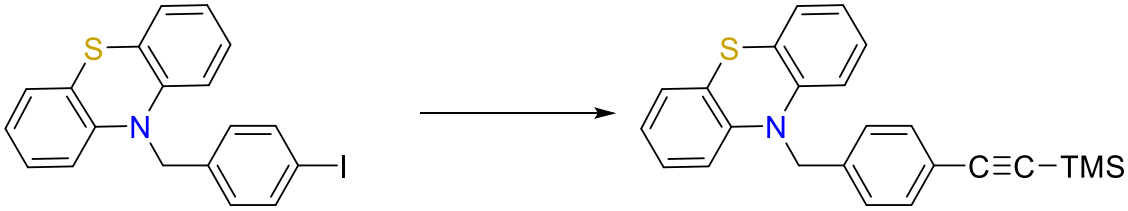

N-(4-iodobenzyl)-phenothiazine (1.00 g, 2.410 mmol), bis(triphenylphosphine) palladium chloride (90 mg, 0.128 mmol, 5 mol %), and copper iodide (53 mg, 0.278 mmol, 12 mol %) were dissolved in deaerated benzene (50 ml). Trimethylsilylacetylene (1.35 ml, 0.69 g ml^{-1}, 9.552 mmol) was added slowly to the solution which was stirred at room temperature for 10 minutes. Distilled, deaerated triethylamine (3.5 ml, 0.726 g ml^{-1}, 25.1 mmol) was added to the reaction mixture resulting in a colour change from orange to dark brown. The reaction mixture was stirred at room temperature for 5 days before the solvent being removed *in vacuo* and the product purified by column chromatography (SiO2, 1:5 CH_2Cl_2: hexane) to yield the product as a white solid (0.78 g, 84 %).

^{1}H NMR (400 MHz, $CDCl_3$) δ 7.42 (d, *J* = 8.28 Hz, 2H), 7.25 (d, *J* = 8.16 Hz, 2H), 7.09 (dd, *J* = 1.56, 7.56 Hz, 2H), 6.96 (td, *J* = 1.60, 7.68 Hz, 2H), 6.86 (td, *J* = 1.08, 7.44 Hz, 2H), 6.59 (dd, *J* = 0.96, 8.16 Hz, 2H), 5.06 (s, 2H), 0.23 (s, 9H).

5.2.2.9 Synthesis of N-(4-trimethylsilyl-C^{13}≡C^{13}-benzyl)-phenothiazine (5.9)

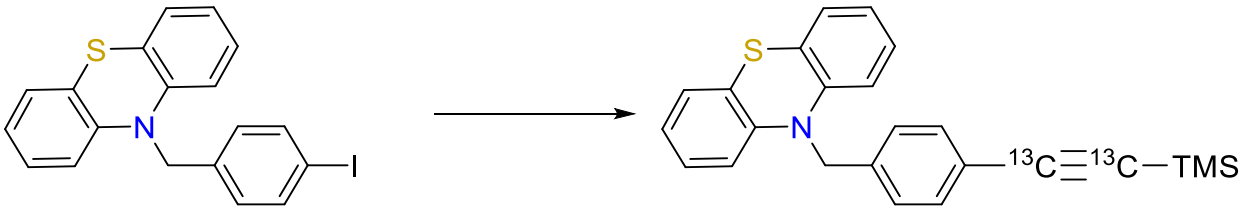

N-(4-iodobenzyl)-phenothiazine (0.25 g, 0.60 mmol), bis(triphenylphosphine) palladium chloride (2 mg, 0.03 mmol, 5 mol %), and copper iodide (14 mg, 0.07 mmol, 12 mol %) were dissolved in deaerated benzene (50 ml). Trimethylsilylacetylene (0.35 ml, 0.24 g, 2.4 mmol) was added slowly to the solution which was stirred at room temperature for 10 minutes. Distilled, deaerated triethylamine (0.84 ml,6 mmol) was added to the reaction mixture resulting in a colour change from orange to dark brown. The reaction mixture was stirred at room temperature for 5 days before the solvent being removed *in vacuo* and the product purified by column chromatography (SiO_2, 1:5 CH_2Cl_2: hexane) to yield the product as a white solid (216 mg, 88 %).

^{1}H NMR (400 MHz, $CDCl_3$) δ 7.42 (d, *J* = 8.28 Hz, 2H), 7.25 (d, *J* = 8.16 Hz, 2H), 7.09 (dd, *J* = 1.56, 7.56 Hz, 2H), 6.96 (td, *J* = 1.60, 7.68 Hz, 2H), 6.86 (td, *J* = 1.08, 7.44 Hz, 2H), 6.59 (dd, *J* = 0.96, 8.16 Hz, 2H), 5.06 (s, 2H), 0.23 (s, 9H).

5.2.2.10 Synthesis of N-(4-C≡CH-benzyl)-phenothiazine (5.10)

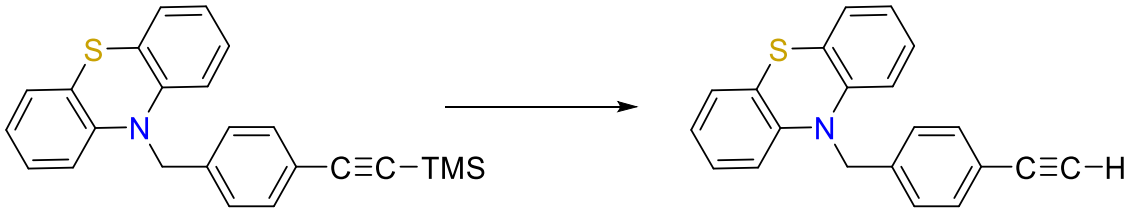

N-(4-trimethylsilyl-C≡C-benzyl)-phenothiazine (0.78 g, 2.02 mmol) was added to a suspension of potassium carbonate (0.7 g, 5.05 mmol) in deaerated 1:1 MeOH:THF (v/v) (50 ml). The reaction mixture was stirred rapidly for 24 hours at room temperature. H_2O (40 ml) was added to the reaction mixture to quench it and the organic solvent was removed *in vacuo* to give a solid foam like substance suspended in the water.

The aqueous suspension was washed with CH_2Cl_2 (3 x 100 ml) causing dissolution of the solid into the organic layer, the organic layers were combined and dried ($MgSO_4$) and the solvent removed *in vacuo* to give the crude product as a brown oil. The crude product was purified by column chromatography (SiO_2, 1:9 CH_2Cl_2: hexane) to yield *N*-(4-C≡CH-benzyl)-phenothiazine as a clear oil (0.56 g, 89 %).

^{1}H NMR (400 MHz, $CDCl_3$) δ 7.44 (d, *J* = 8.23 Hz, 2H), 7.27 (d, *J* = 8.34 Hz, 2H), 7.09 (dd, *J* = 1.56, 7.52 Hz, 2H), 6.96 (td, *J* = 1.60, 7.51 Hz, 2H), 6.86 (td, *J* = 1.11, 7.46 Hz, 2H), 6.59 (dd, *J* = 0.96, 8.16 Hz, 2H), 5.06 (s, 2H), 3.05 (s, 1H).
ESMS: m/z = 314.1 (MH^+, 100 %).

5.2.2.11 Synthesis of N-(4-C^{13}≡C^{13}H-benzyl)-phenothiazine(5.11)

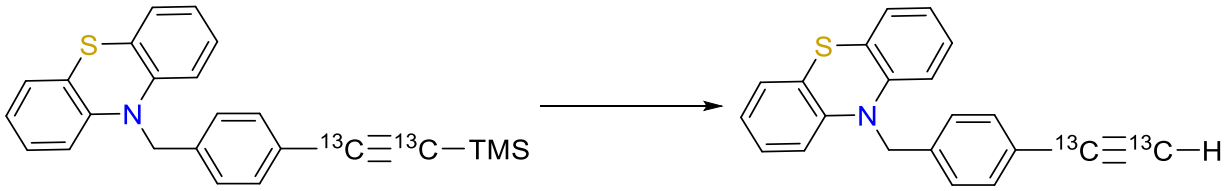

N-(4-trimethylsilyl-C≡C-benzyl)-phenothiazine (0.216 g, 0.56 mmol) was added to a suspension of potassium carbonate (193 mg, 1.4 mmol) in deaerated 1:1 MeOH:THF (v/v) (50 ml). The reaction mixture was stirred rapidly for 24 hours at room temperature. H_2O (40 ml) was added to the reaction mixture to quench it and the organic solvent was removed *in vacuo* to give a solid foam like substance suspended in the water. The aqueous suspension was washed with CH_2Cl_2 (3 x 100 ml) causing dissolution of the solid into the organic layer, the organic layers were combined and dried ($MgSO_4$) and the solvent removed *in vacuo* to give the crude product as a brown oil. The crude product was purified by column chromatography (SiO_2, 1:9 CH_2Cl_2: hexane) to yield *N*-(4-C≡CH-benzyl)-phenothiazine as a clear oil (158 mg, 91 %).

^{1}H NMR (400 MHz, $CDCl_3$) δ 7.44 (d, *J* = 8.23 Hz, 2H), 7.27 (d, *J* = 8.34 Hz, 2H), 7.09 (dd, *J* = 1.56, 7.52 Hz, 2H), 6.96 (td, *J* = 1.60, 7.51 Hz, 2H), 6.86 (td, *J* = 1.11, 7.46 Hz, 2H), 6.59 (dd, *J* = 0.96, 8.16 Hz, 2H), 5.06 (s, 2H), 3.05 (s, 1H). ESMS: m/z = 316.1 (MH^+, 100 %).

5.2.2.12 Synthesis of trans-Pt(PBu$_3$)$_2$(4-C≡C-N-octyl-1,8-naphthalimide)Cl (5.12)

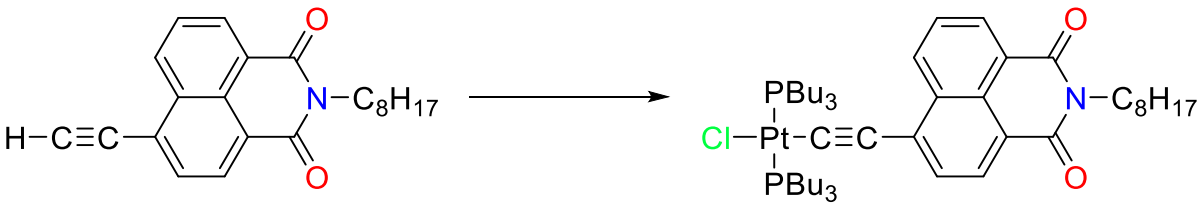

4-C≡CH-*N*-octyl-1,8-naphthalimide (178 mg, 0.532 mmol) was dissolved in distilled deaerated diisopropylamine (50 ml), to this *cis*-Pt(PBu$_3$)$_2$Cl$_2$ (0.5 g, 0.746 mmol) was added and the reaction mixture was refluxed at 84 ^{o}C in the dark for 20 hours. The reaction mixture was allowed to cool to room temperature and the solvent removed *in vacuo* to give the crude product as an orange solid. The crude product was purified by column chromatography (SiO_2, CH_2Cl_2) to give the product Pt(PBu$_3$)$_2$Cl(C≡C-NAP-C_8H_{17}) as the first bright yellow band, with the second band being the Pt(PBu$_3$)$_2$(C≡C-NAP-C_8H_{17})$_2$ complex. The solvent was removed *in vacuo* to give Pt(PBu$_3$)$_2$Cl(C≡C-NAP-C_8H_{17}) as a bright yellow film (268 mg, 52 %)

^{1}H NMR (400 MHz, $CDCl_3$) δ 8.72 (dd, *J* = 8.3, 1.1 Hz, 1H), 8.57 (dd, *J* = 7.3, 1.0 Hz, 1H), 8.45 (d, *J* = 7.7 Hz, 1H), 7.67 (dd, *J* = 8.2, 7.4 Hz, 1H), 7.58 (d, *J* = 7.7 Hz, 1H), 4.20 – 4.13 (m, 2H), 2.10 – 1.91 (m, 12H), 1.72 (dt, *J* = 15.3, 7.5 Hz, 2H), 1.67 – 1.49 (m, 12H), 1.49 – 1.19 (m, 22H), 0.98 – 0.79 (m, 21H).

APMS: m/z = 967.5 (MH^+, 100 %).

5.2.2.13 Synthesis of trans-Pt(PBu$_3$)$_2$(4-C^{13}≡C^{13}-N-octyl-1,8-naphthalimide)Cl (5.13)

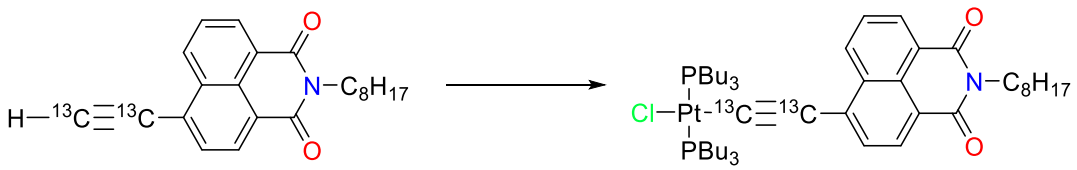

4-C^{13}≡C^{13}H-*N*-octyl-1,8-naphthalimide (167 mg, 0.498 mmol) was dissolved in distilled deaerated diisopropylamine (50 ml), to this *cis*-Pt(PBu$_3$)$_2$Cl$_2$ (468 mg, 0.697 mmol) was added and the reaction mixture was refluxed at 84 ^{o}C in the dark for 24 hours. The reaction mixture was allowed to cool to room temperature and the solvent

removed *in vacuo* to give the crude product as an orange solid. The crude product was purified by column chromatography (SiO_2, CH_2Cl_2) to give the product $Pt(PBu_3)_2Cl(C^{13}{\equiv}C^{13}\text{-NAP-}C_8H_{17})$ as the first bright yellow band, with the second band being the $Pt(PBu_3)_2(C^{13}{\equiv}C^{13}\text{-NAP-}C_8H_{17})_2$ complex. The solvent was removed *in vacuo* to give $Pt(PBu_3)_2Cl(C^{13}{\equiv}C^{13}\text{-NAP-}C_8H_{17})$ as a bright yellow film (212 mg, 44 %)

^{1}H NMR (400 MHz, $CDCl_3$) δ 8.72 (dd, *J* = 8.3, 1.1 Hz, 1H), 8.57 (dd, *J* = 7.3, 1.0 Hz, 1H), 8.45 (d, *J* = 7.7 Hz, 1H), 7.67 (dd, *J* = 8.2, 7.4 Hz, 1H), 7.57 (dd, *J* = 7.6, 5.1 Hz, 1H), 4.20 – 4.13 (m, 2H), 2.10 – 1.91 (m, 12H), 1.72 (dt, *J* = 15.3, 7.5 Hz, 2H), 1.67 – 1.49 (m, 12H), 1.49 – 1.19 (m, 22H), 0.98 – 0.79 (m, 21H).
APMS: m/z = 969.5 (MH^+, 100 %).

5.2.2.14 Synthesis of trans-Pt(PBu$_3$)$_2$(4-C≡C-N-octyl-1,8-naphthalimide)(N-(4-C≡C-benzyl)-phenothiazine (5.14)

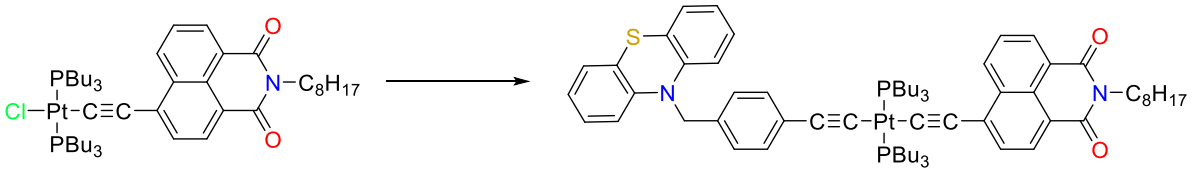

$Pt(PBu_3)_2Cl(C{\equiv}C\text{-NAP-}C_8H_{17})$ (100 mg, 0.1 mmol) and *N*-(4-C≡CH-benzyl)-phenothiazine (93 mg, 0.03 mmol) were both dissolved in diisopropylamine (15 ml) in separate flasks and deaerated with bubbling argon. The solution of *N*-(4-C≡CH-benzyl)-phenothiazine was added to the solution of $Pt(PBu_3)_2Cl(C{\equiv}C\text{-NAP-}C_8H_{17})$ via cannula transfer and copper(i) iodide (6 mg, 0.03 mmol) was added. The reaction mixture was heated in the dark to 40 ^{o}C with stirring for 24 hours. The solvent was reduced *in vacuo* to give an orange/brown solid as the crude product which was purified by column chromatography (SiO_2, 9:1 CH_2Cl_2: hexane). The product eluted first as a bright yellow band.

^{1}H NMR (400 MHz, $CDCl_3$) δ 8.77 (dd, *J* = 8.3, 1.1 Hz, 1H), 8.57 (dd, *J* = 7.3, 1.1 Hz, 1H), 8.44 (d, *J* = 7.7 Hz, 1H), 7.66 (dd, *J* = 8.1, 7.5 Hz, 1H), 7.59 (d, *J* = 7.8 Hz, 1H),

7.25 – 7.21 (m, 2H), 7.15 (d, *J* = 8.1 Hz, 2H), 7.08 (dd, *J* = 7.5, 1.5 Hz, 2H), 6.97 (td, *J* = 8.1, 1.6 Hz, 2H), 6.86 (td, *J* = 7.5, 1.0 Hz, 2H), 6.64 (dd, *J* = 8.1, 0.8 Hz, 2H), 5.03 (s, 2H), 4.18 – 4.13 (m, 2H), 2.21 – 2.03 (m, 12H), 1.77 – 1.67 (m, 2H), 1.67 – 1.50 (m, 12H), 1.50 – 1.19 (m, 22H), 0.96 – 0.81 (m, 21H).

^{31}P NMR (400 MHz, $CDCl_3$) δ 3.80 ($J_{Pt\text{-}P}$ = 2332 Hz).

5.2.2.15 Synthesis of trans-Pt(PBu$_3$)$_2$(4-C≡C-N-octyl-1,8-naphthalimide)(N-(4-C^{13}≡C^{13}-benzyl)-phenothiazine (5.15)

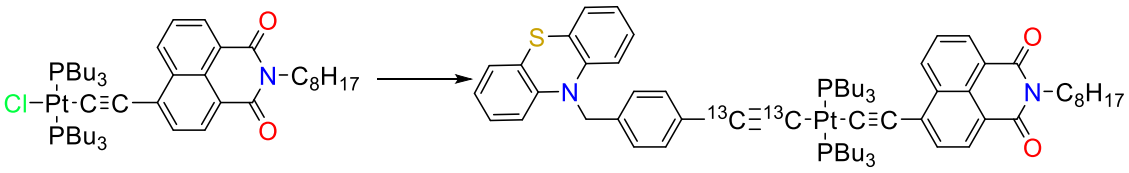

$Pt(PBu_3)_2Cl(C{\equiv}C\text{-}NAP\text{-}C_8H_{17})$ (105 mg, 0.109 mmol) and *N*-(4-$C^{13}{\equiv}C^{13}$H-benzyl)-phenothiazine (95 mg, 0.03 mmol) were both dissolved in diisopropylamine (15 ml) in separate flasks and deaerated with bubbling argon. The solution of *N*-(4-$C^{13}{\equiv}C^{13}$H-benzyl)-phenothiazine was added to the solution of $Pt(PBu_3)_2Cl(C{\equiv}C\text{-}NAP\text{-}C_8H_{17})$ via cannula transfer and copper(i) iodide (6 mg, 0.03 mmol) was added. The reaction mixture was heated in the dark to 40 °C with stirring for 24
hours. The solvent was reduced *in vacuo* to give an orange/brown solid as the crude product which was purified by column chromatography (SiO_2, 9:1 CH_2Cl_2: hexane). The product eluted first as a bright yellow band.

^{1}H NMR (400 MHz, $CDCl_3$) δ 8.77 (dd, *J* = 8.3, 1.1 Hz, 1H), 8.57 (dd, *J* = 7.3, 1.1 Hz, 1H), 8.44 (d, *J* = 7.7 Hz, 1H), 7.66 (dd, *J* = 8.1, 7.5 Hz, 1H), 7.59 (d, *J* = 7.8 Hz, 1H), 7.25 – 7.21 (m, 2H), 7.15 (d, *J* = 8.1 Hz, 2H), 7.08 (dd, *J* = 7.5, 1.5 Hz, 2H), 6.97 (td, *J* = 8.1, 1.6 Hz, 2H), 6.86 (td, *J* = 7.5, 1.0 Hz, 2H), 6.64 (dd, *J* = 8.1, 0.8 Hz, 2H), 5.03 (s, 2H), 4.18 – 4.13 (m, 2H), 2.21 – 2.03 (m, 12H), 1.77 – 1.67 (m, 2H), 1.67 – 1.50 (m, 12H), 1.50 – 1.19 (m, 22H), 0.96 – 0.81 (m, 21H).

^{31}P NMR (400 MHz, $CDCl_3$) δ 3.80 ($J_{Pt\text{-}P}$ = 2330 Hz).

5.2.2.16 Synthesis of trans-Pt(PBu$_3$)$_2$(4-C^{13}≡C^{13}-N-octyl-1,8-naphthalimide)(N-(4-C≡C-benzyl)-phenothiazine (5.16)

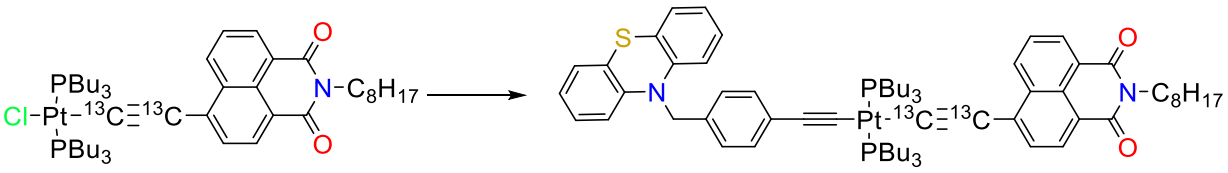

Pt(PBu$_3$)$_2$Cl(C^{13}≡C^{13}-NAP-C$_8$H$_{17}$) (110 mg, 0.113 mmol) and *N*-(4-C≡CH-benzyl)-phenothiazine (95 mg, 0.3 mmol) were both dissolved in diisopropylamine (15 ml) in separate flasks and deaerated with bubbling argon. The solution of *N*-(4-C≡CH-benzyl)-phenothiazine was added to the solution of Pt(PBu$_3$)$_2$Cl(C^{13}≡C^{13}-NAP-C$_8$H$_{17}$) via cannula transfer and copper(i) iodide (6 mg, 0.03 mmol) was added. The reaction mixture was heated in the dark to 40 ^{o}C with stirring for 24 hours. The solvent was reduced *in vacuo* to give an orange/brown solid as the crude product which was purified by column chromatography (SiO$_2$, 9:1 CH$_2$Cl$_2$: hexane). The product eluted first as a bright yellow band.

^{1}H NMR (400 MHz, CDCl$_3$) δ 8.77 (dd, *J* = 8.3, 1.1 Hz, 1H), 8.57 (dd, *J* = 7.3, 1.1 Hz, 1H), 8.44 (d, *J* = 7.7 Hz, 1H), 7.66 (dd, *J* = 8.1, 7.5 Hz, 1H), 7.59 (dd, *J* = 7.6, 5.1 Hz, 1H), 7.25 – 7.21 (m, 2H), 7.15 (d, *J* = 8.1 Hz, 2H), 7.08 (dd, *J* = 7.5, 1.5 Hz, 2H), 6.97 (td, *J* = 8.1, 1.6 Hz, 2H), 6.86 (td, *J* = 7.5, 1.0 Hz, 2H), 6.64 (dd, *J* = 8.1, 0.8 Hz, 2H), 5.03 (s, 2H), 4.18 – 4.13 (m, 2H), 2.21 – 2.03 (m, 12H), 1.77 – 1.67 (m, 2H), 1.67 – 1.50 (m, 12H), 1.50 – 1.19 (m, 22H), 0.96 – 0.81 (m, 21H).

^{31}P NMR (400 MHz, CDCl$_3$) δ 3.80 (J_{Pt-P} = 2330 Hz).

5.2.2.17 Synthesis of trans-Pt(PBu$_3$)$_2$(4-C^{13}≡C^{13}-N-octyl-1,8-naphthalimide)(N-(4- C^{13}≡C^{13}-benzyl)-phenothiazine (5.17)

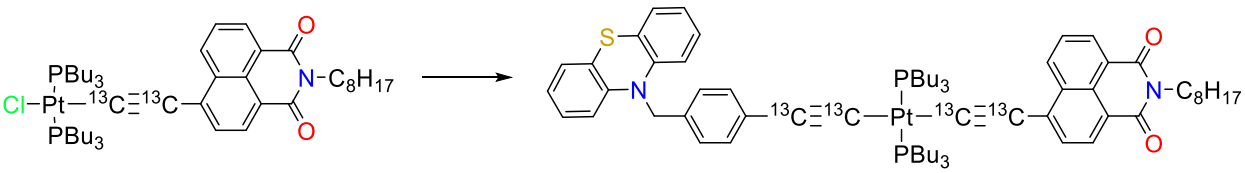

Pt(PBu$_3$)$_2$Cl(C^{13}≡C^{13}-NAP-C$_8$H$_{17}$) (102 mg, 0.105 mmol) and *N*-(4-C^{13}≡C^{13}H-benzyl)-phenothiazine (95 mg, 0.3 mmol) were both dissolved in diisopropylamine (15 ml) in

separate flasks and deaerated with bubbling argon. The solution of *N*-(4-C1^{3}≡C^{13}H-benzyl)-phenothiazine was added to the solution of Pt(PBu$_3$)$_2$Cl(C^{13}≡C^{13}-NAP-C$_8$H$_{17}$) via cannula transfer and copper(i) iodide (6 mg, 0.03 mmol) was added. The reaction mixture was heated in the dark to 40 ^{o}C with stirring for 24 hours. The solvent was reduced *in vacuo* to give an orange/brown solid as the crude product which was purified by column chromatography (SiO_2, 9:1 CH_2Cl_2: hexane). The product eluted first as a bright yellow band.

^{1}H NMR (400 MHz, $CDCl_3$) δ 8.77 (dd, *J* = 0.96, 8.28 Hz, 1H), 8.56 (dd, *J* = 0.92, 7.24 Hz, 1H), 8.44 (d, *J* = 7.72 Hz, 1H), 7.66 (t, *J* = 7.84 Hz, 1H), 7.59 (dd, *J* = 7.6, 5.1 Hz, 1H), 7.24 (d, *J* = 8.20 Hz, 2H), 7.15 (d, *J* = 8.20 Hz, 2H), 7.07 (dd, *J* = 1.48, 7.56 Hz, 2H), 6.97 (td, *J* = 1.48, 7.86 Hz, 2H), 6.85 (td, *J* = 0.88, 7.44 Hz, 2H), 6.63 (d, *J* = 8.16 Hz, 2H), 5.03 (s, 2H), 4.15 (t, *J* = 7.64 Hz, 2H) 2.05-2.20 (m, 12H), 1.67-1.76 (m, 2H), 1.58-1.67 (m, 12H), 1.20-1.47 (m, 22H), 0.84-0.92 (m, 21H).
^{31}P NMR (400 MHz, $CDCl_3$) δ 3.80 ($J_{Pt\text{-}P}$ = 2330 Hz).

5.3 Results and discussion

5.3.1 NMR

The terminal acetylene proton is very easy to identify in the carbon-13 labelled complexes by NMR spectroscopy when comparing them to the unlabelled version. For example the acetylene proton in C$_8$H$_{17}$-NAP-C≡CH produces a resonance with singlet multiplicity at 3.73 ppm (in deuterated chloroform), in contrast the resonance in the carbon-13 labelled analogue produces a resonance at the same chemical shift the multiplicity is a doublet of doublets with large coupling constants 250 Hz and 54Hz (Figure 5.3). The doublet of doublet resonance originates from the splitting from the carbon-13 nuclei present in the labelled complex which have a spin of -1/2. The closest carbon-13 is one bond away from the acetylene proton and therefore has a large coupling constant of 250 Hz whilst the other carbon-13 nucleus is 2 bonds away and has a smaller coupling constant of 54 Hz (Figure 5.4).

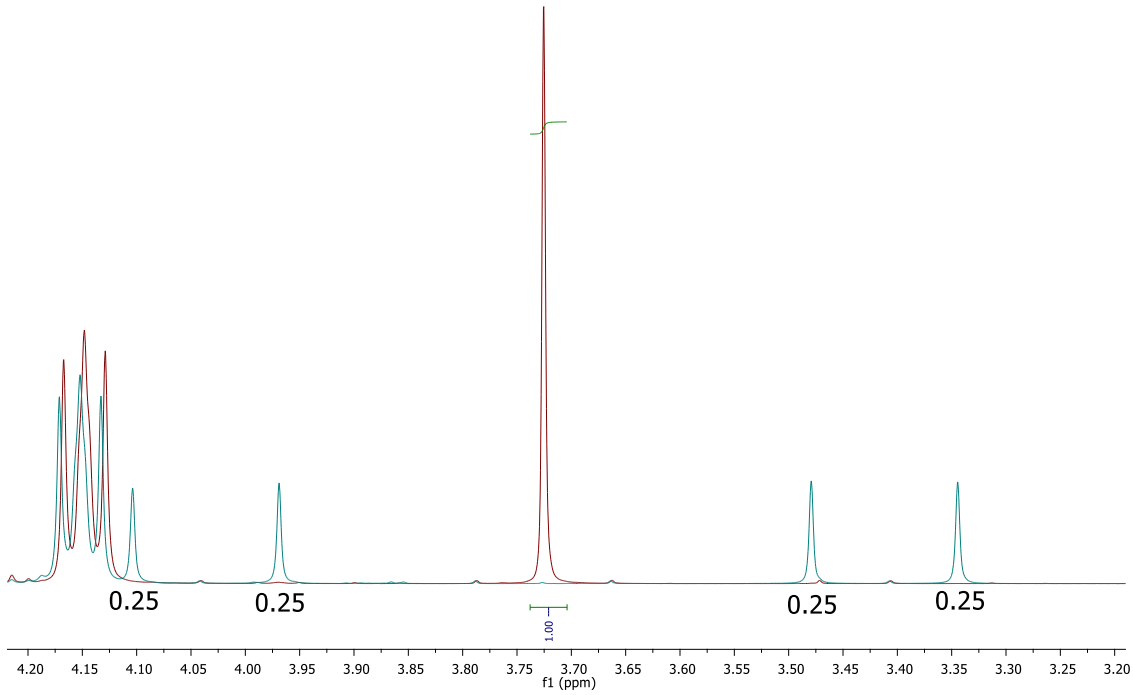

Figure 5.3. The resonance corresponding to the acetylene proton in C_8H_{17}-NAP-C≡CH ^1H NMR (red) at 3.73 ppm as a singlet and the acetylene proton in C_8H_{17}-NAP-C^{13}≡C^{13}H ^1H NMR (blue) as a doublet of doublets.

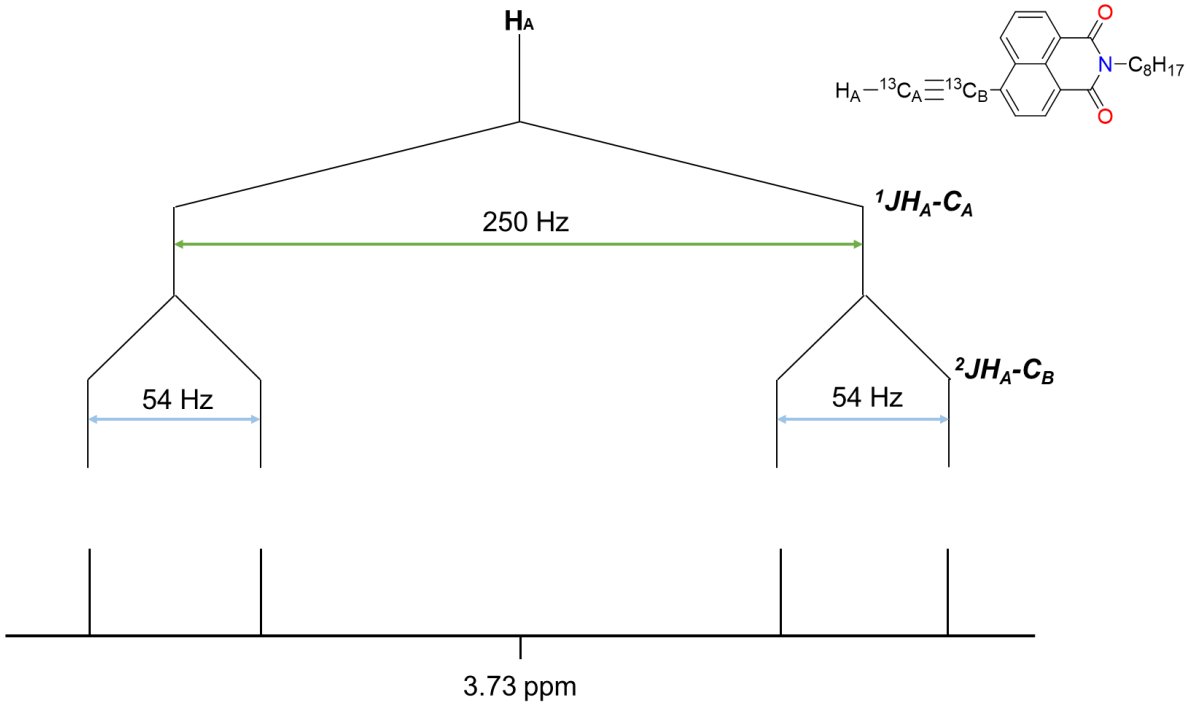

Figure 5.4. The splitting tree for proton H_A in the complex C_8H_{17}-NAP-C^{13}≡C^{13}H resulting in a resonance with a doublet of doublet multiplicity.

The introduction of a carbon-13 labelled acetylene also changes the multiplicity of the nearest aromatic proton's resonance from a doublet with a coupling constant of 7.5 Hz to a doublet of doublets with coupling constants of 7.5 Hz and 6.0 Hz (Figure 5.5). In both molecules the proton H_B is coupled to the proton three bonds away, H_C, with a coupling constant of 7.5 Hz, in the labelled molecule the proton is also coupled to the nearest carbon-13 nucleus through 3 bonds with a coupling constant of 6.0 Hz (Figure 5.6).

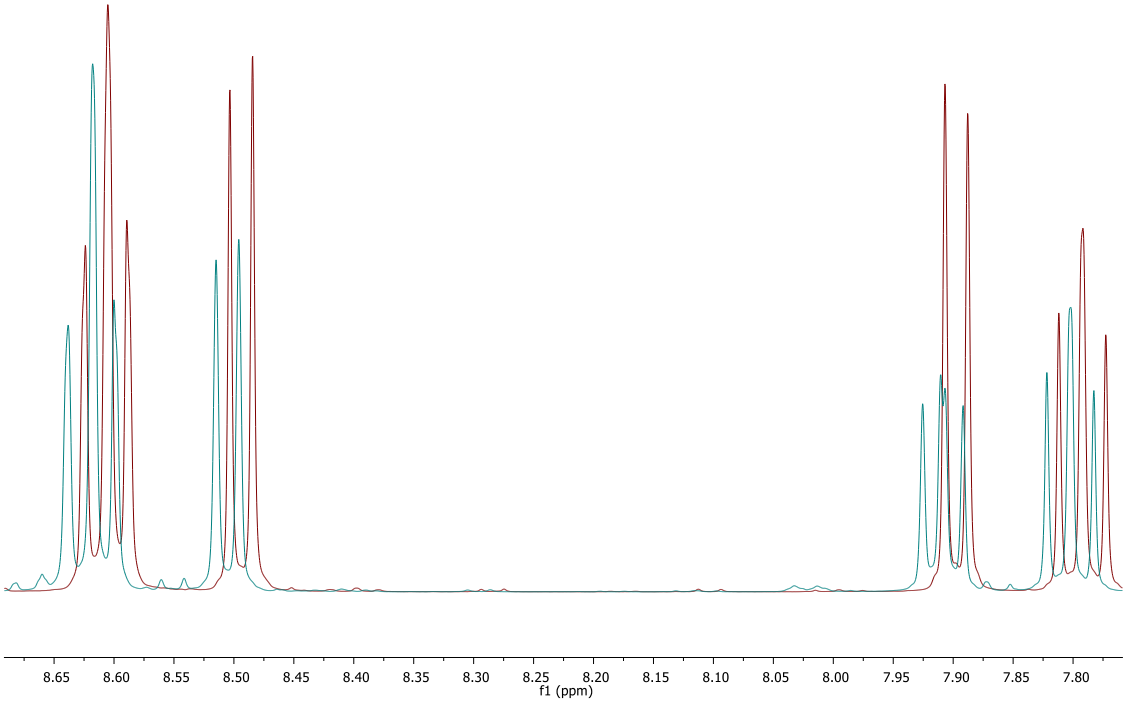

Figure 5.5. The aromatic region in C_8H_{17}-NAP-C≡CH ^{1}H NMR (red) and C_8H_{17}-NAP-C^{13}≡C^{13}H ^{1}H NMR (blue).

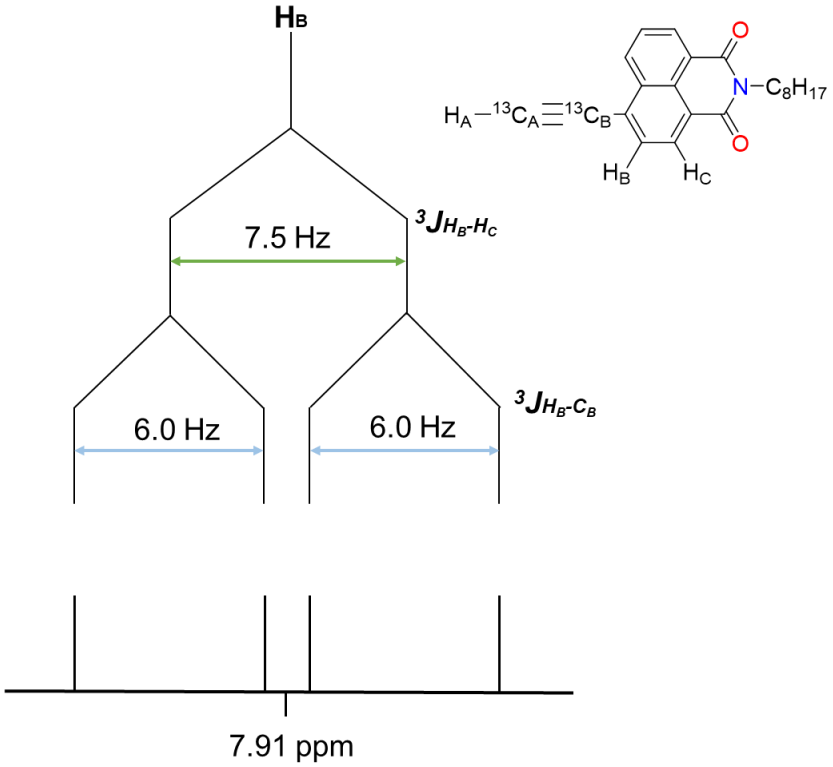

Figure 5.6. The splitting tree for proton H_B in the complex C_8H_{17}-NAP-$C^{13}{\equiv}C^{13}H$ resulting in a resonance with a doublet of doublet multiplicity.

The origin of this additional splitting was confirmed by recording the carbon-13 decoupled ^{1}H NMR of the labelled molecule. One would expect to see the resonance at 3.73 ppm, that usually has a doublet of doublet multiplicity, corresponding to the terminal acetylene proton in C_8H_{17}-NAP-$C^{13}{\equiv}C^{13}H$ appear as a singlet as in the unlabelled molecule. However, the resonance in the $^1H\{^{13}C\}$ NMR spectrum coalesces to one with triplet multiplicity indicating that the carbon resonances are not fully decoupled (Figure 5.7).

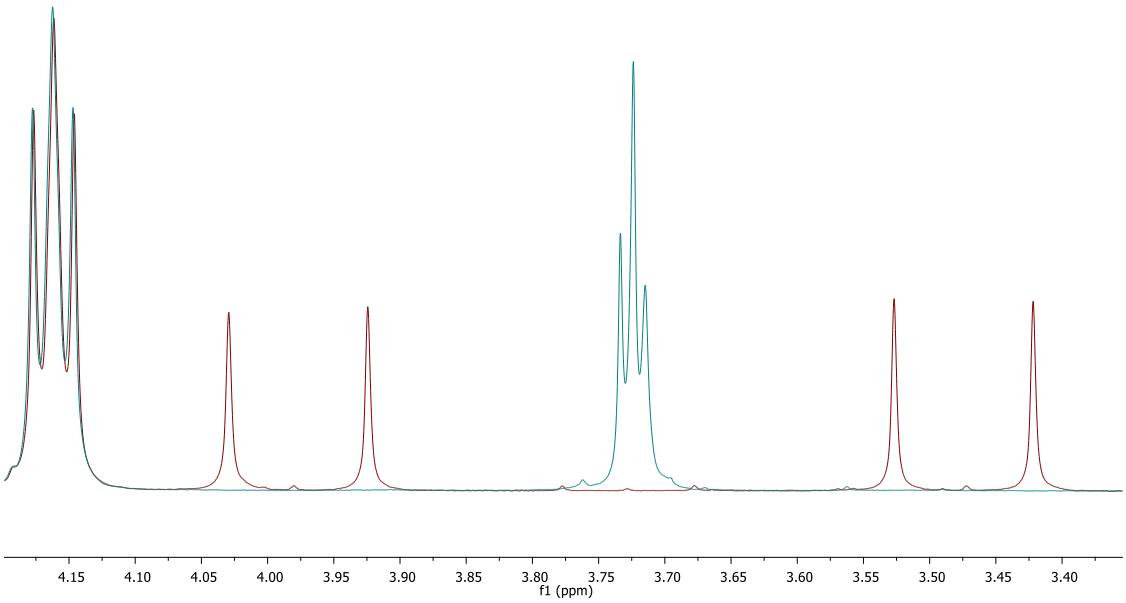

Figure 5.7. The acetylene proton resonance in C_8H_{17}-NAP-$C^{13}{\equiv}C^{13}H$ ^1H NMR (red) and in the $^1H\{^{13}C\}$ NMR (blue).

The aromatic region of the $^1H\{^{13}C\}$ NMR spectrum shows the resonance at 7.91 ppm fully decoupled from a doublet of doublets to a doublet (Figure 5.8). It is likely easier to decouple these resonances as the atoms a spaced further apart relative to the acetylene proton.

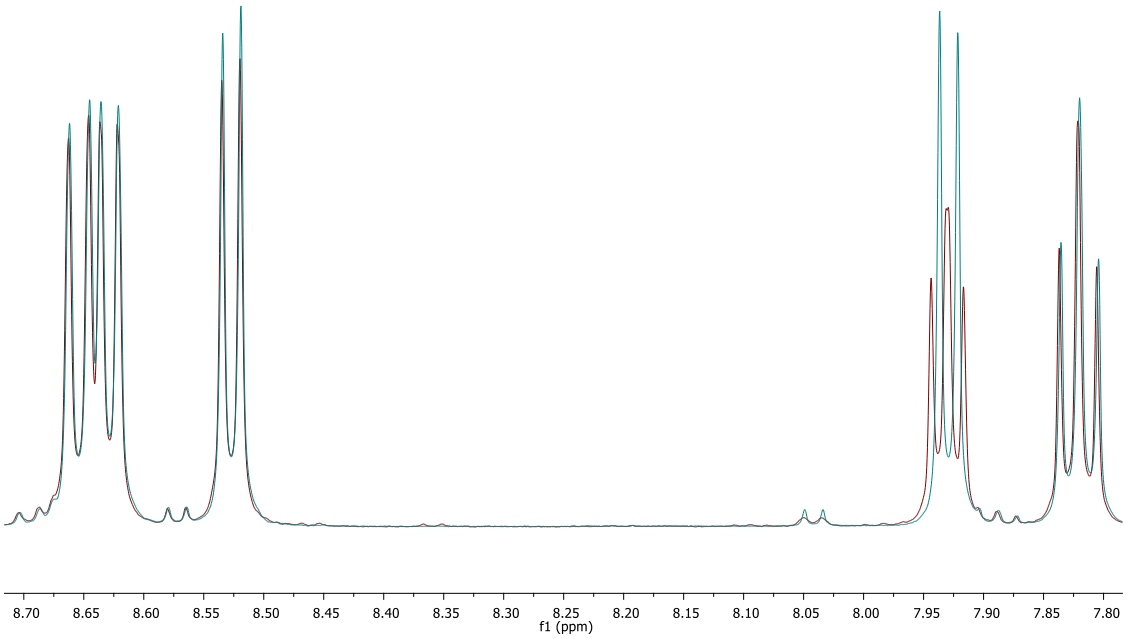

Figure 5.8. The aromatic region C_8H_{17}-NAP-$C^{13}{\equiv}C^{13}H$ ^1H NMR (red) and in the $^1H\{^{13}C\}$ NMR (blue).

5.3.2 FTIR vibrational absorption spectroscopy

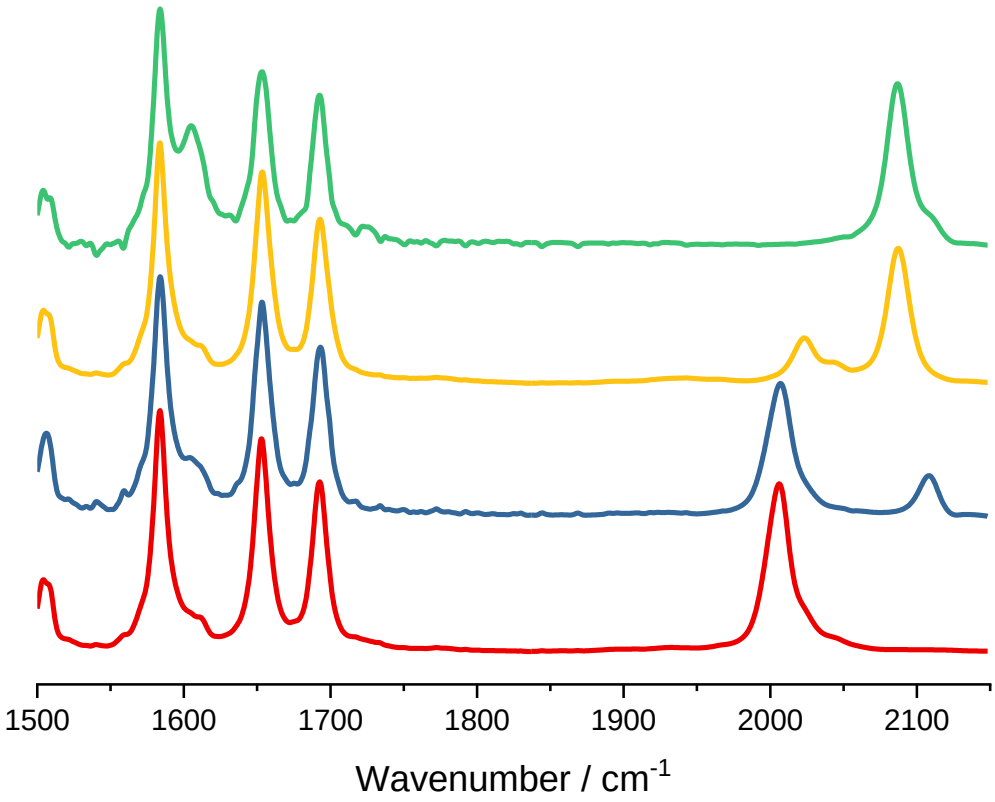

Figure 5.9. The region between 1500-2150 cm^{-1} showing the acetylide stretches for the complexes PTZ-Ph-C≡C-Pt-C≡C-NAP (green), PTZ-Ph-C^{13}≡C^{13}-Pt-C≡C-NAP (yellow), PTZ-Ph-C≡C-Pt-C^{13}≡C^{13}-NAP (blue), PTZ-Ph-C^{13}≡C^{13}-Pt-C^{13}≡C^{13}-NAP (Red). Recorded in CH_2Cl_2 at r.t.

Table 5.1. Vibrational absorption bands for complexes PTZ-Ph-C≡C-Pt-C≡C-NAP in CH_2Cl_2 at r.t

Complex	**ṽ / cm^{-1}**
PTZ-Ph-C≡C-Pt-C≡C-NAP	1583, 1605, 1653, 1692, 2090, 2110
PTZ-Ph-C^{13}≡C^{13}-Pt-C≡C-NAP	1583, 1605, 1653, 1692, 2020, 2043, 2090
PTZ-Ph-C≡C-Pt-C^{13}≡C^{13}-NAP	1583, 1605, 1653, 1692, 2010, 2110
PTZ-Ph-C^{13}≡C^{13}-Pt-C^{13}≡C^{13}-NAP	1583, 1605, 1653, 1692, 2010, ~2020

Ground state FTIR spectra of the complexes show the same four bands in the region 1500-1700 cm^{-1} at 1583, 1605, 1653, 1692 cm^{-1}. These signals are assigned as follows; 1583 and 1605 cm^{-1} ν(NAP), 1653 cm^{-1} ν(CO) asymmetric stretch, 1692 cm^{-1}

v(CO) symmetric stretch. The signals between 2000-2150 cm^{-1} are assigned to the acetylide stretches. For the unlabelled complex, PTZ-Ph-C≡C-Pt-C≡C-NAP, there is an intense peak at 2090 cm^{-1} corresponding to v($C^{12}C^{12}$) asymmetric stretch and a weaker shoulder at 2110 cm^{-1} corresponding to v($C^{12}C^{12}$) symmetric stretch. For the complex that has isotopically labelled acetylides on both the donor and acceptor sides, PTZ-Ph-C^{13}≡C^{13}-Pt-C^{13}≡C^{13}-NAP, there is an strong peak at 2010 cm^{-1} corresponding to v($C^{13}C^{13}$) asymmetric stretch and a weaker shoulder at approximately 2020 cm^{-1} corresponding to v($C^{13}C^{13}$) symmetric stretch however this is less defined that the asymmetric stretching frequency in the unlabelled complex. For the complex that has an isotopically labelled acetylide on the donor side only, PTZ-Ph-C^{13}≡C^{13}-Pt-C≡C-NAP, there are weak signals at 2020 and 2043 cm^{-1} which likely arise from a resonance between v($C^{13}C^{13}$) and another combination mode, the intense peak at 2090 cm^{-1} corresponds to v($C^{12}C^{12}$). For the complex that has an isotopically labelled acetylide on the acceptor side only, PTZ-Ph-C≡C-Pt-C^{13}≡C^{13}-NAP, there is an intense signal at 2010 cm^{-1} that corresponds to v($C^{13}C^{13}$) and there is a weak signal at 2110 cm^{-1} which likely arises from a resonance between v($C^{13}C^{13}$) and another combination mode, similar to those described in Archer *et al.*[5]

5.4 Conclusions

A series of isotopically labelled ($C^{13}C^{13}$) platinum(II) *trans*-acetylides were synthesised with the aim of separating their acetylide vibrational frequencies so that they could be selectively probed in “vibrational control” experiments. It was estimated that the isotopic labelling would shift the vibrations by ~80 cm^{-1} and this was observed in the ground state FTIR spectra.

5.5 Future work

The complexes synthesised in this chapter have been studied in depth at Rutherford Appleton laboratories using ultrafast spectroscopy. The data is currently in the process of being analysed.

5.6 References

1 M. Delor, T. Keane, P. A. Scattergood, I. V. Sazanovich, G. M. Greetham, M. Towrie, A. J. H. M. Meijer and J. A. Weinstein, *Nat. Chem.*, 2015, **7**, 689–695.

2 P. A. Scattergood, M. Delor, I. V Sazanovich, O. V Bouganov, S. A. Tikhomirov, A. S. Stasheuski, A. W. Parker, G. M. Greetham, M. Towrie, E. S. Davies, A. J. H. M. Meijer and J. A. Weinstein, *Dalt. Trans.*, 2014, **43**, 17677–17693.

3 M. Delor, I. V. Sazanovich, M. Torie and J. A. Weinstein, *Acc. Chem. Res.*, 2015, **48**, 1131–1139.

4 M. Delor, P. A. Scattergood, I. V Sazanovich, A. W. Parker, G. M. Greetham, A. J. H. M. Meijer, M. Towrie and J. A. Weinstein, *Science*, 2014, **346**, 1492–5.

5 S. A. Archer, T. Keane, M. Delor, A. J. H. M. Meijer and J. A. Weinstein, *Inorg. Chem.*, 2016, **55**, 8251–8253.